HAL
archives-ouvertes.fr

Des scalaires dans les dimensions supplémentaires (courbes) : modèles effectifs et réalisations concrètes

Andrei Angelescu

▶ **To cite this version:**

Andrei Angelescu. Des scalaires dans les dimensions supplémentaires (courbes) : modèles effectifs et réalisations concrètes. High Energy Physics - Phenomenology [hep-ph]. Université Paris-Saclay, 2017. English. <NNT : 2017SACLS312>. <tel-01680119>

HAL Id: tel-01680119
https://tel.archives-ouvertes.fr/tel-01680119

Submitted on 10 Jan 2018

HAL is a multi-disciplinary open access archive for the deposit and dissemination of scientific research documents, whether they are published or not. The documents may come from teaching and research institutions in France or abroad, or from public or private research centers.

L'archive ouverte pluridisciplinaire **HAL**, est destinée au dépôt et à la diffusion de documents scientifiques de niveau recherche, publiés ou non, émanant des établissements d'enseignement et de recherche français ou étrangers, des laboratoires publics ou privés.

NNT: 2017SACLS312

THÈSE DE DOCTORAT
DE
L'UNIVERSITÉ PARIS-SACLAY
PREPARÉE À
L'UNIVERSITÉ PARIS-SUD

ÉCOLE DOCTORALE N°576
Particules Hadrons Énergie et Noyau : Instrumentation, Image, Cosmos et Simulation (PHENIICS)
Spécialité de doctorat : Physique des particules

Par
M. Andrei Angelescu

Scalars in (Warped) Extra Dimensions: Climbing from the Bottom to the Top

Thèse présentée et soutenue à Orsay, le 29 septembre 2017 :

Composition de jury:

M. Aldo Deandrea	*Professeur, Université Claude Bernard Lyon*	Rapporteur
M. Abdelhak Djouadi	*Directeur de recherche, Université Paris-Saclay*	Co-directeur de thèse
M. Emilian Dudas	*Professeur, Université Paris-Saclay*	Président
M. Florian Goertz	*Chargé de Recherche, Institut de Physique Nucléaire Max Planck*	Examinateur
M. Grégory Moreau	*Maître de conférences, Université Paris-Saclay*	Directeur de thèse
M. José Santiago	*Professeur, Université de Grenade*	Rapporteur

Titre: Des scalaires dans les dimensions supplémentaires (courbes): modèles effectifs et réalisations concrètes
Mots clés: *Nouvelle Physique, Dimensions Supplémentaires, Boson de Higgs, LHC, Phenomenologie, Matiére Noire*
Résumé: Il y a près de deux décennies, l'utilisation des modèles à dimensions supplémentaires pour résoudre le problème de hiérarchie des théories de jauge a reçu beaucoup d'attention, grâce à d'élégantes propositions: des dimensions supplémentaires (DS) étendues et plates – le modèle d'Arkani-Hamed-Dimopoulos-Dvali, ou ADD – ainsi que des DS courbées – le modèle de Randall-Sundrum, ou RS. Dans cette thèse, nous discutons plusieurs modèles inspirés de tels scénarios de dimension supèrieure. Pour commencer, nous introduisons des éléments-clés de la théorie des champs en cinq dimensions, et nous montrons comment de tels scénarios apportent une réponse au problème de hiérarchie. Ensuite, dans une première partie, nous adoptons une approche "de bas en haut" et étudions plusieurs modèles contenant des fermions vectoriels (FV), prédits génériquement dans les modèles de DS. Nous montrons qu'en ajoutant des quarks vectoriels (QV) au Modèle Standard (MS), on peut expliquer en même temps les anomalies (i) d'asymétrie avant-arrière des quarks b ($A_{\rm FB}^b$) mesurée au Large Electron-Positron collider (LEP) et (ii) de section efficace de production de $t\bar{t}h$ mesurée au Large Hadron Collider (LHC). En utilisant des rapports de taux de désintégration du Higgs, nous estimons aussi la sensibilité du LHC amélioré, le LHC à haute luminosité, à la présence de QV. Puis nous considérons un modèle à deux doublets de Higgs (2HDM), accompagné de leptons vectoriels (LV) pour expliquer le mystérieux excès à 750 GeV observé au LHC fin 2015. Dans un modèle similaire, nous expliquons également l'abondance de matière noire (MN) dans l'Univers, notre candidat pour la MN étant un LV neutre, stabilisé par une symétrie $\mathbb{Z}_2$ appropriée. Dans une deuxième partie de la thèse, nous nous penchons sur le scénario plus concret des DS courbées dotées d'une symétrie custodiale dans l'espace à cinq dimensions, qui protège le modèle vis-à-vis de larges corrections aux observables de précision électrofaibles. Dans ce cadre, nous interprétons tout d'abord la résonance à deux bosons observée à 2 TeV au LHC comme étant une superposition de bosons de jauge de Kaluza-Klein, produits dans le canal s. Dans un deuxième temps, nous étudions la phénoménologie du secteur scalaire du modèle susdit, qui mélange le boson de Higgs et le radion. En particulier, nous estimons la sensibilité du LHC et d'un futur collisionneur électron-positron (l'International Linear Collider - ILC) à la présence d'un radion, via la production de celui-ci en association avec un boson Z.

Title: Scalars in (Warped) Extra Dimensions: Climbing from the Bottom to the Top
Key words: *New Physics, Extra Dimensions, Higgs Boson, LHC, Phenomenology, Dark Matter*
Abstract: Almost two decades ago, the paradigm of extra-dimensional models addressing the gauge hierarchy problem attracted much attention through the elegant proposals of large, flat extra dimensions (EDs) – the Arkani-Hamed-Dimopoulos-Dvali or ADD model – and warped EDs – the Randall-Sundrum or RS model. In this thesis, we discuss several models inspired from such extra-dimensional scenarios. We start by introducing some key elements of field theory in five space-time dimensions and showing how such scenarios provide a solution to the hierarchy problem. Afterwards, in a first part of this work, we adopt a bottom-up approach and study several models containing Vector-Like Fermions (VLFs), which are typically predicted in ED frameworks. We show how adding Vector-Like Quarks (VLQs) to the Standard Model (SM) allows one to simultaneously explain the anomalies in the (i) b-quark forward-backward asymmetry ($A_{\rm FB}^b$) measured at the Large Electron-Positron collider (LEP) and (ii) the $t\bar{t}h$ production cross section measured at the Large Hadron Collider (LHC). Using the so-called Higgs decay ratios, we also estimate the sensitivity of the upgraded LHC, the High-Luminosity LHC, to the presence of VLQs. Then, we consider a Two-Higgs Doublet Model (2HDM) extended with Vector-Like Leptons (VLLs) in order to fit the mysterious 750 GeV excess observed at LHC in late 2015. Within a similar model, we also explain the Dark Matter (DM) abundance in the Universe, our DM candidate being a neutral VLL, which is rendered stable by a suitable $\mathbb{Z}_2$ symmetry. Later on, in a second part of the thesis, we focus on the more concrete warped ED scenario endowed with a bulk custodial symmetry, which protects the model from large electroweak (EW) corrections. In this framework, we first interpret the 2 TeV diboson bump observed at LHC in 2015 as a superposition of Kaluza-Klein (KK) gauge bosons produced in the s-channel. Afterwards, we study the phenomenology of the mixed Higgs-radion scalar sector of the aforementioned model. In particular, we estimate the sensitivity of the LHC and of a future electron-positron collider (the International Linear Collider - ILC) to the existence of a radion via its production in association with a Z boson.

Université Paris-Saclay
Espace Technologique / Immeuble Discovery
Route de l'Orme aux Merisiers RD 128 / 91190 Saint-Aubin, France

Contents

List of Tables

List of Figures

Résumé en français

Jusqu'au présent, le Modèle Standard (MS) de la Physique des Particules est la théorie décrivant le mieux la dynamique aux echelles subatomiques. Avec la découverte du boson de Brout-Englert-Higgs, qui a été prédit pendant les années soixantes, découverte qui a eu lieu au Grand Collisioneur Hadronique (Large Hadron Collider - LHC), le MS de la Physique des Particules est finalement complet.

Plusieurs fois, des expériences dans le passé (i.e. Le Grand Collisioneur Electron-Positron - LEP et Tevatron) et dans le présent (LHC) ont confirmé du point de vue expérimental les prédictions théoriques du Modèle Standard. Malgré cela, il y a des raisons à croire que le Modèle Standard n'est pas la théorie fondamentale qui décrive la Nature.

Du côté observationel, le Modèle Standard n'arrive pas a décrire les oscillations de saveur des neutrinos, qui ont été mésurées dans le passée. Plus précisement, dans le cadre du MS, les trois neutrinos sont de masse nulle, ce qui implique qu'ils ne peuvent pas osciller d'une saveur à l'autre. Un autre défaut du MS en ce qui concerne la partie observationelle est relié à la Matière Sombre (MS) ou Matière Noire. Des mésures cosmologique effectuées par le satellite Planck indique que approximativement 27% du budget énérgetique de l'Univers est composé par la Matière Sombre. Parmi le $\sim 73\%$ qui reste, seulement 5% est constitué de matiére ordinaire/lumineuse, tandis que 68% restant est représenté par la encore plus mysteriuse Energie Noire (i.e. Constante Cosmologique).

Le MS a aussi plusieures problèmes d'origine théorique. Deux examples proéminents sont (i) son inabilité d'inclure de manière consistente une théorie quantique de la gravité et (ii) le probème de l'hiérarchie. Dans le prémier cas, le probléme vient du fait que la théorie de gravité d'Einstein est une théorie non-renormalizable: a chaque ordre en théorie des perturbations, des nouvelles divergences apparaissent, qui impose l'introduction d'une infinité de contre-termes dans le Lagrangian qui décrive la gravité. Or, étant donné que chaque contre-terme doit être fixé par une mésure expérimentale, on voit immédiatement l'impossibilité d'inclure d'une maniére consistente la gravité dans le MS: pour faire cela, on aurait besoin d'une infinité des mesures expérimentales. Malgré cela, c'est possible d'interpreter les collisions gravitationelles des particules si elles ont lieu aux énérgies beaucoup plus basses que la masse du Planck, M_{Pl}, qui est l'échelle énérgetique à laquelle la gravité devient fortement coupleé.

Peut-être le probléme le plus étudié du Modèle Standard est le deuxième example donné dans le paragraphe précedent, c'est à dire le probléme de l'hiérarchie de jauge. Ce problé est relié aux corrections que la masse du boson de Higgs reçoit au niveau quantique (au niveau des boucles). Une maniére simple d'enoncer le probléme de l'hiérarchie est la suivante. Considérons un boson scalaire générique S, ayant une masse M et plus lourd que le boson de Higgs de 125 GeV h, qui couple au scalaire du MS avec un couplage g_*. Si on fait un "matching" à une boucle à l'échelle $\mu = M$ entre le model Ultra-Violet (UV) contenant le scalaire lourd et la théorie effective de champs (Effective Field Theory - EFT) avec S intégré,

on trouve les correctons suivantes à la masse physique du Higgs:

$$m^2_{h,\text{phys}} \simeq m^2_{h,\text{bare}} - \text{const} \times \frac{g^2_*}{16\pi^2} M^2, \tag{1}$$

ou const est une constante numérique d'ordre 1 (la valeur de cette constante varie selon le type d'interaction entre les deux scalaires, i.e. des vertex trilineaires/quartiques). Il y a aussi des autres corrections, proportionelles à $\log(M/m_h)$, mais on a decidé de ne pas les détailler car elles sont pas essentielles dans cette discussion. Si S est beaucoup plus lourd que h, i.e. $M \gg m_{h,\text{phys}}$, la masse "nue" $m_{h,\text{bare}}$ doit être de même ordre de grandeur que M (modulo $g^2_*/(16\pi^2)$), mais tré finement reglée afin de reproduir la masse mésurée du boson de Higgs. Cela represent l'idée central dérrière le problème de hiérarchie, qui est connu aussi comme le problè de réglage fine du MS. Alternativement, dans une formulation moins précise, le probléme de l'hiérarchie a ses origines dans la faibless des intéractions gravitationelles par rapport aux autre intéractions fondamentales. De manière équivalente, le probléme de l'hiérarchie peut être formule comme une simple questions: pourquoi l'échelle électrofaible est si basse par rapport à l'échelle de Planck, M_{Pl}?

Pendant les dérnières décades, le probléme de l'hiérarchie a reçu beaucoup d'attention. Cela est du au fait que chaque théorie qui propose une solution viable au probléme du réglage fine du MS prédit, en principe, des nouvelles particules qui ne devraient pas être beaucoup plus lourdes que le Higgs mésuré, tel que il n'y a pas besoin de fines annullations dans l'équation (1). Il y a, cependant, des théories qui ne respectent pas cet argument, comme le "relaxion" et le mechanisme de "Higgsplosion".

Une théorie particuliérement populaire qui résout le problème de l'hiérarchie est le Modèle Standard Supersymmétrique Minimal (Minimal Supersymmetric Standard Model - MSSM). Dans le MS, les masses physique des fermions et des bosons de jauge reçoivent des corrections proportionelles à leurs masses nues, i.e. $m_{\text{phys}} - m_{\text{bare}} \propto m_{\text{bare}} \log(M/m)$, qui est une conséquence de la symmetrie chirale (de jauge) pour le cas des fermions (bosons de jauge). D'une façon similaire, la SuperSymmétrie (SuSy) offre un méchanisme de protection pour le scalaire de Higgs. En MSSM, chaque particule du Modéle Standard est associée à son superpartenaire, qui a les même nombre quantiques que la particule originale, sauf le spin, qui diffère d'une unité de 1/2 par rapport à celui de la particule du MS. Par conséquent, le boson de Higgs est associé a son superpartenaire de spin-1/2, appellé le "higgsino". Cette dérnière particule est protégée par une symétrie chirale, qui, via SuSy, protége le Higgs aussi.

Une autre solution elegante au problèm de l'hiérarchie est d'ajouter des dimensions spatiales supplémentaires (extra-dimensions - EDs) à l'éspace-temps quatre-dimensionel habituel (espace Minkowski). Dans des modèles aux dimensions supplémentaire étendues (plates), le MS se propage dans une variété 4-dimensionelle (4D), tandis que la gravité se propage non seulement dans l'espace 4D, mais aussi au long des dimensions supllémentaires. Par conséquent, la gravité est diluée dans le volume extra-dimensionel, ce qui, dans ce type de modéles, explique pourquoi la gravité est si faible dans la description effective 4D. Comme rémarque intéréssante, on mentionne que la SuSy et les dimesions supplémentaires sont des elements indispensable dans des théories des Supercordes (Superstrings).

Une autre théorie aux dimensions supplémentaires qui résout le probléme de l'hiérarchie est basée sur la proposition elegante de Randall et Sundrum. Les deux auteurs ont considéré une construction geométrique avec une dimensions spatiale supplémentaire qui est courbée et qui s'étend entre deux 3-branes (i.e. variétés 4D). La métrique non-factorizable et de type Anti-de-Sitter (Ads) et l'espace-temps résultant est une "tranche" de AdS_5, qui est habituellement appellé le "bulk". Les deux bords 4D (ou branes) de l'ED sont la brane ultra-violet (UV)/Planck, avec une échelle unique de la gravité, egale à l'échelle de Planck,

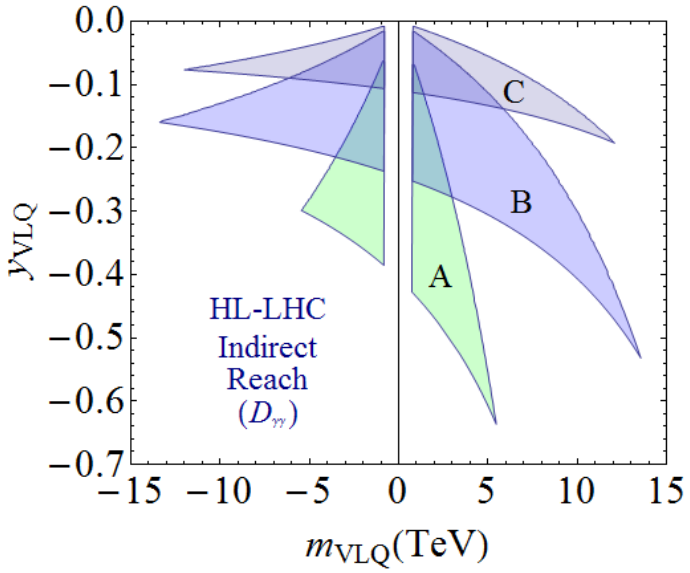

Figure 1 – Régions dans le plan $[m_{\rm VLQ}, y_{\rm VLQ}]$ pour les versions simplifiées des modèles **A**, **B** et **C**, auxquelles une mesure précise de $D_{\gamma\gamma}$ au HL-LHC, avec $\Delta D_{\gamma\gamma} = 1\%$, sera sensible. Les autres paramètres entrant dans le analyse sont discutées dans le troisième chapitre.

et la brane infra-rouge (IR)/TeV, avec une échelle d'énérgie exponentiellement supprimée, qui est proche de échelle du TeV. Dans un tel scénario aux dimensions supplémentaires, la hiérarchie entre les échlles de Planck et electrofaible est expliqué d'une manière naturelle á travers le facteur de courbure exponentiel entre les deux branes. Afin de résoudre le problème de l'hiérarchie de jauge, ce scenario a besoin d'un boson de Higgs localisé sur ou proche de la brane TeV. Par conséquent, l'échlle typique de la brane TeV ((exponentiellement supprimée)) joue le rôle d'un "cutoff" pour les corrections quantique à la masse de Higgs.

Dans cette thèse de doctorat, on s'est concentré sur les aspects phénomenologiques des modèles aux dimensions supplémentaires courbes. Dans les premiers chapitres, on a étudié des modèles effectives inspirés des constructions aux dimensions supplémentaires. On appelle ces modèles "effeives" car ils contiennent des Fermions Vecteurs (Vector-Like Fermions - VLFs), qui peuvent être réalisés comme des excitations Kaluza-Klein (KK), qui sont prédites dans des théories aux dimensions supplémentaires. Ensuite, dans les dérniers chapitres, on a considéré des scenarios plus concrets aux dimensions supplémentaires. Dans les deux parties, les secteurs scalaires des modéles qu'on a considérés ont été au centre de nos études. Ces secteures incluent le Higgs du MS, des nouveaux champs de Higgs lourds, qui apparaissent typiquement dans des Modéles à Deux Doublets de Higgs (Two Higgs Doublet Models - 2HDMs) ou dans le MSSM, et un scalaire plus exotique, appellé le radion. Dans des modéles cinq-dimensionels, c'est à dire à une seule dimension supplémentaire, le radion est un champ scalaire associé à la fluctuation de la cinqième composante de la métrique. Egalement, le radion joue un rôle dans la stabilisation de la longueur de la dimension supplémentaire.

Maintenant, on va discuter briévement chaque chapitre de cette thèse, en détaillant trois résultats centrals qu'on a obtenu. Le premier chapitre représente une introduction générale au sujet de cette thése, tandis que chaque chapitre suivant aura à son début une introduction plus precise. Le deuxième chapitre est une discussion concise sur les modéles aux dimensions supplémentaires en physique des particules. Ici, on introduise les dimensions supplémentaire plates et courbes aussi.

Dans le troisième chapitre, on propose plusieures extensions du MS aux Quark Vecteurs

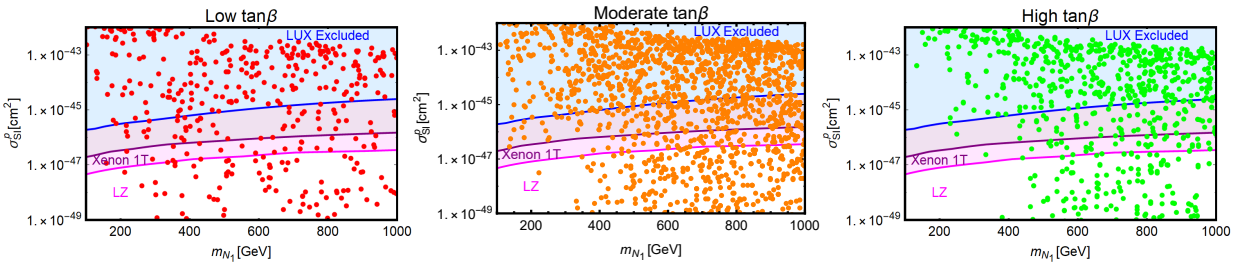

Figure 2 – Graphiques récapitulatifs comprenant toutes les contraintes discutées tout au long du cinquième chapitre. Chacun des trois panneaux de la figure fait référence à un régime de valeurs différent de $\tan\beta$ (voir le texte principal pour plus de détails), indiqué en haut de chaque panneau.

(Vector-Like Quarks - VLQ), ayant le but d'expliquer (i) l'anomalie de LEP pour la mésure de l'asymmétrie avant-arrière de la production des quarks b, et aussi (ii) l'anomalie plus récente, à 2σ, dans la section efficace de production associée d'un boson de Higgs avec une paire des quarks t, $\sigma(pp \to t\bar{t}h)$. On analyse aussi la sensibilité du LHC à haute luminosité (High Luminosity LHC ou HL-LHC) à la présence des VLQs.

Un des résultats centrales du troisième chapitre est représenté dans la Fig. 1, qui montre la sensibilité du HL-LHC à la présence des VLQs de charge éléctrique $Q = 5/3, 2/3$ et $-4/3$. Plus précisémment, les régions colorées de la Fig. 1 indiquent les regions auxquelles une mésure très précise de $\Delta D_{\gamma\gamma}$, atteignable au HL-LHC, sera sensible. Les deux axes représentent la masse du VLQ, $m_{\rm VLQ}$, et son couplage Yukawa au Higgs du MS, $y_{\rm VLQ}$. $\Delta D_{\gamma\gamma}$ est une observable définie dans le troisième chapitre. Ce qui est remarcable et le fait que l'observable $\Delta D_{\gamma\gamma}$ sera (indirectement) sensible aux masses des VLQs de l'ordre de 10 TeV, tandis que les recherches directes des VLQs au HL-LHC atteigneront une sensibilité de $1.5 - 2$ TeV.

Le quatrième chapitre est dédié à une interpretaion de la mystérieuse resonance de 750 GeV observée dans le canal diphoton au LHC en 2015 (mais qui n'a pas êtê confirmée par les données ultérieures). Dans notre interpretion, le rôle de la resonance de 750 GeV est joué par un scalaire lourd provenant d'un Modèle à Deux Doublets de Higgs, tandis que son rapport de branchement en deux photons est augmenté par l'introduction des Leptons Vecteurs (Vector-Like Leptons - VLLs) avec une chargé electrique non-nule.

Dans le cinquième chapitre, on essaye d'expliquer l'abondance de Matière Sombre dans l'Univers en considérant un modéle similaire à celui du quatrième chapitre. La différence principale est le fait qu'on considére des VLLs neutres (sans charge electrique) aussi, dont un est le candidat pour la matiére sombre.

Les résultats de l'étude fait dans ce chapitre sont résumés en Fig. (2). Ici, on met ensemble les résultats de la phénoménologie de la matière sombre avec les contraintes théoriques venant des é du group de renormalization pour le couplage quartique des scalaires, les contraintes des testes de précision électrofaible, les limites venant des recherches aux LHC (surtout (pseudo)scalaire lourd se désintegrant en $\tau\tau$), et contraintes venant des mésures à basse énergie.

Les trois images de la fig. (2) montrent, pour trois régimes de valeurs de $\tan\beta$, i.e. basse (1-7), modérée (10-20) et haute (40-45), dans le plan $(m_{N_1}, \sigma^{\rm SI}_{N_1 p})$, les points du modèle reproduisant la densité relique correcte de la matière sombre et satisfaisant les contraintes listées ci-dessus.

Les résultats présentés sur la fig. (2) peuvent être expliqués comme suit. Les distributions

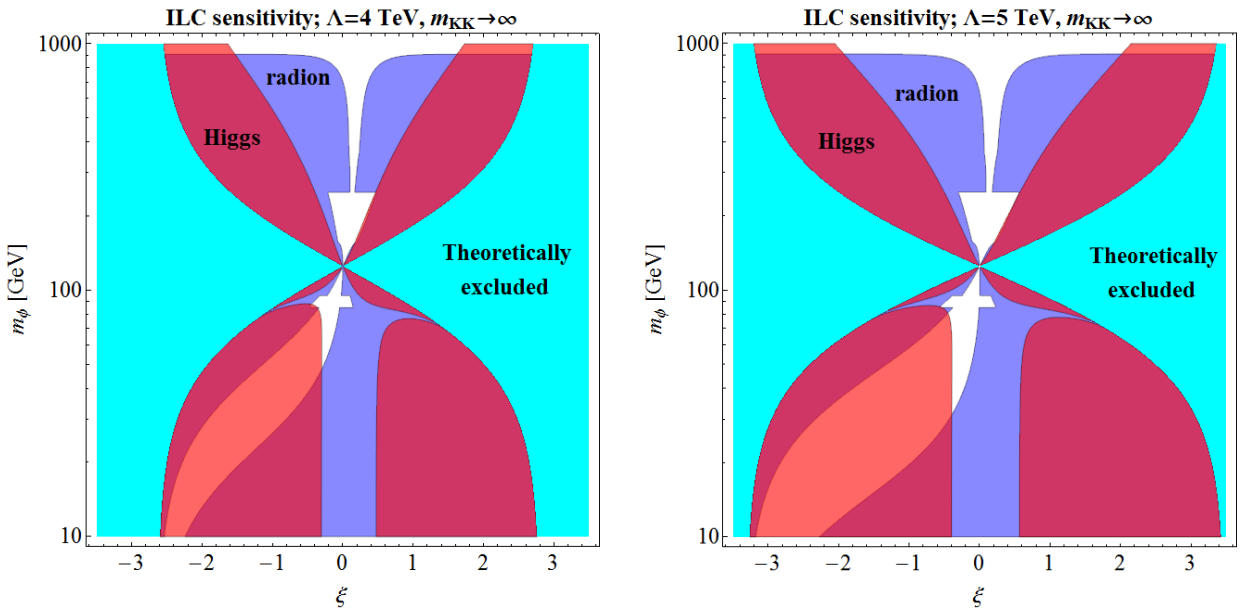

Figure 3 – Graphique récapitulatifs pour les recherches directes et indirectes du radion aux trois étapes de fonctionnement de l'ILC ($\sqrt{s} = 250$ GeV, 500 GeV, and 1 TeV), dans le plan $\{\xi, m_\phi\}$, pour (gauche) $\Lambda = 4$ TeV et (droite) $\Lambda = 5$ TeV, avec m_{KK} infini. La région bleue couvre l'espace des paramètres Higgs-radion estimé d'être sondé par l'ILC par des recherches directes de radion, tandis que la région rouge représente le domaine potentiellement sondé par la mesure précise du couplage hZZ. Le domaine cyan est exclus par des contraintes théoriques.

des points dans les trois panneaux de la figure semblent plutôt similaires. Comme discuté dans le troisième, en supposant que les VLLs puissent coupler aux deux doublets de Higgs, la dépendance sur $\tan\beta$ des couplages de la matière est réabsorbée dans la définition des couplages eux-mêmes. Nous remarquons néanmoins que les masses réduite du DM, c'est-à-dire plus légères qu'environ 400 GeV, deviennent progressivement désavantagées quand la valeur de $\tan\beta$ augmente. Les limites venant de la détection directe sont en général évitées si la densité relique est atteinte soit par des résonances en canal s, soit par des annihilations impliquant des Higgses lourdes, en particulier ceux chargés, comme états finaux. La première possibilité devient de plus en plus artificielle à des valeurs plus élevées de $\tan\beta$ car la réduction de la largeur de désintégration des états H/A nécessite un réglage fin dans la difference $|m_{N_1} - m_{A,H}/2|$. Ce problème est partiellement évité en considérant des valeurs assez élevées des masses de H et A. Le cas des annihilations en Higgs lourds est influencé par plusieurs aspects, selon le type de 2HDM, c'est-à-dire le type I, le type II, lepton spécifique ou "flipped". La configuration de type II est exclue pour m_A inférieure à 400 GeV dans le régime modéré de $\tan\beta$, et pour des masses considérablement plus grandes dans le régime $\tan\beta$ élevé, par les recherches LHC dans le canal $\tau\tau$. Les valeurs de m_A inférieures à 400 GeV sont également exclues dans la configuration "flipped" pour $\tan\beta$ élevé. Ces contraintes partiellement influencent les autres masses de Higgs car pour des valeurs modérés / élevés de $\tan\beta$ les contraintes favorisent un spectre dégénéré pour les Higgs lourds. Dans le modèle de type II, la masse du Higgs chargé est cependant individuellement forcée de se situer au-dessus d'environ 400 GeV par des contraintes provenant des processus à basse énergie.

Dans le sixième chapitre, nous considérons un modèle aux dimensions suppèmentaires courbes pour expliquer l'anomalie diboson à 2 TeV observée en 2015 au LHC (et, encore une

fois, non confirmée par des données ultérieures). Notre candidat pour l'excès est en fait une superposition de bosons de jauge de Kaluza-Klein (KK) presque dégénérés en masse, qui sont prédits par le groupe de jauge étendu (custodial) que nous considérons.

Ensuite, dans le septième chapitre, nous adoptons le même modèle qu'au chapitre précédent, mais nous nous concentrons plutôt sur la phénoménologie de son secteur scalaire, qui inclut le Higgs et le radion. Plus précisément, nous calculons les couplages du Higgs et du radion et estimons la sensibilité du LHC et d'un futur collisionneur linéaire (tel que ILC - International Linear Collider) à la présence du radion.

Sur la figure 3, nous résumons sur un graphique unique les régions couvertes par les trois possibles stages de fonctionnement ILC, respectivement à 250 GeV, 500 GeV et 1 TeV, pour des résonances KK découplées ($m_{KK} \to \infty$) et pour deux valeurs du VEV du radion, $\Lambda = 4,5$ TeV. Une analyse plus précise serait nécessaire pour évaluer de manière consistente ces performances, mais il est clair que l'ILC peut creuser dans le scénario de radion avec une excellente sensibilité.

Enfin, dans le huitième chapitre, on résume les résultats et on donne un bref aperçu.

Chapter 1

Introduction

Up to date, the so-called Standard Model (SM) of Particle Physics [8–10] is undoubtedly the most successful theory describing dynamics at the subatomic level. With the discovery of the long-predicted Brout-Englert-Higgs boson [11–13] at the Large Hadron Collider (LHC) in 2012 by the ATLAS [14] and CMS [15] collaborations, the SM of Particle Physics is finally complete.

Time and again, past (i.e. LEP - The Large Electron-Positron collider, Tevatron) and present (LHC) colliders have experimentally confirmed the theoretical predictions of the SM. Nevertheless, there are reasons to believe that the SM is not the fundamental theory describing Nature.

On the observational side, the SM fails to describe the neutrino flavour oscillations, which have been measured in the past [16]. More precisely, in the SM, the three neutrinos are massless, which implies that they should not oscillate from one flavour into another. Another shortcoming of the SM regarding observation is related to the so-called Dark Matter [17–20]. Cosmological measurements carried out by the Planck satellite [21] indicate that approximately 27% of total energy budget of the Universe is made out of Dark Matter. Among the rest of $\sim 73\%$, only 5% is represented by ordinary, luminous matter, whereas the remaining 68% is made out of the even more mysterious Dark Energy (i.e. Cosmological Constant).

The SM also suffers from several problems of theoretical origin. Two prominent examples are (i) its inability to consistently incorporate a quantum theory of gravity and (ii) the so-called hierarchy problem. In the first case, the problem lies in the fact that gravity is a non-renormalizable theory: at each order in perturbation theory, new divergences appear, which mandate the introduction of an infinity of counter-terms in the renormalized Lagrangian describing gravity. Or, each counter-term needs to be fixed by an experimental measurement, meaning that one has to perform an infinity of measurements to make sense of gravity at the quantum level, hence the impossibility to consistently incorporate quantum gravity in the SM.[1]

Perhaps the most widely studied problem of the SM is the second example given in the previous paragraph, namely the gauge hierarchy problem. It is related to the corrections that the Higgs boson mass receives at the loop (quantum) level. A simple way of stating the hierarchy problem is the following. Consider a generic scalar S with mass M, heavier than the 125 GeV Higgs boson h, having a generic coupling g_* to the SM scalar. If a matching at one loop at the scale $\mu = M$ is performed between the UV model containing the heavy

[1] Nevertheless, one can make sense of quantum gravitational particle collisions if they occur at energies well below the Planck Scale M_{Pl} by retaining only the leading order(s) in E/M_{Pl}, where E is, for example, the center-of-mass energy of the collision.

scalar and the effective field theory (EFT) with S integrated out, one finds the following corrections to the physical mass of the Higgs: [2]

$$m^2_{h,\text{phys}} \simeq m^2_{h,\text{bare}} - \text{const} \times \frac{g_*^2}{16\pi^2} M^2, \tag{1.1}$$

where const is a number of order 1.[3] There are also other corrections proportional to $\log(M/m_h)$, but we choose to not display them as they are not relevant for the current discussion. If S is much heavier than h, i.e. $M \gg m_{h,\text{phys}}$, then $m_{h,\text{bare}}$ has to be of the same order as M (modulo $g_*^2/(16\pi^2)$), but very precisely tuned in order to reproduce the much smaller measured Higgs mass. This is the crux of the so-called gauge hierarchy problem, which is also called the fine-tuning problem of the SM.[4]

In the last few decades, the hierarchy problem has received lots of attention. This is because any theory which provides a viable solution to the fine-tuning problem of the SM predicts, in principle, new particles that should be not much heavier than the measured Higgs, such that no fine cancellations are needed in eq. (1.1).[5]

One particularly popular theory addressing the gauge hierarchy problem is the Minimal Supersymmetric Standard Model or MSSM [24]. In the SM, the fermion and gauge boson physical masses receive corrections proportional to their bare masses, i.e. $m_{\text{phys}} - m_{\text{bare}} \propto m_{\text{bare}} \log(M/m)$, which is a consequence of chiral (gauge) symmetry in the case of fermions (gauge bosons). Similarly, Supersymmetry (SuSy) provides a protection mechanism for the Higgs scalar. In SuSy, each SM particle is paired up with one so-called superpartner, which retains the same quantum numbers as the original SM particle but whose spin differs by 1/2 with respect to the spin of the SM particle. Consequently, the Higgs boson gets paired with its spin-1/2 superpartner, dubbed the Higgsino, from which the SM scalar "inherits", via supersymmetry, the protection that the Higgsino receives through chiral symmetry.

Another popular solution to the hierarchy problem is the addition of compact (i.e. finite) extra spatial dimensions (EDs) to the ordinary 4-dimensional (4D) Minkowski space. In models with large (flat) extra dimensions, the SM is confined to the usual 4D world, whereas gravity propagates not only in 4D, but also along the extra-dimensions. As a consequence, gravity gets diluted in the extra-dimensional volume, which is why, in such models, gravity appears so weak in the effective 4D description. Interestingly, both Supersymmetry and extra dimensions appear as ingredients in in Superstring theories.

A different extra-dimensional scenario addressing the hierarchy problem is based on an elegant proposal by Randall and Sundrum [25]. The two authors considered a geometrical setup with one additional warped spatial dimension, which extends between two branes (i.e. 4D worlds). The non-factorisable metric is of Anti-de-Sitter (AdS) type and the resulting space-time is a so-called AdS_5 slice (or throat), which is referred to as the bulk. The two 4-dimensional boundaries or branes are the ultra-violet (UV) boundary (or the Planck brane), with a (unique) gravity scale at the Planck scale, and the infra-red (IR) brane (or the TeV brane), with an exponentially suppressed scale close to the TeV scale. In such a higher-dimensional framework, the hierarchy between the electroweak (EW) and Planck

[2] Our argument follows the one from Adam Falkowski's lectures, given in April-May 2017 at IPhT Saclay: `https://courses.ipht.cnrs.fr/?q=fr/node/167`.

[3] This constant depends on whether one considers only $hhSS$ or both hhS and $hhSS$ couplings. In any case, specifying the type of interactions between the two scalars is not important in this case.

[4] In a less precise formulation, the hierarchy problem has its origins in the relative weakness of the gravitational interaction compared to other fundamental interactions. Equivalently, it tries to answer to the following question: why is the electroweak scale much lower than the Planck scale, M_{Pl}?

[5] There are, however, exceptions to this statement, as, for example, the so-called relaxion mechanism [22] or the recently proposed Higgsplosion scenario [23].

scales is achieved in a natural way through the exponential warping between the two branes. In order to solve the gauge hierarchy problem, such a scenario needs to have the Higgs boson localized close to or at the so-called TeV brane. In this way, the (exponentially suppressed) typical energy scale of the TeV brane acts as a cutoff on the Higgs mass corrections.

In this PhD thesis, we focus on phenomenological aspects of warped extra-dimensional models. In the first chapters, we start from the "bottom" and study effective models that are inspired from extra-dimensional constructions. We call these models effective in the sense that they feature Vector-Like Fermions (VLFs), which can be realised as Kaluza-Klein excitations predicted in higher-dimensional theories. Afterwards, in the final chapters, we "climb towards the top" and consider more concrete extra-dimensional scenarios. Throughout both parts, special attention is dedicated to the scalar sectors of the considered models. These sectors comprise the SM Higgs, new heavy Higgs fields, which typically arise in Two Higgs Doublet Models (2HDM) or in Supersymmetry), and a more "exotic" scalar, the so-called radion. In 5D models, the latter appears as a scalar fluctuation of the 5th component of the metric. Also, it plays a role in stabilizing the length of the extra dimension.

This thesis is organized as follows. The current chapter serves as a general introduction for this work, whereas each of the upcoming chapters has a more precise introduction at its beginning. Chapter 2 serves as a brief overview of extra-dimensional models in particle physics. Here, we dedicate a short discussion to both flat and warped extra dimensions. In chapter 3, we propose several Vector-Like Quark (VLQ) extensions of the SM with the purpose of explaining both the forward–backward asymmetry in b–quark production at LEP, $A_{\rm FB}^b$, but also the more recent 2σ deviation of the cross section for the associated Higgs production with top quark pairs at the LHC, $\sigma(pp \to t\bar{t}h)$. We also analyze the sensitivity of the High Luminosity LHC (HL-LHC) to the presence of VLQs. Chapter 4 is dedicated to an interpretation of the putative 750 GeV diphoton excess observed at CERN in 2015 (but discarded as a statistical fluctuation in 2016). The role of the 750 GeV resonance is played by a heavy scalar coming from a Two Higgs Doublet Model (2HDM), while its branching ratio to two photons is enhanced by introducing electrically charged Vector-Like Leptons (VLLs). In chapter 5, we aim at explaining the Dark Matter (DM) abundance in the Universe by considering a model similar to the one in chapter 4. The main difference is that we consider also electrically neutral VLLs, one of which is a DM candidate. In chapter 6, we arrive at the "top" and consider a concrete warped extra-dimensional model to accommodate the 2 TeV diboson anomaly observed in 2015 at the LHC (and, again, not confirmed by subsequent data). Our candidate for the excess is actually a superposition of nearly degenerate Kaluza-Klein (KK) gauge bosons, which are predicted by the custodially-extended gauge group that we consider. Afterwards, in chapter 7, we adopt the same custodially protected warped extra-dimensional framework, but focus instead on the phenomenology of its mixed Higgs-radion sector. More precisely, we calculate the relevant Higgs and radion couplings and estimate the sensitivity of the LHC and of a future linear collider (such as ILC - the International Linear Collider) to the presence of the radion. Finally, in chapter 8, we summarize our results and give a brief outlook.

Chapter 2

Extra Dimensions in Particle Physics

In this chapter, we summarize the basic properties of models containing extra dimensions. We divide these models in two types, in correspondence with the flat or warped geometry of the extra dimension (ED).

The idea that the space-time has more than 3 spatial dimensions dates from almost one century ago, when T. Kaluza and O. Klein published their idea of unifying gravity and electromagnetism in a five dimensional space-time [26,27]. However, as the other fundamental interactions were discovered in the meantime, their elegant proposal became no longer valid. In more recent times, the two Superstring Revolutions that took place during the last three decades boosted the popularity of EDs. But, within Superstring Theory, there was no reason to believe that the EDs would be visible at the energy scales of particle colliders. However, with the proposal of the warped extra-dimensional (Randall-Sundrum or simply RS) [25] and the ADD [28, 29] scenarios, the possibility of having EDs whose effects could be visible at colliders prompted the development of phenomenological model building in this direction.

As they have escaped detection up to date, extra spatial dimensions have to be fundamentally different from the conventional three spatial dimensions that we are acquainted with. Such differences can be achieved if:

- the length R of the extra dimension is smaller than the typical energy scale probed at colliders such as LEP or LHC, i.e. $R \lesssim \mathcal{O}(\text{TeV}^{-1})$;
- a subset of the particle spectrum is not allowed to propagate into the extra-dimensional volume. For example, if only gravity propagates into the full extra-dimensional space-time and the rest of the SM fields are confined to 4 dimensions [28], the typical bounds, on R coming from experiments testing the inverse square law for gravity, are relaxed to the order of 100 microns;
- the extra dimensions are strongly curved [25], which, roughly speaking, leads to a localization of low energy physics towards the boundary of the extra-dimensional volume, such that it appears to be four-dimensional.

We now proceed to summarizing the main features of flat and warped extra-dimensional models.

2.1 Flat Extra Dimensions

2.1.1 Introduction and Motivation

The paradigm of large, flat extra dimensions addressing the gauge hierarchy problem was introduced in a series of papers in 1998 [28–30]. Such models are commonly referred to as "ADD" models–the initials of the authors–or as "large extra dimensions". In order to explain the apparent weakness of gravity with respect to the other fundamental interactions, the authors imagined a $4+n$-dimensional space-time, with n compact (i.e. finite) EDs, in which gravity propagates freely. On the other hand, they considered the SM to live on a 3-brane, i.e. to be confined to a 4D world. Their solution to the hierarchy problem relied on the following observation: as gravity can freely propagate in every space-time direction, the 4D-confined fields would experience only a small fraction of the gravitational force. In layman terms, gravity appears much weaker than the other interactions simply because it is "leaking" in the extra-dimensional volume, whereas the other forces act only in 4D.

More precisely, ADD models suppose that the electroweak scale, m_{EW}, is the only fundamental short distance scale in nature, thus being the scale of gravity as well. To explain the weakness of gravity, the authors take the radius of each of the n extra dimensions equal to R, and then estimate the Newtonian potential at two distances, one much smaller and the other much larger than R. For two test masses $m_{1,2}$ separated by a distance $r \ll R$, the $4+n$-dimensional Gauss law dictates a potential of the form

$$V(r \ll R) \sim \frac{m_1 m_2}{M_{Pl(4+n)}^{n+2}} \frac{1}{r^{n+1}}, \tag{2.1}$$

where $M_{Pl(4+n)}$ is the $4+n$-dimensional Planck scale. On the other hand, for separations much greater than the size of the EDs, the gravitational flux lines are no longer able to escape into the EDs, which leads to the recovery, at large distances, of the usual $1/r$ potential:

$$V(r \gg R) \sim \frac{m_1 m_2}{M_{Pl(4+n)}^{n+2} R^n} \frac{1}{r}. \tag{2.2}$$

Matching the long-distance potential with its ordinary Newtonian counterpart leads to an effective 4D Planck scale M_{Pl} given by

$$M_{Pl}^2 \sim M_{Pl(4+n)}^{n+2} R^n. \tag{2.3}$$

To solve the hierarchy problem, $M_{Pl(4+n)}$ is taken to be of the order of m_{EW}, which gives an estimate on the typical size of the EDs:

$$R \sim 10^{\frac{30}{n}-17}\,\text{cm} \times \left(\frac{1\,\text{TeV}}{m_{EW}}\right)^{1+\frac{2}{n}} \;\Rightarrow\; R^{-1} \sim 10^{12-\frac{30}{n}}\,\text{eV} \times \left(\frac{m_{EW}}{1\,\text{TeV}}\right)^{1+\frac{2}{n}}. \tag{2.4}$$

Clearly, the case $n = 1$ is experimentally excluded, as it would imply deviations from the inverse-square law on interplanetary scales. However, for $n \geq 2$, modifications of gravity appear only on distances not yet probed by experiment.

Although elegant, the ADD model has a conceptual problem: it explains the hierarchy between the Planck and the EW scales by introducing a third scale, namely the inverse radius of the EDs, R^{-1}. For $n = 2$, for example, the inverse radius is of the order of meV, which is far below m_{EW} and thus reintroduces a hierarchy problem. For $n \sim 30$, R^{-1} is in the 100 GeV range, which indeed explains the hierarchy between M_{Pl} and m_{EW}; nevertheless,

minimality is lost for such a high value of n. For proposals of addressing this issue of ADD models, see, for example, Ref. [31].

Even if flat extra dimensions have some difficulties in solving the gauge hierarchy problem, such theories have many other interesting motivations. To start with, if one allows all the SM fields to propagate in the extra-dimensional volume, then $4+n$-dimensional momentum conservation implies KK number conservation in the 4D effective theory. Thus, in such scenarios, dubbed Universal Extra Dimensions or UEDs [32], the lightest KK particle, if electrically neutral, becomes a viable Dark Matter candidate [33]. Moreover, gauge (and even Yukawa) coupling unification can be easily achieved in flat extra dimensions through power-law running of the couplings [34, 35]. Finally, we also mention that it is possible to explain the SM fermion mass hierarchy [36] or the neutrino masses/oscillations [37, 38] in scenarios with flat EDs.

2.1.2 Kaluza-Klein Decomposition and Boundary Conditions

A central concept in theories with ED is the so-called Kaluza-Klein (KK) decomposition. Simply put, as shown in the following, the KK decomposition phrases the effects of a 5D theory in a 4D language.

For clarity, we consider the simple case where the ordinary Minkowski space-time is extended by a flat, compact extra dimension of length L. We denote the coordinates as $x^M \equiv (x^\mu, y)$, with $M = 0, \ldots, 3, 5$ labeling the whole 5D space-time and $\mu = 0, \ldots, 3$ only its 4D submanifold. The metric of such a space is given simply as $g_{MN} = \mathrm{diag}(+1, -1, -1, -1, -1)$. Consequently, fields now depend also on y,

$$\Phi(x^\mu) \to \Phi(x^\mu, y) \tag{2.5}$$

Since the y dependence is on a compact support, $y \in [0, L]$, one can Fourier decompose the 5D fields in the y variable, leaving thus the x_μ dependence in the coefficients of the decomposition:

$$\Phi(x^\mu, y) = \sum_{n=0}^{\infty} \phi^n(x^\mu)\, g^n(y). \tag{2.6}$$

To anticipate, it is clear that each ϕ_n denotes a 4D field. On the other hand, solving for the g^n functions can only be done by considering a concrete theory. For simplicity, we take the free action of a 5D real scalar field

$$S = \frac{1}{2} \int d^4x \int_0^L dy \left[\partial_M \Phi\, \partial^M \Phi \right]. \tag{2.7}$$

Plugging eq. (2.6) into the action and integrating by parts with respect to y, we obtain

$$S = \frac{1}{2} \sum_{n,m=0}^{\infty} \int d^4x \left[K_{nm} \partial_\mu \phi^n\, \partial^\mu \phi^m - M_{nm} \phi^n \phi^m \right] \tag{2.8}$$

where

$$K_{nm} = \int_0^L dy\, g^n g^m, \quad M_{mn} = \int_0^L dy\, \partial_y f_m \partial_y f_n = m_n \delta_{mn} + \text{boundary term} \tag{2.9}$$

A particularly simple form of the action is achieved if the g^n functions are chosen to be orthonormal:

$$K_{nm} = \delta_{nm}, \tag{2.10}$$

which corresponds to canonically normalized kinetic terms for the ϕ^n fields. Moreover, if the g^n's are eigenfunctions of the operator ∂_y^2, such that $\partial_y^2 g^n = -m_n^2 g^n$, we have that

$$\mathcal{M}_{nm} = -\delta_{nm}\, m_n^2 \quad \text{(no sum)}. \tag{2.11}$$

Once boundary conditions for the field are specified, this is a Sturm-Liouville problem whose solutions are orthonormal functions. Even if the algebra gets more involved, this point remains valid also when considering a warped ED. In either case, we arrive at

$$S = \frac{1}{2}\sum_{n=0}^{\infty} \int d^4x \left[\partial_\mu \phi^n\, \partial^\mu \phi^n - m_n^2 \phi^n \phi^n\right]. \tag{2.12}$$

This is the action of an infinite tower of scalar fields with masses m_n. The particles arising from the quantization of the $\phi^{n\geq 1}(x)$ fields will henceforth be called Kaluza-Klein (KK) modes/partners/excitations, and the functions $g^{n\geq 0}(y)$ wave functions/profiles. The $\phi^0(x)$, which usually corresponds to a SM particle, will be called the 0-mode. The expansion from eq. (2.6) in mass eigenmodes and substitution into the action (2.12) is thus referred to as KK decomposition.

In the example above, the only point left to discuss is the boundary term from eq. (2.9), which, in explicit form, reads

$$\text{boundary term} = -\frac{1}{2}\sum_{n,m}[g^n \partial_y g^m]\Big|_0^L. \tag{2.13}$$

The standard procedure is to set these terms to 0, which leaves two options:

$$\Phi\Big|_{y_0} = 0 \quad \text{or} \quad \partial_y \Phi\Big|_{y_0} = 0,\ y_0 = 0, L, \tag{2.14}$$

which correspond, respectively, to Dirichlet and Neumann boundary conditions (BCs). From now on, the Dirichlet BCs will be referred to as "$(-)$" BCs, whereas the Neumann counterparts will be referred to as "$(+)$" BCs. Thus, there are four choices of BCs for the wave functions:

- $(++)$ BCs: Neumann BCs at both $y = 0$ and $y = L$.
- $(+-)$ BCs: Neumann BCs at $y = 0$ and Dirichlet BCs at $y = L$;
- $(-+)$ BCs: Dirichlet BCs at $y = 0$ and Neumann BCs at $y = L$;
- $(--)$ BCs: Dirichlet BCs at both $y = 0$ and $y = L$.

The choice of boundary conditions has important consequences on the 4D theory resulting after KK decomposition: among the 4 possibilities above, only $(++)$ BCs allow to have $g^0(y) \neq 0$. In other words, a 5D field has a 0-mode only if it is assigned with $(++)$ BCs; all the other options for the BCS imply $g^0(y) = 0$ and thus eliminate the 0-mode from the 4D physical spectrum. Even if this example considers a 5D scalar, the point discussed in this paragraph applies also to fermions and gauge bosons. There are, however, some fundamental differences between 5D scalar and 5D fermions and gauge bosons.

In a 5D space-time, chirality cannot be defined (a simple way of seeing it is that all the γ matrices are used to define the 5D Clifford algebra and there is none left to construct a chirality operator), which means that all 5D fermions are Dirac. However, it is an established fact that the 4D fermions from the SM are Weyl, i.e. chiral fermions. Fortunately, this problem is solved by the boundary conditions.

In fact, if one considers a 5D fermion Ψ, its KK decomposition gives rise, as expected, to two KK towers of Weyl fermions, one left-handed (Ψ_L) and the other right-handed (Ψ_R). The two towers are not completely independent, though: if we fix the type of boundary condition at y_0 ($= 0$ or L) for one tower, then, through the Euler-Lagrange equations evaluated at y_0, the other tower is forced to have an opposite type of BC at y_0. As an example, if we assign $(++)$ BCs to Ψ_R, then Ψ_L automatically satisfies $(--)$ BCs. As a consequence, because of the BCs, the 4D theory contains only one chiral zero-mode, Ψ_R^0, whereas Ψ_L^0 is removed from the physical spectrum. Thus, one is left with a 4D effective theory containing (also) chiral fermions.

Nonetheless, both $\Psi_L^{n\geq 1}(x)$ and $\Psi_R^{n\geq 1}(x)$ fields remain in the 4D effective theory, as they are not removed by BCs. These KK modes are the so-called "Vector-Like Fermions" (VLFs) predicted by extra-dimensional theories. For a given $n \geq 1$, $\Psi_L^n(x)$ and $\Psi_R^n(x)$ share the same quantum numbers under, for example, the SM gauge group $SU(3)_c \times SU(2)_L \times U(1)_Y$. Owing to this fact, the Dirac fermion $\Psi^n(x)$ would thus have a purely vectorial coupling to the W and Z bosons: hence the name vector-like. Therefore, in 5D theories, each 4D chiral fermion, left- or right-handed, comes together with a KK tower of vector-like fermions.

We now turn our attention to 5D gauge bosons, $V_M = (V_\mu, V_5)$. Compared to 4D theories, the new element that could raise questions is the 5th component V_5, which, if treated inappropriately, could lead to the existence of a non-desireable light scalar zero-mode, $V_5^0(x)$, in the 4D effective theory. Again, the BCs come to the rescue: as for the fermions, assigning a type of BCs to V_μ leads to an opposite type of BCs for V_5. For example, choosing $(++)$ BCs for V_μ would enforce $(--)$ BCs for V_5, which in turn would remove $V_5^0(x)$ from the effective 4D physical spectrum. As for the 4D scalars $V_5^{n\geq 1}(x)$, they are nothing else than the longitudinal polarizations of the massive $V_\mu^{n\geq 1}(x)$ vectors.

2.1.3 On the Non-Renormalizability of Extra-Dimensional Field Theories

As opposed to the more conventional 4D quantum field theories (QFTs), theories in $D > 4$ dimensions do not have the property of renormalizability. In the early days of QFT, an important difficulty (both conceptually and technically) was dealing with the infinities that appeared when considering quantum corrections to the classical field theory. However, Quantum Electrodynamics (QED), through its formidable success, proved that infinities can consistently removed by absorbing them into the fundamental parameters of the theory. This was the idea of renormalization, which was deemed to be an essential property of every healthy QFT, and proving that the SM obeys this property brought 't Hooft and Veltman the Nobel Prize in 1999.

Nevertheless, in the past decades, it was realized that non-renormalizable QFTs can be sensible theories for describing low energy effects dictated by dynamics accessible only at much higher energies. However, there is a price to pay for abandoning renormalizability: a non-renormalizable theory can be valid only up to a certain cut-off energy scale, commonly denoted by Λ, where new degrees of freedom come into play and the predictive power of the theory is therefore lost. The most famous example in this sense is the Fermi theory for beta decays [39], whose coupling constant G_F has the same dimensions as an inverse squared energy. For a given scattering process involving the Fermi interaction, as long as the collision energy E is much lower than the inverse square root of the Fermi constant, $E^2 G_F \ll 1$, the Fermi theory gives a result in agreement with observation. This result follows simply from naive dimensional analysis, which also tells us that, at energies approaching $\sim G_F^{-1/2}$, new degrees of freedom have to appear in order to cure the non-unitarity of the theory. Indeed

this is the case: the Fermi theory is UV-completed by the W and Z bosons. Exactly the same happens to theories involving flat or warped extra space-time dimensions: the 4D effective theories resulting from integrating out the ED are valid up to a certain energy cutoff Λ, beyond which the ED can no longer be treated classically, because a quantum theory of 5D gravity enters into the picture.

2.2 Warped Extra Dimensions

2.2.1 Introduction and Motivation

In the context of particle physics, the idea of warped extra dimensions was put forward by Randall and Sundrum (RS) in two seminal papers published in 1999 [25, 40]. In these papers, it was shown that a slice of 5D anti-de-Sitter space, AdS_5, is a dynamical solution to the Einstein equations in 5D provided that

- two 3-branes exist at the boundaries of the ED and
- the two 4D (for each brane) and the 5D cosmological constant are suitably chosen.

Moreover, Randall and Sundrum showed that such a setup can solve the hierarchy problem related to the UV sensitivity of the Higgs mass. Since then, warped ED model became very popular in both the theory and phenomenology community. Interestingly, two years before the RS model appeared, Maldacena conjectured [41] the famous AdS/CFT correspondence, which says that that a weakly coupled theory living in AdS_5 is dual to a strongly coupled 4D conformal field theory (CFT).

Apart from the gauge hierarchy problem, there are several motivations for the RS model. While in the original RS model the SM fields were confined on a 3-brane, it was soon realized that allowing fermions and gauge bosons to propagate in 5D could provide solutions to other problems of the SM. For example, both the flavour hierarchy [42] and neutrino mass [43] problems can be solved if the SM fermions and gauge bosons propagate in the bulk. Additionally, within the same setup, it was shown that Grand Unification can also be achieved [44, 45]. Furthermore, if an appropriate discrete symmetry is imposed in the ED, a variation on the RS model can provide a suitable candidate for explaining the Dark Matter abundance in the Universe [46].

2.2.2 The Randall-Sundrum Model as a Solution to the Gauge Hierarchy Problem

In order to explain how the hierarchy problem is tackled in the RS model, we start by considering a 5D space-time, where the usual infinite 4D space-time is extended by a finite ED spanning the interval $0 \leq y \leq L$. At the endpoints of the interval, there are two 3-branes (4D worlds), which are commonly referred to as the Planck/UV/hidden brane at $y = 0$ and the TeV/IR/visible brane at $y = L$. The 5D space-time between the two branes ($0 < y < L$) is usually called the 5D bulk or simply the bulk. The classical action for this setup is given by

$$S = S_{bulk} + S_{Planck} + S_{TeV} \tag{2.15}$$

where the three pieces read

$$S_{bulk} = \int d^4x \int_0^L dy \left(\mathcal{L}_{bulk} + \sqrt{g}(2M_*^3 R - \Lambda)\right) \tag{2.16}$$

$$S_{Planck} = \int d^4x \int_0^L dy \left(\mathcal{L}_{Planck} - \sqrt{g}\Lambda_{Planck}\right) \delta(y) \tag{2.17}$$

$$S_{TeV} = \int d^4x \int_0^L dy \left(\mathcal{L}_{TeV} - \sqrt{g}\Lambda_{TeV}\right) \delta(y - L) \tag{2.18}$$

For the moment, since we are interested in the dynamics of the metric, we neglect the back-reaction of the matter and gauge fields on the geometrical background and set $\mathcal{L}_{bulk}$, $\mathcal{L}_{Planck}$, and $\mathcal{L}_{TeV}$ to 0. In the previous equations, Λ is the 5D cosmological constant and M_* the fundamental scale of 5D gravity. Meanwhile, R is the 5D Ricci scalar and $g = \det(g_{MN})$. Furthermore, Λ_{Planck} and Λ_{TeV} are the 4D cosmological constants, also known as the (brane) tensions of the Planck- and TeV-branes, respectively.

Solving the 5D Einstein equations derived from the action above, the following expression for the metric is found [25]:

$$ds^2 = g_{MN}dx^M dx^N = e^{-2ky}\eta_{\mu\nu}dx^\mu dx^\nu - dy^2 m \tag{2.19}$$

where $\eta_{\mu\nu} = \text{diag}(+1, -1, -1, -1)$ is the 4D Minkowski metric, and, as before, $y \in [0, L]$. The parameter k, which represents the curvature scale of the extra dimension, is given by

$$k = \sqrt{\frac{-\Lambda}{24M_*^3}}. \tag{2.20}$$

This validity of this solution requires an additional condition:

$$\Lambda_{Planck} = -\Lambda_{TeV} = 24M_*^3 k, \tag{2.21}$$

which has to be imposed in order to obtain a null effective 4D cosmological constant on the TeV brane. In fact, eq. (2.21) hides a fine-tuning associated with the cosmological constant problem, which is not addressed in the RS scenario.

Clearly, the solution for k is meaningful only if $\Lambda < 0$. While in the case $\Lambda = 0$ a flat extra dimension is recovered, for $\Lambda < 0$ the 5D bulk $0 < y < L$ is a slice of 5D Anti-de-Sitter space (AdS_5), which is generally referred to as warped space. Note that, for a fixed value of y, the metric respects 4D Poincaré invariance.

At an energy scale μ much lower than the inverse length of the extra dimension, $\mu \ll 1/L$, one can obtain the corresponding effective 4D theory by integrating over the extra dimension, a procedure that is called dimensional reduction. To this end we insert the warped metric (2.19) into the bulk action (2.16), and obtain for the curvature term

$$\int d^4x \int_0^L dy\, \sqrt{g}\, 2M_*^3 g^{\mu\nu} R_{\mu\nu} \to \int d^4x \underbrace{\int_0^L dy\, 2M_*^3 e^{-2ky}}_{\equiv M_{Pl}^2} \sqrt{-\bar{\eta}}\bar{R}, \tag{2.22}$$

where $\bar{\eta} = \det(\bar{\eta}_{\mu\nu})$ and $\bar{R}$ denotes the 4D Ricci scalar constructed out of $\bar{g}_{\mu\nu}$. Here,

$$\bar{\eta}_{\mu\nu} = \eta_{\mu\nu} + h_{\mu\nu}(x) \tag{2.23}$$

is the four-dimensional metric containing the physical 4D graviton field, $h_{\mu\nu}(x)$, i.e. the fluctuations around the Minkowski background metric $\eta_{\mu\nu}$. As a low energy effective field,

$h_{\mu\nu}$ is independent of y. Thus, one can perform the y integral explicitly and obtain the effective 4D Planck scale of gravity as a function of parameters of the 5D theory:

$$M_{Pl}^2 \equiv \frac{M_*^3}{k}\left[1 - e^{-2kL}\right] \sim \frac{M_*^3}{k} \quad \text{for} \quad kL \gg 1. \tag{2.24}$$

Bleary, M_{Pl} depends very weakly on the size of the extra dimension, L, such that in the limit $kL \gg 1$ the 4D effective scale of gravity is determined only by M_* and k.

We now focus our attention on the matter Lagrangian on the TeV brane, $\mathcal{L}_{TeV}$, and determine the energy scales to which it is associated. Let us consider a fundamental scalar H (the Higgs boson) living on the TeV brane and acquiring a vacuum expectation value (VEV), $\langle H \rangle = v_0$. Its effective 4D action reads

$$S_{Higgs}^{4D} = \int d^4x \sqrt{-g_{TeV}} \left(g_{TeV}^{\mu\nu} \partial_\mu H^\dagger \partial_\nu H - \lambda (H^\dagger H - v_0^2)^2 \right) \tag{2.25}$$

with $g_{TeV}^{\mu\nu} = g^{\mu\nu}(y = L) = e^{2kL}\eta^{\mu\nu}$, and $g_{TeV} = \det(g_{TeV}) = e^{-8kL}$. In order to have a canonical kinetic term for H, we rescale it by e^{kL}, $H \to e^{kL}H$, and thus obtain

$$S_{Higgs}^{4D} = \int d^4x \left(\eta^{\mu\nu} \partial_\mu H^\dagger \partial_\nu H - \lambda (H^\dagger H - e^{-2kL} v_0^2)^2 \right) \tag{2.26}$$

Quite remarkably, the effective symmetry breaking scale is given not by v_0, but instead by

$$v \equiv e^{-kL} v_0. \tag{2.27}$$

This result has profound consequences: while the 4D effective gravity scale M_{Pl} is fixed by M_* and k, but almost completely insensitive to the ED length L, the effective symmetry breaking scale depends exponentially on L, as v is suppressed by the e^{-kL} factor with respect to the fundamental scale v_0. In order to avoid large hierarchies between the fundamental parameters of the 5D theory, we assume that $M_*, k, v_0 \sim \mathcal{O}(M_{Pl})$. Given this choice, only a moderate hierarchy, $kL \sim 35$, is needed in order to obtain

$$v \sim 10^{-16} v_0 \sim \mathcal{O}(1) \text{ TeV} \tag{2.28}$$

for the 4D effective scale of electroweak symmetry breaking.

Thus, the RS geometric construction provides an elegant solution to the hierarchy problem, as it reduces the 16 orders of magnitude hierarchy between M_{Pl} and the EW energy scale, m_{EW}, to a mere hierarchy of ~ 35 between the curvature scale k of the ED and its inverse length, $1/L$. We emphasize the RS metric in eq. (2.19) is not an ad-hoc choice that leads to the good result: it is in fact a solution to the 5D Einstein equation with a negative bulk cosmological constant. $\Lambda < 0$, and suitably adjusted brane tensions, Λ_{Planck} and Λ_{TeV}.

However, the are two theoretical issues that remain unaddressed in this model. The first one is related to how can one ensure the relation in eq. (2.21) between the 5D cosmological constant and the two brane tensions. As hinted at before, the answer is that this relation has to be imposed "by hand", implying thus a fine tuning: it corresponds to the notorious cosmological constant problem, which remains unsolved in the RS model. The second theoretical issue concerns the stability of the ED length, L, against gravitational fluctuations. Soon after the publication of the RS papers, it was shown that, indeed, the length of the ED can be stabilized through the so-called Goldberger-Wise (GW) mechanism [47]. In short, this mechanism relies on the presence of a bulk scalar, called the GW scalar, which has a 5D mass term and a different 4D potential on each brane. Consequently, the GW scalar acquires a VEV on the IR brane, v_{IR} and a different VEV on the Planck brane, $v_{UV} \neq v_{IR}$. By a moderate hierarchy of order ~ 10 between k and 5D mass of the GW scalar and for $v_{UV}/v_{IR} = \mathcal{O}(1)$, it is indeed possible to stabilize the ED length such that $kL \sim 35$.

Chapter 3

Vector-Like Quarks: Explaining the A_{FB}^{b} and tth Anomalies and Prospects from Higgs Precision Measurements

3.1 General Properties of Vector-Like Quarks

Vector-like quarks (VLQs) are spin-1/2 particles which transform as triplets under the $SU(3)$ color gauge group. Their name reflects the fact that both left- and right-handed chiralities of a vector-like quark (or, more generally, fermion) transform the same way under the SM gauge group, from which it follows that their coupling to a W boson is purely vectorial. Owing to this fact, such new fermionic states do not lead to radiative breaking of gauge symmetries through chiral anomalies.

Concerning fermionic extensions of the Standard model, vector-like fermions are the only option which is not excluded by experiment [48–50]. In order to have an anomaly-free theory [51, 52], new chiral fermions should come in full families, identical to the ones in the SM ("fourth family"). In turn, a fourth family of chiral fermions would couple to the Higgs boson similarly to their SM counterparts, which would lead to a factor 3 enhancement with respect to the SM [48–50] of the gluon-gluon fusion (ggF) production mechanism of the Higgs boson. However, ggF has been measured at the LHC and the experminental result is in good agreement with the SM prediction [53], meaning that a fourth fermionic family is basically excluded. However, for a way around this argument, see, for example, Refs. [54, 55].

Besides being triplets of $SU(3)_c$, vector-like quarks can carry various non-trivial quantum numbers under $SU(2)_L$ and $U(1)_Y$, leading to conventional electric charges, such as 2/3 (top-like) or $-1/3$ (bottom-like), or more exotic ones, as, for example, $-4/3$ or 5/3. Moreover, if the VLQs are embedded into isospin singlets, doublets, or triplets, they can couple to the Higgs doublet and a SM quark through gauge-invariant and renormalizable Yukawa terms. Furthermore, due to their vector-like nature, VLQs can possess bare mass terms of the type $m\,\overline{q}_L q_R +$ h.c.. Upon electroweak symmetry breaking (EWSB), they can mix with the SM quarks[1] and generate deviations in their couplings to other SM states.

A common assumption in models containing VLQs is that the new coloured spin 1/2 states mix only with third generation SM quarks. Besides simplicity and convenience, there is also a theoretical motivation behind this assumption: because of the large Yukawa couplings of the top and bottom quarks, one expects a closer connection between these states and

[1] In the case where such a mixing is very small or even forbidden by, say, a $\mathbb{Z}_2$ symmetry, the new quarks can form exotic QCD bound states, similar to the so-called "R-hadrons" (QCD bound states involving supersymmetric particles), which are searched for at the LHC [56].

possible new physics related to EWSB. Suppressed mixing with the first two generations is favoured also by experiment, since such a mixing pattern would avoid problems related to precisely measured flavour observables (for a review, see Ref. [57]).

Several extensions of the Standard Model (SM) of particle physics, including some that address the gauge hierarchy problem, predict the existence of VLQs. Such states arise, for instance, as:

- Kaluza-Klein excitations in warped extra-dimension scenarios [25] (in the version with SM fields in the bulk, which explains the fermion mass hierarchy - see for example [42, 43, 58–61]);
- excited resonances in the context of composite Higgs models [62–65];
- partners of the top quark in little Higgs theories [66, 67];
- additional states in the extended group representations of grand unified theories [68, 69].

As their masses are expected to be in the vicinity of the TeV scale, these particles can be produced at the Large Hadron Collider (LHC) and their search is therefore of prime importance. For phenomenological analyses concerning VLQs, see [70–94] (for more specific scenarios involving VLQs, see, for example, [95–98]).

At the LHC, direct experimental searches have imposed, almost independently of the VLQ electric charge, the model independent bound $m_{\rm VLQ} \gtrsim 800$ GeV [99–101] on VLQ masses from pair-production through strong interactions. There exist also indirect constraints on the masses and couplings of these particles from electroweak precision tests (EPWT)–they give, for example, radiative contributions to the so–called oblique corrections that affect the W–boson mass m_W and the effective mixing angle, $\sin^2\theta_W$ [102, 103]. In addition, through their mixing with SM 3rd generation quarks, VLQs alter the properties of the heavy top and bottom quarks. Therefore, strong constraints can be obtained, for example, from the Z–boson decay into bottom quarks, $Z \to b\bar{b}$, as measured at the LEP e^+e^- collider at energies close to the Z–pole [104, 105]. Concerning $Z \to b\bar{b}$, VLQs are (together with Kaluza–Klein excitations of electroweak gauge bosons [106]) among the few possibilities that can provide an explanation to the long-standing puzzle of the bottom quark forward-backward asymmetry, $A^b_{\rm FB}$, whose value measured at LEP differs by $\sim 2.5\sigma$ from the SM expectation [107].

Indirect constraints on VLQs also come from the data collected on the 125 GeV scalar particle that has been observed at the LHC [1, 2, 53]. Firstly, these new quarks contribute to the loop induced Higgs couplings to pairs of gluons and photons, either through their additional exchange in the triangular loops or when modifying the dominant top quark loop contribution through mixing [108–112]. Secondly, the Higgs decay channels in the various final states detected so far by the ATLAS and CMS collaborations, namely the $h \to \gamma\gamma, ZZ, WW$ and eventually $\tau^+\tau^-$ final states with the Higgs state dominantly produced in the gluon fusion mechanism $gg \to h$, set strong limits on VLQ masses and couplings [1, 2, 53]. The sensitivity in these leading Higgs production channels, supplemented by the one in the Higgs–strahlung process, $q\bar{q} \to Vh$, with the $V = W, Z$ boson decaying leptonically and the Higgs state decaying into $b\bar{b}$ final states, will significantly improve as the LHC will reach higher integrated luminosities.

At a later LHC stage, a very efficient indirect probe of VLQ effects would come from associated Higgs production with top quark pairs, $pp \to t\bar{t}h$, through a modification of the top quark Yukawa coupling y_t, as the cross section is directly proportional to y_t^2. Although the sensitivity is still rather low, the combination of the data collected so far by the ATLAS and CMS collaborations in this channel displays a $\sim 2\sigma$ deviation from the SM expectation [53]

(the deviation is close to $\sim 1\sigma$ in the ATLAS data and is much larger, being at the $\sim 2.1\sigma$ level, in the case of CMS [1, 2]). This excess in the production rate would correspond to an enhancement of the top–quark Yukawa coupling y_t by a factor ~ 1.4.[2] Even if rather premature, it is tempting to attribute this excess to the indirect presence of VLQs and this should soon be confirmed or ruled out.

In order to introduce the notation and to fix some basic ideas, we will briefly discuss a simple VLQ model, which contains, apart from the SM particle spectrum, a new charge 2/3 isosinglet VLQ, which we shall denote by t':

$$t'_{L,R} \sim (3,1)_{2/3}, \tag{3.1}$$

where 3, 1, and 2/3 represent the $SU(3)_c$, $SU(2)_L$, and $U(1)_Y$ charges, respectively. Denoting by $Q_L = (t\ b)_L$ the third generation (left-handed) quark doublet and by t_R, b_R the right-handed top and bottom quarks, the most general gauge-invariant Yukawa Lagrangian of this simple model becomes

$$\mathcal{L} = Y_{t_1} \overline{Q}_L \tilde{H} t_R + Y_{t_2} \overline{Q}_L \tilde{H} t'_R + m\, \overline{t}'_L t'_R + \text{h.c.}, \tag{3.2}$$

where $H = \begin{pmatrix} H^+ \\ H^0 \end{pmatrix}$ represents the SM Higgs doublet, $\tilde{H} = i\sigma_2 H^*$ its charge conjugate, L/R the left and right fermion chiralities, the Y's dimensionless Yukawa coupling constants and the m's the VL masses of the new colored states. Upon EWSB, $H_0 \to v' + h/\sqrt{2}$ and thus the mass and Yukawa matrices in the interaction basis read:

$$\mathcal{M} = \begin{pmatrix} v' Y_{t_1} & v' Y_{t_2} \\ 0 & m \end{pmatrix}, \quad \mathcal{C} = \frac{1}{\sqrt{2}} \begin{pmatrix} Y_{t_1} & Y_{t_2} \\ 0 & 0 \end{pmatrix}. \tag{3.3}$$

The resulting mass eigenstates are the SM-like top quark, which we shall denote as t_1, and a heavier quark t_2. The mass eigenvalues $m_{t_{1,2}}$ are the square roots of the eigenvalues of $\mathcal{M}^\dagger \mathcal{M}$ (or $\mathcal{M}\,\mathcal{M}^\dagger$). The Yukawa couplings in the mass basis are obtained by a biunitary transformation $\mathcal{C} \to U_L\, \mathcal{C}\, U_R^\dagger$, where the unitary/rotation matrices $U_{L,R}$ are determined from

$$U_L\, \mathcal{M}\mathcal{M}^\dagger\, U_L^\dagger = U_R\, \mathcal{M}^\dagger \mathcal{M}\, U_R^\dagger = \text{diag}\,(m_{t_1}^2, m_{t_2}^2). \tag{3.4}$$

Also, the unitary matrices are related through $U_L\, \mathcal{M}\, U_R^\dagger = \text{diag}\,(m_{t_1}, m_{t_2})$. In the current simple case of only two fields mixing, assuming all the parameters from Eqs. (3.2) and (3.3) are real, the rotation matrices can be expressed in their usual form as

$$U_{L,R} = \begin{pmatrix} \cos\theta_{L,R} & \sin\theta_{L,R} \\ -\sin\theta_{L,R} & \cos\theta_{L,R} \end{pmatrix}, \tag{3.5}$$

where $\theta_{L,R}$ are the mixing angles for the left (L) and right (R) chiralities. For the mixing of more than two VLQs, the rotation matrices can still be expressed with the help of (several) mixing angles, but, as the expressions of these matrices are not particularly illuminating, we will not quote them here. The mass basis couplings are straightforwardly obtained by matrix multiplication of the interaction basis coupling matrix with the unitary matrices from eq. (3.5). For example, the Yukawa couplings in the mass basis are the entries of the matrix product $U_L\, \mathcal{C}\, U_R^\dagger$, with $\mathcal{C}$ defined in eq. (3.3).

In this chapter, which is based on Ref. [116], we analyze the sensitivity of present and future LHC Higgs data to the vector–like partners of the heavy top and bottom quarks. We

[2] For an alternative explanation of the $t\bar{t}h$ excess, see Ref. [113]. Other explanations, similar to ours, can be found in Refs. [114, 115].

consider several VLQ representations under the SM gauge group, such that the obtained scenarios can be embedded into various realistic high-energy frameworks. We first explore the possibility that some VLQs modify the Yukawa couplings of the heavy top and/or bottom quarks through fermion mixing and discuss the impact of this mixing on electroweak observables, including those in $Z \to b\bar{b}$ decays. We also analyze the constraints that can be obtained from the LHC data on the observed Higgs particle. In particular, we focus on constraints coming from the measured loop–induced Higgs couplings to gluons and photons, as well as from the rates in the Higgs–strahlung production process followed by the decay $h \to b\bar{b}$.

As a main outcome of this study, we provide a simultaneous explanation of the two possible deviations from SM expectations in heavy quark observables: the $pp \to t\bar{t}h$ cross section at the LHC and the $A_{\rm FB}^b$ asymmetry at LEP. For the production rate $\sigma(pp \to t\bar{t}h)$, the increase of the top Yukawa coupling that is necessary to explain the $\sim 2\sigma$ excess has to be compensated by a destructive interference between the top and the VLQ loop contributions to the $gg \to h$ production and $h \to \gamma\gamma$ decay rates[3]. Such an interpretation of the anomaly in $\sigma(pp \to t\bar{t}h)$ predicts VLQs with masses in the range of 1–1.5 TeV, which should thus be directly produced at the current and future LHC runs.

Finally, we show that VLQs with masses up to ~ 10 TeV can be probed by measuring precisely the ratios of the $h \to \gamma\gamma$ to $h \to ZZ^*$ and $h \to b\bar{b}$ to $h \to WW^*$ production times decay rates [117, 118], which are free of the large theoretical ambiguities that affect the absolute rates or the signal strengths [119–121] and which could be determined with a percent-level accuracy the high–luminosity LHC option [122–124].

The chapter is structured as follows. In the next section, we introduce and describe three VLQ models which could allow for an enhancement of the top quark Yukawa coupling and, simultaneously, for a resolution of the $A_{\rm FB}^b$ puzzle. In Section 3, we summarize the presently available constraints that can be set on VLQS, in particular from high precision electroweak measurements LEP and from the LHC Higgs data. We then present in Section 4 our numerical results for each studied model and delineate the allowed parameter space for the masses and couplings of VLQs that accommodates the anomalies in $\sigma(pp \to t\bar{t}h)$ and $A_{\rm FB}^b$. Finally, in Section 5, we discuss the sensitivity to VLQs that can be achieved at the high–luminosity LHC through precision measurements of Higgs decay ratios. The results are then summarized and discussed in Section 6.

3.2 Theoretical Models for the $A_{\rm FB}^b$ and tth Anomalies

In this section, we discuss the simplest models that include vector-like quarks and start by analyzing those which could accommodate the two possible anomalies in the heavy quark sector, namely an increase of the $pp \to t\bar{t}h$ production cross section and a deviation of the $A_{\rm FB}^b$ asymmetry from the SM expectation. We focus on scenarios that lead to modifications of the top quark Yukawa coupling, defined in the SM as $y_t^{\rm SM} = m_t/v$ (when neglecting the three SM generation mixing with respect to the top–VLQ mixing), $m_t = 174 \pm 1$ GeV being the measured top–quark mass [107] and $v = v'\sqrt{2} \simeq 246$ GeV the Higgs vacuum expectation value. The VLQs responsible for such modifications will be denoted as top partners, $t', t'', \ldots$, since they should have an electric charge $Q = 2/3$ in order to mix with the top quark.

It turns out that the simplest SM extension, which would involve a single t' quark and

[3] Independently of the present excess in the $pp \to t\bar{t}h$ production rate, this study highlights the importance of and provides a motivation for a direct measurement of the top quark Yukawa coupling, as the indirect determination from the $gg \to h$ and $h \to \gamma\gamma$ processes might be differently altered by new physics.

which was given as an example in the previous section, leads to a reduction of the top Yukawa coupling with respect to its SM value. This conclusion holds for a t' embedded in a singlet, a doublet or a triplet under the $\mathrm{SU(2)_L}$ group, because the mass matrix in the (t, t') field basis has the same texture in each of the three cases and generates identical mixing angles. The embedding of a single t' component into a quadruplet or a higher $\mathrm{SU(2)_L}$ multiplet forbids gauge invariant Yukawa couplings for the extra t' and, hence, a t–t' mixing. Consequently, one should include at least two extra top partners. The embedding of vector–like t', t'' quarks in two $\mathrm{SU(2)_L}$ singlets would lead to a mass matrix in the (t, t', t'') field basis of the type (from now on, we denote by "Y" the interaction basis couplings and by "y" the mass basis couplings):

$$\mathcal{M}_t = \begin{pmatrix} Y_{t_1} v' & Y_{t_2} v' & Y_{t_3} v' \\ 0 & m_1 & 0 \\ 0 & 0 & m_2 \end{pmatrix}, \tag{3.6}$$

which turns out to have an insufficient number of free parameters to increase y_t without significantly altering the measured m_t value. The same holds for two extra isodoublets, for which the mass matrix is simply the transpose of $\mathcal{M}_t$. Therefore, in order to increase y_t, the minimal top sector should include one t' embedded in an $\mathrm{SU(2)_L}$ doublet and one $\mathrm{SU(2)_L}$ singlet, t''. Here, by minimal sector we understand scenarios with the least possible number of heavy quark $SU(2)_L$ n-plets, with $n \leq 3$.

In the case of the forward–backward asymmetry A_{FB}^b, one can use similar arguments to construct a minimal sector. The main goal is to reduce the A_{FB}^b tension with data through tree-level changes of the $Zb\bar{b}$ couplings, induced by the mixing of the SM b–quark with its VLQ partners (see next section). However, one should keep the ratio $R_b \equiv \Gamma(Z \to b\bar{b})/\Gamma(Z \to \text{hadrons})$ in agreement at the $\lesssim 1\sigma$ level with its SM value when the tree-level $Zb\bar{b}$ coupling constants g_{b_L} and g_{b_R} are modified. This problem has been studied previously and a possible solution is to increase g_{b_R} by $\sim$30% and to decrease the absolute value of g_{b_L} by $\sim$1% with respect to their SM values [106, 125].

The need of such a large increase in the right–handed component of the $Zb\bar{b}$ coupling g_{b_R} gives an idea on the required minimal bottom–quark sector. In the interaction basis, the coupling matrix of the Z–boson to the b–quark and its VL partners has the diagonal form

$$G_{L/R}^b = \mathrm{diag}(I_{3L/R}^{(1)} + \frac{1}{3}\sin^2\theta_W,\, I_{3L/R}^{(2)} + \frac{1}{3}\sin^2\theta_W,\, I_{3L/R}^{(3)} + \frac{1}{3}\sin^2\theta_W, \ldots), \tag{3.7}$$

where $I_{3R}^{(1)} = 0$ and $I_{3L}^{(1)} = -\frac{1}{2}$ are the SM b_L and b_R isospin projections and $I_{3L/R}^{(2,3)}$ stand for the first and second VL left-handed/right-handed b''s isospin projections. Rotating to the mass basis by a unitary transformation U_R^b, one finds that, for the characteristic case of two b' states, the $Zb_R\bar{b}_R$ coupling becomes

$$G_{R,11}^b \equiv \tilde{g}_{b_R} = \sum_{i=1}^{3} I_{3R}^{(i)} \left(U_{R,1i}^b\right)^2 + \frac{1}{3}\sin^2\theta_W \equiv I_{3R,\mathrm{eff}}^{(1)} + \frac{1}{3}\sin^2\theta_W, \tag{3.8}$$

where $I_{3R,\mathrm{eff}}^{(1)}$ is the "effective isospin" of the SM bottom quark after mixing with its VLQ partners. Thus, after b–b' mixing, the change in g_{b_R} is equal to $I_{3R,\mathrm{eff}}^{(1)}$, since $I_{3R}^{(1)} = 0$. As unitarity implies $\sum_{i=1}^{3} \left(U_{R,1i}^b\right)^2 = 1$, one concludes that the effective isospin of the SM b quark is actually a weighted mean of the isospins of all the bottom–like quarks present in the model. Since the measured values of A_{FB}^b and R_b point towards $I_{3R,\mathrm{eff}}^{(1)} > 0$, the minimal model should contain one bottom–like VLQ with positive isospin and none with negative isospin, which from the start excludes a (t', b') doublet. (Less minimal models could contain

additional b' quarks with negative isospins but non-significant mixings with the SM b_R field, i.e. $U^b_{R,1i} \ll 1$.)

Therefore, in the sense of the minimality mentioned above, experimental constraints in the bottom sector favor a b' VLQ embedded with a $-\frac{4}{3}$ electric charge VLQ, $q_{4/3}$, in a $-\frac{5}{6}$ hypercharge isodoublet,

$$B_{L,R} = \begin{pmatrix} b' \\ q_{4/3} \end{pmatrix}^{Y=-5/6}_{L,R} , \tag{3.9}$$

with the addition of a singlet b'', which guarantees that there are enough parameters to produce a significant deviation of the couplings to the Z boson [126]. The electric charge of the multiplet components is fixed by the relation $Q = Y + I_3$ coming from the assumption that the symmetry breaking occurs as in the SM. The hypercharge is fixed by the gauge symmetry itself, which imposes the same Y value for the components of a given multiplet. In addition, as the bottom sector measurements disfavor a (t', b') doublet and the minimal top sector imposes a t' embedded in a doublet, one concludes that the t' should pair up with an exotic electric charge $+\frac{5}{3}$ VLQ, $q_{5/3}$, in an $\mathrm{SU(2)_L}$ doublet,

$$T_{L,R} = \begin{pmatrix} q_{5/3} \\ t' \end{pmatrix}^{Y=7/6}_{L,R} . \tag{3.10}$$

Along these lines, one can construct a minimal VLQ model, that we denote here as model **A**, which addresses simultaneously the excess of the $pp \to t\bar{t}h$ cross section at the LHC and the anomaly in the A^b_{FB} asymmetry as measured at LEP. Besides the SM fields, model **A** will have the following content:

$$\text{Model } \mathbf{A} : T_{L,R},\ B_{L,R},\ t''_{L,R} \text{ and } b''_{L,R}, \tag{3.11}$$

where $B_{L,R}$ and $T_{L,R}$ are the two isodoublets defined in eqs. (3.9) and (3.10) respectively, whereas $b''_{L,R}$ and $t''_{L,R}$ are two isosinglets. Denoting the SM left-handed (t, b) doublet as Q_L, the most general Lagrangian containing all possible terms invariant under the SM $\mathrm{SU(3)_C \times SU(2)_L \times U(1)_Y}$ gauge symmetry reads

$$\begin{aligned} \mathcal{L} = {} & Y_{t_1}\, \overline{Q}_L \tilde{H}\, t_R \,+\, Y_{t_2}\, \overline{Q}_L \tilde{H}\, t''_R \,+\, Y_{t_3}\, \overline{T}_L H\, t_R \,+\, Y_{t_4}\, \overline{T}_L H\, t''_R \,+\, Y_{t_5}\, \overline{T}_R H\, t''_L \\ & +\, Y_{b_1}\, \overline{Q}_L H\, b_R \,+\, Y_{b_2}\, \overline{Q}_L H\, b''_R \,+\, Y_{b_3}\, \overline{B}_L \tilde{H}\, b_R \,+\, Y_{b_4}\, \overline{B}_L \tilde{H}\, b''_R \,+\, Y_{b_5}\, \overline{B}_R \tilde{H}\, b''_L \\ & +\, m_1\, \overline{T}_L T_R \,+\, m_2\, \overline{t}''_L t''_R \,+\, m_3\, \overline{B}_L B_R \,+\, m_4\, \overline{b}''_L b''_R \,+\, \text{H.c.}, \end{aligned} \tag{3.12}$$

where $H = \begin{pmatrix} H^+ \\ H^0 \end{pmatrix}$ represents the SM Higgs doublet, $\tilde{H} = i\sigma_2 H^*$ its charge conjugate, L/R the left and right fermion chiralities, the Y's dimensionless Yukawa coupling constants and m's the masses of the various VLQs.

Without loss of generality, the coefficients of the $\bar{t}''_L t_R$ and $\bar{t}_L t'_R$ terms can be rotated away [127]. The Yukawa couplings for the first two generations of fermions are omitted in the Lagrangian of eq. (3.12) as their mixings with the top-partners t', t'' are expected to be much smaller than the t–t' and t–t'' mixings as a consequence of the larger mass differences. Since the CKM angles [107] are typically small, the first two up–quark flavors naturally decouple from the top quark. A similar discussion holds for the down–type quark sector and the b', b'' components[4].

[4]The t' or b' states could contribute to the severely constrained Flavor Changing Neutral Current (FCNC) reactions which rely precisely on the whole SM set of Yukawa couplings for quarks. This issue, which leads to a large number of parameters, is beyond our scope.

The top Yukawa couplings and mass terms generated after symmetry breaking by the Lagrangian of eq. (3.12) can be synthesized respectively in the $h\bar{\psi}^t_L \mathcal{C}_t \psi^t_R$ and $\bar{\psi}^t_L \mathcal{M}_t \psi^t_R$ terms (the "t" superscript stands for "top", while the T superscript stands for matrix transposition). Within the interaction basis defined by $\psi^t = (t, t', t'')^T$, the coupling and mass matrices read

$$\mathcal{C}_t \;=\; \frac{1}{\sqrt{2}} \begin{pmatrix} Y_{t_1} & 0 & Y_{t_2} \\ Y_{t_3} & 0 & Y_{t_4} \\ 0 & Y_{t_5} & 0 \end{pmatrix} \;, \quad \mathcal{M}_t \;=\; \begin{pmatrix} v' Y_{t_1} & 0 & v' Y_{t_2} \\ v' Y_{t_3} & m_1 & v' Y_{t_4} \\ 0 & v' Y_{t5} & m_2 \end{pmatrix} \;. \tag{3.13}$$

In the mass basis ("m" superscript), one has $\mathcal{C}^m_t = U^t_L \mathcal{C}_t (U^t_R)^\dagger$, where the unitary matrices $U^t_{L/R}$ are obtained by bi–diagonalizing the model dependent mass matrix, $U^t_L \mathcal{M}_t (U^t_R)^\dagger = \text{diag}(m_{t_1}, m_{t_2}, m_{t_3})$. The argument stays the same for the b–quark sector, but with the replacements $t \to b$, $m_1 \to m_3$ and $m_2 \to m_4$. As for the $\frac{5}{3}$ and $-\frac{4}{3}$ charged exotic partners, their masses are given by $|m_1|$ and $|m_3|$, respectively. The mass eigenstates are ordered by increasing absolute value and thus, for example, the observed top quark (after mixing) will be represented by t_1, while the lightest bottom-like VLQ will be denoted by b_2.

We will show later that indeed, there is a region in the parameter space of this minimal model where all the LEP and LHC constraints, as well as the constraints from the oblique corrections that affect the W/Z propagators, are satisfied. However, for the sake of completeness, we will also consider two other models that respect too the requirement of minimality and pass the constraints mentioned above. The two additional models contain, besides the SM fields, the VLQ multiplets enlisted below:

$$\text{Model } \mathbf{B} : T_{L,R},\; B_{L,R},\; X_{L,R} = \begin{pmatrix} t'' \\ b'' \\ q'_{4/3} \end{pmatrix}^{Y=-1/3}_{L,R} \quad \text{and } t'''_{L,R}. \tag{3.14}$$

This is simply a copy of the minimal model **A** with the replacement $b'' \to X$, with the top–like singlet from model **A** being renamed into t'''. The triplet is chosen such that the isospin of b'' is equal to 0, which, together with b' having a positive isospin, solves the A^b_{FB} discrepancy. Also, with the choice of this triplet, this model has the same number of parameters as model **A**, namely 14.

$$\text{Model } \mathbf{C} : T_{L,R},\; B_{L,R},\; Z_{L,R} = \begin{pmatrix} q_{8/3} \\ q'_{5/3} \\ t'' \end{pmatrix}^{Y=5/3}_{L,R} \;, \; b''_{L,R} \text{ and } t'''_{L,R}. \tag{3.15}$$

Just as in the previous model, the top–like singlet gets the most primes, becoming t'''. In both models, the B and T VLQ doublets are the ones defined earlier in eqs. (3.9) and (3.10).

We close this general discussion by presenting the Lagrangians and the mass matrices of the additional models **B** and **C**. We denote the interaction basis vectors as $\psi^q = (q, q', q'', \ldots)^T$, where q stands for the quark type, namely b, t, $q_{4/3}$ and $q_{5/3}$, while $(\ldots)^T$ stands for the matrix transpose operation. The Yukawa coupling matrices will not be written, since they are obtained in a straightforward manner by differentiating the corresponding mass matrices with respect to the Higgs VEV, v (recall that $v = v'\sqrt{2}$).

Model **B**: the corresponding Lagrangian is given by

$$\begin{aligned} \mathcal{L} = {} & Y_{t_1}\, \overline{Q}_L \tilde{H}\, t_R \,+\, Y_{t_2}\, \overline{Q}_L H\, X_R \,+\, Y_{t_3}\, \overline{Q}_L \tilde{H}\, t'''_R \,+\, Y_{t_4}\, \overline{T}_L H\, t_R \,+\, Y_{t_5}\, \overline{T}_L H\, t'''_R \\ & +\, Y_{t_6}\, \overline{T}_R H\, t'''_L \,+\, Y_{b_1}\, \overline{Q}_L H\, b_R \,+\, Y_{b_2}\, \overline{B}_L \tilde{H}\, b_R \,+\, Y_{b_3}\, \overline{B}_L \tilde{H}\, X_R \,+\, Y_{b_4}\, \overline{B}_R \tilde{H}\, X_L \\ & +\, m_1\, \overline{T}_L T_R \,+\, m_2\, \overline{X}_L X_R \,+\, m_3\, \bar{t}'''_L t'''_R \,+\, m_4\, \overline{B}_L B_R \,+\, \text{H.c.}, \end{aligned} \tag{3.16}$$

For the top, bottom and $-\frac{4}{3}$ electric charge quarks, the mass matrices are given by

$$\mathcal{M}_t = \begin{pmatrix} v'Y_{t_1} & 0 & v'Y_{t_2} & v'Y_{t_3} \\ v'Y_{t_4} & m_1 & 0 & v'Y_{t_5} \\ 0 & 0 & m_2 & 0 \\ 0 & v'Y_{t_6} & 0 & m_3 \end{pmatrix}, \; \mathcal{M}_b = \begin{pmatrix} v'Y_{b_1} & 0 & \frac{v'Y_{t_2}}{\sqrt{2}} \\ v'Y_{b_2} & m_4 & \frac{v'Y_{b_3}}{\sqrt{2}} \\ 0 & \frac{v'Y_{b_4}}{\sqrt{2}} & m_2 \end{pmatrix},$$
$$\mathcal{M}_{4/3} = \begin{pmatrix} m_4 & v'Y_{b_3} \\ v'Y_{b_4} & m_2 \end{pmatrix}. \tag{3.17}$$

Additionally, the physical mass of $q_{5/3}$ is given by $|m1|$. Note that, in the bottom quark mass matrix from above, the Y_{t_2}, Y_{b_3} and Y_{b_4} terms are divided by $\sqrt{2}$. The extra $1/\sqrt{2}$'s are just Clebsch-Gordan factors arising from the direct product of the Higgs doublet with a VL doublet into a triplet, i.e. the **3**-representation from the group product decomposition $\mathbf{2} \otimes \mathbf{2} = \mathbf{3} \oplus \mathbf{1}$.

Model **C**: the Lagrangian is given by

$$\begin{aligned} \mathcal{L} = {} & Y_{t_1}\, \overline{Q}_L \tilde{H}\, t_R \, + \, Y_{t_2}\, \overline{Q}_L \tilde{H}\, t'''_R \, + \, Y_{t_3}\, \overline{T}_L H\, t_R \, + \, Y_{t_4}\, \overline{T}_L \tilde{H}\, Z_R \, + \, Y_{t_5}\, \overline{T}_L H\, t'''_R \\ & + \, Y_{t_6}\, \overline{Z}_L H\, T_R + Y_{t_7}\, \overline{T}_R H\, t'''_L \, + \, Y_{b_1}\, \overline{Q}_L H\, b_R \, + \, Y_{b_2}\, \overline{Q}_L H\, b''_R \, + \, Y_{b_3}\, \overline{B}_L \tilde{H}\, b_R \\ & + \, Y_{b_4}\, \overline{B}_L \tilde{H}\, b''_R \, + \, Y_{b_5}\, \overline{B}_R \tilde{H}\, b''_L \, + \, m_1\, \overline{T}_L T_R \, + \, m_2\, \overline{Z}_L Z_R \, + \, m_3\, \bar{t}'''_L t'''_R \\ & + \, m_4\, \overline{B}_L B_R \, + \, m_5\, \bar{b}''_L b''_R \, + \, \text{H.c.}, \end{aligned} \tag{3.18}$$

and the mass matrices for the t, b and $\frac{5}{3}$ electric charge quarks are given by

$$\mathcal{M}_t = \begin{pmatrix} v'Y_{t_1} & 0 & 0 & v'Y_{t_2} \\ v'Y_{t_3} & m_1 & v'Y_{t_4} & v'Y_{t_5} \\ 0 & v'Y_{t_6} & m_2 & 0 \\ 0 & v'Y_{t_7} & 0 & m_3 \end{pmatrix}, \; \mathcal{M}_b = \begin{pmatrix} v'Y_{b_1} & 0 & v'Y_{b_2} \\ v'Y_{b_3} & m_4 & v'Y_{b_4} \\ 0 & v'Y_{b_5} & m_5 \end{pmatrix},$$
$$\mathcal{M}_{5/3} = \begin{pmatrix} m_1 & \frac{v'Y_{t_4}}{\sqrt{2}} \\ \frac{v'Y_{t_6}}{\sqrt{2}} & m_2 \end{pmatrix}. \tag{3.19}$$

The novelty of this model is the appearance of an electric charge $\frac{8}{3}$ exotic quark, $q_{8/3}$, whose mass is given by $|m_2|$. Also, the mass of $q_{4/3}$ is given by $|m_4|$.

3.3 Present Constraints on VLQ Properties

3.3.1 Bounds from the LHC Higgs Data

The first set of constraints that we consider is due to Higgs production and detection at the LHC; for a review of the relevant processes see e.g. Ref. [128]. The data collected by the ATLAS and CMS collaborations at 7+8 TeV c.m. energies in the main search channels, namely the $h \to \gamma\gamma, ZZ, WW, \tau\tau$ detection modes with the Higgs boson produced in the gluon (ggF) and in the vector boson (VBF) fusion channels plus the $h \to b\bar{b}$ decay mode with the Higgs produced in the $q\bar{q} \to Vh$ mode (Vh) with $V = W, Z$, seem to be in good agreement with the SM expectations [1, 2, 53]. One can thus use the signal strengths μ_{XX} in these Higgs detection channels, defined as the measured cross section times the decay branching ratio relative to the SM prediction,

$$\mu_{XX} = \frac{\sigma(pp \to h)}{\sigma(pp \to h)_{\text{SM}}} \times \frac{\text{BR}(h \to XX)}{\text{BR}(h \to XX)_{\text{SM}}}, \tag{3.20}$$

to constrain possible effects of extra vector–like top and bottom partners which would impact several of them.

The cross section for the gluon fusion mechanism ggF is by far the dominant Higgs production process at the LHC as it provides $\sim 85\%$ of the total Higgs sample before kinematical cuts are applied. In the SM, the process is mediated by triangular top and (to a lesser extent) bottom quark loops. VLQs that are top and bottom partners would affect the ggF production rate either through mixing, i.e. by modifying the t, b loop contributions, or via their exchange in the loop. The various quark contributions to the loop-induced hgg coupling are summarized below. [5]

Noting the Yukawa couplings for the VL mass eigenstates as y_{t_i} and y_{b_i}, (labeled by $i = 1, 2, \ldots$), the ratio of the ggF cross section over its SM prediction reads as

$$\mu_{\rm ggF} \equiv \frac{\sigma^{\rm VL}_{\rm ggF}}{\sigma^{\rm SM}_{\rm ggF}} = \frac{\Big|\sum_i \frac{v\, y_{t_i}}{m_{t_i}} A[\tau(m_{t_i})] + \sum_i \frac{v\, y_{b_i}}{m_{b_i}} A[\tau(m_{b_i})]\Big|^2}{\Big|A[\tau(m_t)] + A[\tau(m_b)]\Big|^2}, \tag{3.21}$$

where $A[\tau(m)]$ is the form factor for spin 1/2 particles [128] normalized such that $A[\tau(m) \ll 1] \to \frac{4}{3}$ and $A[\tau(m) \gg 1] \to 0$ with $\tau(m) = m_h^2/4m^2$. It is useful to use this large mass limit, which is a reasonable approximation (except for the bottom quark), so that the first sum from eq. (3.21) simplifies [129],

$$\sum_i \frac{v y_{t_i}}{m_{t_i}} A[\tau(m_{t_i})] \simeq \sum_i \frac{v y_{t_i}}{m_{t_i}} = v\, {\rm Tr}\Big(\frac{\partial \mathcal{M}_t}{\partial v} \mathcal{M}_t^{-1}\Big) = v \frac{\partial}{\partial v} \log\det \mathcal{M}_t. \tag{3.22}$$

A similar expression holds for the sum over the bottom quark states, with the difference that, since the bottom form factor is almost zero, one has to add and then subtract its contribution. Thus, we can write an approximate form for the ggF ratio from eq. (3.21):

$$\mu_{\rm ggF} \simeq v^2 \left| \frac{\partial}{\partial v} \log\det \mathcal{M}_t + \frac{\partial}{\partial v} \log\det \mathcal{M}_b - \frac{y_{b_1}}{m_{b_1}} \right|^2, \tag{3.23}$$

which can be used as a guide to stay in regions where the ggF rate is not too far from its SM value. Nevertheless, in our numerical analyses, we use the exact expression of eq. (3.21).

The impact of VLQs in the hgg vertex can be probed essentially through the signal strength in the $h \to ZZ^* \to 4\ell^\pm$ channel, which is among the most precisely measured ones (we refrain here from adding the information from the $h \to WW^* \to 2\ell 2\nu$ search channel that is affected by larger theoretical and experimental uncertainties). Averaging the Run 1 ATLAS and CMS measurements [1, 2, 53], one obtains[6] [1, 2]

$$\mu_{ZZ}^{\rm (comb)} = 1.17^{+0.23}_{-0.22}\,. \tag{3.24}$$

The loop induced $h \to \gamma\gamma$ decay mode bears many similarities with the ggF process. It is mediated by top and bottom quark triangular loops but also receives a contribution from

[5] The discussion of the $h\gamma\gamma$ loop proceeds in a similar fashion, but with the strong coupling replaced by the QED coupling, and with an additional loop contribution from the W boson. Also, the diphoton loop coupling depends on the electric charges of the particles running in the loop.

[6] We will not discuss here the subtleties in the treatment of the theoretical uncertainties that are expected to be at the level of 15–20% in this channel, referring the reader to Ref. [119, 121, 130] for a recent discussion (note that the QCD corrections to the VLQ contributions to the ggF and $h \to \gamma\gamma$ loop processes should be approximately the same as for the top quark contribution; see Ref. [131] for instance). We also note that a combination of the ATLAS and CMS Higgs results at the first LHC run [53] gives slightly different values for the signal strengths in some channels; the difference is nevertheless so small that our analysis is unaffected.

the W boson. In fact, the latter contribution is dominating and interferes destructively with the one from the heavy SM quarks. Again, additional contributions come from VLQs, in particular through their exchange in the $h\gamma\gamma$ vertex. Given their smaller electric charge, VLQ bottom–quark partners barely contribute to the vertex but exotic VLQs with higher electric charge, e.g. $+\frac{5}{3}$ or $-\frac{4}{3}$, could more significantly affect the loop [110]. Run I ATLAS and CMS data [1, 2], when combined, give the even stronger constraint

$$\mu_{\gamma\gamma}^{(\rm comb)} = 1.14 \pm 0.18\,. \tag{3.25}$$

Additional bottom–like VLQ partners would alter, besides the $Zb\bar{b}$ vertex, the $hb\bar{b}$ coupling as well. Consequently, one should also enforce the constraint from the Higgs–strahlung process with the Higgs boson decaying into $b\bar{b}$. Combining the ATLAS and CMS results [1, 132], one obtains for this channel[7]

$$\mu_{bb}^{(\rm comb)} = 0.69 \pm 0.29\,. \tag{3.26}$$

Note that here, the production cross section in the Vh process is not altered at tree level by the presence of VLQ and only the $h \to b\bar{b}$ branching ratio is affected. In fact, this branching ratio, $\sim 60\%$, is the dominant one [133]. It controls the total decay width and therefore enters in all the other Higgs branching ratios and hence all signal strengths. We will thus simultaneously include the various effects and impose the three constraints from $\mu_{ZZ}, \mu_{\gamma\gamma}$ and μ_{bb} at the same time, ignoring the other signal strengths that are less stringently constrained [1, 2, 53].

Finally, we will also consider the signal in the associated $pp \to t\bar{t}h$ production channel for which the combined ATLAS and CMS measurement [1, 2, 53]

$$\mu_{tth}^{(\rm comb)} = 2.23^{+0.64}_{-0.61} \tag{3.27}$$

exhibits a $\sim 2\sigma$ excess compared to the SM value, that is very tempting to attribute to new physics. The experimental value for the μ_{tth} signal strength assumes SM Higgs decay rates, a feature that is consistent as the decays modified by VLQs such as the $h \to b\bar{b}$ and $h \to \gamma\gamma$ modes will be separately tested here to be close to their SM values.

In our discussion, this deviation will be attributed to an enhancement of the top quark Yukawa coupling as a result of mixing with VLQ partners. However, because the non–SM–like y_t coupling would also affect the top–quark contributions to the hgg and $h\gamma\gamma$ vertices, one could compensate the y_t enhancement by another (negatively interfering) contribution due to VLQ exchanges in the loops as these effective couplings seem to be in agreement with the SM prediction.

3.3.2 Constraints from High Precision Tests

There are also indirect constraints on VLQs from high precision electroweak data. First, for the third generation quark sector, there are tree-level corrections induced by the t–t' or b–b' mixings directly on the t or b vertices but, because of the heaviness of t' states, the value for the CKM matrix element V_{tb} [107] including quark mixing is expected to be SM–like. In addition, there are radiative corrections to the gauge boson vacuum polarization functions induced by the exchange of VLQs [134, 135]. These can be cast into the so–called "oblique" parameters S, T and U [102] that must lie inside the 1σ regions induced by a long list of electroweak precision observables [107]. Three crucial observables, the W boson

[7] Here, the theoretical uncertainty is small and the error is largely dominated by the experimental one.

mass M_W, the leptonic partial width $\Gamma(Z \to \ell\ell)$ and the longitudinal polarization and forward–backward asymmetries for leptons that give $\sin^2\theta_W$ play a prominent role [107]. Given the fact that none of our considered models exhibit an explicit custodial symmetry, it is a non–trivial question whether they will respect these oblique parameter constraints. Also, trying to impose custodial symmetry, as in Ref. [126], would not be a valid solution, since a strong mixing between the SM quarks and the VLQs is needed to explain the μ_{ttH} enhancement. Moreover, such a symmetry would require a high number of VLQ multiplets, which goes against the idea of minimality.

We will analyze the 2σ excursions of the correlated S and T values (with the usual assumption that $U = 0$), obtained for our models, from the experimental values of the two parameters, which are given by

$$S|_{U=0} = 0.06 \pm 0.09 \quad \text{and} \quad T|_{U=0} = 0.10 \pm 0.07, \tag{3.28}$$

with a correlation coefficient of 0.91 [136]. We find that the theoretical prediction for the S parameter typically does not deviate too much from its central value, while T has a very high sensitivity to the addition of VLQs. Disentangling the deviations of the observable T that are due to mixing effects or to the VLQ loop contributions is rather difficult in practice. In particular, the mixing effects between (at least) three states are very cumbersome to handle; they can be treated only numerically and one then needs to resort to a scan approach as will be done in our analysis.

The other set of constraints comes from $Z \to b\bar{b}$ decays at LEP. For the experimental [107] and theoretical [107, 137] values of the ratio of partial widths R_b and the asymmetry $A_{\rm FB}^b$, one has the following:

$$R_b^{(\rm exp)} = 0.21629 \pm 0.00066 \quad \text{vs} \quad R_b^{(\rm SM)} = 0.2158 \pm 0.00015, \tag{3.29}$$

$$A_{\rm FB}^{b\,(\rm exp)} = 0.0992 \pm 0.0016 \quad \text{vs} \quad A_{\rm FB}^{b\,(\rm SM)} = 0.1029 \pm 0.0003. \tag{3.30}$$

As already mentioned in several instances, the models that we consider address the $A_{\rm FB}^b$ anomaly. They can be realized within concrete warped extra-dimensional [125] or their dual composite Higgs scenarios [138, 139]. Indeed, in model **A**, the VLQs could be interpreted as Kaluza-Klein excitations of SM quarks in extra-dimensional scenarios. The presence of Kaluza-Klein excitations of the bottom quark would induce b–b' mixing and thus corrections to the $Zb\bar{b}$ couplings that affect $A_{\rm FB}^b$ and R_b. Furthermore, extra t' modes would be simultaneously added to enhance the top quark Yukawa coupling. These t' states would then typically have a negative $\mathrm{SU}(2)_{\rm L}$ isospin, as explained in Section 2. Such a t' isospin arises in several embeddings in a $\mathrm{SU}(2)_{\rm L} \times \mathrm{SU}(2)_{\rm R}$ custodial symmetry gauged in the bulk which allows a protection with respect to all electroweak precision data [125, 138–140]. In other words, the extra-dimensional scenarios that comply with the S, T constraints could naturally predict an enhanced y_t coupling and a smaller value for $A_{\rm FB}^b$, at least from the point of view of the field content and their gauge group embedding.

Note that since we are considering a unique set of VLQ fields and not a replica per generation, it means that the so-called custodians $(t', b', ...)$ for the first two quark (and three lepton) SM generations would decouple, which can be realistic in such frameworks [125, 139]. Higgs data imply then large masses for the Kaluza-Klein excitations of gauge bosons and the Higgs sector would essentially feel only the effects of the VLQs (custodians) from the various effective **A**–**C** models.

3.3.3 Other Constraints

Apart from the constraints coming from the LEP and LHC, one should also incorporate various constraints concerning the eigenmasses of the physical states and their couplings to the scalar Higgs field. First, one should reproduce the observed top and bottom quark masses. However, since we are neglecting the mixing between the 3 flavors and also the running from the VLQ mass down to the heavy quark pole masses m_t and m_b, we will allow for an uncertainty for both eigenmasses. In the case of the top quark t_1, we require its mass to lie between 157 and 191 GeV, which represents a 10% excursion from the measured value of $m_{t_1} \sim 174$ GeV. As for the bottom quark b_1, we impose for its mass a value between 3 GeV and 5 GeV.

Indeed, as the Cabibbo-Kobayashi-Maskawa (CKM) matrix is close to the identity matrix, the simplest theoretical quark mixing configuration corresponds to having both rotation matrices for the up and down quark sectors close to identity as well, with a similar assumption for the matrices of the right-handed sector, for simplicity. Since the deviation of the CKM matrix from identity (its off-diagonal elements) is between less than 1% and $\sim 20\%$ [107], one can expect deviations of order 10% in these up and down rotation matrices. Hence, the top quark mass could be affected by a correction of this order. Such mixing effects can induce an even larger uncertainty for the bottom quark due to its mass being closer to the light generation ones.

Besides, the running effect between the VLQ and the top quark pole masses could be of order $\sim 10\%$ [141, 142], depending on the considered model. The bottom quark mass can be even more affected due to its proximity to the QCD scale, Λ_{QCD}.

Second, one should take into account the mass constraints coming from direct searches for VLQs at the LHC. Up to date, the most severe bounds on the VLQ masses come from the ATLAS experiment and are as follows:

- for a top-like VL partner, $m_{t_2} > 950$ GeV for $\mathrm{BR}(t_2 \to h t_1) = 1$ [100];
- for a bottom-like VLQ, $m_{b_2} > 813$ GeV for $\mathrm{BR}(b_2 \to W t_1) = 1$ [100];
- for a $+\frac{5}{3}$ charged VLQ, $m_{5/3_1} > 840$ GeV for $\mathrm{BR}(q_{5/3_1} \to W t_1) = 1$ [99];
- for a $-\frac{4}{3}$ charged VLQ, $m_{4/3_1} > 770$ GeV for $\mathrm{BR}(q_{4/3_1} \to W b_1) = 1$ [99].

To be conservative, we have considered for each type of VLQ the decay branching ratio values that give the most stringent lower bound on their eigenmass.

However, since it contains an electric charge $+\frac{8}{3}$ VLQ, model **C** needs an additional discussion. At LHC, there are no dedicated searches for such a resonance, but the authors of Ref. [143] have recast the LHC exclusion limits for an electric charge $\frac{5}{3}$ VLQ giving same–sign dilepton final states into the bound $m_{8/3} > 940$ GeV at 95% CL. In our analysis, this is the limit that we will use.

Besides one $\frac{8}{3}$ VL quark, model **C** contains two $\frac{5}{3}$ VLQs, which in general are not degenerate in mass. Given this situation, one must reinterpret the mass exclusion limits on a $\frac{5}{3}$ top partner. Supposing that the heavier 5/3 charge partner decays always to the lighter $\frac{5}{3}$ VLQ (plus a Z or a Higgs boson) and knowing that $\mathrm{BR}(q_{8/3} \to q_{5/3} + W) = 1$, one can infer a lower bound on the mass of the electric charge $\frac{5}{3}$ partner. A conservative bound can be obtained by considering that $m_{8/3} \simeq m_{5/3_2} \simeq m_{5/3_1}$ (mass differences of $\mathcal{O}(m_W)$, thus negligible), which, together with the previous assumption, amounts to multiplying by a factor 3 the QCD pair-production cross section of the charge 5/3 states. This assumption gives the most conservative bound because, by minimizing the masses of the VLQs, we maximize their production cross section. Reinterpreting the search for electric charge 5/3 colored resonances

from Ref. [99] in this way, we obtain, in the particular case of model **C**, the conservative bound $m_{5/3} \gtrsim 1$ TeV at 95% CL.

Finally, to make our predictions reliable at leading order in perturbation theory, we impose a perturbativity bound on the Yukawa couplings in the mass basis. Using naive dimensional analysis, we thus enforce the conservative constraint $\max(|y_{ij}|) < \sqrt{4\pi}$ for all four types of quarks, namely top, bottom, $q_{4/3}$ and $q_{5/3}$ states.

3.4 Numerical analysis

We now present our numerical results on the constraints on VLQ masses and couplings from current data. We first summarize the approximations that we use when enforcing the various constraints from the Higgs signal strengths as defined in eq. (3.20) and as measured at the first run of the LHC, eqs. (3.24)–(3.26). As discussed previously, on the production side, the additional VLQs alter only the ggF production mechanism. On the other hand, they do not affect the hVV couplings that enter in the subdominant VBF and Vh processes. Since the ggF process is responsible for most of the Higgs production cross section at the LHC, we assume that, in both the SM and in our VLQ models, one simply has $\sigma(pp \to h) \simeq \sigma(gg \to h)$ for all signal strengths, with the exception of the $h \to b\bar{b}$ decay. In the latter case, the production mode is instead the Higgs-strahlung process which should be SM–like. Moreover, we consider that only the decay $h \to b\bar{b}$, which has the largest branching ratio, is modified in the presence of the VLQs ($h \to \gamma\gamma$ is also modified, but this decay has a negligible branching ratio). Indeed, the other decay mode that involves third generation quark couplings, namely $h \to gg$, has a small branching ratio and is expected to be close to its SM value, as the vertex is tested directly via the production process. Thus, we consider that the modification of the total decay width of the Higgs boson, which enters in all signal strengths, comes only from the altered $hb\bar{b}$ vertex.

Considering model **A**, we present in the left–hand side of Fig. 3.1 the constraints that we obtain in the $[Y_{t_3}, Y_{t_4}]$ plane. The solid black and grey lines delineate, respectively, the domains where the signal strengths μ_{ZZ} and $\mu_{\gamma\gamma}$ respect the LHC measurements given in eqs. (3.24,3.25), at the 1σ level. The black dashed lines delineate the areas in which the constraints from the oblique parameters S and T are satisfied at 1 and 2σ, with $U = 0$, while at the right of the red line, the top quark mass is reproduced within an uncertainty of $\pm 10\%$ (the lower value does not appear in this frame). The regions excluded by the non-perturbativity of the Yukawa couplings or by too low VLQ masses are included but their impact in also not shown in the figure. Finally, the region in which the top quark Yukawa coupling y_{t_1} needs to be enhanced so as to explain the observed excess in the $t\bar{t}h$ production rate relative to the SM prediction is given by the blue lines: the lines for $\mu_{ttH} = 2.87$ and $\mu_{ttH} = 1.62$, which correspond respectively to the $+1\sigma$ and -1σ deviation of the experimental value as given in eq. (3.27), as well as the central value $\mu_{ttH} = 2.23$, are shown.

Turning to the bottom sector, we display in the right–hand side of Fig. 3.1 the regions in the $[Y_{b_2}, Y_{b_3}]$ plane where the various experimental (and theoretical, as we also include the perturbativity of the couplings) constraints are satisfied. Apart from imposing no more than 1σ deviation compared to the SM for the measured values of the $A_{\rm FB}^b$ asymmetry (purple lines) and the R_b ratio of widths (green lines), we allow for the bottom quark mass to take values between 3 and 5 GeV (to account for the neglected effects of running and flavor mixing), a constraint that is not displayed in the figure as it is satisfied in the entire plane. Also not displayed, the LHC constraint on the μ_{bb} signal strength is compatible with data at the 1σ level in the whole plane (the experimental central value given in eq. (3.26)

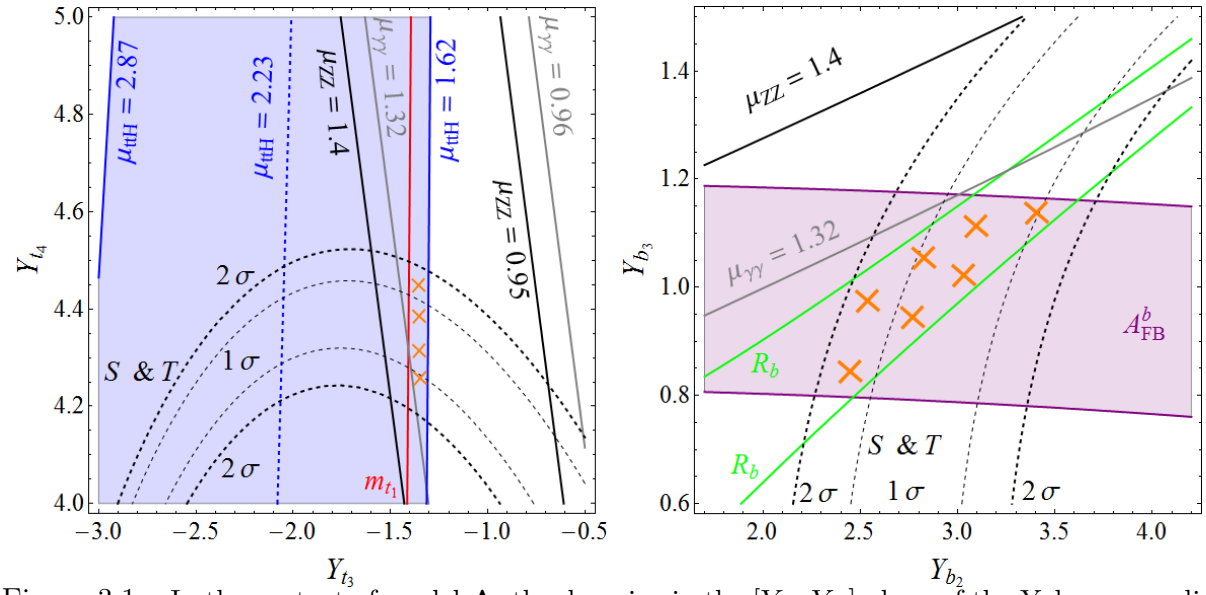

Figure 3.1 – In the context of model **A**, the domains in the $[Y_{t_3}, Y_{t_4}]$ plane of the Yukawa couplings in the top sector (left plot) and $[Y_{b_2}, Y_{b_3}]$ of the Yukawa couplings in the bottom sector (right plot) in which the various experimental constraints are satisfied at the 1σ level. The constraints discussed in the text but not displayed (such as the one from the perturbativity of the Yukawa couplings and the lower limits on the VLQ masses) are satisfied in the entire planes. The regions complying with all constraints are highlighted by the orange crosses.

is $\sim 1\sigma$ smaller than the expectation in the SM). This is not the case of the μ_{ZZ} and $\mu_{\gamma\gamma}$ constraints which, as in the top sector case, are depicted by the solid black and the solid gray lines respectively. Here, the additional constraints on the mass of the VL bottom–quark partners from direct LHC searches play an important role. Naturally, the constraints on the top quark mass m_{t_1} and the signal strength μ_{tth} do not appear in the plot as they essentially depend on parameters from the top sector (likewise, the constraints from $A^b_{\rm FB}$ and R_b do not appear on the left plot of Fig. 3.1 as they also do not depend on the top sector parameters).

In Fig. 3.1, the regions with the orange crosses are the ones that are compatible, at the 68% confidence level (95% CL for for S and T), with all considered constraints. In the bottom sector plot, we fix the Y_{t_3} and Y_{t_4} interaction basis parameters at $Y_{t_3} = -1.45$ and $Y_{t_4} = 4.32$, while in the top sector plot we take $Y_{b_2} = -3.15$ and $Y_{b_3} = -1.08$. The values of the other parameters of the considered model **A** that appear in the Lagrangian of eq. (3.12) are given by $Y_{t_1} = -0.98$, $Y_{t_2} = 3.05$, $Y_{t_5} = 3.81$, $Y_{b_1} = -0.02$, $Y_{b_4} = -2.2$, $Y_{b_5} = -0.05$, for the Yukawa couplings and $m_1 = 1.77$ TeV, $m_2 = 1.61$ TeV, $m_3 = -0.85$ TeV and $m_4 = -5.69$ TeV for the VLQ masses.

The outcome of the discussion is that, indeed, there is a set of parameter values for which the observed excess in the $t\bar{t}h$ production cross section and the measured departure from the SM of the $A^b_{\rm FB}$ asymmetry are both accommodated. In addition, for the same set of parameter values, both the LHC Higgs data and the EW precision measurements at LEP are satisfied. As already mentioned, this is a rather non–trivial result. As the masses of the majority of the VLQs that result from the fit lie in the range between 1 and 2 TeV, this scenario is currently being tested at the LHC through the direct production the additional VLQ states.

The same considerations apply for models **B** and **C**: we show in Fig. 3.2 and Fig. 3.3 respectively the impact of the various constraints in the $[Y_{t_3}, Y_{t_4}]$ (left plots) and $[Y_{b_2}, Y_{b_{3,4}}]$ (right plots) planes. The regions in which (i) the b–quark related constraints $m_{b_1}, A^b_{\rm FB}, R_b, \mu_{bb}$,

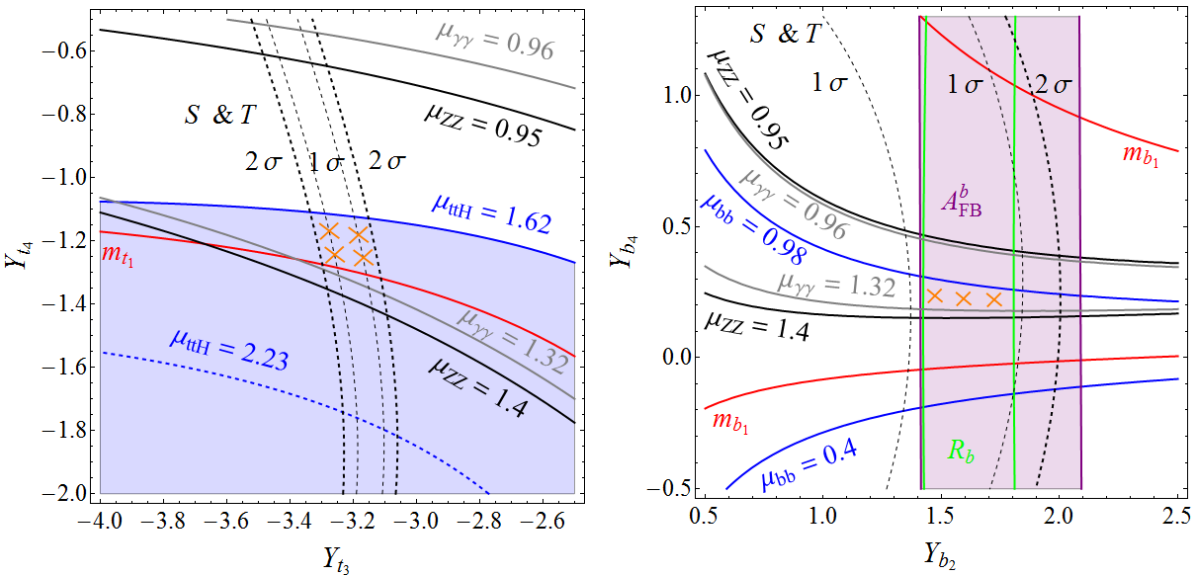

Figure 3.2 – The same as in Fig. 3.1 but in the context of model **B**.

(ii) the t–quark related constraints m_{t_1}, μ_{tth}, (iii) the general constraints $\mu_{\gamma\gamma}, \mu_{ZZ}$, (iv) the EW constraints from S and T, and (v) the LHC lower bounds on the VLQ masses are satisfied at the 1σ level (2σ for $S\,\&\,T$), i.e. the allowed regions, are again highlighted by orange crosses. We have also enforced the perturbativity of all Yukawa couplings and the impact of this constraint is now visible in the plots: the dark coloured areas are those where at least one Yukawa coupling in the mass basis is larger than $\sqrt{4\pi}$ in absolute value. Also, we imposed the direct exclusion limit on the VLQ mass $m_{b_2} > 813$ GeV [100]. One constraint is particularly important in the two models **B** and **C**, namely the $h \to \gamma\gamma$ signal strength, as both models contain VLQs with high electric charge, $-\frac{4}{3}$ and $\frac{5}{3}$, which could lead to important contributions to the $h\gamma\gamma$ vertex. Note that in the left plot of Fig. 3.3, only the line for the -1σ value of the $t\bar{t}h$ rate is displayed as we have selected the areas in which the top Yukawa coupling is sufficiently enhanced to accommodate the observed excess. Moreover, one can see that in the bottom sector plot of model **C** (right plot of Fig. 3.3) there are two disjoint regions where all the phenomenological constraints mentioned above are satisfied. Although they are situated roughly symmetrically with respect to the $Y_{b_2} = 0$ line, their shapes are different. This shows that, with all the other parameters fixed, flipping the sign of Y_{b_2} is of physical importance. Indeed, such a transformation changes the value of $\det \mathcal{M}_b$, which enters directly in the rate expression for the loop-induced ggF mechanism and $h \to \gamma\gamma$ decay (as described earlier)).

In the two models, the values of the various parameters appearing (and defined) in eq. (3.17) for model **B** and eq. (3.19) for model **C** and not shown in the planes are as follows. In model **B**, we have: $Y_{t_1} = -0.98$, $Y_{t_2} = 0.68$, $Y_{t_5} = -3.6$, $Y_{t_6} = 4.4$, $Y_{b_1} = 0.019$, $Y_{b_2} = 1.47$, $Y_{b_3} = 0.28$, $Y_{b_4} = 0.17$, $m_1 = 1.42$ TeV , $m_2 = 1.1$ TeV, $m_3 = -2.32$ TeV and $m_4 = 1.5$ TeV, with $Y_{b_2} = 1.61$ and $Y_{b_4} = 0.23$ in the top sector plot (left) plus $Y_{t_3} = -3.22$ and $Y_{t_4} = -1.21$ in the bottom sector plot (right). In model **C**, we have: $Y_{t_1} = -1.01$, $Y_{t_2} = -1.19$, $Y_{t_5} = -5.61$, $Y_{t_6} = -4.03$, $Y_{t_7} = 3.81$, $Y_{b_1} = 0.024$, $Y_{b_2} = 0.5$, $Y_{b_3} = 1.75$, $Y_{b_4} = 0.64$, $Y_{b_5} = 0.02$, $m_1 = -4.8$ TeV , $m_2 = -3.12$ TeV, $m_3 = 1.11$ TeV, $m_4 = 1.5$ TeV and $m_5 = 1.1$ TeV, with $Y_{b_2} = 0.52$ and $Y_{b_3} = 1.75$ in the top sector plot (left) plus $Y_{t_3} = -4.59$ and $Y_{t_4} = -4.51$ in the bottom sector plot (right).

We observe from the three sets of plots Figs. 3.1–3.3 that the allowed regions in the $[Y_{t_3}, Y_{t_4}]$ and the $[Y_{b_2}, Y_{b_3,b_4}]$ planes are rather sizeable. Nevertheless, other choices of the remaining

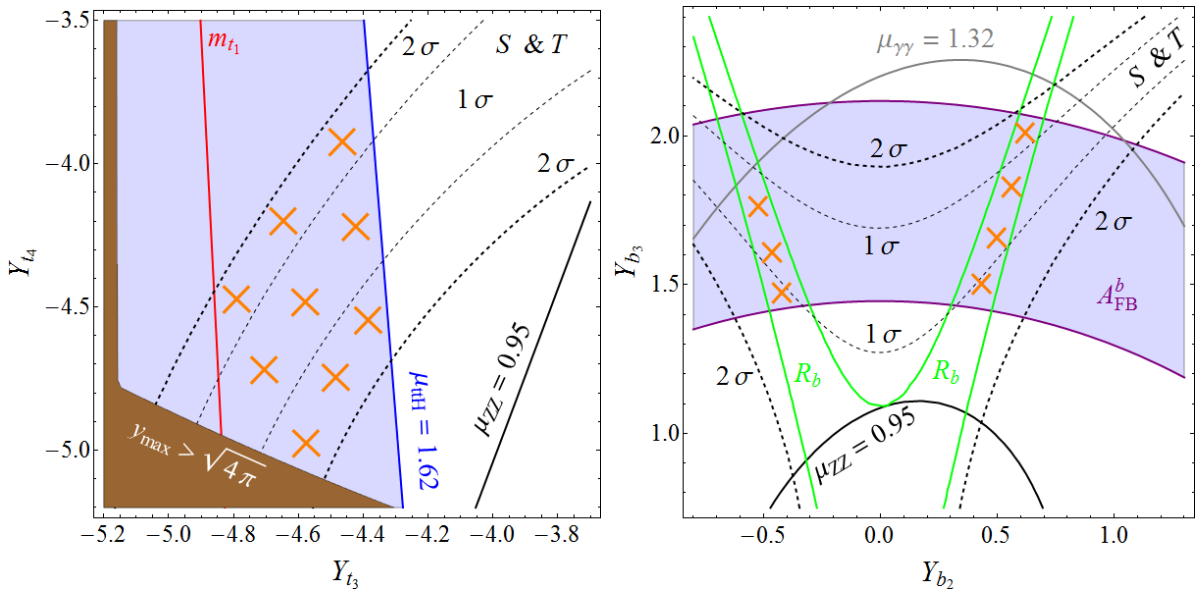

Figure 3.3 – The same as in Fig. 3.1 but in the context of model **C**.

parameters do not allow to significantly increase those domains. In general, besides S and T, the most important constraint in the top sector come from enforcing the enhancement of the $t\bar{t}h$ rate without significantly altering the top quark mass. Simultaneously respecting these two constraints calls for a strong mixing with the extra quarks, which translates into larger Yukawa couplings Y_{t_i}, with $i = 1, 2, 3, \ldots$. As a consequence, the allowed regions are driven close to the areas ruled out by non-perturbativity, with the highest Higgs–VLQ couplings reaching values typically higher than 3 (for model **C**, the allowed region and the area ruled out by non-perturbativity are adjacent). Another possibility of enhancing the mixing would be to lower the VLQ mass parameters m_i, but this approach fails, since it leads to VLQ masses that are too low and experimentally excluded. Concerning the bottom sector, the strongest constraints come clearly from the LEP observables $A^b_{\rm FB}$ and R_b, which are measured at the per mille level, as well as from the S and T oblique parameters, measured (indirectly) also at LEP.

Note that our choice for presenting the results (Figs. 3.1–3.3) in the the $[Y_{t_3}, Y_{t_4}]$ and the $[Y_{b_2}, Y_{b_3,b_4}]$ planes was only for illustration, as any other choice would have been equally valid. Nonetheless, when searching for the allowed regions, we varied all the parameters involved in our models. Even though the parameter space of each of our models has a dimensionality larger than 10, varying by a significant amount the couplings Y_{t_i,b_i} and/or the VLQ mass parameters m_i that we kept fixed in the plots would have restrained the starred regions, where all the constraints are satisfied. Thus, is was not possible to decrease the large values of some of the interaction basis couplings, which were $Y_{t_i,b_i} > 3$. Nevertheless, we remind the reader that the displayed regions involve only perturbative couplings in the mass basis.

Interestingly, the considered models predict the existence of top, bottom (t_2 and b_2 eigenstates) and even exotic partners around the TeV scale, to which the LHC Run II might be sensitive. While model **B** predicts 7 VLQs with masses $\lesssim 2$ TeV, models **A** and **C** both predict 4 VLQs with masses $\lesssim 2$ TeV. Such states will be thus accessible through direct production at the upgraded LHC.

Another feature that can be noticed from the plots is the fact that in the allowed regions, the top quark mass attains rather large values, usually above 185 GeV, while the $t\bar{t}h$ signal strength has a value around 1.65, which is approximately 1σ below its central value, 2.23. In fact, the considered VLQ models can more closely reproduce simultaneously the measured

top mass $m_t \simeq 174$ GeV and a higher value of the $t\bar{t}h$ signal strength, typically $\mu_{tth} \simeq 2$ (i.e. only $\sim 0.3\sigma$ away from the central value), but at the expense of having S and T values outside their 2σ ranges. One can argue that S and T, which are measured with a higher accuracy than the Higgs couplings, could be also sensitive to the presence of other sources of new physics, such as extra gauge bosons that appear in many scenarios with VLQs[8], allowing to increase the range of validity of the Yukawa couplings with the data in Figs. 3.1–3.3.

Note that the three VLQ models that we consider improve the discrepancies in $A_{\rm FB}^b$ not only on the Z–pole but also off the Z–pole. For instance, in model **A**, for the allowed region of the parameter space in the lower part of Fig. 3.1, the χ^2 function of the fit of all the asymmetry measurements is reduced from $\chi^2_{\rm SM} \simeq 33$ down to typically $\chi^2_{\rm VLQ} \simeq 15$.

To summarize the discussion of this section, we present in Fig. 3.4 a "summary plot" containing, for each considered model, the predicted values of $c_t \equiv |y_{t_1}/y_t^{\rm SM}|$ and m_{t_2} (upper plots) plus $c_b \equiv |y_{b_1}/y_b^{\rm SM}|$ and m_{b_2} (lower plots), where y_{Q_1} is the Yukawa coupling (in the mass basis) of the Q_1 mass eigenstate, i.e. the observed top and bottom quarks, and $y_Q^{\rm SM}$ is the SM prediction (the two values are equivalent in the interaction or mass basis if no fermion mixing is present). Thus, c_t and c_b measure the relative departure from the SM of the Yukawa couplings of the top and bottom quarks. As already mentioned throughout the chapter, m_{t_2} (m_{b_2}) represents the mass of the lightest top–like (bottom–like) VLQ in each of the three obtained models. For completeness, we also quote, for the allowed regions in each model, the typical masses of the lightest electric charge $Q = -\frac{4}{3}, \frac{5}{3}, \frac{8}{3}$ VLQs:

- In model **A**, $m_{5/3_1} = |m_1| \simeq 1.77$ TeV and $m_{4/3_1} = |m_3| \simeq 0.85$ TeV;
- In model **B**, $m_{5/3_1} = |m_1| \simeq 1.42$ TeV and $m_{4/3_1} \simeq 1.07 - 1.1$ TeV;
- In model **C**, $m_{8/3_1} = |m_2| \simeq 3.12$ TeV, $m_{5/3_1} \simeq 2.95 - 3$ TeV, $m_{4/3_1} = |m_4| \simeq 1.5$ TeV. Note that, in this model, the bounds mentioned in Section 3.3, $m_{8/3} > 940$ GeV and $m_{5/3} > 1$ TeV, are both respected.

In the figure, the varied parameters and their corresponding variation ranges are $Y_{t_3} \in [-1.6, -1.2]$, $Y_{t_4} \in [4, 4.6]$ and $Y_{b_2} \in [2, 4]$, $Y_{b_3} \in [0.7, 1.2]$ for model **A**, $Y_{t_3} \in [-3.4, -3]$, $Y_{t_4} \in [-1.4, -1]$ and $Y_{b_2} \in [1, 2]$, $Y_{b_4} \in [0, 1]$ for model **B**, plus $Y_{t_3} \in [-5, -4.2]$, $Y_{t_4} \in [-5.5, -3.5]$ and $Y_{b_2} \in [-0.8, 0.8]$, $Y_{b_3} \in [1.3, 2.2]$ for model **C**. These intervals cover roughly the allowed regions in Figs. 3.1–3.3 and, for each model, the remaining parameters are fixed at the same values as in these figures. Obviously, the Yukawa couplings with "t" and "b" subscripts correspond respectively to the top and bottom sectors.

The two quantities c_t and c_b are defined as absolute values as the sign of the Yukawa couplings in the mass basis is not physical. Instead, the signs of y_{t_1}/m_{t_1} and y_{b_1}/m_{b_1} are of physical relevance since such ratios appear directly in the loop-mediated $gg \to h$ and $h \to \gamma\gamma$ amplitudes. For example, in the $h \to \gamma\gamma$ process, a negative y_{t_1}/m_{t_1} ratio would mean that the top quark loop amplitude would interfere constructively with the W–loop amplitude, leading to an increase of $\Gamma(h \to \gamma\gamma)$ with respect to the SM value. In principle, this is possible in general VLQ scenarios but it is not the case in our chosen models. In the regions where all phenomenological constraints are satisfied, we find that in the three models y_{t_1}/m_{t_1} is positive, as in the SM, but slightly higher as a result of the enhancement of the top Yukawa coupling. Depending on the model, the new VLQ mass eigenstates propagating

[8] This is for instance the case in extra–dimensional models where one would have Kaluza–Klein excitations of gauge bosons and top and bottom quark partners. These could contribute to the S and T parameters but not to the Yukawa couplings. Note that the $A_{\rm FB}^b$ puzzle can be solved by contributions from both extra bosons and/or extra fermions, as discussed in Refs. [106, 125].

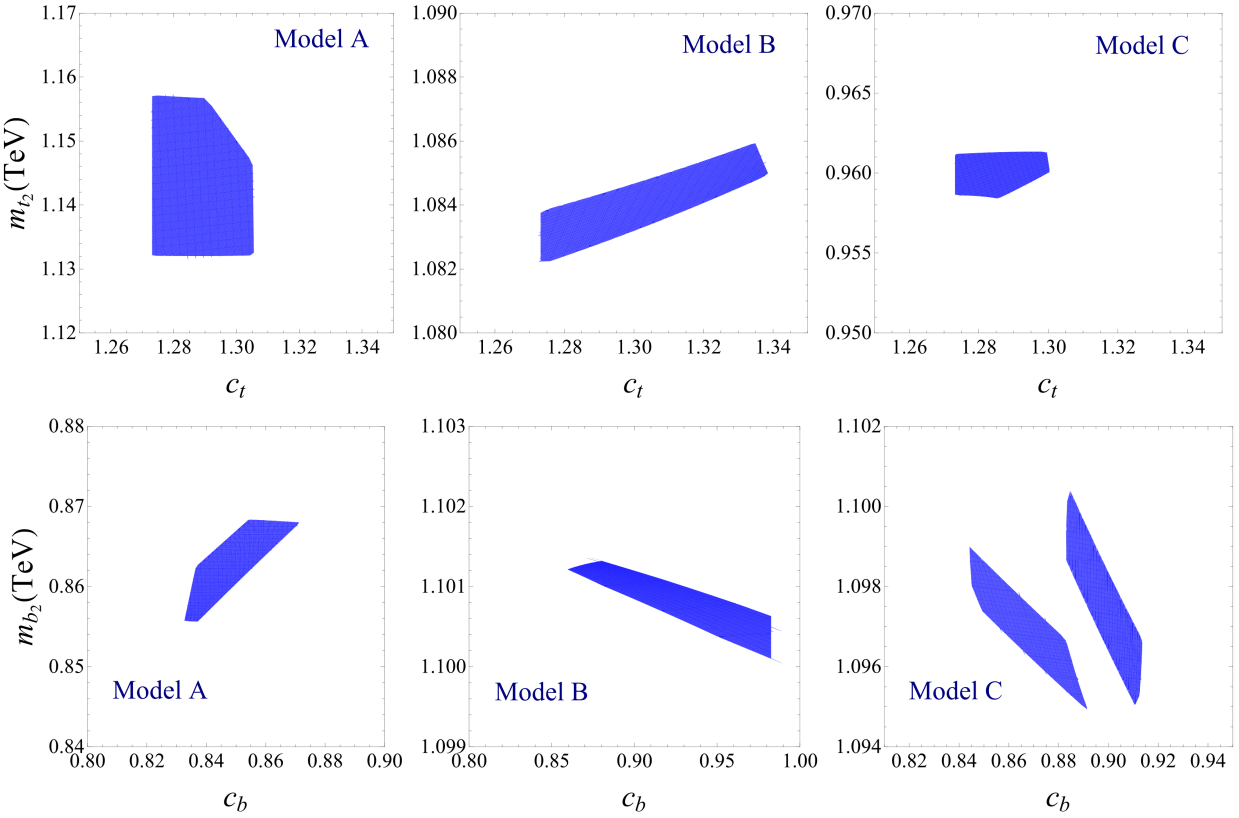

Figure 3.4 – Regions in the $[c_t, m_{t_2}]$ plane (upper plots) and the $[c_b, m_{b_2}]$ plane (lower plots) where all the phenomenological constraints enlisted in the previous section are satisfied. The varied parameters and their corresponding ranges for the three models are given in the text.

in the loop interfere either constructively or destructively with the top quark exchange. Nevertheless, their contribution to the triangular loop is modest since their masses are rather large and their couplings to the Higgs boson are small, being induced only through quark mixing[9].

As a final remark, there is no complete cancellation between the effects of the enhanced top Yukawa coupling and the contribution of the new VLQ states in the triangular loop. Instead, it turns out that in each of the models that we have considered, the gluon fusion cross section is increased by 10–15% compared to the SM value. Meanwhile, relative to its SM value, the diphoton partial width is suppressed by $1-2\%$ in models **A** and **B**, whereas in model **C** it is enhanced by $\sim 15\%$. However, these slight deviations from the SM are below the experimental accuracy on the signal strengths measured by the ATLAS and CMS collaborations [1, 2, 53].

3.5 Testing VLQs through Higgs Precision Measurements

We now discuss the sensitivity on VLQs that could be achieved at the upgraded LHC with $\sqrt{s} = 14$ TeV center of mass energy when 3000 fb^{-1} of data will be collected, the so–called high–luminosity option of the LHC (HL-LHC). We start with a discussion of the observables that can be measured with high precision in this case.

[9]The Higgs–VLQ couplings are given by the diagonal entries of the mass basis Yukawa matrix, $y_{t_{i>1}}$. These entries are zero in the interaction basis so that the mass basis couplings are mixing-induced.

3.5.1 Precision Higgs Observables at High–Luminosity

Compared to $\sqrt{s} = 8$ TeV, the Higgs production cross sections at $\sqrt{s} = 14$ TeV are enhanced by a factor of approximately 2.5 in the case of gluon fusion, 2 in the case of Higgs–strahlung and 5 in the case of associated $t\bar{t}h$ production. The statistical uncertainties on the measurement of the signal strengths values μ_{XX} for the various processes listed in Section 3.1 and obtained at $\sqrt{s} = 7$+8 TeV with ~ 25 fb^{-1} data, will be thus significantly reduced at this LHC upgrade. For instance, in the ggF mode, the statistical error which is presently the largest uncertainty will be reduced by a factor $\sqrt{300} \approx 15$ with 3000 fb^{-1} data and would lead to a precision of the order of 1–2% in the case of the $\mu_{\gamma\gamma}$ and μ_{ZZ} signal strengths and 3–5% in the case of μ_{bb}. The smaller systematical uncertainties could also be reduced so that one could hope that the total experimental errors would be reduced to the few percent level, in agreement with the ATLAS and CMS projection at $\sqrt{s} = 14$ TeV with 3000 fb^{-1} data [123, 124].

The theoretical uncertainties that affect the production cross sections (which are at the level of 5% in the ggF and 5% in the Vh cases for instance) and the decay branching ratios (which are presently of order 5% in most channels) would turn then to be the largest source of uncertainty and would limit the interest of these measurements if they are not significantly reduced. Nevertheless, one could construct ratios of observables that are free of these uncertainties. In particular, the ratio of production times decay rates [117, 118]

$$D_{\gamma\gamma} = \frac{\sigma(pp \to h \to \gamma\gamma)}{\sigma(pp \to h \to ZZ^*)} \simeq \frac{\Gamma(h \to \gamma\gamma)}{\Gamma(h \to ZZ^*)}, \tag{3.31}$$

$$D_{bb} = \frac{\sigma(q\bar{q} \to Vh \to Vb\bar{b})}{\sigma(q\bar{q} \to Vh \to VWW^*)} \simeq \frac{\Gamma(h \to b\bar{b})}{\Gamma(h \to WW^*)}, \tag{3.32}$$

will be free of all these theoretical uncertainties (including also possible ambiguities in the Higgs total decay width that affect all the branching ratios), provided that the fiducial cross sections for the processes in the numerator and in the denominator are measured within the same kinematical configurations. The two observables will be then limited only by the experimental error and, in particular, the statistical one (at least for $D_{\gamma\gamma}$). At the HL–LHC, one expects that accuracies of the order of

$$\Delta D_{\gamma\gamma} \approx 1\% \quad \text{and} \quad \Delta D_{bb} \approx 5\% \tag{3.33}$$

could be achieved. The decay ratios above, which measure only the ratio of Higgs couplings squared g^2_{hXX}, would be then extremely powerful tools to indirectly probe new physics effects and, in particular, those of heavy VLQs of the third generation.

Another Higgs decay ratio which could also be very useful in general is $D_{\tau\tau} = \Gamma(h \to \tau\tau)/\Gamma(h \to WW^*)$, with the Higgs state produced in the ggF+1j and VBF modes. However, we will ignore it in our discussion, since the VLQs that we are analyzing here do not affect the $h\tau\tau$ and hVV couplings and will thus have no impact in this context.

Finally, the signal strength in the associated Higgs production with top quark pairs, $pp \to t\bar{t}h$, is also important in the context of VLQs. At the HL–LHC, both the ATLAS and CMS collaborations expect a measurement of the cross section $\sigma(pp \to t\bar{t}h)$ with an experimental accuracy of the order of 15% [123, 124]. This error is largely dominated by the statistical one. In addition to that, the process, which is known at NLO in the QCD and electroweak couplings [144–147], is affected by a theoretical uncertainty of about 15–20% from the variation of the renormalisation and factorisation scales and from the parton distribution functions and the value of α_s. This leads then to a total uncertainty of about

30%. Nevertheless, it has been advocated that considering the ratio of cross sections for associated $t\bar{t}h$ and $t\bar{t}Z$ boson production[10], $C_{tt} = \sigma(pp \to t\bar{t}h)/\sigma(pp \to t\bar{t}Z)$, will also significantly reduce the theoretical uncertainties to the level of $\sim 5\%$ [148]. One would then have a total error on the ratio at the level of 15% when combining the ATLAS and CMS measurements at HL–LHC.

Hence, the ratio C_{tt} is expected to be affected by a much larger error than the $D_{\gamma\gamma}$ and even D_{bb} ratios, thus reducing its capacity to probe tiny VLQ effects. For this reason, although providing a complementary information as it is exclusively sensitive to the $t - t'$ mixing, we will not include this ratio in the rest of our VLQ analysis.

3.5.2 Probing VLQs Using the Higgs Decay Ratios

Using the $D_{\gamma\gamma}$ and D_{bb} decay ratios, with the total uncertainties given in eq. (3.33) and their projected central values equal to their SM values, we now estimate the sensitivities that could be achieved on VLQs at the HL–LHC. In this analysis, it would be useful to simplify to a certain extent the previously considered models in order to keep the discussion as transparent as possible but still at a rather general level. We will thus make the following three simplifying assumptions.

First, since we would like to study the new physics effects only and not the mixing effects between the SM and the physics beyond it, we will assume the VLQs to decouple from the top and bottom quarks, thus leaving the latter's couplings to the Higgs boson SM-like. This is a good approximation in general since the VLQs that we are investigating have masses well above the electroweak scale and, thus, are supposed to mix weakly with the SM states. At this stage, we will no longer attempt to explain the LHC hint for an increased top Yukawa coupling nor the anomaly in the $A_{\rm FB}^b$ asymmetry. We will thus allow the new physics that we are considering to communicate with the SM only via the Higgs boson, an assumption which guarantees that the models which we are investigating comply with the currently available phenomenological constraints[11]. For all the other phenomenological constraints, in particular for the electroweak oblique observables S and T, we assume the same central values and errors as presently (we thus ignore for simplicity some potential improvement such as the one that would come from a better measurement of the W boson mass at the LHC). The constraints from reproducing the measured top and bottom quark masses and from the perturbativity of the Yukawa couplings, as well as the lower bounds on the masses of the VLQs (which might be improved by the time of the HL–LHC if no signal is found, but will be superseded by the limits that will be obtained in our analysis) will also be assumed to be the same.

Second, to focus as much as possible on the effect of a single VLQ and not consider the cumulative contribution of several ones (for instance in the contributions to the $h \to \gamma\gamma$ or $gg \to h$ loop processes), we will retain for each model only two vector–like multiplets and decouple completely the others. The reason for keeping two multiplets and not only one is that, in the absence of mixing between VLQs and SM quarks, at least two VLQ fields are needed to have interactions of the new color triplets with the Higgs boson. This interaction with the Higgs field generates, after electroweak symmetry breaking, a mixing term between the two vector–like fields. However, to still concentrate on the effect of a single VLQ, we consider the VL mass parameter of one of the two multiplets to be larger than the other

[10] Note that in our models, both the $t\bar{t}h$ and $t\bar{t}Z$ vertices will be affected via top quark mixing with the VLQs, so that their ratio C_{tt} would not probe solely the $t\bar{t}h$ vertex.

[11] Note that there exist also model–building justifications for such a decoupling of the SM and new physics effects, such as symmetries forbidding the Yukawa coupling terms between SM fields and VLQs.

(this guarantees a small effect of the heavier VLQ in the loop induced $h\gamma\gamma$ and hgg vertices for instance). Nevertheless, at the same time, this mass splitting significantly reduces the Yukawa coupling of the lighter VLQ as a result of mixing factors. In this case, only a one percent measurement of the $D_{\gamma\gamma}$ ratio could signal the new physics effects. Our goal will be simply to estimate the power of high–precision measurements in the Higgs sector to probe heavy VLQ states with small couplings to the Higgs bosons.

Finally, also for simplicity reasons, we will assume that the two possible Higgs–VLQ–VLQ couplings in the interaction basis are equal, which means that, in the same basis, the VLQ mass matrices are symmetric. The latter have the simple texture

$$\mathcal{M}_{\rm VLQ} = \begin{pmatrix} m & m_Y \\ m_Y & M \end{pmatrix}. \tag{3.34}$$

In this expression, m (M) is the lighter (heavier) VLQ mass parameter, while m_Y is, up to a possible Clebsch–Gordan factor, equal to $v'Y$ (as the highest multiplet we consider is a triplet, $1/\sqrt{2}$ is the only possibility for a Clebsch-Gordan coefficient). In each model, M will be fixed to a high value, while m and Y will be treated as variable parameters.

In the three discussed models, the various multiplets that we retain and their impact on the $D_{\gamma\gamma}$ ratio and hence on the $h\gamma\gamma$ loop are as follows (as already stated, VLQ states are also exchanged in the loop induced ggF production mechanism but the production rates cancel in the $D_{\gamma\gamma}$ ratio):

- In model **A**, $(q_{5/3}, t')$ is the lighter doublet, with mass parameter m, while the heavier VL field (with the larger mass parameter M) is the t'' singlet. Both top quark partners will enter in the $h\gamma\gamma$ loop and affect the amplitude.
- In model **B**, the $(b', q_{4/3})$ doublet is the lighter multiplet while the heavier one is the $(t'', b'', q'_{4/3})$ triplet. Here, the main actors will be the exotic $q_{4/3}$ states, while the bottom–quark partners would generate a tiny effect on the triangular Higgs–diphoton loop, of order $(Q_{\rm em}(q_{4/3})/Q_{\rm em}(b))^2 = 16$ times smaller than the contribution of the electrically charged $-4/3$ quarks.
- For model **C**, the $(q_{5/3}, t')$ doublet has a mass parameter m and the $(q_{8/3}, q'_{5/3}, t'')$ triplet, a mass M. Here, the main contribution will be that of the exotic $q_{5/3}$ states. The contribution of the the top quark partners is approximately $\frac{1}{\sqrt{2}}(Q_{5/3}/Q_{top})^2 \simeq 4.42$ times smaller than that of the $q_{5/3}$ states ($1/\sqrt{2}$ is a Clebsch-Gordan).

In each of these cases, the eigenmass of the lighter VLQ will be denoted by $m_{\rm VLQ}$, and its coupling (in the same mass basis) to the Higgs boson by $y_{\rm VLQ}$. These two quantities are deduced from the diagonalization of the matrix in eq. (3.34). Due to the fact that $M \gg m$, one has $m_{\rm VLQ} \sim m$ and $y_{\rm VLQ} \sim -vY^2/(M-m)$. We consider only $Y \leq 5$ because, for $Y \gtrsim 5$, at least one of the four Yukawa couplings in the mass basis becomes non-perturbative, i.e. greater than $\sim \sqrt{4\pi}$. Moreover, while we allow m to attain both negative and positive values, M is chosen to be positive for all the models, since only the relative sign of the two parameters is physical. The values of M for each model are taken such that the largest resolvable $m_{\rm VLQ}$ is roughly half of M, which avoids too much feedback in the $h \to \gamma\gamma$ loop from the heavier VLQ and thus isolates, to some extent, the contribution to $D_{\gamma\gamma}$ of the lighter VLQ.

For the case of the $hb\bar{b}$ vertex, which can be probed directly in the measurement of the $h \to b\bar{b}$ partial width, the discussion concerning the D_{bb} decay ratio will be even simpler. As the $hb\bar{b}$ vertex is unaffected in the absence of mixing, we will consider here a non-vanishing mixing between the b quark and its VL partners. In turn, we will consider only bottom-like

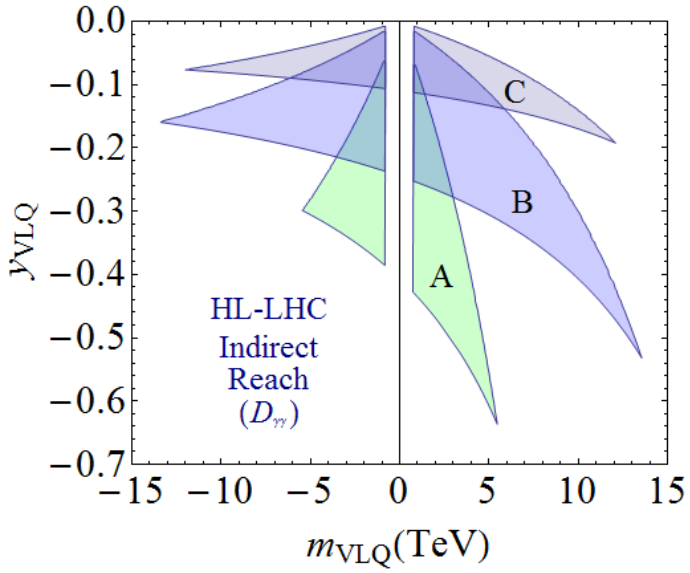

Figure 3.5 – Regions in the $[m_{\rm VLQ}, y_{\rm VLQ}]$ plane for the simplified versions of models **A**, **B** and **C**, to which a precise measurement of $D_{\gamma\gamma}$ at the HL-LHC, with $\Delta D_{\gamma\gamma} = 1\%$, will be sensitive. The other parameters entering the analysis are discussed in the text.

VLQs since only such states affect the $hb\bar{b}$ coupling through b–b' mixing. For simplicity, we shall study the case of only one bottom-like VL partner b'. The choice of the $\mathrm{SU}(2)_{\rm L}$ representation of the b' extra quark will be qualitatively irrelevant due to similar mass matrix textures (the only quantitative difference could come from various Clebsch-Gordan factors, depending on the $\mathrm{SU}(2)_{\rm L}$ embedding of b'). Thus, a single picture could be representative of all three considered models. By minimality, we shall take the b' as a singlet under $\mathrm{SU}(2)_{\rm L}$, which, together with the SM b quark, will lead to a mass matrix given by

$$\mathcal{M}_b = \begin{pmatrix} m_{Y_1} & m_{Y_2} \\ 0 & M \end{pmatrix}, \tag{3.35}$$

with $m_{Y_{1,2}} \equiv v' Y_{1,2}$. We shall denote by $y_{b'}$ the Higgs-VLQ coupling in the mass basis and by $m_{b'}$ the bottom-like VLQ eigenmass, both being obtained from the bi-diagonalization of the mass matrix in eq. (3.35).

In the analysis, we will treat Y_2 and M, defined in eq. (3.35), as variable parameters. The remaining parameter, Y_1, also appearing in eq. (3.35), will be expressed in terms of Y_2 and M by demanding that m_b, the observed b quark mass, is reproduced. Since $M \gg m_{Y_{1,2}}$ in most of the interesting part of the parameter space, we have, to a very good approximation, $m_b \approx m_{Y_1}(1 - m_{Y_2}^2/2M^2)$, which can easily be inverted in order to re-express Y_1 as a function of Y_2 and M. For this purpose, the value of the bottom quark mass in our numerical analysis will be taken to lie between the $\overline{\rm MS}$ value $m_b(\overline{\rm MS}) \approx 4.18$ GeV, and the on-shell value $m_b(1{\rm S}) \approx 4.65$ GeV [107], with a mean value $m_b = 4.43$ GeV. Apart from this constraint, we shall enforce the perturbativity condition of the mass basis Yukawa couplings, $y \lesssim \sqrt{4\pi}$, and the LHC bottom-like VLQ exclusion limit, $m_{b'} > 813$ GeV [100].

We display in Fig. 3.5, for the simplified versions of models **A**-**C**, regions in the plane $[m_{\rm VLQ}, y_{\rm VLQ}]$ to which a precise measurement with $\Delta D_{\gamma\gamma} = 1\%$ will be sensitive. In this figure, we have assumed that the future central experimental value of $D_{\gamma\gamma}$ would be equal to its SM prediction. The choices for the heavy VLQ mass parameters are $M_A = 15$ TeV, $M_B = 25$ TeV and $M_C = 28$ TeV. For each model, the ranges of the parameters are $m \in [-15, 15]$ TeV and $Y \in [0, 5]$. The lower boundary of each region is given by the $Y = 5$ curve, which typically marks the transition to the non-perturbativity regime, while the upper

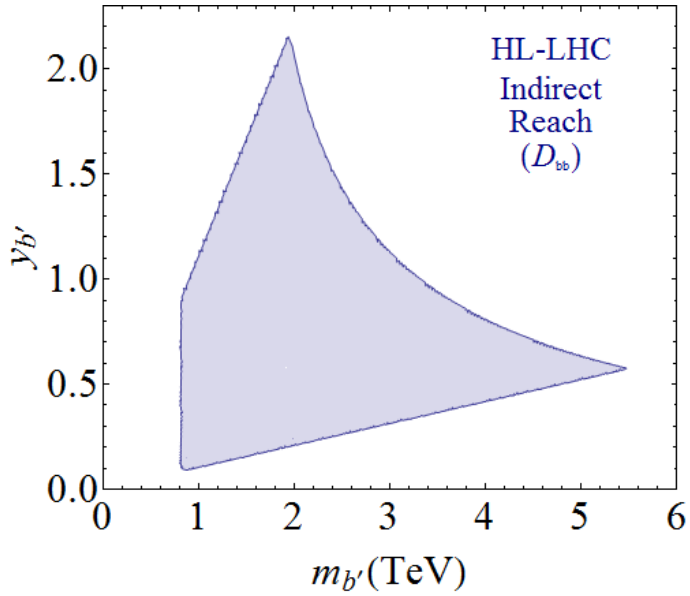

Figure 3.6 – Regions in the $[m_{b'}, y_{b'}]$ plane for the a simplified VLQ model to which a precise measurement of D_{bb} at the HL-LHC, with $\Delta D_{bb} = 5\%$, will be sensitive. The other parameters entering the analysis are discussed in the text.

boundary is dictated by the $\Delta D_{\gamma\gamma} = 1\%$ condition. The region defined by $|m_{\rm VLQ}| \lesssim 0.8$ TeV, delimiting the third boundary, is excluded by direct VLQ searches.

It might seem peculiar that in Fig. 3.5 we show also negative values of the VLQ mass, $m_{\rm VLQ}$. However, this is just a matter of convention: only the $y_{\rm VLQ}/m_{\rm VLQ}$ ratio enters in the expression of $D_{\gamma\gamma}$ (see eq. (3.21) for the comparable structure of the ggF loop amplitude). Consequently, we have plotted only negative values for $y_{\rm VLQ}$, while letting $m_{\rm VLQ}$ have any sign. Thus, the left half of Fig. 3.5 corresponds to taking both $y_{\rm VLQ}$ and $m_{\rm VLQ}$ positive.

Also, it is interesting to note in Fig. 3.5 the asymmetry of the regions with respect to the $m_{\rm VLQ} = 0$ axis. This is due to the fact that, in the case of $m_{\rm VLQ} > 0$, the interference of the lighter VLQ with its heavier counterpart is destructive, while for $m_{\rm VLQ} < 0$ the exact opposite happens. Thus, the (absolute) values of $y_{\rm VLQ}$ that can be probed are higher in the case of $m_{\rm VLQ} > 0$.

Similarly, we present in Fig. 3.6 regions of the $[m_{b'}, y_{b'}]$ plane to which a 5% accuracy measurement of D_{bb} will be sensitive. In this figure, we have assumed, as in the case of $D_{\gamma\gamma}$, that the future central experimental value of D_{bb} would be equal to its SM prediction. Here, the ranges of the parameters are $M \in [0.5, 6]$ TeV and $Y_{b_2} \in [0, 6]$. The lower boundary of the obtained region is determined by the $\Delta D_{bb} = 5\%$ condition, while the upper right one signals the passage to non-perturbativity. The upper left boundary delimits the zone where the observed bottom quark becomes too light, whereas the left boundary shows the lower limit $m_{b'} \lesssim 0.8$ TeV from direct searches of b-like VL partners.

Figs. 3.5 and 3.6 constitute our main prospective results and one can see that VLQ masses up to several TeV can be probed. With the precise measurement of $D_{\gamma\gamma}$ top partners with masses up to 5 TeV can be resolved in the loop, while exotic quarks (with $Q_{\rm em} = -\frac{4}{3}, \frac{5}{3}$) with masses as high as ~ 13 TeV are probed. Meanwhile, a 5% error in the measurement of D_{bb} can be sensitive to the presence of bottom-like VLQs with masses up to ~ 5 TeV. It is interesting to observe the complementarity between the two measurements: while with $D_{\gamma\gamma}$ one can efficiently resolve multi-TeV scale top and exotic VL partners, very heavy bottom VL partners can be probed through D_{bb}.

As expected, $D_{\gamma\gamma}$ is more sensitive to the VLQs with higher electric charge that occur in

models **B** and **C**. The mass limits above are much higher than the ones obtained from *direct* VLQ searches which, even at the HL–LHC, would only reach the 2 TeV range [123]. It may be surprising that the mass reach for the $q_{4/3}$'s of model **B** is higher than the one for the $q_{5/3}$'s of model **C**, but the explanation is simple. As it is visible from the figure, model **C** has a lower sensitivity on $m_{\rm VLQ}$ but for a lower coupling $y_{\rm VLQ}$. The relative smallness of the couplings in model **C** has two reasons: on the one hand, the Yukawa couplings for model **C** are suppressed by a Clebsch-Gordan factor of $1/\sqrt{2}$ and, on the other hand, the mass parameter M is larger in model **C** ($M \sim 28$ TeV) than in model **B** ($M \approx 25$ TeV), which leads to a smaller mixing between the two VLQs and hence a smaller coupling for the lighter ones to the Higgs boson.

We should also mention that, in the $D_{\gamma\gamma}$ discussion, for models **B** and **C**, the oblique parameters S and T are well within 2σ for all values of m and Y not excluded by non-perturbativity or by direct searches of VLQs. The situation is not as good in model **A**, where, for $m_{\rm VLQ} \leq 3$ TeV, S and T deviate by more than 3σ. However, since we are interested in knowing the highest possible VL mass that can be resolved in the $h \to \gamma\gamma$ loop, this is not a serious problem. The case of D_{bb} is similar to the one in model **A**: for $m_{b'} \gtrsim 3$ TeV, S and T are within 2σ from their central values.

3.6 Summary and Discussion

In this chapter, we have analyzed in the sensitivity of present and future LHC Higgs data to heavy vector–like partners of the top and bottom quarks that appear in many extensions of the SM, such as warped extra dimension scenarios and composite Higgs models. Working in an effective approach and considering several VLQ representations under the SM gauge group, we have thoroughly investigated three models that simultaneously address the longstanding puzzle of the forward–backward asymmetry $A^b_{\rm FB}$ at LEP and the recently observed deviation of the $pp \to t\bar{t}h$ production cross section at the LHC from its SM value. On the other hand, the three models fulfill all other experimental and theoretical constraints, in particular those coming from the electroweak precision measurements and from the LHC data in the Higgs decay and main production channels.

We have used the principle of minimality as a guide to select representative examples of the t' and b' multiplets, which should be related through their contributions to the highly constrained electroweak precision data and address the two aforementioned anomalies. Among the multiplets that involve t', b' and VLQs with exotic electric charge, one has, for example, t', b' singlets, $(q_{5/3}, t')$, $(b', q_{4/3})$ doublets and/or $(t', b', q_{4/3})$, $(q_{8/3}, q_{5/3}, t')$ triplets. These states mix with the SM top and bottom quarks and modify their Yukawa and gauge couplings. In addition, they would contribute to the loop induced $gg \to h$ production and $h \to \gamma\gamma$ decay processes. For instance, the mixing with the additional states in the bottom sector allows for a sufficiently large increase of the Zb_Rb_R coupling to explain the $A^b_{\rm FB}$ anomaly. At the same time, an enhancement of the $ht\bar{t}$ Yukawa coupling by a factor up to ~ 1.4 can occur, which would instead explain the $\sim 2\sigma$ apparent increase of the cross section $\sigma(pp \to t\bar{t}h)$ at the LHC. The rates for the loop induced processes would stay SM–like due to either small VLQ contributions or compensating effects between fermion mixing and loop contributions. Interestingly, the considered models predict the existence of VLQ with masses in the range 1–2 TeV that might be discovered at the current Run II of the LHC with a c.m. energy of 13 to 14 TeV.

In a second part of the chapter, we left aside the anomalies in the asymmetry $A^b_{\rm FB}$ and the cross section $\sigma(pp \to t\bar{t}h)$ and focused instead on the VLQ mass scale that could be

probed in the future by precision measurements in the Higgs sector at the high–luminosity LHC option. In this context, the ratios of the partial widths of the $h \to \gamma\gamma$ vs $h \to ZZ^*$ and $h \to b\bar{b}$ vs $h \to WW^*$ decay modes, $D_{\gamma\gamma}$ and D_{bb}, would play an important role as they can be determined with an accuracy at the level of, respectively, $\Delta D_{\gamma\gamma} = 1\%$ and $\Delta D_{bb} = 5\%$. Assuming the worst-case scenario in which the new physics scale would lie far above the electroweak scale and all other measured observables would appear to be SM-like, we have shown that, in some simplified VLQ frameworks, the precise measurement of the two decay ratios would probe VLQs with masses above the multi–TeV range. In particular, VLQs contributing to the the $h\gamma\gamma$ loop vertex or altering at tree–level the $hb\bar{b}$ coupling would be visible at the HL-LHC if the mass scales are ~ 5 TeV for top and bottom partners and up to ~ 13 TeV for VLQs with higher electric charge, such as $-\frac{4}{3}$ or $\frac{5}{3}$. These mass values are much higher than those attainable in direct VLQ searches at the LHC in the present [99–101] or even in the future [123, 124].

Chapter 4

Interpretations for the LHC Diphoton Excess: Two Higgs Doublets and Vector-Like Fermions

4.1 Generalities of Two Higgs Doublet Models

4.1.1 Introduction and Motivation

Out of the many possible extensions of the Standard Model, a particularly simple one is the scalar extension called the Two Higgs Doublet Model (2HDM). As their name suggests, the new feature of 2HDMs with respect to the SM is the presence of a second Higgs doublet, which has the same quantum numbers as its usual SM counterpart.

An appealing feature of 2HDMs is the fact that they preserve, at tree level, the value of the ρ parameter at 1:

$$\rho \equiv \frac{m_W^2}{c_W^2 m_Z^2} = 1. \tag{4.1}$$

In other words, 2HDMs do not violate custodial symmetry at tree level. For multiplets of general isospin I acquiring a VEV, this statement does not always apply. The particular cases for which tree-level custodial symmetry is preserved is the addition of multiplets with $I = 0, 1/2$ (i.e. singlets and doublets) acquiring a VEV.[1]

One of the main motivations of 2HDMs is the fact that they are a generalization of the scalar potential that one encounters in the Minimal Supersymmetric Standard Model (MSSM). In the MSSM, having only one scalar doublet would lead to an anomalous gauge symmetry: the fermionic superpartner of the Higgs boson, the higgsino, would render the $U(1)_Y$ and $SU(2)_L$ gauge symmetries anomalous. In order to cure this problem, one has to introduce a second Higgs doublet, the resulting extra higgsino cancelling the anomaly caused by the first one.

Introducing another Higgs doublet could also increase the amount of CP violation (CPV) with respect to the SM (in fact, this was the motivation behind the first proposal of 2HDMs [149]). A well studied problem of the SM is its inability to explain the mechanism that generates the baryon asymmetry in the universe (BAU), which proceeds through CP-violating interactions. More precisely, one has only one CP-violating phase in the SM, namely the one in the CKM matrix. Adding a second Higgs doublet increases the number of quartic

[1] The case of isospin multiplets with no VEV is trivial, since they do not contribute to ρ at tree level.

couplings in the scalar potential, some of which could carry a complex phase, thus increasing the amount of CPV and allowing for an explanation of the BAU.

Even if 2HDMs appear as simple extensions of the SM, they nevertheless possess a rich phenomenology. In the following, we briefly summarize the most important features of 2HDMs. For a more extensive review we refer instead, for example, to [150].

4.1.2 The Scalar Potential and The Mass Eigenstates

The two doublets are both color singlets and have a hypercharge equal to 1/2 [2], and they can be parametrized as follows:

$$H_{1,2} = \begin{pmatrix} \phi^+_{1,2} \\ \frac{1}{\sqrt{2}}\left(v_{1,2} + \rho_{1,2} + i\phi^Z_{1,2}\right) \end{pmatrix} \sim (1,2)_{-1/2}, \tag{4.2}$$

where v_i are the VEVs, ρ_i, ϕ_i^Z, and $\phi_i^\pm$ are, respectively, the neutral CP-even, neutral CP-odd, and charged interaction eigenstates. The most general potential that one can write for the two scalars is

$$\begin{aligned} V(H_1,H_2) = {} & m_{11}^2 H_1^\dagger H_1 + m_{22}^2 H_2^\dagger H_2 - \left(m_{12}^2 H_1^\dagger H_2 + \text{h.c.}\right) \\ & + \frac{\lambda_1}{2}\left(H_1^\dagger H_1\right)^2 + \frac{\lambda_2}{2}\left(H_2^\dagger H_2\right)^2 + \lambda_3\left(H_1^\dagger H_1\right)\left(H_2^\dagger H_2\right) + \lambda_4\left(H_1^\dagger H_2\right)\left(H_2^\dagger H_1\right) \\ & + \left[\frac{\lambda_5}{2}\left(H_1^\dagger H_2\right)^2 + \lambda_6\left(H_1^\dagger H_1\right)\left(H_1^\dagger H_2\right) + \lambda_7\left(H_2^\dagger H_2\right)\left(H_1^\dagger H_2\right) + \text{h.c.}\right]. \end{aligned} \tag{4.3}$$

Out of the total of 10 mass parameters and quartic couplings appearing in the scalar potential, m_{12}^2 and $\lambda_{5,6,7}$ are complex, whereas the others are real. In the following, we will not consider CP violation, meaning that we will take all the parameters to be real.

General 2HDMs feature tree-level flavour-changing neutral currents (FCNCs), which are absent in the SM and would impose very tight constraints on 2HDMs. The standard way to avoid this shortcoming of 2HDMs is to impose a $\mathbb{Z}_2$ symmetry under which, by convention, H_1 is odd and H_2 is even. Imposing such a symmetry results in the vanishing of λ_6 and λ_7 terms from the scalar potential in Eq. (4.3). Nevertheless, this symmetry is softly broken by the $-m_{12}^2 H_1 H_2$ term in the potential. The presence of this term is necessary in order to comply with direct searches of new Higgs states: setting it to 0 would imply that the extra scalars should be close in mass to the 125 GeV scalar, which would be in strong tension with experiments (see, for example, the bounds on MSSM heavy scalars derived in Ref. [151]).

Concerning the physical spectrum of 2HDMs, a straightforward degree-of-freedom counting shows that the mass eigenstates resulting after mixing are the following:

- two CP-even scalars, h and H, with H being, by convention, heavier than h. Throughout this thesis, we assume that h corresponds to the 125 GeV scalar discovered in 2012 at the LHC.
- one CP-odd scalar, A, and a neutral Goldstone boson, which becomes the longitudinal polarization of the Z boson;
- one electrically charged scalar, $H^\pm$, plus a charged Goldstone boson, which is eaten by the W boson.

[2] The convention used for hypercharge is $Y = Q - I^3$, where Q is the electric charge and I^3 the third component of weak isospin.

We now introduce the mass matrices for the three types of scalars, assuming that $\lambda_6 = \lambda_7 = 0$, as follows from imposing the $\mathbb{Z}_2$ symmetry that forbids tree level FCNCs. The mass matrix for the CP-even scalars is given by

$$\mathcal{M}^2_{\text{CP}-\text{even}} = \begin{pmatrix} m^2_{12}\frac{v_2}{v_1} + \lambda_1 v_1^2 & -m^2_{12} + \lambda_{345} v_1 v_2 \\ -m^2_{12} + \lambda_{345} v_1 v_2 & m^2_{12}\frac{v_1}{v_2} + \lambda_2 v_2^2 \end{pmatrix}, \tag{4.4}$$

with $\lambda_{345} \equiv \lambda_3 + \lambda_4 + \lambda_5$. By definition, α is the mixing angle that diagonalizes the CP-even mass matrix, the resulting eigenmasses being $m_h < m_H$. In the CP-odd and charged sectors, the mass matrices are similar:

$$\mathcal{M}^2_{\text{CP}-\text{odd}} = \frac{m_A^2}{v_1^2 + v_2^2}\begin{pmatrix} v_2^2 & -v_1 v_2 \\ -v_1 v_2 & v_1^2 \end{pmatrix}, \quad \mathcal{M}^2_{\pm} = \frac{m_\pm^2}{v_1^2 + v_2^2}\begin{pmatrix} v_2^2 & -v_1 v_2 \\ -v_1 v_2 & v_1^2 \end{pmatrix}, \tag{4.5}$$

where the physical pseudo- and charged scalar masses are given by, respectively:

$$m_A^2 = (v_1^2 + v_2^2)\left(\frac{m_{12}^2}{v_1 v_2} - 2\lambda_5\right), \quad m_\pm^2 = (v_1^2 + v_2^2)\left(\frac{m_{12}^2}{v_1 v_2} - \lambda_4 - \lambda_5\right). \tag{4.6}$$

As expected, both the CP-odd and charged scalar mass matrices have a null eigenvalue, which corresponds to the neutral and charged Goldstone bosons that are eaten by the Z and $W^\pm$ gauge bosons. Both mass matrices are diagonalized by a rotation of angle β, which can be expressed in its more familiar form as

$$\tan\beta \equiv t_\beta \equiv \frac{v_2}{v_1}. \tag{4.7}$$

The $\tan\beta$ parameter plays an important role in 2HDMs, as it determines, together with the angle α, the couplings of the physical scalars to the SM fermions and gauge bosons.

4.1.3 Scalar Couplings to Fermions and Gauge Bosons

As stated in the previous subsection, the transition from the interaction basis $(H_1, H_2)^T$ to the mass basis $(h, H, A, H^\pm)$ depends on two mixing angles, α and β. Throughout all this work we will assume to be in the so-called alignment limit, i.e. $\alpha \simeq \beta - \pi/2$. This is a reasonable assumption since, in most scenarios, as also shown in fig. 4.1, only small deviations from the alignment limit are experimentally allowed. In this limit, the h boson becomes completely SM-like. A second relevant implication is that the couplings of the second CP-even Higgs H with W and Z bosons are zero at tree level, being proportional to $\cos(\beta - \alpha)$ (analogous tree-level couplings for the A boson are forbidden by CP conservation). For a more detailed treatment of the alignment limit, we refer the reader to e.g. Refs. [152–156].

The couplings of the SM fermions with the Higgses are described by the following Lagrangian:

$$\begin{aligned} -\mathcal{L}^{\text{SM}}_{\text{Yuk}} = &\sum_{f=u,d,l} \frac{m_f}{v}\left[\xi_h^f \overline{f} f h + \xi_H^f \overline{f} f H - i\xi_A^f \overline{f}\gamma_5 f A\right] \\ &- \frac{\sqrt{2}}{v}\left[\overline{u}\left(m_u \xi_A^u P_L + m_d \xi_A^d P_R\right) d H^+ + m_l \xi_A^l \overline{\nu_L} l_R H^+ + \text{h.c.}\right], \end{aligned} \tag{4.8}$$

where the parameters $\xi^f_{h,H,A}$ depend the couplings of the SM fermions with the two doublets $H_{1,2}$. Motivated by the non-observation of flavour-changing neutral currents (FCNCs) we consider four different sets of $\xi^f_{h,H,A}$ corresponding to four 2HDM models, i.e.

Type-I, Type-II, lepton specific and flipped, featuring the absence of tree-level FCNCs [150]. The values of the ξ's for theses four flavour-conserving types of 2HDMs are listed below in table 4.1.

The Yukawa couplings of the SM fermions are dictated exactly by the choices of t_β and of the 2HDM type. In all four types, the up-type quarks couple to H_2. In order to couple an SM fermion to H_1, the right-handed said fermion should be odd under the $\mathbb{Z}_2$ symmetry under which H_1 is odd as well. For Type-I, no SM fermions couple to H_1, whereas for type-II, down-type quarks and leptons couple to H_1. A lepton-specific 2HDM features only leptons coupling to H_1, while in a flipped 2HDM only the down-type quarks couple to H_1.

	Type I	Type II	Lepton-specific	Flipped
ξ_h^u	$c_\alpha/s_\beta \to 1$	$c_\alpha/s_\beta \to 1$	$c_\alpha/s_\beta \to 1$	$c_\alpha/s_\beta \to 1$
ξ_h^d	$c_\alpha/s_\beta \to 1$	$-s_\alpha/c_\beta \to 1$	$c_\alpha/s_\beta \to 1$	$-s_\alpha/c_\beta \to 1$
ξ_h^l	$c_\alpha/s_\beta \to 1$	$-s_\alpha/c_\beta \to 1$	$-s_\alpha/c_\beta \to 1$	$c_\alpha/s_\beta \to 1$
ξ_H^u	$s_\alpha/s_\beta \to -t_\beta^{-1}$	$s_\alpha/s_\beta \to -t_\beta^{-1}$	$s_\alpha/s_\beta \to -t_\beta^{-1}$	$s_\alpha/s_\beta \to -t_\beta^{-1}$
ξ_H^d	$s_\alpha/s_\beta \to -t_\beta^{-1}$	$c_\alpha/c_\beta \to t_\beta$	$s_\alpha/s_\beta \to -t_\beta^{-1}$	$c_\alpha/c_\beta \to t_\beta$
ξ_H^l	$s_\alpha/s_\beta \to -t_\beta^{-1}$	$c_\alpha/c_\beta \to t_\beta$	$c_\alpha/c_\beta \to t_\beta$	$s_\alpha/s_\beta \to -t_\beta^{-1}$
ξ_A^u	t_β^{-1}	t_β^{-1}	t_β^{-1}	t_β^{-1}
ξ_A^d	$-t_\beta^{-1}$	t_β	$-t_\beta^{-1}$	t_β
ξ_A^l	$-t_\beta^{-1}$	t_β	t_β	$-t_\beta^{-1}$

Table 4.1 – Couplings of the Higgses to the SM fermions as a function of the angles α and β, in the alignment limit where $(\beta - \alpha) \to \pi/2$.

4.2 A Diphoton Resonance at 750 GeV?

At the end of 2015, it was reported that the approximately 4 fb^{-1} of data, delivered in LHC run with a center of mass energy of 13 TeV, hinted at the presence of a resonance that decays into two photons, with a mass of about 750 GeV and a width of ~ 50 GeV [157, 158]. The local significance of this signal was only at the 3σ level in the case of the ATLAS collaboration and slightly less for the CMS collaboration. Hence, it was likely that this excess of data was simply yet another statistical fluctuation which would be washed away with more data. Indeed, this was the case: the 2016 data discarded the resonance as a statistical fluctuation [159, 160]. Nevertheless, in the absence of any firm sign of the long awaited new physics beyond the SM, it was interesting to contemplate at that time that the effect was indeed due to a new resonance. This is, in fact, the subject of this chapter: our interpretation for the 750 GeV "resonance", as outlined in Ref. [161].

Let us start by briefly sketching the various possibilities for such a resonance and considering its spin–parity quantum numbers. The observation of the $\gamma\gamma$ signal rules out the option that it comes from the decay of a spin–1 particle by virtue of the Landau–Yang theorem [162, 163]. This leaves the spin 0 and spin ≥ 2 possibilities. A graviton–like spin–2 is extremely unlikely since it has universal couplings and it should have also decayed into other states such as WW, ZZ, dileptons and dijets which have not been observed up to very high masses [164, 165]. The most likely possibility for the resonance particle is thus to have spin–0.

Furthermore, the resonance should be Higgs–like and couple only very weakly to light quarks as, if produced in $q\bar{q}$ annihilation, it should have already been observed at the

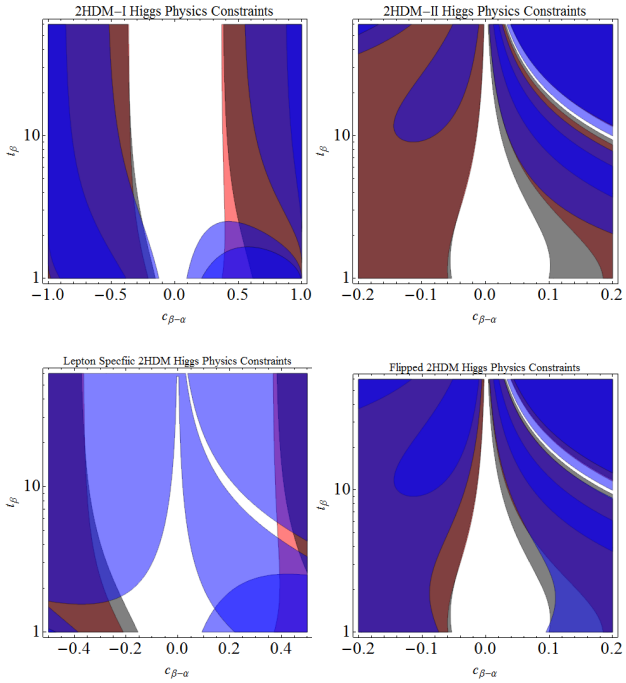

Figure 4.1 – Constraints in the $(c_{\beta-\alpha}, t_\beta)$ plane on the four types of flavour-conserving 2HDMs, coming from Higgs signal strength measurements [1, 2]. The signal strengths we have considered are $\mu_{\gamma\gamma}$ (red), $\mu_{ZZ,WW}$ (grey), and $\mu_{bb,\tau\tau}$ (blue).

first LHC run with $\sqrt{s} = 8$ TeV and 20 fb^{-1} data. Indeed, for a 750 GeV resonance, just considering naively the $q\bar{q}$ parton luminosities for a given c.m. energy, there should be an increase of only a factor of 2.5 for the production rate when moving from 8 to 13 TeV c.m. energy [166]. Instead, if the resonance is produced in gg fusion, the jump in cross section would be a factor of 4.5 so that the collected data sets at $\sqrt{s} = 8$ and 13 TeV would be equivalent. Note that there was an ATLAS search for a two-photon scalar resonance performed at $\sqrt{s} = 8$ TeV [167] but it did not extend beyond the scale of 600 GeV. CMS searched also for diphoton resonances [168] and observed a slight excess of about 2σ at a mass of 750 GeV. The present diphoton excess is, thus, not a complete surprise.

In this chapter, we explore the possibility that the diphoton events originate from the decays of the heavy neutral CP–even and CP–odd Higgs particles that are present in two Higgs doublet models [150, 169] and, in particular, in their minimal supersymmetric incarnation, the MSSM [169, 170]. We show that to achieve such a strong diphoton signal, additional particles should contribute to the loop induced production and decay processes and we investigate some scenarios with vector–like quarks and leptons that occur in many extensions of the Standard Model (SM) [78, 109, 171]. We show that indeed, vector–like leptons can account for the observed signal without altering the properties of the lightest h boson.

4.3 The Diphoton Rate in 2HDMs and the MSSM

As presented in the previous section, the 2HDM is a straightforward extension of the SM that involves additional Higgs states. Another theory predicting new scalars is the minimal supersymmetric extension of the SM (MSSM), whose scalar sector is a type II 2HDM, but

with the interesting feature that supersymmetry imposes strong constraints on the parameters and only two of them, e.g. $\tan\beta$ and m_A, are independent. This is true not only at tree level but approximately also at higher orders if the constraint $m_h = 125$ GeV, which fixes the important radiative corrections to the Higgs sector [170], is enforced; this is the so–called hMSSM discussed recently [151, 172]. Because the LHC Higgs data indicate that h state is SM–like [173] and that the pseudoscalar Higgs boson should be rather heavy [6, 7], one is also in the so–called decoupling limit, where one has $\cos(\beta-\alpha) \approx 0$ and $m_H \approx m_{H^\pm} \approx m_A \gg m_Z$. This simplifies considerably the phenomenology of the model.

In this section, we consider both the MSSM in the decoupling limit and the 2HDMs of type I and II in the alignment limit; a departure from these limits (in particular alignment) by 10% , i.e. being close to the upper bound $\cos^2(\beta-\alpha) \approx 0.1$ indicated by LHC Higgs data [173] does not significantly change our discussion. In the latter case, we assume in addition that the CP–even H and CP–odd A states are approximately degenerate in mass, $m_A \approx m_H$, as is the case in the MSSM. Hence, the 750 GeV diphoton resonance consists of both the H and A bosons. As motivated below, we specialize in the low $\tan\beta$ region, and more precisely to $\tan\beta \approx 1$, which allows for strong Yukawa couplings of the top quark. The possibility of extremely large Yukawa for bottom quarks requires large $\tan\beta$ values (for type II 2HDMs), $\tan\beta \gtrsim 30$ and even 50, which for $m_\Phi \approx 750$ GeV, $\Phi = H, A$, are excluded by the $\Phi \to \tau^+\tau^-$ searches performed at the run I of the LHC [6, 7]. Hence, only the top quark Yukawa coupling is kept in our following discussion and all other Yukawa couplings are considered to be negligible.

Let us now discuss the decays of the two Higgs resonances. In the configuration that we have chosen, with large Higgs masses and low $\tan\beta$ values, the only relevant tree level decay of the $\Phi = H, A$ bosons is into top quark pairs with a partial width [128]

$$\Gamma(\Phi \to t\bar{t}) = \frac{3G_F m_t^2}{4\sqrt{2}\pi} (\xi_\Phi^t)^2 \, m_\Phi \, \beta_t^{p_\Phi} \tag{4.9}$$

where $\beta_t = (1-4m_t^2/m_\Phi^2)^{1/2}$ is the quark velocity and $p_\Phi = 3\,(1)$ for the CP–even (odd) Higgs boson. In principle, the decays of the two resonances into two photons also proceeds through the top–quark loop only (for the CP–even H state, we ignore the W–loop contribution; there are also small charged Higgs contributions to be discussed shortly), but we allow for additional contributions of new fermions that we explicit later. The partial decay widths are given by [128, 169]

$$\Gamma(\Phi \to \gamma\gamma) = \frac{G_F \alpha^2 m_\Phi^3}{128\sqrt{2}\pi^3} \left| \frac{4}{3} \xi_\Phi^t A_{1/2}^\Phi(\tau_t) + \mathcal{A}_{\rm new}^\Phi \right|^2 \tag{4.10}$$

The form factors $A_{1/2}^\Phi(\tau_f)$ which depend on the variable $\tau_f = m_\Phi^2/4m_f^2$ are the only place in which the H and A states behave differently. They are shown in Fig. 4.2. While the amplitudes are real for $m_\Phi \leq 2m_f$, they develop an imaginary part above the kinematical threshold. At low Higgs masses compared to the internal fermion mass, $m_\Phi \ll 2m_f$, the amplitudes for a scalar and a pseudoscalar[3] states reach constant but different values $A_{1/2}^H(\tau_f) \to 4/3$ and $A_{1/2}^A(\tau_f) \to 2$ (in fact these limits are attained quickly as soon as $m_\Phi \lesssim 2m_f$ and are almost exact for $m_f \gtrsim m_\Phi$). The maximal values of the amplitudes occur at the kinematical threshold $m_\Phi = 2m_f$, where one has $\mathrm{Re}(A_{1/2}^H) \sim 2$ and $\mathrm{Re}(A_{1/2}^A) \sim 5$ for the real parts. For a resonance with a mass $m_\Phi \approx 700$ GeV, one has $\tau_t \approx 4$ for the top quark

[3]Note that when including the QCD corrections to the quark loops, there is a Sommerfeld enhancement of the amplitudes near threshold which is significant in the case of the pseudoscalar Higgs boson. Outside this threshold the QCD corrections are very small; see Ref. [131].

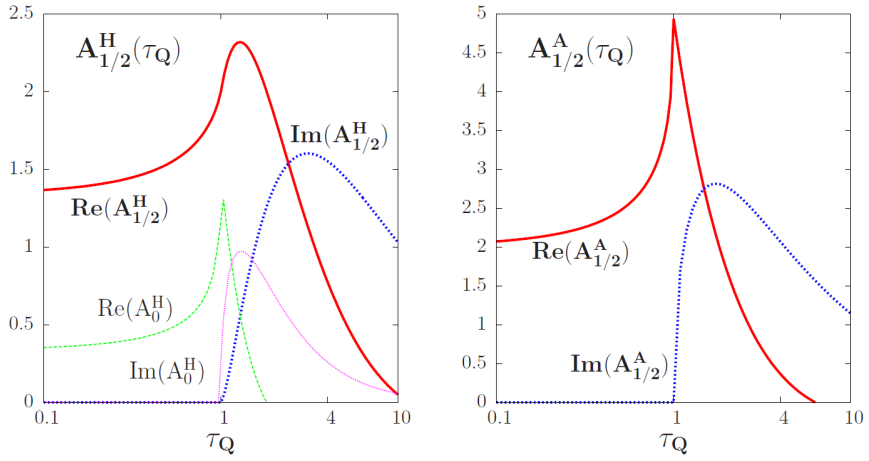

Figure 4.2 – The form factors $A^{\Phi}_{1/2}$ of the Higgs–gg and Higgs–$\gamma\gamma$ fermion loops in the case of the CP–even (left) and CP–odd (right) Higgs particles as a function of $\tau_f = m^2_{\Phi}/4m^2_f$. The smaller form factor for spin–0 particle exchange in the H case is shown for comparison.

and this leads to values for the form factors of $\mathrm{Re}(A^H_{1/2}) \approx \frac{3}{4}, \mathrm{Im}(A^H_{1/2}) \approx \frac{3}{2}$ in the CP–even case and $\mathrm{Re}(A^A_{1/2}) \approx \frac{1}{3}, \mathrm{Im}(A^A_{1/2}) \approx 2$ in the CP–odd case.

Assuming that there are no new physics contributions to the $\Phi\gamma\gamma$ loop besides that of the top quark, the branching ratio of the decay $\Phi \to \gamma\gamma$ is simply given by

$$\mathrm{BR}(\Phi \to \gamma\gamma) \simeq \frac{\Gamma(\Phi \to \gamma\gamma)}{\Gamma(\Phi \to t\bar{t})} = \frac{\alpha^2}{54\pi^2} \frac{m^2_{\Phi}}{m^2_t} \frac{|A^{\Phi}_{1/2}|^2}{\beta^{p_{\Phi}}_t} \approx 10^{-7} \frac{m^2_{\Phi}}{m^2_t} \frac{1}{\beta^{p_{\Phi}}_t} \tag{4.11}$$

and does not depend on $\tan\beta$. For $m_{\Phi} \approx 750$ GeV, one obtains fractions $\mathrm{BR}(A \to \gamma\gamma) \approx 7 \times 10^{-6}$ and $\mathrm{BR}(H \to \gamma\gamma) \approx 6 \times 10^{-6}$ and total decay widths, with $\Gamma^{\Phi}_{\rm tot} \sim \Gamma(\Phi \to t\bar{t})$, of $\Gamma^H_{\rm tot} \approx 32\ \mathrm{GeV}/\tan^2\beta$ and $\Gamma^A_{\rm tot} \approx 35\ \mathrm{GeV}/\tan^2\beta$ [133, 174]. To arrive at a total width of ≈ 50 GeV as experimentally observed, one thus needs $\tan\beta \approx 1$. Hence, besides requiring the equality[4] $m_H \approx m_A$, one should not allow for new H/A decay channels in order to not increase this total width. In fact, even if the total width issue could be ignored, $\tan\beta$ values much smaller than unity, say $\tan\beta \lesssim 1/3$, should be avoided in order to keep a perturbative top quark Yukawa coupling. We will thus stick to $\tan\beta \approx 1$ in our analysis.

In a similar way, the cross section for Φ production in the dominant gluon–gluon fusion process is proportional to the Higgs decay width into two gluons which is given by [128, 169]

$$\sigma(gg \to \Phi) \propto \Gamma(\Phi \to gg) = \frac{G_F \alpha^2_s m^3_{\Phi}}{64\sqrt{2}\pi^3} \left| \xi^t_{\Phi} A^{\Phi}_{1/2}(\tau_t) + \mathcal{A}^{\Phi}_{\rm new} \right|^2 \tag{4.12}$$

First, one notices that the production cross section at $\sqrt{s} = 13$ TeV for a SM–like Higgs boson of mass $m_H = 750$ GeV is $\sigma(H_{\rm SM}) \approx 0.85$ pb [151, 172] and that in our case, one has $\sigma(H)/\sigma(H_{\rm SM}) = \cot^2\beta$ and $\sigma(A)/\sigma(H_{SM}) = \cot^2\beta \times |A^A_{1/2}/A^H_{1/2}|^2 \approx 2\cot^2\beta$ as the form factor is different in the CP–odd case. One obtains then for the cross section times branching fraction when the two channels are added (the numbers are for the hMSSM),

$$\sum_{\Phi} \sigma(gg \to \Phi) \times \mathrm{BR}(\Phi \to \gamma\gamma) \approx 1.5 \times 10^{-2} \cot^2\beta\ [\mathrm{fb}] \tag{4.13}$$

[4] Note that if we assume the hMSSM with $m_A \approx 750$ GeV, this leads $m_H \approx 765$ GeV for $\tan\beta \approx 1$ [151,172]; in a 2HDM, the H/A masses can also be different. A significant $m_H - m_A$ difference will make the observed resonance wider, which is not our interest here, so we assume equal masses also in 2HDMs.

to be compared with a cross section of $\mathcal{O}(10\,\text{fb})$ observed by the ATLAS collaboration.

Thus, for $\tan\beta \approx 1$, we are more than two orders of magnitude away from the diphoton signal and, even if we allow for $\tan\beta \approx 1/3$, we are still more than an order of magnitude below. Very large additional contributions are thus needed.

An important remark is that if the enhancement of the diphoton signal has to come from the production cross section, then we would have a large rate for $gg \to \Phi \to t\bar{t}$ that is constrained from the search of resonances decaying into top quark pairs at the 8 TeV LHC. Indeed a 95% confidence limit of $\sigma(gg \to \Phi) \times \text{BR}(\Phi \to t\bar{t}) \lesssim 1$ pb [175,176] has been set and, since at this energy one has $\sigma(gg \to H+A) \approx 0.5\cot^2\beta$ pb and $\text{BR}(\Phi \to t\bar{t}) \approx 1$, $\tan\beta$ cannot take values much smaller than unity. This leads to the important conclusion that the two orders of magnitude enhancement needed to accommodate the observed diphoton resonance in our context should essentially come from the $\Phi \to \gamma\gamma$ decay.

Nevertheless, let us briefly consider slight departures from our $\tan\beta \simeq 1$ choice. For instance, $\tan\beta \lesssim 1/\sqrt{2}$ would violate the limit from the search of $t\bar{t}$ resonances at the $\sqrt{s} = 8$ TeV LHC, while values $\tan\beta \gtrsim \sqrt{2}$ would reduce by more than a factor of two the Φ total decay width so that the possibility $\Gamma_\Phi \approx 45$ GeV hinted for by ATLAS cannot be explained anymore (this would also call for an additional enhancement of the $gg \to \Phi \to \gamma\gamma$ rate by a factor $\gtrsim 2$). Hence, $\tan\beta$ values close to unity are strongly favored in our scenario. Note again that for such values of $\tan\beta$, the b–quark and τ–lepton Yukawa couplings are so small that there is no difference in practice between Type I and II scenarios, as in both cases, the t–quark Yukawa coupling is the same.

Although obviously unlikely, we nevertheless considered the various additional contributions that can affect the $\Phi\gamma\gamma$ and Φgg loops in the minimal versions of 2HDMs and the MSSM and checked that such a huge enhancement cannot be obtained (this is clearly also the case for the lightest h boson as it has recently been discussed in Ref. [118]).

A first contribution to the $\Phi\gamma\gamma$ loops which can be considered is that of a charged Higgs boson in the case of H (because of CP–invariance there is no AH^+H^- coupling) given by $\mathcal{A}^H_{H^\pm} = g_{HH^+H^-}(m_W^2/m^2_{H^\pm}) \times A_0^H(\tau_{H^\pm})$. The form factor A_0^H is smaller than the fermionic one, as shown in Fig. 4.2. In the MSSM, as $m_{H^\pm} \approx m_H$ and $g_{HH^+H^-} = \mathcal{O}(1)$, the contribution is negligible. Even in a general 2HDM, although $g_{HH^+H^-}$ is not fixed and can be made relatively large, the $H^\pm$ contributions are also very small[5].

In the case of the MSSM, additional contributions are provided by supersymmetric particles running in the loops. The contributions of the charginos in $\Phi \to \gamma\gamma$ are in general small if we are above the $m_\Phi \gtrsim 2m_{\chi^\pm}$ thresholds that are needed to keep the total decay widths of the resonances small. But also for small chargino masses, $\text{BR}(\Phi \to \gamma\gamma)$ cannot be enhanced by more than a few ten percent[6]. There are also contributions of sleptons and squarks to the CP–even $H \to \gamma\gamma$ decay and squarks to the $gg \to H$ production; the CP–odd A state does not couple to identical sfermions and there is no contribution at lowest order. Here again, the Higgs–sfermion couplings are not proportional to sfermions masses and the contributions, $\mathcal{A}^H_{\tilde{f}} \propto \sum_{\tilde{f}_i} g_{H\tilde{f}_i\tilde{f}_i}/m^2_{\tilde{f}_i} \times A_0^H(\tau_{\tilde{f}})$, are damped by powers of $m^2_{\tilde{f}_i}$ leading to small loop contributions for sufficiently heavy sfermions. This is particularly true in the slepton case where the dominant contribution due to light stau's cannot be enhanced by strong

[5]For $m_{H^\pm} \approx 160$ GeV which satisfies the constraints set at the 8 TeV LHC [107], the form factor is small and negative giving a destructive interference with the top contributions. Instead, the contribution can be increased by sitting close to the $m_{H^\pm} = \frac{1}{2}m_\Phi$ threshold so that A_0^H reaches it maximal value, $\text{Re}(A_0^H) \sim 1.5$ and $\text{Im}(A_0^H) \sim 1$ for $\tau \sim 1$. Still these values are too small and the damping factor $m_W^2/m^2_{H^\pm}$ too strong and even for extremely large $g_{HH^+H^-}$, the contributions stay modest.

[6]For the choice of SUSY parameters $\tan\beta = 1, M_2 = -\mu = 200$ GeV which leads to $\chi_1^\pm$ with masses close to the experimental bounds $m_{\chi_1^\pm} \approx 100$ GeV [107], and maximally coupled to the H/A states, one makes only a 25% and 10% change of the $H \to \gamma\gamma$ and $A \to \gamma\gamma$ branching ratios respectively [133,174].

couplings for the low $\tan\beta$ values that we are considering here.

Finally, squarks and particularly relatively light top squarks can make significant contributions to $H \to \gamma\gamma$ and $gg \to H$. In the MSSM, however, for the low $\tan\beta$ values that we are considering, the stops (which contribute to the radiative corrections that enhance the lighter h boson mass) should be extremely heavy for $m_h = 125$ GeV to be reached. Even if by some means one can accommodate this mass values with light stop (e.g. by invoking an additional singlet–like Higgs as in the NMSSM or by incorporating some additional particles to increase the radiative corrections to the h mass) it is difficult to increase $\sigma(gg \to H) \times \text{BR}(H \to \gamma\gamma)$ significantly[7]. In fact, in general, when the SUSY contributions are large, they are also large in the case of the lightest h boson [118] which is unacceptable as its couplings have been measured to be SM–like.

Therefore, it is difficult to enhance the production cross section and the $\gamma\gamma$ decay branching ratios of the MSSM H and A bosons to a level close to what is experimentally observed, even if extreme configurations for the superparticle masses and couplings are chosen. Other more radical measures are needed and we discuss them now.

4.4 Introducing Vector–Like Quarks and Leptons

In order to increase significantly the Higgs couplings to gluons and/or photons, one could consider the contributions of new heavy fermions to the triangular loops[8]. These fermions should have vector–like couplings to the electroweak gauge bosons in order to avoid generating their masses through the Higgs mechanism only and then cope with the the LHC Higgs data[9]. Vector–like fermions appear in many extensions of the SM and recent discussions have been given in Refs. [78, 109, 171]. In our analysis, we do not rely on any specific model (as e.g. Ref. [179]) and simply adopt an effective approach in which the properties of these fermions are adjusted in order to fit our purpose.

In addition to the two Higgs doublets, for which we still assume the alignment limit and the mass equality $m_H \approx m_A$, we first consider vector–like quarks (VLQs) with the following minimal Lagrangian describing their Yukawa couplings in the interaction basis:

$$
\begin{aligned}
-\mathcal{L}_{\rm VLQ} = \Bigg\{ & \frac{y_L^b}{\sqrt{2}} \begin{pmatrix} 0 \\ v_1 + \rho_1 + i\phi_1^Z \end{pmatrix} \overline{\begin{pmatrix} t' \\ b' \end{pmatrix}}_L b''_R + \frac{y_L^t}{\sqrt{2}} \begin{pmatrix} v_2 + \rho_2 - \phi_2^Z \\ 0 \end{pmatrix} \overline{\begin{pmatrix} t' \\ b' \end{pmatrix}}_L t''_R + \{\text{L} \leftrightarrow \text{R}\} \\
& + m_1 \overline{\begin{pmatrix} t' \\ b' \end{pmatrix}}_L \begin{pmatrix} t' \\ b' \end{pmatrix}_R + m_2\, \overline{t''_L} t''_R + m_3\, \overline{b''_L} b''_R \Bigg\} + \text{h.c.}\,, \qquad (4.14)
\end{aligned}
$$

where we have coupled the top- and bottom-like VLQs similarly to the SM top and bottom quarks in a Type-II 2HDM, i.e. to the H_2 and H_1 doublets, respectively. Such representations of the VLQs make possible the presence of Yukawa couplings invariant under the SM gauge symmetry, hence including also terms mixing the VLQs with SM quarks. However, this mixing would represent only a higher order correction to the main enhancement effect of interest; we have therefore omitted for simplicity such Yukawa couplings in the Lagrangian

[7] For instance, assuming $m_{\tilde{t}_1} \approx m_{\tilde{t}_2} \approx \frac{1}{2} m_H \approx 350$ GeV in order to maximize the A_0^H amplitude, one obtains a factor of ≈ 2 enhancement of $\sigma(gg \to H) \times \text{BR}(H \to \gamma\gamma)$. Instead, for a trilinear stop coupling $A_t \approx 2$ TeV that strongly enhances the coupling $g_{H\tilde{t}_1\tilde{t}_1} \propto m_t A_t$, one obtains a more modest change [133, 174].

[8] One can of course consider also the introduction of scalars, such as doubly charged Higgs bosons from see-saw mechanisms [177, 178] for instance, but we will not consider this option here.

[9] The easiest option would have been the introduction of a fourth generation of fermions, which could have increased both the $gg \to H/A$ cross section and the $H/A \to \gamma\gamma$ decay rates by an order of magnitude each. This is nevertheless ruled out by the observation of the light h state with SM–like couplings [48–50].

of eq. (4.14). The key point here is that, to fulfill gauge invariance, at least two vector-like multiplets need to be introduced in order to generate direct VLQ Yukawa couplings that are not suppressed by SM–VLQ mixing angles. This allows to have significant VLQ loop contributions.

Similarly to VLQs, one can introduce Vector–Like leptons (VLLs) in the model. The VLLs are subject to weaker direct mass bounds [180–182] than the ones of order 1 TeV on the VLQ masses [79, 100, 183, 184]. For the particle content, an interesting possibility would be to introduce several replica of vector–like lepton doublets and singlets

$$\begin{pmatrix} \ell'^{-} \\ \ell^{=} \end{pmatrix}_{L/R} , \ \ell''^{-}_{L/R} , \ \ell'^{=}_{L/R}, \tag{4.15}$$

which will couple to the 2HDM Higgs states exactly as shown in the Lagrangian of eq. (4.14) with the replacement $t', t'' \to \ell'^{-}, \ell''^{-}$ and $b', b'' \to \ell^{=}, \ell'^{=}$. The reason to consider this specific pattern for the $\mathrm{SU(2)_L}$ doublet, that includes a singly and a doubly charged lepton, is that it allows both its components to contribute to the diphoton triangular loop.

Based on the particle content of eqs. (4.14)–(4.15) and recalling that $\alpha = \beta - \frac{\pi}{2}$ (alignment limit) is the mixing angle between the CP-even interaction eigenstates ρ_1 and ρ_2, one can express the new fermion contributions to the loop induced $\Phi = H, A$ couplings to photons and gluons in the following form:

$$\mathcal{A}^{\Phi}_{\mathrm{VLF}}(gg) \ \propto \ \mathcal{A}^{\Phi}_{\mathrm{top}}(gg) + N_f^{\mathrm{VLQ}} \left(\cot\beta \sum_{i=1}^{2} \frac{v g^{\Phi}_{t_{ii}}}{m_{t_i}} A^{\Phi}_{1/2}(\tau_{t_i}) \pm \tan\beta \sum_{i=1}^{2} \frac{v g^{\Phi}_{b_{ii}}}{m_{b_i}} A^{\Phi}_{1/2}(\tau_{b_i}) \right) \tag{4.16}$$

$$\begin{aligned} \mathcal{A}^{\Phi}_{\mathrm{VLF}}(\gamma\gamma) \ \propto \ & \mathcal{A}^{\Phi}_{\mathrm{top}}(\gamma\gamma) + \mathcal{A}^{\Phi}_{W}(\gamma\gamma) + N_f^{\mathrm{VLF}} \left(\cot\beta \ \sum_{u} N_c^u Q_u^2 \sum_{i=1}^{2} \frac{v g^{\Phi}_{u_{ii}}}{m_{u_i}} A^{\Phi}_{1/2}(\tau_{u_i}) \right. \\ & \left. \pm \ \tan\beta \ \sum_{d} N_c^d Q_d^2 \sum_{i=1}^{2} \frac{v g^{\Phi}_{d_{ii}}}{m_{d_i}} A^{\Phi}_{1/2}(\tau_{d_i}) \right), \end{aligned} \tag{4.17}$$

where the "+" sign corresponds to $\Phi = A$, while the "−" sign corresponds to $\Phi = H$. In order to describe generically either VLQ or VLL, we introduce sums over u (d) to account for fermions with different electric charges coupling to H_2 (H_1), while $i = 1, 2$ indicate the heavy fermion mass eigenstates. For up–type and down–type vector–like leptons, the mass eigenvalues m_{u_i, d_i} are obtained from bidiagonalizing the mass matrices

$$\mathcal{M}_u = \begin{pmatrix} m_1 & \frac{1}{\sqrt{2}} v y^u_L \sin\beta \\ \frac{1}{\sqrt{2}} v y^u_R \sin\beta & m_2 \end{pmatrix}, \quad \mathcal{M}_d = \begin{pmatrix} m_1 & \frac{1}{\sqrt{2}} v y^d_L \cos\beta \\ \frac{1}{\sqrt{2}} v y^d_R \cos\beta & m_3 \end{pmatrix}, \tag{4.18}$$

in the $(\ell'^{-}, \ell''^{-})_{L/R}$ and $(\ell^{=}, \ell'^{=})_{L/R}$ bases respectively. The $g^{\Phi}_{u_{ii}, d_{ii}}$ denote the diagonal elements of the mass basis Yukawa coupling matrix of $\Phi = H, A$ to the VL states. The aforementioned coupling matrices are obtained from the biunitary transformations of

$$y_u = \frac{\sin\beta}{\sqrt{2}} \begin{pmatrix} 0 & y^u_L \\ \pm y^u_R & 0 \end{pmatrix}, \quad y_d = \frac{\cos\beta}{\sqrt{2}} \begin{pmatrix} 0 & y^d_L \\ \pm y^d_R & 0 \end{pmatrix}, \tag{4.19}$$

with "+" for the h, H states and "−" for the A state. As usual, N_c and Q_f are the color and electric charges whereas N_f^{VLF} stands for the number of vector–like fermion families (taken here, for simplicity, decoupled one from another). The top quark contributions to the loops are simply given by $\mathcal{A}^{H,A}_{\mathrm{top}}(\gamma\gamma) = \frac{4}{3} \cot\beta A^{\Phi}_{1/2}(\tau_t)$ and $\mathcal{A}^{H,A}_{\mathrm{top}}(gg) = \cot\beta A^{\Phi}_{1/2}(\tau_t)$. Also, we have introduced a W contribution to the $\gamma\gamma$ amplitude, which, in the decoupling limit, is zero in

the case of the H state (the AWW vertex is forbidden at tree level by CP-invariance), but not for the lighter h state.

In the narrow width approximation, fully justified for resonances with total decay width of about 5% of their masses, the production rates $\sigma(gg \to \Phi \to \gamma\gamma)$ are simply proportional to the product of the two amplitudes squared, $\sigma \times \text{BR} \propto |\mathcal{A}^{\Phi}(\gamma\gamma)|^2 \times |\mathcal{A}^{\Phi}(gg)|^2$.

An important requirement for the vector–like content contributing to the Φgg and $\Phi\gamma\gamma$ couplings is to not alter significantly the absolute values of the loop induced couplings of the lightest h state with a mass of 125 GeV, which has already been observed to be approximately SM–like [173]. Indeed, the amplitudes for h are almost exactly the same as those of H given by eqs. (4.16)–(4.17), but with a non–zero W loop contribution, $\mathcal{A}^h_W(\gamma\gamma) \simeq -8.3$, included in the diphoton case. An important difference though is that one has to make the replacement $\pm \tan\beta \to 1$ and $\cot\beta \to 1$.

For the values of the parameter β that we are considering and for $\left(\sum A^h_{1/2}(\tau_{\ell_i^-}) g^h_{\ell_{ii}^-}/m_{\ell_i^-}\right) \times \left(\sum A^h_{1/2}(\tau_{\ell_i^=}) g^h_{\ell_{ii}^=}/m_{\ell_i^=}\right) < 0$, a different sign holds between the ℓ_i^- and $\ell_i^=$ eigenstate contributions to the h-diphoton loop. Such a sign configuration can generally be accommodated by controlling the VL Yukawa couplings and masses in the interaction basis. With a suitable choice of parameter values, this configuration could lead to an approximate cancellation in the $h \to \gamma\gamma$ loop between the singly and doubly charged contributions, leading to a SM-like $h\gamma\gamma$ effective coupling. Although efficiently keeping under control the $h\gamma\gamma$ coupling, this configuration entails an important isospin symmetry breaking, leading to an unacceptably large value for the Peskin-Takeuchi T parameter [102].

Another way to cope with the $h\gamma\gamma$ constraint is to choose one of the interaction basis Yukawa couplings close to zero, i.e. $y_R^{u,d} \simeq 0$ in eqs. (4.18) and (4.19), which strongly suppresses the VLL contributions to the $h\gamma\gamma$ loop. More precisely, for $\Phi = h, H$, one has

$$\sum_{i=1}^{2} \frac{g^{\Phi}_{u_{ii},d_{ii}}}{m_{u_i,d_i}} = \partial_v \log\det \mathcal{M}_{u,d} \simeq 0 \tag{4.20}$$

for $y_R^{u,d} \simeq 0$ (for $\Phi = A$, the sum in eq. (4.20) is null for any value of $y_R^{u,d}$). This means that the contribution to $\Phi \to \gamma\gamma$ of a VLL sector will be proportional to $A^{\Phi}_{1/2}(\tau_{u_1,d_1}) - A^{\Phi}_{1/2}(\tau_{u_2,d_2})$, which, for $\Phi = h$, translates into almost no VLL contribution to the diphoton loop, since $m_{u_i,d_i} > m_h$ and thus both form factors reach their asymptotic value, $A^h_{1/2}(\tau_{u_1,d_1}) \simeq A^h_{1/2}(\tau_{u_2,d_2}) \simeq \frac{4}{3}$. However, for H and A, the difference between the two $A^{\Phi}_{1/2}$-factors is in general non-zero and can be maximized if we take one mass at the threshold, $m_{u_1,d_1} \simeq \frac{1}{2} m_{\Phi}$, and the other in the asymptotic region, $m_{u_2,d_2} > m_{\Phi}$, thus leading to a sizable impact in the H, A diphoton loop.

In the case of VLQs, this mechanism is equally efficient in suppressing their contribution to the hgg and $h\gamma\gamma$ loops. However, due to the experimental limits on the VLQ masses($\gtrsim$ 800 GeV) and thus greater than m_{Φ}, such a mechanism would also suppress their contribution to the H, A diphoton loops, since both form factors would reach their asymptotic values (see previous paragraph). Therefore, we do not consider VLQs in the following.

We present now some numerical results that can be obtained in a specific model. We consider a particle spectrum with six identical copies[10] of the VLL multiplets presented in

[10]It is possible that the number of VLL families can be reduced, for same order diphoton rates, if non-vanishing Yukawa couplings between the different families are considered. Note also that diphoton rates around the femtobarn can be reached through the H production with only three VLL generations, in the specific case where negative relative-sign VLL contributions overcompensate the W contribution to the SM h–diphoton amplitude (which stays then compatible with the measured h signal strength).

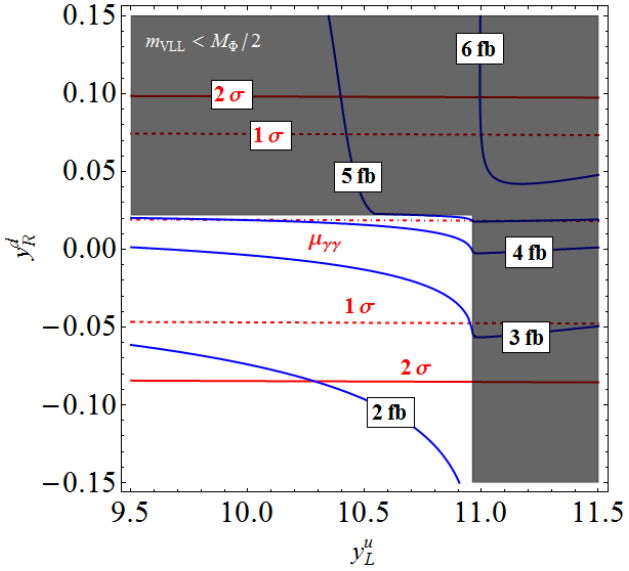

Figure 4.3 – Contours of constant $\sum \sigma(gg \to \Phi) \times \mathrm{BR}(\Phi \to \gamma\gamma)$ (blue, in fb) and $\mu_{\gamma\gamma}$ (red) in the $[y_L^u, y_R^d]$ plane. The dot-dashed line represents the experimental central value of the $h \to \gamma\gamma$ signal strength, $\mu_{\gamma\gamma} = 1.16 \pm 0.18 \pm 0.15$, while the dashed (solid) lines represent the 1σ (2σ) bands. The gray shaded region corresponds to at least one VLL eigenmass being smaller than $\frac{1}{2}m_\Phi \simeq 375$ GeV. The values of the other parameters are given by $y_R^u \simeq 0$, $y_L^d \simeq 11$, $m_1 \simeq m_2 \simeq m_3 \simeq 800$ GeV.

eq. (4.15). For simplicity, we assume that these six copies do not mix between themselves and that they are described by identical parameter values. In order to maximize the impact of the VLL contributions to the $\Phi\gamma\gamma$ loops, an immediate possibility would be to choose the interaction basis parameters in such a way that all the new VLLs have equal masses which are close to the threshold $\frac{1}{2}m_\Phi$ (i.e. $\tau_f = 1$), where the $A_{1/2}^\Phi$ form factors are close to their maximal value, as shown in Fig. 4.2. However, such a choice would set to zero both the up–type (singly charged) and down–type (doubly-charged) VLL contributions to the $A \to \gamma\gamma$ process; see also Ref. [79, 184]. Instead, to take at least partly advantage of the sizable form factor, we arrange the parameter values such that only one up–like and one down–like VLL per copy have masses close to the threshold. Also, as discussed before, we only consider the regions of the parameter space where the singly and doubly-charged contributions to the $h \to \gamma\gamma$ loop are strongly suppressed, leaving thus the $h\gamma\gamma$ effective coupling SM-like.

In Fig. 4.3, we present isocontours of $\sum_{\Phi=H,A} \sigma(gg \to \Phi) \times \mathrm{BR}(\Phi \to \gamma\gamma)$ and the signal strength for the previously observed SM–like state $\mu_{\gamma\gamma} = \sigma(gg \to h) \times \mathrm{BR}(h \to \gamma\gamma)/\sigma(gg \to h) \times \mathrm{BR}(h \to \gamma\gamma)|_{\rm SM}$ in the $[y_L^u, y_R^d]$ plane. The signal strength for the lighter h boson has been evaluated according to the discussion in Ref. [116]: we took the latest combined experimental value obtained at the previous run of the LHC, $\mu_{\gamma\gamma} = 1.16 \pm 0.18$ [173], and added a theoretical uncertainty of order 15% [120, 121, 130]. We chose to vary the y_L^u and y_R^d parameters because each one is representative for its own sector (up/singly–charged and down/doubly–charged). Also, to avoid a too large width of the scalar resonances, we constrained the VLL eigenmasses to be slightly higher than $\frac{1}{2}m_\Phi \simeq 375$ GeV. Albeit the high values of some of the interaction basis Yukawa parameters, the mass basis Yukawa couplings have values well below the perturbativity limit of 4π: the highest values are $g_{d_{22}}^A \simeq g_{d_{22}}^H \simeq 4.5$.

As mentioned earlier, the highest values of the total cross section times branching ratio $\sigma \times \mathrm{BR}$ for the H and A resonances occur in the region where $m_{l_1^-} \simeq m_{l_1^=} \simeq \frac{1}{2}m_\Phi$. For completeness, we quote the other two VLL masses, which, in the region where $\sigma \times \mathrm{BR}$ is

maximized, are approximately equal, i.e. $m_{l_2^-} \simeq m_{l_2^=} \simeq 1.7$ TeV. Moreover, in the total diphoton cross section, $\sum_\Phi \sigma(gg \to \Phi) \times \text{BR}(\Phi \to \gamma\gamma)$, the pseudoscalar contribution is ~ 56 times larger than the H contribution. We also note that, as evident from eqs. (4.16) and (4.17), for the $H \to \gamma\gamma$ decay, the up-like/singly-charged and down-like/doubly-charged VLL sectors interfere destructively, whereas for the $A \to \gamma\gamma$ process the two sectors interfere constructively.

Finally, let us make two remarks about the constraints on the scenario above. Concerning the electroweak precision data, in the language of the S/T parameters [102], VLFs have no impact on the T parameter if there is only a small mass difference between the components of the isospin doublets (as it is the case above where an approximate custodial symmetry is imposed), while the impact on the S parameter is reduced for not too numerous VLFs (in the opposite case, the tension could be reduced by including the additional contribution of the extended Higgs sector and/or mixing between different fermion generations). In addition, other theoretical constraints should in principle be considered, such as the stability of the electroweak vacuum. However, in this case, one should be more specific about the models that incorporate these new particles. In any case, a detailed discussion of the two issues is postponed to the next chapter.

In conclusion, by adding charged VLLs, one can obtain values of $\sum_\Phi \sigma(gg \to \Phi) \times \text{BR}(\Phi \to \gamma\gamma) \simeq$4–5 fb for the diphoton rate in the MSSM or in a 2HDM case, while keeping the $h \to \gamma\gamma$ signal strength in agreement with the LHC Higgs data [173]. By comparing with the value of the diphoton rate for the H/A resonances that can be obtained in our 2HDM scenarios with $\tan\beta = 1$, i.e. $\sigma \times \text{BR} \approx 1.5 \times 10^{-2}$ fb, we see that the VLL loop contributions allow to enhance the decay rate of the A and H bosons to $\gamma\gamma$ final states by a factor of $\mathcal{O}(100)$. Such an important enhancement is due to (i) the high electric charges of the VLLs, (ii) the several VLL families and (iii) the fact that half of the VLLs have masses $\gtrsim \frac{1}{2} m_\Phi$, for which the form factors attain their maximal values.

4.5 Discussion

The first searches performed at the new LHC with a center of mass energy of 13 TeV, albeit with a moderate accumulated luminosity, look very promising as the ATLAS and CMS collaborations have reported the observation of a diphoton resonance at an invariant mass of about 750 GeV. The significance of the signal is well below the required five standard deviations and it can well be a statistical fluctuation. It is nevertheless tempting to consider the possibility that it is the first sign of new physics beyond the SM.

In this first exploratory work, we have investigated the possibility that the diphoton resonance is one of the heavy neutral CP–even or CP–odd Higgs particles (and in fact a superposition of the two) that arise in two–Higgs doublet scenarios that are considered as a straightforward extension of the SM and widely studied, especially in the context of supersymmetric theories like the MSSM. We show that clearly such a strong diphoton signal cannot be achieved in the usual versions of 2HDMs and the MSSM and additional charged particles should contribute to the loop induced production and decay processes.

We have thus considered the possibility that these new particles are vector–like quarks and leptons that couple strongly to the heavy Higgs bosons. We have shown that, for instance, six families of VL leptons can easily enhance the diphoton rate of the 750 GeV resonance to accommodate the observed signal, without affecting the properties of the standard–like 125 Higgs boson and still satisfying the electroweak precision data.

If this diphoton excess would have not been a statistical fluctuation and would have been

indeed confirmed by subsequent data as being a real physics signal, it would have had far reaching consequences. Not only a new scalar would have been discovered, but it would have most likely implied the existence of new electrically charged particles, so as to enhance the scalar's decay into photon pairs. Regrettably, the 2016 data discarded the resonance as a statistical fluctuation [159, 160].

Chapter 5

Dark Matter Phenomenology of SM and Enlarged Higgs Sectors Extended with Vector Like Leptons

5.1 The WIMP Paradigm

Among the features which make Weakly Interacting Massive Particles (WIMPs) an attractive class of Dark Matter (DM) candidates, it is for sure worth mentioning the production mechanism. WIMP DM particles were indeed part of the primordial thermal bath at early stages of the history of the Universe and decoupled via freeze-out at later stages, when the temperature was below their mass (i.e. non-relativistic decoupling), since their interactions with the SM particles were not efficient anymore with respect to the Hubble expansion rates. Under the assumption of standard cosmological history, the comoving abundance of the DM is set by a single particle physics input, namely the thermally averaged pair annihilation cross-section. The experimentally favored value of DM abundance, expressed by the quantity $\Omega h^2 \approx 0.12$ [21] corresponds to a thermally averaged cross-section $\langle \sigma v \rangle \sim 10^{-26} \mathrm{cm}^3 \mathrm{s}^{-1}$. Interactions of this size are potentially accessible to a broad variety of search strategies, ranging from Direct/Indirect Detection to production at colliders, making the WIMP paradigm highly testable.

From the point of view of model building, WIMP frameworks feature interactions between pairs of Dark Matter particles (in order to guarantee the cosmological stability of the DM, operators with a single DM field are in general forbidden, e.g. through a symmetry) and pair of SM states, induced by suitable mediator fields. The simplest option, in this sense, is probably represented by s-channel electrically neutral mediators, dubbed "portals", which can couple the DM with SM fermions (see e.g. [185–187]), although couplings with the SM gauge bosons might also be viable [188–191]. The DM relic density is thus determined via s-channel exchange of the mediator states. By simple crossing symmetry arguments, these processes can be, for example, related to the rate of DM Direct Detection, induced by the t-channel interaction between the DM and the SM quarks, and to the ones of DM pair production at colliders, which can be probed mostly through mono-jet events [192–195].

Interestingly, the SM features two potential s-channel mediators, namely the Z and the Higgs bosons. One possible implementation are the so-called "Z-portal" DM [196] scenarios. However, they are rather contrived, since, because of gauge invariance, interaction between a SM singlet DM and the Z can arise only at the non-renormalizable level [197, 198]. "Higgs portal" models are instead quite popular, although rather constrained [199–203], since a spin-0 (or 1) DM, even if it is a singlet with respect to the SM gauge group, can interact

with the SM Higgs doublet H via four-field operators connecting the bilinear $HH^\dagger$ with a DM pair and giving rise, after electroweak (EW) symmetry breaking, to an effective vertex between a DM pair and the physical Higgs field h.

The fermionic "Higgs portal" is instead realized through a dimension-5 operator. Furthermore this is strongly constrained, also with respect to the scalar and vector DM cases, because of the strong direct detection rates accompanied by a velocity suppressed annihilation cross-section [201, 202].

In order to couple at the renormalizable level to the Z and/or Higgs bosons, the fermionic DM should feature a (small) hyper- and $SU(2)$ charged component. This could be realized through the mixing of a pure SM singlet with extra states posessing non-trivial quantum numbers under $SU(2) \times U(1)$ (see e.g. [204–207] for some constructions). The DM should then be a stable neutral state belonging to a new, non-minimal particle sector.

As argued in the third chapter, new chiral fermions, with mass originating from EWSB, are strongly disfavored experimentally [208]. More suitable options are instead represented by fermions belonging to a real representation or forming vector-like pairs.

In this chapter, base on Ref. [209], we consider the latter option and then extend the fermionic content of the SM with a family of new fields. By "family" we understand vector-like fermions with analogous quantum numbers as the SM leptons and the right-handed neutrinos, and with bare mass terms, which are allowed by gauge symmetry due to the vector-like nature of the new states. In analogy with their color triplet counterparts discussed in Chapter 3, these fields are dubbed as vector-like leptons (VLLs). In absence of mixing with the SM leptons, the lightest new fermionic state, if electrically neutral, constitutes a DM candidate. In this setup, the DM is coupled to the SM Higgs and the Z and W bosons, as it features, in general, an admixture of a fermionic field with non-zero hypercharge and weak isospin.

This kind of scenario is, unfortunately, very strongly constrained since the Higgs and Z-boson mediate Spin Independent (SI) interactions between the DM and the nucleons, which are in increasing tension with experimental constraints. Similarly to the Higgs and Z-portal models, it is possible to comply with these limits, and achieve, at the same time, the correct relic density only for rather heavy DM masses or, possibly, in presence of coannihilation processes, thus implying (approximate) mass degeneracies in the new fermionic sector.

A more interesting option would consist in enlarging the mediator sector by considering two Higgs doublets (2HDM). Besides the still rather fine-tuned possibility of s-channel resonances, it is possible, in this scenario, to enhance the DM annihilation cross-section, marginally affecting its scattering rate on nucleons, through annihilation into extra Higgs bosons, especially the charged ones, as final states, provided that the latter are light enough. This last possibility evidences an interesting complementarity with collider searches of extra Higgs bosons. Lower limits on their masses would automatically constrain the range of viable DM masses.

LHC searches of new scalar states can be themselves influenced by the presence of new vector-like fermions since electrically charged VL fermions (which is embedded in the $SU(2)$ multiplet which the DM belongs to) or even color charged VL fermions (we won't consider explicitly this possibility here) can modify di-boson signal rates. For this reason, 2HDM+VLFs models have attracted significant attention in the recent times since they allowed for the interpretation of the 750 GeV diphoton excess (see previous chapter and Refs. [161, 210–221], announced by the LHC collaboration in December 2015 [158, 222–224], but not confirmed by the 2016 data [225, 226].

The parameters of the theory are constrained not only by the DM and collider phenomenology. The couplings of the new fermions to the 125 GeV Higgs are constrained by

Electro-Weak Precision Tests (EWPT). A further upper bound on these couplings, as well as the ones to the other Higgs states, comes from the RG running of the the gauge and the quartic couplings of the scalar potential. In particular, the latter get negative contributions proportional to the fourth power of the Yukawa couplings of the VLLs, such that the scalar potential might be destabilized even at collider energy scales, unless new degrees of freedom are added.

This chapter proposes an extensive phenomenological overview of the SM and several realizations of 2HDMs, which are extended by a sector or family of vector-like fermions. This VL sector incorporates stable neutral states, the lightest of which is stable and thus provides a viable DM candidate.

This chapter is organized as follows. We start by introducing, at the beginning of section 5.2, the family of vector-like fermions. The remainder of the section is dedicated to a brief overview of the SM+VLLs scenario. Firstly, we briefly illustrate the general constraints coming from the modification of the Higgs signal strengths and the Electroweak Precision Tests (EWPT), and afterwards focus on the DM phenomenology. Along similar lines, an analysis for the 2HDM is then performed in section 5.3. Next, we perform a more detailed analysis of the constraints from EWPT and Higgs signal strengths and add to them the Renormalization Group Equation (RGE) constraints. After the analysis of the DM phenomenology, we briefly discuss the limits and prospects, for our scenario, of collider searches. Finally, we summarize our results in section 5.3.8 and conclude in section 5.4.

5.2 Vector-Like Extensions of the Standard Model

In this section we review how introducing vector-like leptons affects the SM Higgs sector. As already pointed out, the impact is mostly twofold. First of all, they generate additional loop contributions to the couplings of the Higgs boson to two photons, giving rise to deviations of the corresponding signal strengths with respect to the SM prediction. In addition, the presence of vector-like leptons is typically associated with potentially sizeable contributions to the EW precision observables. In order to have viable values of the Higgs signal strengths and precision observables, one should impose definite relations for the Yukawa couplings and masses of the new VLLs. The same relations hold, up to slight modifications, also in the 2HDM case.

5.2.1 The Vector-Like "Family"

In this chapter, we assume that the SM and, afterwards, the 2HDM scalar sectors can be extended by "families" of vector like fermions (VLFs). By family we understand a set of two $SU(2)_L$ singlets and one $SU(2)_L$ doublet, belonging to a $SU(3)_c$ representation R_c, and with their hypercharge determined by a single parameter, Y. For the moment, we keep the discussion general and later on specialize on possible DM candidates. The new fields can be schematically labeled as:

$$\mathcal{D}_{L,R} \sim (R_c, 2, Y - 1/2) \ , \quad U'_{L,R} \sim (R_c, 1, Y) \ , \quad D'_{L,R} \sim (R_c, 1, Y - 1) \ , \tag{5.1}$$

so that the couplings to the SM Higgs doublet, $H = \left(0 \ \frac{v+h}{\sqrt{2}}\right)^T$, are parametrized by the following Lagrangian:

$$\begin{aligned} -\mathcal{L}_{\rm VLF} = {} & y^{U_R}\overline{\mathcal{D}_L}\tilde{H}U'_R + y^{U_L}\overline{U'_L}\tilde{H}^\dagger\mathcal{D}_R + y^{D_R}\overline{\mathcal{D}_L}HD'_R + y^{D_L}\overline{D'_L}H^\dagger\mathcal{D}_R \\ & + M_{UD}\overline{\mathcal{D}_L}\mathcal{D}_R + M_U\overline{U'_L}U'_R + M_D\overline{D'_L}D'_R + \text{h.c.} \ , \end{aligned} \tag{5.2}$$

where we have considered the following decomposition for the $SU(2)$ doublets: $\mathcal{D}_{L,R} \equiv \begin{pmatrix} U & D \end{pmatrix}^T_{L,R}$.

For simplicity we assume that all the couplings are real and that the mixing between the VLFs and the SM fermions is negligible. Later on, when specializing on DM phenomenology, we will forbid the SM fermion-VL fermion mixing through a global $\mathbb{Z}_2$ symmetry.

After electroweak symmetry breaking (EWSB), there is a mixing in the "up" (U', U) and "down" (D', D) sectors. The "up" VL fermions have charge $Q_U = Y$, while the "down" fermions have charge $Q_D = (Y - 1)$. The mass matrices in the two sectors are

$$\mathcal{M}_U = \begin{pmatrix} M_U & y^{U_L} v/\sqrt{2} \\ y^{U_R} v/\sqrt{2} & M_{UD} \end{pmatrix} \ , \ quad \mathcal{M}_D = \begin{pmatrix} M_D & y^{D_L} v/\sqrt{2} \\ y^{D_R} v/\sqrt{2} & M_{UD} \end{pmatrix} \ , \tag{5.3}$$

with $v = 246$ GeV, and they are bi-diagonalized as follows

$$U^F_L \cdot \mathcal{M}_F \cdot \left(U^F_R\right)^\dagger = \begin{pmatrix} m_{F_1} & 0 \\ 0 & m_{F_2} \end{pmatrix} \ , \qquad U^F_L = \begin{pmatrix} c^F_L & s^F_L \\ -s^F_L & c^F_L \end{pmatrix} \ , \quad U^F_R = \begin{pmatrix} c^F_R & s^F_R \\ -s^F_R & c^F_R \end{pmatrix} \ , \tag{5.4}$$

where the sub/superscripts $F = U, D$ distinguish between the two sectors and $c^F_{L/R} = \cos\theta^F_{L/R}$, $s^F_{L/R} = \sin\theta^F_{L/R}$. As done previously, we denote throughout this chapter the lighter mass eigenstate as F_1. The limit where one of the singlets is decoupled, e.g. when $y_{U_R} = y_{U_L} = 0$ and $M_U \to \infty$, has already been studied in detail in [94]. As shall soon be seen, the mixing structure in eq. 5.3 is strongly constrained by the electroweak precision tests (EWPT) and by the Higgs couplings measurements.

5.2.2 Electroweak Precision Tests

Extending the SM with vector-like fermions leads, in general, to the deviation of the Electroweak precision observables S and T from their respective experimental limits. Assuming negligible mixing between the SM and the vector-like fermions, the limits on S and T can be directly translated into limits on the Yukawa couplings and masses of the new fermions; in the limit in which the former go to zero, no constraints from EWPT apply.

Sizeable values of the Yukawa couplings of the VLFs can nevertheless be obtained while still complying with the limits on the T parameter by relying (at least approximately) on a custodial limit:

$$M_D = M_U \ , \qquad y^{U_L} = y^{D_L} \ , \qquad y^{U_R} = y^{D_R} \ , \tag{5.5}$$

which is equivalent to imposing equal mass matrices in the isospin-up and isospin-down sectors. Clearly, the custodial limit can be achieved only by considering "full families" of VLFs, i.e. a corresponding SU(2) singlet for each of the components of the doublet, as done in this chapter.

On the contrary, there is no symmetry protecting the S parameter, which means that, in some cases, it can impose more relevant constraints than the T parameter. The constraints on S can be nevertheless partially relaxed by taking advantage of the correlation among the S and T parameters, illustrated in fig. 5.1, by allowing for a small deviation from the custodial limit, i.e. $T \gtrsim 0$.

5.2.3 Higgs Couplings

We now turn to the second constraint, which comes from the Higgs coupling measurements. In the presence of vector-like fermions, the scalar couplings to gauge bosons receive additional

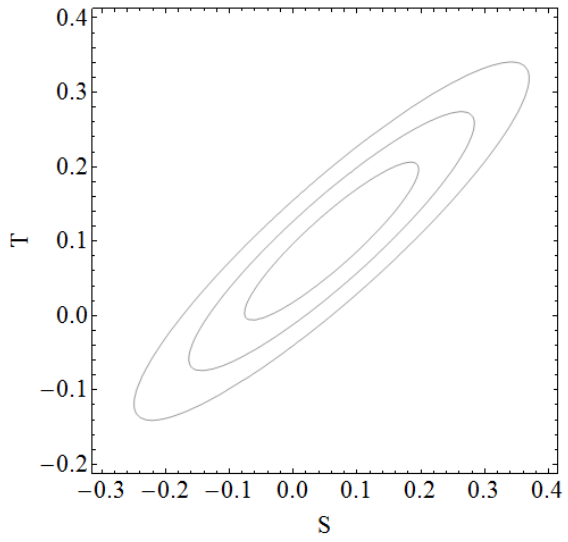

Figure 5.1 – Allowed values of S and T [3] at, from the innermost to the outermost ellipse, 68%, 95.5% and 99.7% confidence level (CL).

contributions, originating from triangle loops in which the new fermions are exchanged. No new decay channels into VLFs are instead present: because of constraints from direct searches at colliders, the VLFs should be heavier than the SM Higgs.

The SM Higgs loop-induced partial decay widths into massless gauge bosons, $\Gamma_{h\mathrm{VV}}$, $\mathrm{V} = g, \gamma$, can be schematically expressed as $\Gamma_{h\mathrm{VV}} \propto |\mathcal{A}^{h\mathrm{VV}}_{\mathrm{SM}} + \mathcal{A}^{h\mathrm{VV}}_{\mathrm{VLF}}|^2$, where $\mathcal{A}^{h\mathrm{VV}}_{\mathrm{SM}}$ and $\mathcal{A}^{h\mathrm{VV}}_{\mathrm{VLF}}$ represent the amplitudes associated, respectively, to the SM and VLF contributions. Throughout this chapter we only consider the case of a family of color-neutral VLFs ($R_c = 1$); as a consequence the new physics sector influences only $\Gamma_{h\gamma\gamma}$ and therefore the $h \to \gamma\gamma$ signal strength, $\mu_{\gamma\gamma}$.[1] The corresponding amplitude is given by:

$$\mathcal{A}^{h\gamma\gamma}_{\mathrm{VLF}} = \sum_{\substack{F=U,D \\ i=1,2}} Q_F^2 \frac{v(\mathcal{C}_F)_{ii}}{m_{F_i}} A^h_{1/2}(\tau^h_{F_i}), \tag{5.6}$$

where $\tau^h_{F_i} = \frac{m_h^2}{4m^2_{F_i}}$, while $A^h_{1/2}$ is a loop form factor whose definition is given e.g. in [170]. The matrix $\mathcal{C}_F$ is defined as:

$$\mathcal{C}_F = U^L_F \cdot \mathcal{Y}_F \cdot (U^R_F)^\dagger, \quad \mathcal{Y}_F = \partial_v \mathcal{M}_F = \frac{1}{\sqrt{2}} \begin{pmatrix} 0 & y_h^{F_L} \\ y_h^{F_R} & 0 \end{pmatrix}. \tag{5.7}$$

For VLFs considerably heavier than 125 GeV Higgs, we can reliably approximate the loop function $A^h_{1/2}(\tau)$ with its asymptotic value, $A^h_{1/2}(0) = 4/3$, such that the expression (5.6) simplifies to:

$$\mathcal{A}^{h\gamma\gamma}_{\mathrm{VLF}} = A^h_{1/2}(0) \sum_{F=U,D} \frac{-2v^2 y_h^{F_L} y_h^{F_R}}{2M_F M_{UD} - v^2 y_h^{F_L} y_h^{F_R}}. \tag{5.8}$$

Experimental measurements do not exhibit statistically relevant deviations of $\mu_{\gamma\gamma}$ from the SM prediction [1,2], which implies essentially two possibilities: $\mathcal{A}^{h\gamma\gamma}_{\mathrm{VLL}} \simeq 0$ or $\mathcal{A}^{h\gamma\gamma}_{\mathrm{VLL}} \simeq -2\mathcal{A}^{h\gamma\gamma}_{\mathrm{SM}}$. As it is clear from eq. (5.8), the first possibility is easily realized by setting (close) to zero one

[1] Note that $\mu_{hZ\gamma}$ is also affected by the VLFs, but the uncertainties on this signal strength are too large to constrain the extended fermionic sector [1,2].

of the $y_h^{F_{L,R}}$ couplings.[2] The other option is instead more complicated to realize. Assuming $Y = 0$ (as is be done for the rest of the chapter), such that only D-type states contribute to $\mu_{\gamma\gamma}$, and setting for simplicity $M_D = M_{UD}$ and $y_h^{D_L} = -y_h^{D_R} = y_h^D$, which implies that the two mass eigenstates will have the same mass m_D, the relation to impose becomes:

$$\mathcal{A}_{\rm VLL}^{h\gamma\gamma} = \frac{4}{3}\left(\frac{y_h^D v}{m_D}\right)^2 \simeq -2\mathcal{A}_{\rm SM}^{h\gamma\gamma} \simeq 13, \tag{5.9}$$

which is impossible to satisfy since $y_h^D v/m_D$ is smaller than 2 (or equal to 2, for $M_D = M_{UD} = 0$).[3] Unless differently stated, we always consider, for both the SM and 2HDM cases, an assignation of the Yukawa couplings of the VLFs such that $\mathcal{A}_{\rm VLL}^{h\gamma\gamma} = 0$.

5.2.4 DM Phenomenology

A DM candidate is introduced, in our setup, by considering a "family" of vector-like leptons coupled to the SM Higgs doublet according to the following Lagrangian:

$$\begin{aligned} -\mathcal{L}_{VLL} = {} & y_h^{N_R}\overline{L}_L\tilde{H}N'_R + y_h^{N_L}\overline{N}'_L\tilde{H}^\dagger L_R + y_h^{E_R}\overline{L}_L H E'_R + y_h^{E_L}\overline{E}'_L H^\dagger L_R \\ & + M_L\overline{L}_L L_R + M_N\overline{N}'_L N'_R + M_E\overline{E}'_L E'_R + \text{h.c.}. \end{aligned} \tag{5.10}$$

To guarantee the stability of the DM candidate, we impose a global $\mathbb{Z}_2$ symmetry under which the vector-like leptons are odd and the SM is even (a supersymmetric analogue is the well-known R-parity). After EW symmetry breaking, the vector like fermions mixed between themselves, as described by the following mass matrices:

$$\mathcal{M}_N = \begin{pmatrix} M_N & v' y_h^{N_L} \\ v' y_h^{N_R} & M_L \end{pmatrix}, \quad \mathcal{M}_L = \begin{pmatrix} M_E & v' y_h^{E_L} \\ v' y_h^{E_R} & M_L \end{pmatrix}. \tag{5.11}$$

where $v' = v/\sqrt{2} \simeq 174$ GeV. Note that the $\mathbb{Z}_2$ symmetry forbids the mixing between the VLLs and the SM fermions. In order to pass from the interaction to the mass basis, one has to bidiagonalize the above matrices as:

$$U_L^N \cdot \mathcal{M}_N \cdot \left(U_R^N\right)^\dagger = \text{diag}(m_{N_1}, m_{N_2}), \quad U_L^E \cdot \mathcal{M}_E \cdot \left(U_R^E\right)^\dagger = \text{diag}(m_{E_1}, m_{E_2}), \tag{5.12}$$

with the unitary matrices $U_{L,R}^F$, $F = N, E$ written explicitly as:

$$U_{L,R}^F = \begin{pmatrix} \cos\theta_{L,R}^F & \sin\theta_{L,R}^F \\ -\sin\theta_{L,R}^F & \cos\theta_{L,R}^F \end{pmatrix},$$

where:

$$\begin{aligned} \tan 2\theta_L^N &= \frac{2\sqrt{2}v\left(M_L y_h^{N_L} + M_N y_h^{N_R}\right)}{2M_L^2 - 2M_N^2 - v^2\left(|y_h^{N_L}|^2 - |y_h^{N_R}|^2\right)}, \\ \tan 2\theta_R^N &= \frac{2\sqrt{2}v\left(M_N y_h^{N_L} + M_L y_h^{N_R}\right)}{2M_L^2 - 2M_N^2 + v^2\left(|y_h^{N_L}|^2 - |y_h^{N_R}|^2\right)}. \end{aligned} \tag{5.13}$$

[2] Alternatively one could think about a cancellation between the contributions of the "up" and "down" sectors. However, in order to have a DM candidate, we consider in this chapter the case that the up sector is made by electrically neutral states, so that they do not actually contribute to $\mu_{\gamma\gamma}$. On general grounds, a cancellation between the up-type and down-type contribution would be anyway difficult to realize, since it would require a strong deviation from the custodially symmetric limit, which is disfavored by EWPT.

[3] This constraint on the Yukawa coupling can be relaxed by adding more families of VLFs and/or considering higher values of Y. However, we do not consider these scenarios throughout this chapter.

The corresponding expressions for $\theta^E_{L,R}$ can be found from the ones above by replacing $M_N \to M_E$ and $y_h^{N_{L,R}} \to y_h^{E_{L,R}}$.

The DM candidate N_1 (i.e. the lighter VL neutrino) is in general an admixture of the $SU(2)$ singlet (with null hypercharge) $N'_{L,R}$ and doublet $N_{L,R}$. As a consequence, N_1 is coupled to the Higgs scalar h. as well as to the SM gauge bosons $W^\pm$ and Z. These couplings are given by:

$$
\begin{aligned}
y_{hN_1N_1} &= \frac{\cos\theta^L_N \sin\theta^R_N y_h^{N_L} + \cos\theta^R_N \sin\theta^L_N y_h^{N_R}}{\sqrt{2}}, \\
y_{V,ZN_1N_1} &= \frac{g}{4\cos\theta_W}\left(\sin^2\theta^N_L + \sin^2\theta^N_R\right), \\
y_{A,ZN_1N_1} &= \frac{g}{4\cos\theta_W}\left(\sin^2\theta^N_L - \sin^2\theta^N_R\right), \\
y_{V,WN_1E_1} &= \frac{g}{2\sqrt{2}}\left(\sin\theta^N_L \sin\theta^E_L + \sin\theta^N_R \sin\theta^E_R\right), \\
y_{A,WN_1E_1} &= \frac{g}{2\sqrt{2}}\left(\sin\theta^N_L \sin\theta^E_L - \sin\theta^N_R \sin\theta^E_R\right),
\end{aligned}
\tag{5.14}
$$

where, for convenience, we have expressed the couplings with the Z and W bosons in terms of vectorial and axial combinations.

The DM relic density can be determined through the WIMP paradigm as a function of the DM thermally averaged pair annihilation cross-section, formally defined (excluding coannihilations) as [227]:

$$
\langle\sigma v\rangle = \frac{1}{8m^4_{N_1} T K_2(m_{N_1}/T)} \int_{4m^2_{N_1}}^{\infty} ds\sigma(s)(s-4m^2_{N_1})\sqrt{s}K_1(\sqrt{s}/T) \tag{5.15}
$$

which is in turn a function of the couplings reported in eq. 5.14. The possible DM annihilation processes are represented by annihilations into SM fermions pairs, induced by s-channel exchange of the h and Z bosons, and into W^+W^-, ZZ, Zh, and hh, induced by t-channel exchange of the neutral states $N_{1,2}$ ($E_{1,2}$ for the W^+W^- final state). In order to precisely determine the DM relic density we have numerically computed (5.15) through the package `MicrOMEGAs` [228]. We nevertheless provide some simple approximations to render more transparent the relationship between the DM relic density and the relevant parameters of the theory, obtained by the conventional velocity expansion [229] $\langle\sigma v\rangle \approx a + 2b/x$ (using $\sigma v \approx a + bv^2/3, \langle v^2\rangle = 6/x$, where $x = m_{\rm DM}/T$). Also, we take only, if non-vanishing, the leading s-wave coefficient a. [4]

In the case of annihilation into $\bar{f}f$ final states, the only non-vanishing contribution in the $v \to 0$ limit is the one associated to the s-channel Z-exchange:

$$
\langle\sigma v\rangle_{ff} \approx \frac{m^2_{N_1}}{8\pi} \frac{g^2 m^2_{N_1}}{\pi((4m^2_{N_1} - m^2_Z)^2 + m^2_Z\Gamma^2_Z)} \sum_f n^f_c(|V_f|^2 + |A_f|^2)|y_{V,ZN_1N_1}|^2, \tag{5.16}
$$

where V_f and A_f are the vectorial and axial couplings of the Z-boson and the SM fermions:

$$
V_f = \frac{g}{2c_W}(-2Q_f s^2_W + T^3_f), \quad A_f = \frac{g}{2c_W} T^3_f, \tag{5.17}
$$

[4] As already pointed out, these expressions should be taken as illustrative. The contribution of the coefficient b is not necessarily negligible. We also remind that the velocity expansion is not valid in presence of s-channel resonances (relevant in the 2HDM section), coannihilations (briefly considered later on) and thresholds corresponding to the opening of new annihilation channels [230].

while n_c^f is the color factor, Q_f the electric charge, and $s_W = \sin\theta_W$ and $c_W = \cos\theta_W$. The cross-sections of the other relevant final states can be instead estimated as [5]:

$$\begin{aligned}\langle\sigma v\rangle_{W^+W^-} \approx & \frac{g^4 t_W}{16\pi m_W^2}((\sin\theta_L^N)^2 + (\sin\theta_R^N)^2)^2 \\ & + \frac{g^4}{64}\left(\frac{1}{2\pi}((\sin\theta_L^N \sin\theta_L^E)^2 + (\sin\theta_R^N \sin\theta_R^E)^2)^2 \frac{m_{N_1}^2}{(m_{N_1}^2 + m_{E_1}^2)^2}\right. \\ & \left. + \frac{2}{\pi}((\sin\theta_L^N \sin\theta_L^E)^2 - (\sin\theta_R^N \sin\theta_R^E)^2)^2 \frac{m_{N_1}^4}{m_W^4}\frac{m_{E_1}^2}{(m_{N_1}^2 + m_{E_1}^2)^2}\right),\end{aligned} \tag{5.18}$$

Here, $t_W = \tan\theta_W$.

$$\begin{aligned}\langle\sigma v\rangle_{ZZ} \approx \frac{g^4}{32\pi c_W^4 m_Z^2}\left[\frac{m_Z^2}{4m_{N_1}^2}\left(\left|(\sin\theta_L^N)^2 + (\sin\theta_R^N)^2\right|^4 + \left|(\sin\theta_L^N)^2 - (\sin\theta_R^N)^2\right|^4\right)\right. \\ \left. + 2\left|(\sin\theta_L^N)^2 + (\sin\theta_R^N)^2\right|^2 \left|(\sin\theta_L^N)^2 - (\sin\theta_R^N)^2\right|^2\right],\end{aligned} \tag{5.19}$$

and

$$\langle\sigma v\rangle_{Zh} \approx \frac{g^2}{4\pi v^2}|y_{V,ZN_1N_1}|^2 \frac{m_Z^2}{m_{N_1}^2}. \tag{5.20}$$

The achievement of the correct relic density through DM annihilations can be potentially in tension with limits from Direct Detection experiments. Indeed, DM interactions with SM quarks, mediated by t-channel exchange of Z and h bosons, induce both Spin Independent (SI) and Spin Dependent (SD) scattering processes of the DM with nuclei of target detectors.

The corresponding cross-sections, focusing for simplicity on the scattering on protons, are given by:

$$\begin{aligned}\sigma_{N_1p,Z}^{SI} &= \frac{\mu_{N_1}^2}{\pi}\frac{1}{m_Z^4}|y_{V,ZN_1N_1}|^2\left[\left(1 + \frac{Z}{A}\right)V_u + \left(2 - \frac{Z}{A}\right)V_d\right]^2, \\ \sigma_{N_1p,h}^{SI} &= \frac{\mu_{N_1}^2}{\pi}\frac{m_p^2}{v^2}\frac{1}{m_h^4}\left|y_{hN_1N_1}\left(\sum_{q=u,d,s} f_q + \frac{2}{27}f_{TG}\sum_{q=c,b,t}\right)\right|^2, \\ \sigma_{N_1p}^{SD} &= \frac{3\mu_{N_1}^2}{\pi m_Z^4}|y_{A,ZN_1N_1}|^2\left[A_u\left(\Delta_u^p S_p^A + \Delta_u^n S_n^A\right)\right. \\ &\quad \left. + A_d\left((\Delta_d^p + \Delta_s^p)S_p^A + (\Delta_d^n + \Delta_s^n)S_n^A\right)\right]^2 \frac{1}{(S_p^A + S_n^A)^2}\end{aligned} \tag{5.21}$$

In the expressions above, $\mu_{N_1} = \frac{m_p m_{N_1}}{m_p + m_{N_1}}$, $f_q, f_{TG}, \Delta_q^{p,n}$ are nucleon form factors, while S_p^A and S_n^A are the contributions of the proton and neutron to the spin of the nucleus A. We have used the values reported in [231].

Among these contributions, the most important one is represented by the SI cross-section from Z-mediated interactions. This allows to estimate the SI cross-section as:

$$\sigma_{N_1p}^{\rm SI} \approx 2\times 10^{-39}\,{\rm cm}^2\left(\sin^2\theta_L^N + \sin^2\theta_R^N\right)^2. \tag{5.22}$$

[5] For simplicity we have assumed that the t-channel diagrams are dominated by the exchange of the lightest mass eigenstate.

In order to comply with the stringent limits by the LUX experiment [232] which impose, for DM masses of the order of few hundreds GeV, a cross section of the order of $10^{-45}\,\mathrm{cm}^2$, [6] we need to require $\sqrt{\sin^2\theta_L^N + \sin^2\theta_R^N} \sim 10^{-(1\div 2)}$.

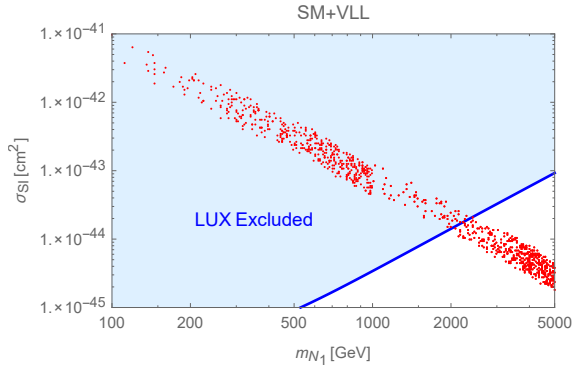

Figure 5.2 – Model points satisfying EWPT and Higgs width constraints and providing the correct DM relic density (see main text for clarification) reported in the bidimensional plane $(m_{N_1}, \sigma_p^{\mathrm{SI}})$. The blue region is excluded by current constraints from DM Direct Detection.

We have computed the main DM observables, i.e. the relic density and the SI scattering cross section, for a sample of model points generating by scanning on the parameters $(y_h^{N_{L,R}}, y_h^{E_L}, M_N, M_E, M_L)$, with $y_h^{E_R} = 0$ such that $\mathcal{A}_{NP}^{h\gamma\gamma} = 0$, over the following range:

$$\begin{aligned} y_h^{N_{L,R}} &\in \left[10^{-3}, 1\right], \\ y_h^{E_L} &\in \left[5\times 10^{-3}, 3\right], \\ M_N &\in \left[100\,\mathrm{GeV}, 5\,\mathrm{TeV}\right], \\ M_E = M_L &\in \left[300\,\mathrm{GeV}, 5\,\mathrm{TeV}\right], \end{aligned} \tag{5.23}$$

with the additional requirement of not exceeding the limits from EWPT.

The results of our analysis are reported in fig. 5.2. The figure shows the set of points featuring the correct DM relic density in the bidimensional plane $(m_{N_1}, \sigma_{\mathrm{SI}})$. Clearly, the very strong constraints from the Z-mediated DM scattering on nucleons rule out the parameter space corresponding to thermal Dark Matter unless its mass is approximately above 2 TeV. This result is similar to what is obtained in the generic Z-portal scenario [196], in which the SM Z boson mediates the interactions between the SM states and a Dirac fermion DM candidate. Notice that in our parameter scan we have anyway considered DM masses heavier than 100 GeV and a sizable mass splitting between the DM and the ligthest electrically charged fermion E_1. If these requirements are dropped, one could achieve an enhanched DM annihilation cross-section at the Higgs "pole", i.e. $m_{N_1} \simeq m_h/2$, or through coannihilations (we will briefly discuss this scenario in the next section in the context of Two Higgs Doublet Models), eventually relaxing the tensions with direct detection. This possibility has been considered e.g. in [181] in a model similar to ours (notice that in this reference the VL neutrinos have also Majorana mass terms and thus their interactions with the Z are weaker than in the model discussed here), but focused on the case of rather light VLLs enhancing the decay branching fraction of the SM Higgs to photon pairs (we have instead considered the case in which this coincides with the SM expectation).

[6] The recently published exclusion limits from the XENON1T collaboration [233] are comparable (i.e. twice as strong) to the ones from LUX.

5.2.5 Vacuum Stability

As will be discussed in greater detail in the next section, the presence of vector like fermions can have a substantial impact on the behavior of the theory with respect to radiative corrections. The RG evolution of the parameters of the scalar potential typically suffers the strongest influence from the introduced New Physics.

The stability of the EW vacuum depends on the sign of the quartic coupling λ of the Higgs potential. This parameter, positive at the electroweak scale, is driven towards negative values, at higher energy scales, by radiative corrections mostly relying on the yukawa coupling of the top quark. Detailed studies, like e.g. [234] have shown that the EW vacuum is stable up to energies close to the Planck scale. A quantitative determination is nevertheless extremely sensitive to the value of the mass of the top quark.

The presence of vector like fermions tends to steepen the decrease of λ at high energy. This fact is reflected by the 1-loop β function for the Higgs quartic, λ:

$$\beta_\lambda = \frac{1}{16\pi^2}\Big[\beta_{\lambda,\mathrm{SM}} + 4\lambda\left((y_h^{N_L})^2 + (y_h^{N_R})^2 + (y_h^{E_L})^2 + (y_h^{E_R})^2\right) \\ -4\left((y_h^{N_L})^4 + (y_h^{N_R})^4 + (y_h^{E_L})^4 + (y_h^{E_R})^4\right)\Big] \tag{5.24}$$

where $\beta_{\lambda,\mathrm{SM}}$ accounts for the SM contribution.

We have then checked the stability of the EW vacuum in presence of the new vector like fermions by solving the coupled RGEs of the Higgs quartic couplings and of the other relevant parameters, such as the VLF and top quark Yukawa couplings and the gauge couplings [7]. For simplicity, we have assumed that all the new particles lie at a same scale, $m_F = 400$ GeV, and that their Yukawa couplings are zero below this scale. As discussed in the previous subsection, the coupling $y_h^{N_L}$ is constrained, by DM phenomenology, to be very small, below 10^{-2}. We also remind that we customarily assume $y_h^{N_R} = y_h^{E_R} = 0$ to automatically comply with the constraints on the Higgs signal strength. In this simplified picture the vacuum stability depends, besides the SM inputs, on just one new parameter, i.e. $y_h^{E_L}$.

The behaviour of the Higgs quartic parameter with the energy is shown, for some assignations of $y_h^{E_L}$, in the left panel of fig. (5.3). Values of $y_h^{E_L}$ equal or greater than one correspond to a fast drop of λ. For $y_h^{E_L} = 2$ we notice indeed that the Higgs quartic coupling becomes negative in the proximity of the energy threshold corresponding to the mass of the VLFs. Our results have been made more quantitative in the second panel of fig. (5.3): here, we have indeed defined the stability scale Λ_{UV} by adopting the criterion $\lambda(\Lambda_{\mathrm{UV}}) = -0.07$ [235]. The energy scale Λ_{UV} is interpreted as the scale below which new degrees of freedom should be added in order to have a stable EW vacuum up to high scales. As will be further remarked throughout this chapter, building a UV complete model is not in the purposes of the work presented in this chapter; as a consequence we will implicitly adopt the minimal requirement that Λ_{UV} lies above the energy scales accessible to collider studies, namely a few TeVs, so that our model provides a reliable low energy description of the relevant phenomenology.

5.3 Two Higgs Doublet Models

Let us now move to the case of 2HDM scenarios. Their most important features have been summarized at the beginning of the previous chapter. In the following, we just display some relations that are necessary in order to discuss the relevant constraints.

[7] Our analysis is rather qualitative, as it is based on one loop β functions. Our results are nevertheless in good agreement with the more detailed study presented in [235].

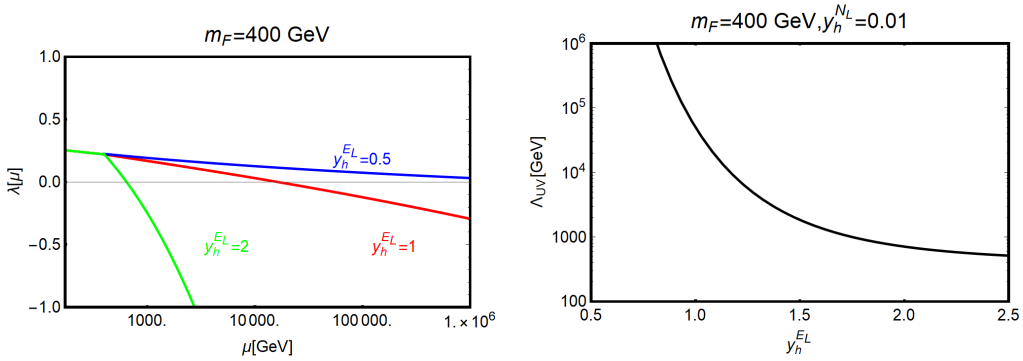

Figure 5.3 – Left panel: Evolution of the Higgs quartic coupling λ with the energy scale μ for three assignations, i.e. 0.5,1 and 2, of the Yukawa coupling $y_h^{E_L}$. The VLL have been assumed to be at a scale $m_F = 400\,\text{GeV}$, while the neutral Yukawa coupling $y_h^{N_L}$ has been set to 0.01. The other two Yukawa couplings $y_h^{N_R}, y_h^{E_R}$ have been set to zero for simplicity and in order to have a SM like diphoton rate for the Higgs boson. Left panel: Variation of the scale Λ_{UV}, defined by $\lambda(\Lambda_{\text{UV}}) = -0.07$ with the coupling $y_h^{E_L}$. The other parameters have been set as in the left panel.

In order impose the theoretical constraints coming from unitarity and boundedness from below of the scalar potential in a transparent way, we begin by expressing the quartic couplings of the scalar potential (4.3) as functions of the masses of the physical states. In the alignment limit, the relevant equations are:

$$\begin{aligned}
\lambda_1 &= \frac{1}{v^2}\left[m_h^2 + \left(m_H^2 - M^2\right) t_\beta^2\right], \\
\lambda_2 &= \frac{1}{v^2}\left[m_h^2 + \left(m_H^2 - M^2\right) t_\beta^{-2}\right], \\
\lambda_3 &= \frac{1}{v^2}\left[m_h^2 + 2m_{H^\pm}^2 - \left(m_H^2 + M^2\right)\right], \\
\lambda_4 &= \frac{1}{v^2}\left[M^2 + m_A^2 - 2m_{H^\pm}\right], \\
\lambda_5 &= \frac{1}{v^2}\left[M^2 - m_A^2\right],
\end{aligned} \tag{5.25}$$

where $M \equiv m_{12}/(s_\beta c_\beta)$. Unitarity and boundedness from below of the scalar potential impose constraints on the value of the couplings $\lambda_{i=1,5}$ [150, 236] which, through eqs. (5.25), are translated into bounds on the physical masses. In particular these bounds imply that it is not possible to assign their values independently one from each other. All these bounds can be found, for example, in Ref. [236, 237], but, for completeness, we report them below. For the scalar potential to be bounded from below, the quartics must satisfy:

$$\lambda_{1,2} > 0,\ \lambda_3 > -\sqrt{\lambda_1\lambda_2},\ \text{and}\ \lambda_3 + \lambda_4 - |\lambda_5| > -\sqrt{\lambda_1\lambda_2}, \tag{5.26}$$

while s-wave tree level unitarity imposes that:

$$|a_\pm|, |b_\pm|, |c_\pm|, |f_\pm|, |e_{1,2}|, |f_1|, |p_1| < 8\pi, \tag{5.27}$$

where:

$$
\begin{aligned}
a_\pm &= \frac{3}{2}(\lambda_1+\lambda_2) \pm \sqrt{\frac{9}{4}(\lambda_1-\lambda_2)^2+(2\lambda_3+\lambda_4)^2},\\
b_\pm &= \frac{1}{2}(\lambda_1+\lambda_2) \pm \sqrt{(\lambda_1-\lambda_2)^2+4\lambda_4^2},\\
c_\pm &= \frac{1}{2}(\lambda_1+\lambda_2) \pm \sqrt{(\lambda_1-\lambda_2)^2+4\lambda_5^2},\\
e_1 &= \lambda_3+2\lambda_4-3\lambda_5, \quad e_2 = \lambda_3-\lambda_5,\\
f_+ &= \lambda_3+2\lambda_4+3\lambda_5, \quad f_- = \lambda_3+\lambda_5,\\
f_1 &= \lambda_3+\lambda_4, \quad p_1 = \lambda_3-\lambda_4.
\end{aligned}
\tag{5.28}
$$

Vacuum stability finally requires [238]:

$$
m_{12}^2\left(m_{11}^2-m_{22}^2\sqrt{\lambda_1/\lambda_2}\right)\left(\tan\beta-\sqrt[4]{\lambda_1/\lambda_2}\right)>0 \tag{5.29}
$$

where the mass parameters m_{11}, m_{22}, m_{12} should satisfy:

$$
\begin{aligned}
m_{11}^2+\frac{\lambda_1 v^2\cos^2\beta}{2}+\frac{\lambda_3 v^2\sin^2\beta}{2} &= \tan\beta\left[m_{12}^2-(\lambda_4+\lambda_5)\frac{v^2\sin 2\beta}{4}\right]\\
m_{22}^2+\frac{\lambda_2 v^2\sin^2\beta}{2}+\frac{\lambda_3 v^2\cos^2\beta}{2} &= \frac{1}{\tan\beta}\left[m_{12}^2-(\lambda_4+\lambda_5)\frac{v^2\sin 2\beta}{4}\right]
\end{aligned}
\tag{5.30}
$$

Later on, we will include these constraints as well when doing our scans.

Turning towards the fermionic sector, we choose to couple the SM fermions to only one doublet, as explained in the first section of the previous chapter. On the contrary, we assume generic couplings of the VL fermions to both the $H_{1,2}$ doublets:[8]

$$
\begin{aligned}
-\mathcal{L}_{\rm VLL} &= y_i^{U_R}\overline{\mathcal{D}_L}\tilde{H}_i U'_R + y_i^{U_L}\overline{U'_L}\tilde{H}_i^\dagger\mathcal{D}_R + y_i^{D_R}\overline{\mathcal{D}_L}H_i D'_R + y_i^{D_L}\overline{D'_L}H_i^\dagger\mathcal{D}_R\\
&\quad + M_{\mathcal{D}}\overline{\mathcal{D}_L}\mathcal{D}_R + M_U\overline{U'_L}U'_R + M_D\overline{D'_L}D'_R + \text{h.c.},
\end{aligned}
\tag{5.31}
$$

where a sum over $i=1,2$ is implied. It is possible to define the Yukawa couplings y_h^X and y_H^X to the physical scalar states through the following rotations:

$$
\begin{pmatrix} y_h^X \\ y_H^X \end{pmatrix} = \begin{pmatrix} c_\beta & s_\beta \\ s_\beta & -c_\beta \end{pmatrix}\begin{pmatrix} y_1^X \\ y_2^X \end{pmatrix}, \quad \begin{pmatrix} H_{\rm SM} \\ H_{\rm NP} \end{pmatrix} = \begin{pmatrix} c_\beta & s_\beta \\ s_\beta & -c_\beta \end{pmatrix}\begin{pmatrix} H_1 \\ H_2 \end{pmatrix}, \tag{5.32}
$$

where we used the superscript $X = U_{L/R}$ or $D_{L/R}$. As we are working in the alignment limit, $H_{\rm SM}$ becomes the SM Higgs doublet, while $H_{\rm NP} = \begin{pmatrix} H^+ \\ (H-iA)/\sqrt{2} \end{pmatrix}$ contains all the new scalar degrees of freedom. Since we are coupling the VL fermions to both doublets, the value of t_β or the chosen type of 2HDM will be irrelevant for the VLF coupling to the scalars.

A DM candidate is again straightforwardly introduced by considering a Lagrangian of the form (5.31) with $U \equiv N$ and $D \equiv E$. Our analysis will substantially follow the same

[8] Since we are coupling the VLFs to both doublets, we cannot rigorously refer to type-I, type-II, lepton specific, or flipped 2HDMs, as flavor violating Yukawa couplings, possibly responsible for FCNCs, might be induced radiatively by the VLLs. We will nevertheless retain the classification of the various 2HDM realizations in order to distinguish the different dependence on $\tan\beta$ of the couplings of the SM fermions and the Higgs mass eigenstates.

lines as in the case of VLL extensions of the SM Higgs sector. Before determining the DM observables and comparing them with experimental constraints, we reformulate, in the next subsections, for the case of the 2HDM, the constraints from the SM Higgs signal strengths and from EWPT. We also consider an additional set of constraints, namely the ones coming from RGEs, which limit the size of the new Yukawa couplings.

5.3.1 Higgs Signal Strengths

Having imposed the alignment limit, the extended Higgs sector does not influence the decay branching fractions of the 125 GeV SM-like Higgs. The only possible source of deviation from the SM expectation is represented by the VLLs, which can affect the $h \to \gamma\gamma$ signal strength, $\mu_{\gamma\gamma}$. The corresponding contribution substantially coincides with the one determined in the one Higgs doublet scenario, namely eq. (5.8). Assuming the presence of only one family of VLLs, the simplest solution for having an experimentally viable scenario is to set to zero one of the $y_h^{E_{L,R}}$ couplings. Unless differently stated, we will assume, in the analysis below, that $y_h^{E_R} = 0$.

5.3.2 EWPT Constraints

In a 2HDM+VLL framework, new contributions (with respect to the SM) to the S and T parameters are generated by both the fermionic and the scalar sector. Regarding the former, these contributions depend, as for the case of one Higgs doublet, on the masses of the new fermions and their couplings $y_h^{N_{L,R},E_{L,R}}$ to the SM-like Higgs, while the couplings with the other Higgs states are unconstrained. The contributions from the scalar sector are instead related to the masses of the new Higgs states. Also in this case it is possible to forbid deviations from the SM expectations of the T parameter by imposing a custodial symmetry. In the alignment limit this is realized by setting $m_H \simeq m_{H^\pm}$ or $m_A \simeq m_{H^\pm}$ [3, 239] and considering only constraints from the S parameter. As already pointed out and further clarified below, this choice would imply excessive limitations to DM phenomenology. For this reason we will not impose a custodial symmetry neither to the fermionic nor to the scalar sector, but rather freely vary the corresponding parameters and require in turn that the S, T parameters do not deviate by more than 3σ from their best fit values.

For illustrative purposes, we have reported in fig. (5.4) the regions allowed by EWPT for some definite choices of model parameters. More specifically, we have fixed the values of the DM candidate mass m_{N_1} and of the lightest charged new fermion m_{E_1}, as well as the Yukawa coupling $y_h^{N_L}$, to, respectively, 120 GeV, 250 GeV and 0.01 (this very low value is motivated by constraints from DM DD), while we have varied the parameter $y_h^{E_L}$, since it will be relevant for the DM relic density as well as for LHC detection prospects. Regarding the scalar sector we have fixed $m_A = 500$ GeV (left panel) and $m_A = 800$ GeV (right panel) and varied the mass of the CP-even Higgs state H and of the charged one $H^\pm$. For $y_h^{E_L} \leq 1$ the effect of the fermionic sector on the EWPT is subdominant such that the allowed regions substantially correspond to the one allowed in the case where no VLLs are present in the theory. On the contrary, once the value of $y_h^{E_L}$ is increased, a cancellation between the contributions from the fermionic and scalar sectors is needed in order to comply with experimental constraints. As a consequence, the allowed regions of the parameter space are reduced to rather narrow bands. We also notice that, in this last case, the constraints from EWPT disfavor mass degenerate $H, A, H^\pm$. We remind that, on the other hand, the variation of the masses of the Higgs states is constrained by perturbativity and unitarity limits, eq.(5.26)-(5.27). We have then reported on fig. (5.4) the regions allowed by these latter constraints, determined by

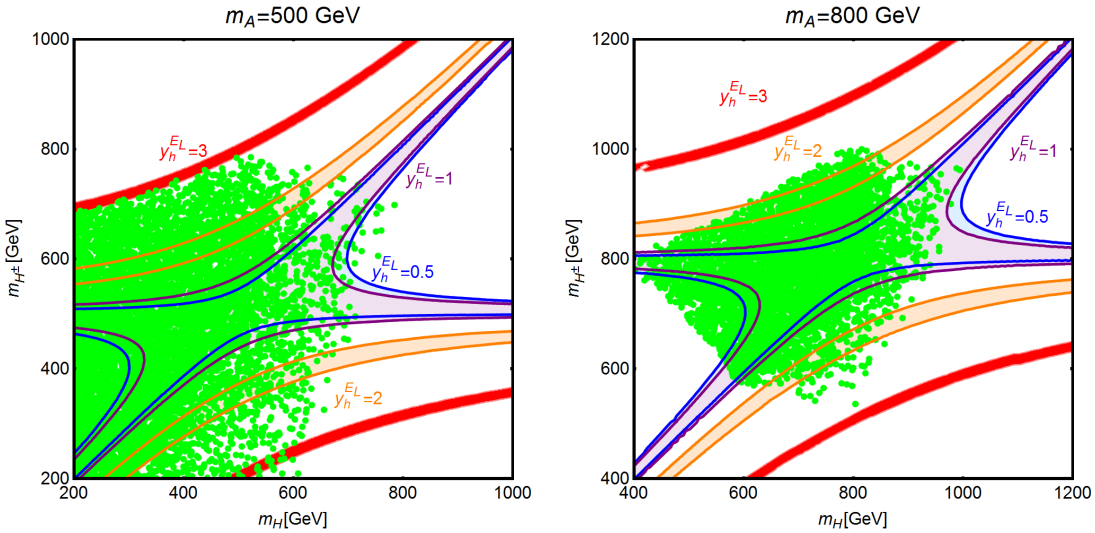

Figure 5.4 – Impact of EWPT constraints in the bidimensional plane $(m_H, m_{H^\pm})$ for two fixed assignations of m_A, i.e. 500 and 800 GeV. The blue,purple,orange and red regions represent the allowed parameter space for, respectively, $y_h^{E_L} = 0.5, 1, 2, 3$. The green points represent the configurations allowed by the constraints reported in eq. (5.26) and (5.27).

varying the input parameters of eq. (5.25) over the same ranges considered in [236] (contrary to this reference we have nevertheless assumed alignment limit). As we can see, values of $y_h^{E_L}$ above 3 are excluded for $m_A = 500\,\text{GeV}$ while for $m_A = 800\,\text{GeV}$ we get the even stronger constraint $y_h^{E_L} \lesssim 2$.

5.3.3 Constraints from RGE Evolution

The extension of the Higgs sector with VLFs is also constrained by demanding theoretical consistency. Indeed, the presence of new fermions affects the RGE evolution of the parameters of the 2HDM, in particular the gauge couplings and the quartic couplings of the scalar potential [240], making it difficult for the new states to induce sizable collider signals, as, for example, diphoton events [241–248] (see also below).

Regarding the gauge couplings, their β functions receive a positive contribution depending on the number of families of vector-like fermions and on their quantum numbers under the SM model gauge group. In the case where these contributions are too high, the gauge couplings can be lead to a Landau pole at even moderate/low energy scales. However, in the case considered in this chapter, i.e. one family of vector like leptons, we have only a small contribution to the β functions of the couplings g_1 and g_2 which does not affect in a dangerous way their evolution with energy.

Instead, the case of the quartic couplings is different. As already seen in the case of a SM-like Higgs sector, the radiative corrections associated to the VLLs depend on their

Yukawa couplings. The β functions are given by:

$$\beta_{\lambda_1} = \beta_{\lambda_1,\text{2HDM}} + \frac{1}{8\pi^2}\left(\lambda_1 \sum_L |y_1^L|^2 - \sum_L |y_1^L|^4\right), \tag{5.33}$$

$$\beta_{\lambda_2} = \beta_{\lambda_2,\text{2HDM}} + \frac{1}{8\pi^2}\left(\lambda_2 \sum_L |y_2^L|^2 - \sum_L |y_2^L|^4\right), \tag{5.34}$$

$$\begin{aligned}\beta_{\lambda_3} = \beta_{\lambda_3,\text{2HDM}} + \frac{1}{16\pi^2}\Bigg(&\lambda_3 \sum_L (|y_1^L|^2 + |y_2^L|^2) \\ &- 2y_1^{E_L} y_2^{E_L} y_1^{N_L} y_2^{N_L} + (|y_1^{N_L}|^2 + |y_1^{E_L}|^2)(|y_2^{N_L}|^2 + |y_2^{E_L}|^2) \\ &- 2y_1^{E_R} y_2^{E_R} y_1^{N_R} y_2^{N_R} + (|y_1^{N_R}|^2 + |y_1^{E_R}|^2)(|y_2^{N_R}|^2 + |y_2^{E_R}|^2)\Bigg),\end{aligned} \tag{5.35}$$

$$\begin{aligned}\beta_{\lambda_4} = \beta_{\lambda_4,\text{2HDM}} + \frac{1}{16\pi^2}\Bigg(&\lambda_4 \sum_L (|y_1^L|^2 + |y_2^L|^2) \\ &- 2y_1^{E_L} y_2^{E_L} y_1^{N_L} y_2^{N_L} + (|y_1^{N_L}|^2 - |y_1^{E_L}|^2)(|y_2^{N_L}|^2 - |y_2^{E_L}|^2) \\ &+ 2y_1^{E_R} y_2^{E_R} y_1^{N_R} y_2^{N_R} + (|y_1^{N_R}|^2 - |y_1^{E_R}|^2)(|y_2^{N_R}|^2 - |y_2^{E_R}|^2)\Bigg),\end{aligned} \tag{5.36}$$

$$\beta_{\lambda_5} = \beta_{\lambda_5,\text{2HDM}} + \frac{1}{16\pi^2}\left(\lambda_5 \sum_L (|y_1^L|^2 + |y_2^L|^2) - 2\sum_L |y_1^L|^2 |y_2^L|^2\right), \tag{5.37}$$

where $\beta_{\lambda_i,\text{2HDM}}$ are the contributions to the β function originating only from the quartic couplings themselves and the Yukawa couplings of the SM fermions. We refer to [150] for their explicit expressions. To simplify the notation, we have expressed, in eqs. (5.33)-(5.37) [9], the Yukawa couplings in the (H_1, H_2) basis.

As evident, the quartic couplings receive large radiative corrections scaling either with the second or the fourth power of the Yukawa couplings. As a consequence, vacuum stability and/or perturbativity and unitarity might be spoiled at some given energy scale unless additional degrees of freedom are introduced in the theory.

A quantitative analysis would require the solution of eqs. (5.33)-(5.37) coupled with RGEs for the gauge and Yukawa couplings as a function of the masses of the Higgs eigenstates and the parameters M and t_β, which determine the initial conditions for $\lambda_{1,5}$, and then verifying conditions (5.26) and (5.27) as functions of the energy scale. A good qualitative understanding can be nevertheless achieved by noticing that for sizable Yukawa couplings the β functions (5.33)-(5.37) are dominated by the negative contributions scaling with the fourth power of the Yukawas themselves (their β function are positive, scaling qualitatively as $\beta_y \propto y^3$). As a consequence one can focus, among (5.26) and (5.27), on the conditions $\lambda_{1,2} > 0$. In an analogous fashion to the case of the SM Higgs sector, discussed in the previous section, we will just require low energy viability of the model. In other words, a given set of model parameters will be regarded as (at least phenomenologically) viable if the scale at which the couplings λ_1, λ_2 become negative is considerably above few TeVs, i.e. far enough from the energy scales probed by collider processes. Additional degrees of freedom at a high energy scale might, at this point, improve the UV behavior of the theory. The study of such explicit scenarios is however beyond the purposes of this study.

According to the discussion above, in a phenomenologically viable setup, the quartic couplings λ_1 and λ_2 should not vary too fast with the energy. As proposed in [249], an

[9] Notice that even if the couplings λ_6 and λ_7 have been set to zero, they are radiatively generated. So one should also consider their β function as well as additional terms in eqs. (5.33)-(5.37). For simplicity we have not explicitly reported these contributions but we have included them in our numerical computations.

approximate but reliable condition consists in imposing $|\beta_{\lambda_{1,2}}/\lambda_{1,2}| < 1$, with $\lambda_{1,5}$ computed according to eqs. (5.25) and the Yukawa couplings set to their input value at the EW scale. In case this condition is not fulfilled, the functions $\beta_{\lambda_{1,2}}$ would vary too fast with the energy so that the theory would manifest a pathological behavior already in the proximity of the energy threshold corresponding to the masses of the VLLs [10].

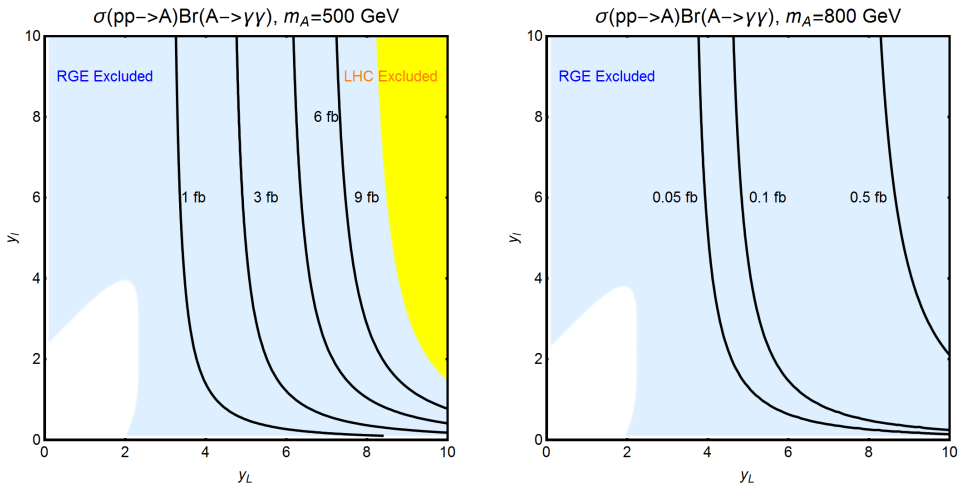

Figure 5.5 – Contours of the process $pp \to A \to \gamma\gamma$ for the two values $m_A = 500\,\text{GeV}$ (upper panel) and $m_A = 800\,\text{GeV}$ (lower panel), as function of the parameters $y_{l,L}$ (see main text). In both plots we have considered type-I 2HDM with $\tan\beta = 1$. The yellow region in the left panel is excluded by present LHC searches. In the region at the left of the 1 fb (left panel) and 0.05 fb (right panel) contours, the production cross-section varies in a negligible way with $y_{l,L}$ and basically coincides with the prediction of the 2HDM without VLLs. The blue region corresponds to theoretically inconsistent, because of RGE effects, values of the Yukawa parameters.

As already pointed out, the requirements of a reliable behaviour of the theory under RG evolution mostly affect possible predictions of LHC signals. As it will be reviewed in greater detail in the next subsections, one of the most characteristic signatures induced by the VLLs are enhanced diphoton production rates from decays of resonantly produced H/A states. This happens because their effective couplings with photons are increased by triangle loops of electrically charged VLLs such that, once their masses are fixed, the corresponding rate depends on the size of the Yukawa couplings. The constraints from RGE can be used to put an upper limit on the size of the Yukawa couplings which imply, in turn, an upper limit on the diphoton production cross-sections which are expected to be observed.

As an illustration, we report in fig. (5.5) the isocontours of $\sigma(pp \to A)Br(A \to \gamma\gamma)$ as a function of $y_l = y_h^{E_L}$ and $y_L = y_H^{E_L} = -y_H^{E_R} = -y_H^{N_L} = y_H^{N_R}$ (see below for clarification), for two values of m_A, namely 500 and 800 GeV. As a further assumption, we have set $m_{E_1} = m_A/2$ in order to maximize the effective coupling between A and the photons [11].

As it is clear, in order to obtain substantial deviations of $\sigma(pp \to A)Br(A \to \gamma\gamma)$ from the prediction of a 2HDM without VLLs, which is approximately 1 fb and 0.05 fb for the

[10] We remark that our discussion has mostly qualitative character since it is based on 1-loop β-functions.

[11] In the computation we have considered only a "perturbative" enhancement. A further enhancement can be achieved through non perturbative effects [250], at the price of a rather strong fine tuning of $|m_A/2 - m_{E_1}|$. We won't consider this case here.

two examples considered, rather high values of the new Yukawas are needed [12], which would induce too large radiative corrections to the quartic couplings of the scalar potential. In theoretically consistent realizations, the VLLs typically have negligible effects on the diphoton production cross-section.

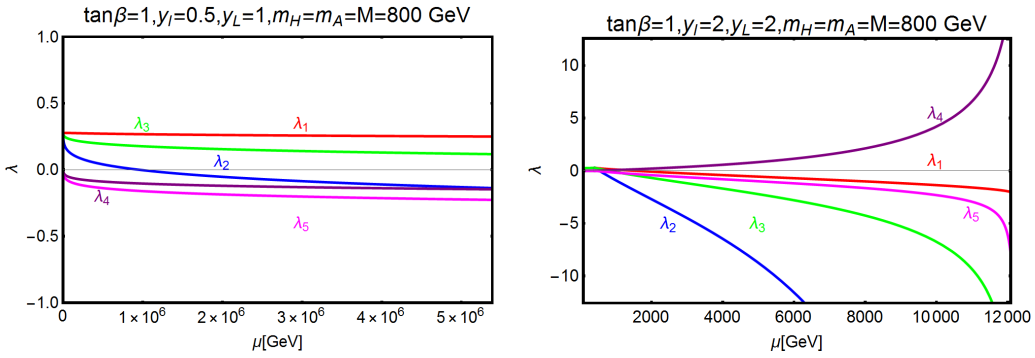

Figure 5.6 – Two examples of resolution of the RGE equations. The corresponding assignations of the relevant model parameters are reported on top of the panels. In the left panel, the initial values of the Yukawa couplings are sufficiently small such that the conditions (5.26)-(5.27) are satisfied up to energy scales of the order of 10^6 GeV. In the right panel the assignation of the Yukawas causes, instead, the couplings $\lambda_{1,2}$ to become negative already at the energy threshold of the VLLs.

We have checked the validity of the criterion $|\beta_{\lambda_{1,2}}/\lambda_{1,2}| \leq 1$ by explicitly solving the RGE for some benchmark models. We present two examples of solutions in fig. (5.6). Here we have considered the same values for the model parameters as in the left panel of fig. (5.5), and chosen two assignations of the Yukawa parameters $y_{l,L}$. In the left panel, we have considered the set $(y_l, y_L) = (0.5, 1)$, lying in the white region of the right panel of fig. (5.5). As evident, the couplings $\lambda_{1,2}$ remain positive up to an energy scale μ of the order of 10^6 GeV, high enough such that the model point is viable at (least from a phenomenological point of view).[13] On the contrary, by choosing parameter values lying in the blue region, RGEs drive the couplings $\lambda_{1,2}$ to negative values already at the energy threshold of the charged VLLs, of the order of 400 GeV for the case considered.

5.3.4 DM Phenomenology

The coupling of the DM to an additional Higgs doublet has a two-fold impact on dark matter phenomenology. First of all, the extra neutral Higgs states constitute additional s-channel mediators for DM annihilations and, only for the case of H, t-channel mediators for scattering processes relevant for Direct Detection. In addition, in the high DM mass regime, they may represent new final states for DM annihilation processes.

The coupling of the DM with the non SM-like Higgs states can be expressed, in the mass

[12] This requirement can be partially relaxed by introducing more than one family of VLL.

[13] We have explicitly checked the other conditions (5.26)-(5.27) as a function of the energy and found that these are violated at a slightly lower scale of 5×10^5 GeV. This difference is acceptable as it does not affect the validity of our results: our goal is not to quantitatively determine the scale at which the theory should be completed, but just to set a qualitative criteria that applies to the theory at low energy.

basis, in terms of the Yukawa couplings y_H^X and of the mixing angles $\theta_X^{L,R}$:

$$\begin{aligned} y_{HN_1N_1} &= \frac{\cos\theta_N^L \sin\theta_N^R y_H^{N_L} + \cos\theta_N^R \sin\theta_N^L y_H^{N_R}}{\sqrt{2}}, \\ y_{AN_1N_1} &= i\frac{\cos\theta_N^L \sin\theta_N^R y_H^{N_L} - \cos\theta_N^R \sin\theta_N^L y_H^{N_R}}{\sqrt{2}}, \\ y_{H^+N_1E_1} &= \cos\theta_N^L \sin\theta_E^R y_H^{E_L} + \sin\theta_N^L \cos\theta_E^R y_H^{E_R} \\ &\quad - \cos\theta_N^R \sin\theta_E^L y_H^{N_R} - \cos\theta_N^L \sin\theta_E^R y_H^{N_L}. \end{aligned} \tag{5.38}$$

The analysis of the DM phenomenology is structured in an analogous way as the one performed in the previous section. We compute the DM annihilation cross-section and verify for which choices of the model parameters the thermally favored value, $\sim 3\times 10^{-26}\,\mathrm{cm^3 s^{-1}}$, is achieved without conflicting with bounds from DM Direct Detection. Given the dependence of the coupling between the DM and the neutral Higgs states on the mixing angles $\theta_N^{L,R}$, the DM scattering cross-section is still dominated by the Z exchange processes so that the new couplings from eq. (5.38) mostly impact the determination of the DM relic density.

For what regards the DM relic density, we distinguish several possibilities:

- $m_{N_1} \leq m_X/2, X = A, H, H^\pm$ and sizable mass splitting between the DM and the other vector-like fermions. In this case the situation is very similar to the case of SM+VLLs. The most relevant DM annihilation channels are again into fermion and gauge boson pairs. Reminding that, in the alignment limit, there is no tree-level coupling between the H, A states and the W, Z bosons, the only annihilation processes substantially influenced by the presence of the additional Higgs bosons are the ones into SM fermions. In particular, s-channel exchange of the CP-odd Higgs gives rise to a new s-wave contribution so that the DM annihilation cross-section can be schematized as:

$$\begin{aligned} \langle\sigma v\rangle_{ff} &= \frac{m_{N_1}^2}{8\pi}\frac{m_t^2}{v^2}|\xi_A^t|^2 \frac{1}{((4m_{N_1}^2 - m_A^2)^2 + m_A^2\Gamma_A^2)}|y_{AN_1N_1}|^2 \\ &+ \frac{g^2 m_{N_1}^2}{\pi((4m_{N_1}^2 - m_Z^2)^2 + m_Z^2\Gamma_Z^2)}\left[\sum n_c^f(|V_f|^2 + |A_f|^2)|y_{V,ZN_1N_1}|^2\right. \\ &\left. + \frac{3m_t^2}{2m_{N_1}^2}(|V_t|^2 + |A_t|^2)|y_{A,ZN_1N_1}|^2\right]. \end{aligned} \tag{5.39}$$

  As evident, the annihilation cross-section depends, through the factor ξ, on $\tan\beta$ and, in turn, on the realization of the couplings of the two Higgs doublets to SM fermions. Given the dependence on the mass of the final state fermions, A-exchange diagrams give a sizable contribution mostly to the $\bar{t}t$ final state, when kinematically open (an exception being a type II/flipped 2HDM for $\tan\beta \gtrsim 45$, when a sizable contribution comes also from $\bar{b}b$).

  As already pointed out, the strong DD limits, mostly originating from t-channel Z exchange, impose that the DM is essentially a $SU(2)$ singlet with, as well, a tiny hypercharged component. This implies also a suppression of the couplings of the DM to the neutral Higgs states, such that the DM is typically overproduced in the parameter regions compatible with DD constraints. It is nevertheless possible to achieve the correct relic density by taking advantage of the resonant enhancement of the DM annihilation cross-section when the condition $m_{N_1} \simeq \frac{m_{H,A}}{2}$ is met. Notice that in this case the DM annihilation cross-section is also sensitive to the total width of the H/A state and thus sensitive to the value of $\tan\beta$. An illustration of the DM constraints in

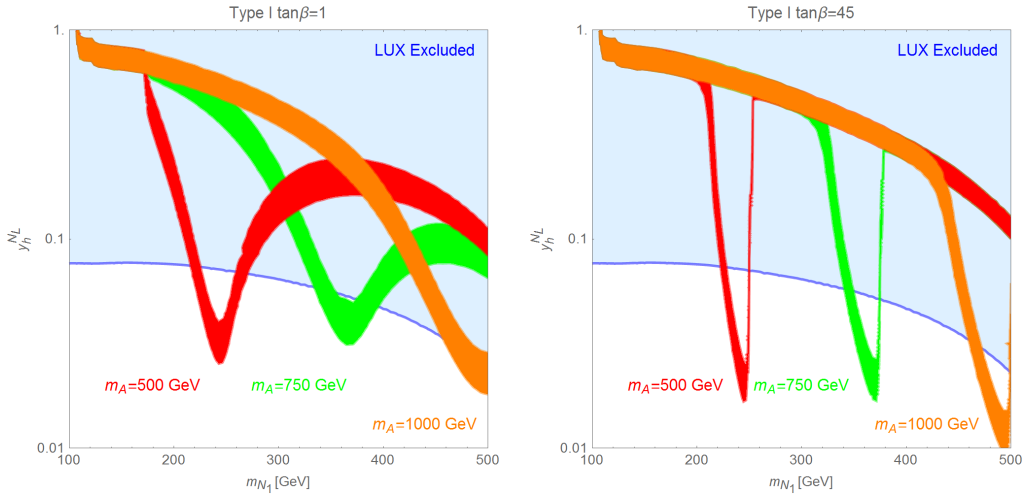

Figure 5.7 – Isocontours of the correct DM relic density in the bidimensional plane $(m_{N_1}, y_h^{N_L})$ for two values of $\tan\beta$, (left panel) 1 and (right panel) 45, and for the following assignations of the other parameters of the fermion sector: $y_h^{N_R} = y_h^{E_R} = 0$, $y_h^{E_L} = 0.5$, $y_H^{N_L} = -y_H^{N_R} = -y_H^{E_L} = y_H^{E_R} = 1$. We have finally set $M = m_H = m_A = m_{H^\pm}$ and considered the three values of 500 GeV, 750 GeV and 1 TeV.

the $m_{N_1} \leq \frac{m_{A,H}}{2}$ regime is provided in fig. (5.7). Here we compare, for two values of $\tan\beta$ (for definiteness we have considered type-I 2HDM), the isocontours of the correct DM relic density, for three choices of $m_A = m_H = m_{H^\pm}$, and the DD exclusion limit, as set by LUX. As already anticipated the only viable regions are the ones corresponding to the s-channel poles. We also notice that the shapes of the relic density contours are influenced by the large (narrow) widths of the resonances occurring for small (high) $\tan\beta$.

Concerning Indirect Detection, possible signals might be originated by residual annihilation processes, at present times, into $\bar{f}f$ (mostly $\bar{b}b$ and $\bar{t}t$ when kinematically accessible), W^+W^-, ZZ and Zh, since their corresponding annihilation cross-section have unsuppressed s-wave (i.e. velocity independent) contributions. These annihilation processes can be probed by searches of gamma-rays produced by interactions of the primary products of DM annihilation. The most stringent constraints come from searches in Dwarf Spheroidal galaxies (DSph) [4]. These kind of constraints can probe thermally favored values of the DM annihilation cross-section only for DM masses below 100 GeV. As evidenced in fig. (5.8) they are then considerably less competitive, with the exception of the resonance region, than the ones from DD. An additional indirect signal might be represented by gamma-ray lines produced in the annihilation process $N_1N_1 \to \gamma\gamma$ originated by a 1-loop induced effective vertex between the pseudoscalar Higgs state A and two photons [189, 251, 252]. In our setup this annihilation channel is, however, rather suppressed so that it is not capable to probe the thermal DM region (see dashed yellow line in fig. 5.8).

- $m_{N_1} < m_X/2, X = A, H, H^\pm$ and DM close in mass with at least the lightest charged VLL. In this case the DM relic density is not only accounted for by pair annihilation of the DM particle N_1, but also by coannihilation processes of the type $N_iE_j \to$

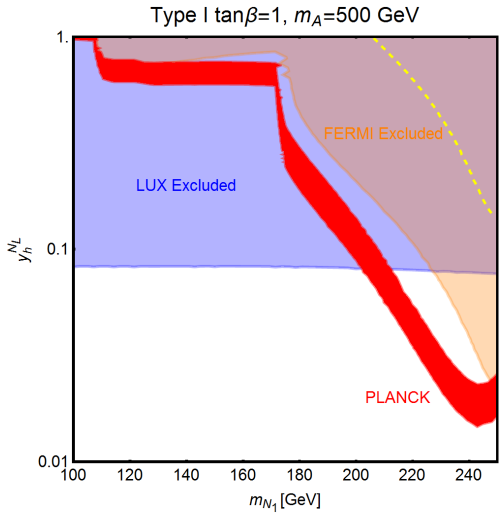

Figure 5.8 – Comparison between the different DM constraints from one of the benchmarks considered in fig. (5.7). In addition to the already considered constraints from relic density and DD, the figure reports (in orange) the excluded region by searches of gamma-rays in DSph [4] as well as the limit (yellow dashed line) from gamma-ray lines [5].

$\bar{f}f', W^{\pm}h, W^{\pm}Z$, $i, j = 1, 2$ [14] (in most of our computations we have assumed $M_E = M_L$ and, then, the charged eigenstates are very close in mass) which occur through s-channel exchange of the $W^{\pm}$ and the $H^{\pm}$ or t-channel exchange of the VLLs themselves. These kinds of process can be easily dominant, provided a low enough mass splitting, with respect to N_1N_1 annihilation since their corresponding annihilation rates depend on the couplings $y_h^{E_L}, y_H^{E_{L,R}}$ which are not subject to the strong constraints from DD. We also notice that coannihilations would be relevant in case that a custodial symmetry is imposed in the VLF sector.

The DM phenomenology in presence of coannihilations is illustrated in fig. (5.9). We show, in the left panel, the isocontours of the correct DM relic density in the bidimensional plane $(m_{N_1}, \frac{m_{E_1}-m_{N_1}}{m_{N_1}})$. For simplicity, we have set $y_h^{E_L} = y_H^{N_L} = -y_H^{N_R} = -y_H^{E_L} = y_H^{E_R}$ and considered two numerical values, i.e. 0.1 and 1. The remaining non-zero coupling, $y_h^{N_L}$, has been set to 10^{-3} in order to evade constraints from DD. The masses of the new Higgs states have been finally set to the value of 1 TeV in order to avoid effects on the relic density for DM masses of a few hundreds GeV. As evidenced in the figure, the correct relic density can be achieved through coannihilation processes, provided that the relative mass splitting between the DM and the lightest charged state is between approximately 2% and 10%.

We emphasize that we have chosen a much lower value of $y_h^{N_L}$ with respect to the limits shown, for example, in fig. 5.7. This is because an approximate degeneracy between m_{N_1} and m_{E_1} implies $M_N \simeq M_L$, which in turn generates an enhancement of the angles $\theta_N^{L,R}$. These angles are responsible of the coupling of the DM with the Z, which accounts for most of the SI cross-section. This last feature is well evidenced in the bottom panel of fig. 5.9, where we have assumed the $y_h^{N_L} = y_h^{E_L}$ limit to easily compare relic density and Direct Detection. As evident, the latter is responsible for very strong constraints, reaching almost $y_h^{N_L} \sim 10^{-3}$ and almost excluding the regions

[14] To a lower extent also the process $N_2N_2 \to W^+W^-$ can be relevant.

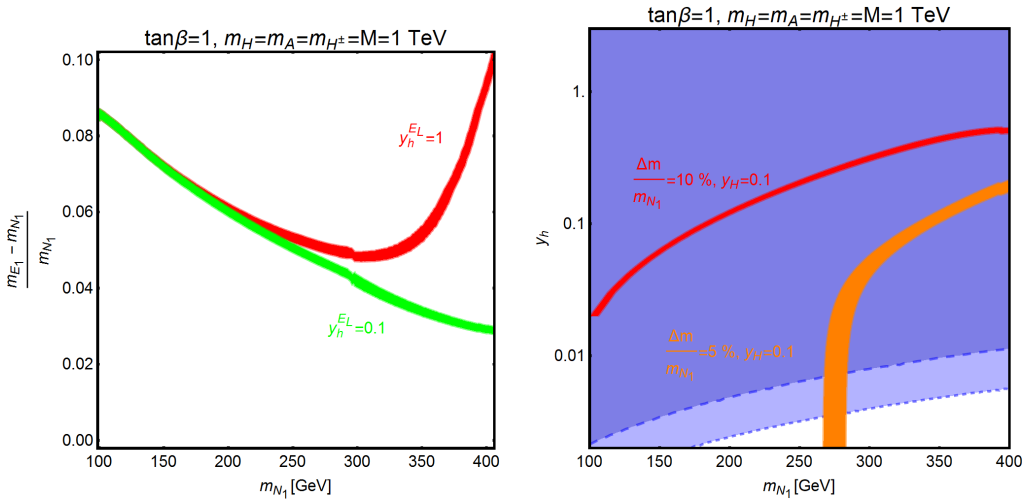

Figure 5.9 – Left panel:Isocontours of the correct DM relic density in the bidimensional plane $(m_{N_1}, \frac{m_{E_1}-m_{N_1}}{m_{N_1}})$ for $\tan\beta = 1$, $y_h^{N_R} = y_h^{E_R} = 0$, $y_h^{N_L} = 5\times10^{-3}$, and two assignations of $y_h^{E_L} = y_H^{N_L} = -y_H^{N_R} = -y_H^{E_L} = y_H^{E_R}$, i.e. 0.1 and 1. Notice that we have set $M = m_H = m_A = m_{H^\pm} = 1\,\text{TeV}$. Right panel: Isocontours of the correct relic density, assuming $y_h^{N_L} = y_h^{E_L}$, for two values of $\frac{m_{E_1}-m_{N_1}}{m_{N_1}}$, namely 5% and 10%, and the corresponding excluded region by LUX, in, respectively, blue and dark blue.

at viable DM relic density.

In the case that the DM relic density is mostly accounted by coannihilation processes we do not expect ID signals, since the rate of this kind of processes is (Boltzmann) suppressed at present times.

- $m_{N_1} > m_X/2, X = A, H, H^\pm$ (no coannihilations): in this case the situation is very different with respect to the case of the SM Higgs sector. Indeed, as the DM mass increases, new annihilation channels become progressively open. We have, first of all, when $m_{N_1} > m_X/2, X = A, H, H^\pm$, the opening of annihilation channels of the type VX where $V = Z, W^\pm, X = A, H, H^\pm$. By further increasing the DM mass, annihilation channels into pairs of Higgs states are finally reached. Among these new channels the most efficient turn out to be the ones into $W^\pm H^\mp$ and into $H^\pm H^\mp$. These processes can occur through t-channel exchange of the lightest charged state E_1, and the corresponding rates depend on the coupling $y_{H^+N_1E_1}$, which depends on parameters not involved in direct detection processes. Moreover, this coupling can be of sizable magnitude even for a SM singlet DM, provided that the charged state E_1 has a sizable $SU(2)$ component. The potentially rich phenomenology offered by the annihilations into Higgs and gauge bosons or into Higgs boson pairs is the reason why we have not strictly enforced a custodial symmetry in the scalar sector, since it would have imposed a too rigid structure to the mass spectrum.

  Concerning possible Indirect Detection constraints, these rely on gamma-ray signals originated in cascade decays of the $H^\pm, W^\pm$ [253]. Annihilations at present times have a smaller rate than at thermal freeze-out and then ID constraints, as shown in one example in fig. 5.10, are marginally relevant.

In order to explore the multi-dimensional parameter space we have then resorted to a

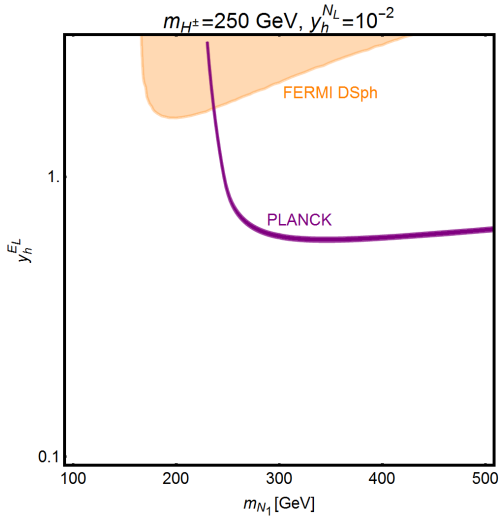

Figure 5.10 – Isocontour (purple line) in the bidimensional plane $m_{N_1}, y_h^{E_L}$ of the correct DM relic density for $m_{H^\pm} = 250\,\text{GeV}$. The orange region is excluded by searches of gamma-ray signals in DSph. The coupling $y_h^{N_L}$ has been set to 10^{-2} to evade constraints from DM direct detection.

scan of the following parameters:

$$\begin{aligned}
&y_h^{N_{L,R}} \in \left[10^{-3}, 1\right], \\
&y_h^{E_L} \in \left[5\times 10^{-3}, 3\right], \\
&M_N \in [100\,\text{GeV}, 1\,\text{TeV}], \\
&M_E = M_L \in [100\,\text{GeV}, 1\,\text{TeV}], \\
&\tan\beta \in [1, 50], \\
&m_A \in [250\,\text{GeV}, 1\,\text{TeV}], \\
&m_H \in [m_h, 1.5\,\text{TeV}], \\
&m_{H^\pm} \in [m_W, 1.5\,\text{TeV}], \\
&|M| \in [0, 1.5\,\text{TeV}],
\end{aligned} \tag{5.40}$$

and required that the model points pass the constraints from EWPT, from perturbativity and unitarity of the scalar quartic couplings, eqs. (5.26)-(5.27), and from satisfying the requirement of stability under RGEs, $|\beta_{\lambda_{1,2}}/\lambda_{1,2}| < 1$. We have finally required that the correct DM relic density is achieved. Similarly to the case discussed in the previous section, we have disregarded the possibility of coannihilations between the DM and other VLLs by further imposing a minimal mass difference between these states. We have repeated this scan for the different 2HDM realizations reported in tab. (4.1). Although the DM results are mostly insensitive to the type of couplings of the Higgs states to SM fermions, the prospects for LHC searches, discussed in the next subsection, will be different in the various cases.

The results of our analysis are again reported, in fig. (5.11), in the bidimensional plane $(m_{N_1}, \sigma_{\text{SI}})$. Similarly to the case of the single Higgs doublet scenario, many points, especially at lower values of the DM mass, are excluded by LUX. Viable model configurations nevertheless exist, already for DM masses of the order of 150 GeV. We notice in particular the presence of points lying beyond the reach of even next generation 1 Ton facilities such as XENON1T and LZ. This is because, for these configurations, the relic density is achieved through the annihilations into $H^\pm H^\mp$ and $H^\pm W^\mp$ final states, relying on the couplings $y_{h,H}^{E_{L,R}}$,

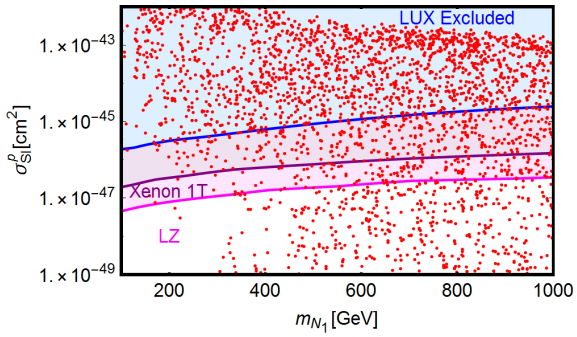

Figure 5.11 – Model points satisfying the correct DM relic density and passing EWPT, perturbativity and unitarity constraints, in the bidimensional plane (m_{N_1}, σ_{SI}). The blue region is excluded by current limits by LUX while the Purple and Magenta regions represent the reach of Xenon1T and LZ.

so that very small values of the neutral Yukawa couplings can be taken (as pointed above, in presence of a single family of VLLs, large deviations from the custodial limit are allowed provided suitable assignments of the masses of the Higgs states.)

5.3.5 Impact on LHC

In this section we discuss the impact on LHC phenomenology of the scenario under investigation. In the subsections below, we provide an overview of the possible relevant processes, which currently are (and will be probed in the near future) at the LHC. These are distinguished in three categories: (i) production of Higgs states and decay into SM fermion, (ii) production of the Higgs states and their subsequent decay into gauge bosons, especially photons, and (iii) direct production of VLLs. VLLs are directly involved only in the last two categories of collider signals; it is nevertheless important to consider as well limits/prospects from the first category of processes since they put constraints on the masses of Higgs states and on $\tan\beta$ which can, in turn, reduce the viable parameter space for DM.

Among this rather broad variety of signals, we dedicate particular attention to the diphoton production. It arises from the resonant production, and subsequent decay into photon pairs, of the neutral Higgs states. The VLL couplings entering in this process are the Yukawa couplings $y_{h,H}^{E_{L,R}}$. These couplings control the annihilation cross-sections into $W^\pm H^\mp$ and $H^\pm H^\mp$ final states, which mostly account for the DM relic density in the high DM mass regime; furthermore, they are influenced, through the S/T parameters, by the values of the neutral couplings $y_{h,H}^{N_{L,R}}$, which are in turn strongly constrained by DM phenomenology.

As a further simplification we consider the CP-even Higgs state A as the only candidate for a diphoton resonance. As explicitly shown in the following, this condition can be achieved by imposing a specific relation between the VLF Yukawa couplings, so as to minimize the impact of VLLs on the effective couplings between the CP-even state H and photons and, at the same time, maximize their impact on the effective $A\gamma\gamma$ coupling. This relation will allow to reduce the number of free parameters. This choice is also motivated by the fact that the production cross-section $pp \to A$ of the CP-odd state is, at parity of masses, bigger than the corresponding one of the CP-even state H. For the specific case of the diphoton production, as already pointed out, a further enhancement is achieved by a specific choice of the masses of the charged VLLs. As a consequence, focusing on the CP-odd Higgs A allows to obtain conservative limits which can be straightforwardly extended to the CP-even H.

Despite these simplifications, there is still a broad variety of factors which influence the collider phenomenology of a diphoton resonance. We thus summarize below the most relevant cases, basically distinguished by the value of $\tan\beta$:

- **Low** $\tan\beta$, i.e $\tan\beta = 1 - 7$: The neutral Higgs states are mostly produced through gluon fusion. Irrespective of the type of couplings with the SM fermions (see table 4.1), the top coupling to the heavy scalars is the dominant among the ones with SM fermions. This last coupling determines almost entirely the production cross sections of the processes $pp \to A/H$. The H/A resonances would then dominantly decay into $\bar{t}t$, or into a lighter neutral scalar (whether kinematically allowed) and a gauge boson,[15] except for the case of sizable decay branching fractions into charged and neutral VLLs (an important branching fraction into the DM would be nevertheless in strong tension with constraints from DM searches). In particular, for $\tan\beta = 1$, one can have very large decay width, $\Gamma/M \sim 5 - 10\%$, given essentially by decays into $\bar{t}t$. The observation of $t\bar{t}$ resonances would be an interesting complementary signature of a possible diphoton resonance. Searches of this kind of signals have been already performed at LHC Run I [175, 176]. The gluon-gluon fusion (ggF) mechanism can provide production cross-sections close to the experimental sensitivity only for $\tan\beta \simeq 1$, while for increasing values of $\tan\beta$ it gets rapidly suppressed.

- **Moderate** $\tan\beta$, i.e. $\tan\beta = 10 - 20$: While gluon fusion is still the most relevant production process, in a 2HDM with enhanced $\xi^d_{H,A}$ (type II and lepton-specific), a sizable contribution arises also from $b\bar{b}$ fusion. Regardless of the type of the 2HDM, the couplings between neutral resonances and SM fermions are suppressed, with respect to the previous scenario, so that they feature rather narrow width, unless sizable contributions arise from decays into VLLs (for $\tan\beta \gtrsim 5$ unitarity and perturbativity constraints favor a degenerate Higgs spectrum.). Large cross sections for the process $pp \to A/H \to \tau\tau$ are expected in a 2HDM with enhanced $\xi^l_{H,A}$, i.e. type II and flipped. Corresponding LHC searches [6, 7] give already strong limits, such that values of $\tan\beta$ above 10 are already excluded for $m_{A,H} < 500\,\text{GeV}$.

- **High** $\tan\beta$, i.e. $\tan\beta \simeq 50$: This regime occurs only for the type-I and flipped 2HDM since the other cases are essentially ruled out, for masses of the neutral Higgses below approximately 1 TeV, by the limits from $pp \to A/H \to \tau\bar{\tau}$. Two rather different scenarios correspond to these two types of 2HDM. In the flipped model the A/H scalars have enhanced couplings to b-quarks, implying $b\bar{b}$-fusion as dominant production process and, possibly, a large decay width dominated by the $b\bar{b}$ final state. In the case of the type-I 2HDM the neutral Higgses are "fermiophobic", since all their couplings to the SM fermions are suppressed by a factor $1/\tan\beta$. Unless the decays into VLLs are relevant, we have very narrow widths, even $\Gamma_{H,A}/m_{H,A} \sim 10^{-2}$, and a strong enhancement of the decay branching fraction into photons.

In the following sub-subsections we provide an overview, for the scenarios depicted above, of the possible relevant LHC signals and the corresponding constraints/prospects of detection. We have indeed identified some relevant subsets among the parameter points providing the correct DM relic density and in agreement with theoretical constraints. We have first of all considered a set of points in the low, namely $1 - 5$, $\tan\beta$ regime (although we mostly refer to type-I 2HDM, the various 2HDM realizations do not substantially differ in this

[15] This possibility is contrived because the very strong HAZ coupling would easily lead to very high decay widths, which would make difficult the observation of resonances.

regime, as already pointed out). To these we have added three subsets, characterized by $10 \leq \tan\beta \leq 40$, for, respectively, type-I, type-II and lepton-specific couplings of the 2 Higgs doublets with the SM fermions. Two subsets at $\tan\beta = 50$, corresponding to type-I and flipped realizations, have been finally included.

For our study we have adopted the cross-sections provided by the LHC Higgs Cross Section Working Group [254], which have been produced with `SusHi` 1.4.1 [255]. More specifically, for the 2HDM types with enhanced bottom quark couplings to heavy scalars (type-II and flipped), we have taken the $gg/\bar{b}b$ fusion cross sections calculated for the hMSSM [151, 172]. For the remaining two realizations, namely type-I and lepton-specific 2HDMs, regardless of the value of $\tan\beta$, the only important production mechanism is gg fusion, since $\bar{b}b$ fusion is suppressed not only by the lower bottom quark luminosity, but also by the $\bar{b}bA/H$ couplings, which scale as $1/\tan\beta$. Therefore, as both top and bottom quark couplings to the heavy scalars are proportional to $1/\tan\beta$ for type-I and lepton specific 2HDMs, it follows that the effective ggA/H couplings have a similar behaviour. Consequently, for these two realizations, we evaluated the gg fusion cross sections by simply taking the hMSSM ggF cross section for $\tan\beta = 1$ and rescaling it by $1/\tan^2\beta$.

$A/H \to \bar{f}f$

We start our analysis by considering the production processes $pp \to \bar{f}f$, with $f = \tau, t$. The associated phenomenology is essentially identical to the pure 2HDM case. Indeed, being singlets under $SU(3)$, the VLF do not modify the gluon fusion production vertex; furthermore, limits from DM phenomenology disfavour a sizable branching fraction of decay of the Higgs states into VLLs. For the case of DM this is easily understood by considering the strong limits from DM Direct Detection which require very suppressed couplings. A numerical check is provided on fig. 5.12 for the case of type-I 2DHM (the outcome would be analogous also for the other types of 2HDM).

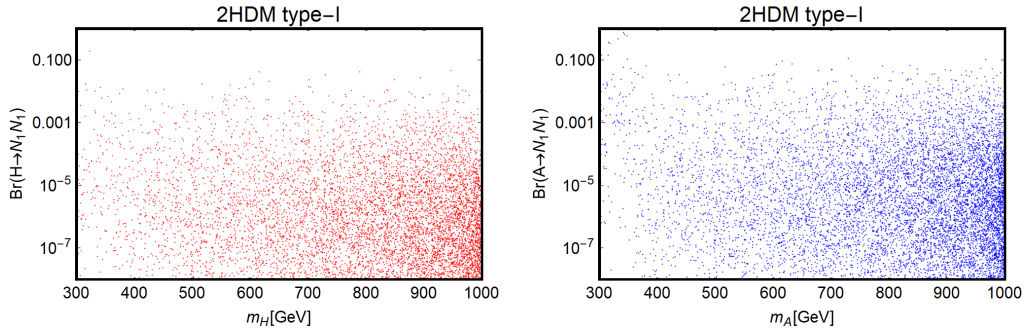

Figure 5.12 – Decay branching ratios of the Heavy CP even (left panel) and CP-odd (right panel) scalar into N_1N_1, as a function of their masses.

In fig. 5.12, we report the branching ratios of decay into DM pairs of the H and A bosons for model points, generated through a parameter scan over the ranges illustrated in the previous section, featuring a DM scattering cross-section below the current limit by the LUX experiment. The figure evidences typically suppressed or even negligible values for these branching fractions.

The couplings of the H/A bosons with the heavier VL neutrino and with the two VL electrons are, on the contrary, not directly constrained by direct detection and in principle could allow for sizable decay branching fractions. However, in two of the pinpointed scenarios

for the correct DM relic density, i.e. s-channel resonances and annihilations into heavy Higgses, these decay processes are kinematically forbidden. Furthermore the coannihilation scenario is as well contrived for what regards collider prospects. We then leave this matter aside for the moment and postpone a dedicated discussion to a following sub-subsection.

Since the branching fractions of the Higgses decaying into fermions depend on the masses of the final state fermions themselves, sizable signals can be achieved only for $\bar{t}t$, $\tau\tau$ and $\bar{b}b$ final states. The observation of the latter is substantially shadowed by huge SM backgrounds, such that only $\bar{t}t$ and $\tau\tau$ feature observational prospects. Tau pair searches can probe type-II 2HDMs at moderate-to-high $t_\beta \gtrsim 5$, depending on the value of m_A, since in this case we have an enhancement of the τ Yukwawa coupling to A, $\xi_A^\tau = t_\beta$. In a complementary manner, $t\bar{t}$ searches provide a discovery avenue for small values of t_β, typically $\lesssim 3$ [256–259], for any type of 2HDM. However, looking for heavy scalars decaying into top quark pairs is challenging from the experimental point of view, since the interference between the signal and the SM background can give rise to non-trivial dip-peak structures in the $\bar{t}t$ invariant mass spectrum, which get smeared after binning, thus reducing the visibility of a potential "bump" [259,260]. We also mention that the search for scalar resonances lighter than 500 GeV decaying to $\bar{t}t$ pairs is not possible, as the t and $\bar{t}$ quark are not boosted enough, the selection cuts thus being inefficient.

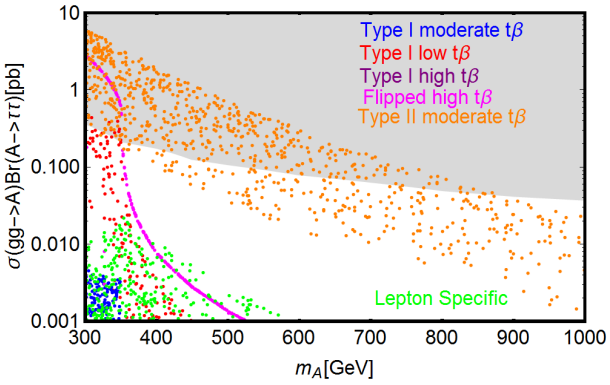

Figure 5.13 – Production cross-section for the process $pp \to \bar{\tau}\tau$ for the set of models with viable relic density. The colors distinguish the type of 2HDM realizations. The gray region is excluded by current limits [6, 7].

We display in fig. 5.13 the $\tau\tau$ production cross-section for the model points passing the theoretical and DM constraints, distinguishing, with different colors, the various 2HDM scenarios depicted above. As already stated, current LHC constraints are mostly efficient in the 2HDM-II. They can nevertheless also exclude low values of m_A for other 2HDM realizations.

We then focus, in the left panel of fig. (5.14), on the 2HDM-II case, highlighting the dependence of the collider limits on the value of $\tan\beta$. As evident, values above 20 are excluded for m_A up to 1 TeV. A similar exercise has been performed in the right panel of fig. (5.14) for the case of the $pp \to A \to \bar{t}t$ process, in the scenario of very low $\tan\beta$, and all the points lie below current experimental sensitivity. Only the points with $\tan\beta \sim 1$ lie close enough to the experimental sensitivity in order to be probed in the near future.

Diphoton Signal

In this sub-subsection we investigate in more detail the prospects for observing a diphoton signal. The corresponding cross-section can be schematically written, in the narrow width

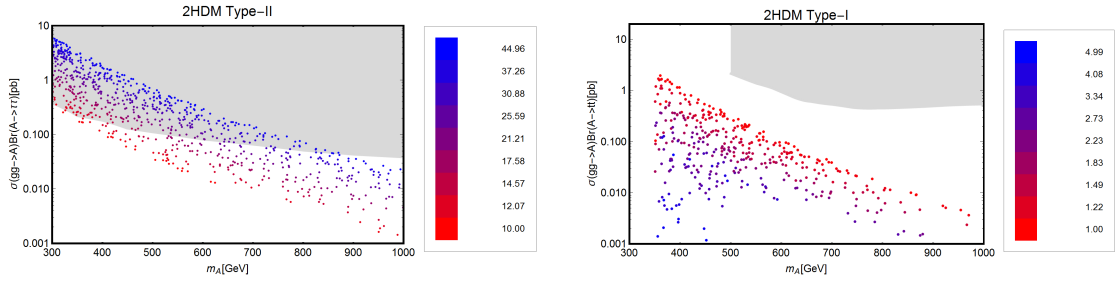

Figure 5.14 – Left panel: $pp \to \bar{\tau}\tau$ cross-section for type-II 2HDM. Right panel: $pp \to \bar{t}t$ for 2HDM type-I realizations in the low $\tan\beta$ regime. In both plots the points follow a color code according to the value of $\tan\beta$. The gray regions are already experimentally excluded.

approximation, as:

$$\sigma(pp \to \Phi \to \gamma\gamma) = \sigma(pp \to \Phi) Br(\Phi \to \gamma\gamma),\ \Phi = H, A, \tag{5.41}$$

with

$$Br(\Phi \to \gamma\gamma) \propto |\mathcal{A}^{\Phi}_{\rm SM} + \mathcal{A}^{\Phi}_{H^\pm} + \mathcal{A}^{\Phi}_{\rm VLL}|^2, \tag{5.42}$$

where $\mathcal{A}^{\Phi}_{\rm SM}$, $\mathcal{A}^{\Phi}_{H^\pm}$ and $\mathcal{A}^{\Phi}_{\rm VLL}$ represent, respectively, the loop induced amplitudes by SM fermions, charged Higgs (only present for the CP-even state H and typically negligible in comparison with the other contributions) and VLLs. The contribution associated to the VLLs can be written as:

$$\mathcal{A}^{\Phi}_{\rm VLL} = \sum_{i=1}^{2} \frac{v \left(\mathcal{C}^{\Phi}_E\right)_{ii}}{m_{E_i}} A^{\Phi}_{1/2}(\tau_{E_i}), \tag{5.43}$$

where we have used the definition:

$$\mathcal{C}^{\Phi}_E = U^E_L \cdot \mathcal{Y}^{\Phi}_E \cdot \left(U^E_R\right)^\dagger. \tag{5.44}$$

The Yukawa couplings between the VLLs and the heavy Higgs states are given by

$$\mathcal{Y}^H_N = \frac{1}{\sqrt{2}} \begin{pmatrix} 0 & y_H^{N_L} \\ y_H^{N_R} & 0 \end{pmatrix}, \quad \mathcal{Y}^H_E = \frac{1}{\sqrt{2}} \begin{pmatrix} 0 & y_H^{E_L} \\ y_H^{E_R} & 0 \end{pmatrix}, \tag{5.45}$$

for the heavy CP-even scalar H and:

$$\mathcal{Y}^A_N = \frac{1}{\sqrt{2}} \begin{pmatrix} 0 & -y_H^{N_L} \\ y_H^{N_R} & 0 \end{pmatrix}, \quad \mathcal{Y}^A_E = \frac{1}{\sqrt{2}} \begin{pmatrix} 0 & y_H^{E_L} \\ -y_H^{E_R} & 0 \end{pmatrix}, \tag{5.46}$$

for the CP-odd scalar A.

A general analytical expression for eq. (5.43) would be rather involved. We consider however two simplifying assumptions. First of all, in order to avoid dangerous contributions to the decay branching fraction into photons of the SM-like Higgs we set, as before, $y_h^{E_R} = 0$. Note that, especially in the case of heavier VLLs, one can relax this assumption, since the $h \to \gamma\gamma$ signal strength is currently measured with only $\sim 10 - 20\%$ accuracy; nevertheless, for simplicity, we take $y_h^{E_R} = 0$. Furthermore, we assume that $M_E = M_L$, such that the mass matrix for the charged VLLs simplifies to [16]

$$\mathcal{M}_E = \begin{pmatrix} M_E & v' y_h^E \\ 0 & M_E \end{pmatrix}. \tag{5.47}$$

[16] In fact, we checked that such a texture for the mass matrix suppresses, in a similar way as for $h \to \gamma\gamma$, the VLL contributions to $h \to Z\gamma$, thus leaving the latter decay SM-like.

Knowing that neither the sign of M_E nor the one of y_h^E are physical (both signs can be absorbed via a field redefinition), we will consider only positive values for these parameters. Thus, the eigenmass splitting reads

$$m_{E_2} - m_{E_1} = v' y_h^E, \tag{5.48}$$

with $M_E = \sqrt{m_{E_1}(m_{E_1} + v' y_h^E)}$ fixed in order to give m_{E_1} as the lowest eigenvalue. Under this assumptions the heavy scalar loop amplitudes can be written as:

$$\begin{aligned}\mathcal{A}^H_{\rm VLL} = \frac{-v'}{2m_{E_1} + v' y_h^E}\Bigg\{ & y_H^{E_L}\left[A^H_{1/2}(\tau_{E_1}) - A^H_{1/2}(\tau_{E_2})\right] \\ & + y_H^{E_R}\left[\frac{m_{E_1} + v' y_h^E}{m_{E_1}} A^H_{1/2}(\tau_{E_1}) - \frac{m_{E_1}}{m_{E_1} + v' y_h^E} A^H_{1/2}(\tau_{E_2})\right]\Bigg\},\end{aligned} \tag{5.49}$$

$$\begin{aligned}\mathcal{A}^A_{\rm VLL} = \frac{-v'}{2m_{E_1} + v' y_h^E}\Bigg\{ & y_H^{E_L}\left[A^A_{1/2}(\tau_{E_1}) - A^A_{1/2}(\tau_{E_2})\right] \\ & - y_H^{E_R}\left[\frac{m_{E_1} + v' y_h^E}{m_{E_1}} A^A_{1/2}(\tau_{E_1}) - \frac{m_{E_1}}{m_{E_1} + v' y_h^E} A^A_{1/2}(\tau_{E_2})\right]\Bigg\}.\end{aligned} \tag{5.50}$$

To improve the detection potential of the heavy scalars decaying into diphotons, it would be desireable maximize the value of $\mathcal{A}^A_{\rm VLL}$. This task is achieved by taking opposite signs for the $y_H^{E_R}, y_H^{E_L}$ couplings. We can thus reduce the number of free couplings by setting $y_H^{E_R} = -y_H^{E_L} \equiv y_H^E$. In this setup the H and A loop amplitudes become:

$$\mathcal{A}^H_{\rm VLL} = \frac{-v'^2 y_h^E y_H^E}{m_{E_1}(2m_{E_1} + v' y_h^E)}\left[A^H_{1/2}(\tau_{E_1}) + \frac{m_{E_1}}{m_{E_1} + v' y_h^E} A^H_{1/2}(\tau_{E_2})\right], \tag{5.51}$$

$$\mathcal{A}^A_{\rm VLL} = \frac{v' y_H^E}{m_{E_1}}\left[A^A_{1/2}(\tau_{E_1}) - \frac{m_{E_1}}{m_{E_1} + v' y_h^E} A^A_{1/2}(\tau_{E_2})\right]. \tag{5.52}$$

Note that, in the case where both $E_{1,2}$ mass eigenstates are much heavier than the scalar masses, i.e. $\tau_{E_{1,2}} \to 0$, the CP-even and CP-odd amplitudes differ only through the loop form factor:

$$\mathcal{A}^{A/H}_{\rm VLL} \simeq \frac{\pm v'^2 y_h^E y_H^E}{m_{E_1}(m_{E_1} + v' y_h^E)} A^{A/H}_{1/2}(0). \tag{5.53}$$

However, in the case where $A^A_{1/2}(\tau_{E_1})$ dominates over the second term in the brackets from eq. (5.52), which happens, for example, if $m_{E_1} \simeq m_A/2$ and $m_{E_2} \gg m_{E_1}$, the CP-odd amplitude is indeed maximized: $\mathcal{A}^A_{\rm VLL} \propto \frac{v'}{m_{E_1}}$, whereas $\mathcal{A}^H_{\rm VLL} \propto \frac{v'^2}{m_{E_1} m_{E_2}}$.

We present and confront with the current experimental limits [261], in fig.(5.15), the predicted cross-section for $pp \to A \to \gamma\gamma$, for the model points providing viable DM candidates. We distinguish between the different regimes described in the previous subsection, identified by the type of interactions with the fermions and by the value of $\tan\beta$. Clearly, the most promising scenarios are the ones corresponding to low $\tan\beta$ and to $\tan\beta \sim 50$ for the flipped 2HDM. These scenarios correspond, indeed, to the configurations which maximize the production vertex of the resonance: as already emphasized, for $\tan\beta \sim 1$ the gluon fusion process is made efficient by the coupling with the top quark, while for $\tan\beta \sim 50$ the production cross-section is enhanced by b-fusion. In the other type-I regimes, the cross-section fastly drops with the value of $\tan\beta$.

In all the considered regimes the diphoton cross-section lies below the current experimental sensitivity; the departure from the experimental sensitivity fastly reaches several orders of magnitude as the value of m_A increases. A signal in diphoton events would be hardly

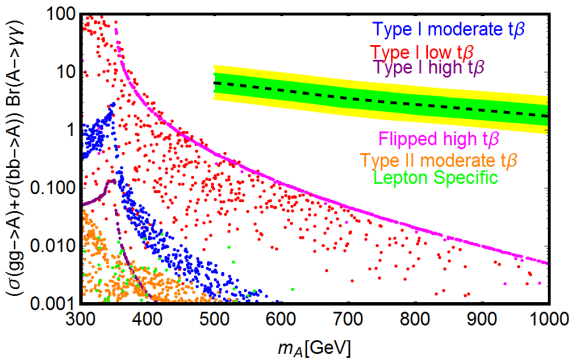

Figure 5.15 – Expected diphoton cross-section, as function of m_A for the model points featuring the correct DM relic density and pass constraints from EWPT, perturbativity and unitarity. The red points refer to type-I couplings of the Higgs doublets while the blue ones to the other type of couplings considered in this chapter.

observable, even in future luminosity upgrades, for $m_A \gtrsim 700\,\text{GeV}$. This outcome is a consequence of the fact that the size of the Yukawa couplings of the charged VLLs are limited from above by the requirement of consistency under RG evolution and, only for $y_h^{E_L}$, by EWPT. Therefore, no substantial enhancement of the diphoton production cross-section, with respect to the 2HDM without VLLs, is actually allowed (if one insists on having a theory which is consistent up to high energy scales). We notice, in addition, that in order to comply with limits from DM phenomenology, the VLLs should be typically heavier than the diphoton resonance. This translates in a further suppression of the VLL triangle loop contribution.

Other Loop-Induced Processes

Given their quantum number assignments (and gauge invariance), VLLs also induce, at one loop, decays of A/H into $Z\gamma, ZZ, WW$, which can be probed at the LHC.

Among these processes, the cleanest signal is likely provided by the $Z\gamma$ channel. It is searched for in events with one photon and dijets or dileptons originating from the decay of the Z. Although the corresponding production rate is suppressed with respect to diphoton signals, the potential signal is particularly clean (i.e. low background), especially in the case of lepton final states. In the setup under investigation, the $A \to Z\gamma$ decay width, to a very good approximation, reads [94, 170]

$$\Gamma(A \to Z\gamma) = \frac{\alpha g^2 m_A^3}{512\pi^4 v^2 c_W^2}\left(1 - \frac{m_Z}{m_A}\right)^3 \left|\mathcal{A}_t^{AZ\gamma} + \mathcal{A}_b^{AZ\gamma} + \mathcal{A}_{\text{VLL}}^{AZ\gamma}\right|^2 . \tag{5.54}$$

The top-loop and bottom-loop amplitudes have simple expressions,

$$\mathcal{A}_{t,b}^{AZ\gamma} = N_c Q_{t,b}\, V_{t,b}\, \xi_A^{t,b} A_{1/2}^A(\tau_{t,b}, \lambda_{t,b}), \tag{5.55}$$

with Q_f the electric charge of the SM fermion f, V_f its vectorial coupling to the Z boson, and $\xi_A^{t,b}$ defined in Table 4.1. For the $A_{1/2}^A(\tau_i, \lambda_i)$ loop form factors, we use the same expressions as in Ref. [94], with $\tau_i \equiv \frac{m_A^2}{m_i^2}$ and $\lambda_i \equiv \frac{m_Z^2}{m_i^2}$.

Concerning the VLL $A \to Z\gamma$ loop amplitude, its general expression, which is again given in the Appendix of Ref. [94] (denoted as $\tilde{\mathcal{A}}_f^{Z\gamma}$ there), is rather contrived, and will not be

displayed here. However, for our particular choice of the charged VLL mass and pseudoscalar Yukawa matrices, it takes the simple form

$$\mathcal{A}_{\rm VLL}^{AZ\gamma} = Q_e\, V_e \frac{v' y_H^E}{m_{E_1}} \left[A_{1/2}^A(\tau_{E_1}, \lambda_{E_1}) - \frac{m_{E_1}}{m_{E_1} + v' y_h^E} A_{1/2}^A(\tau_{E_2}, \lambda_{E_2}) \right], \tag{5.56}$$

with $Q_e = -1$ the electric charge of the VL electron and $V_e = -0.25 + s_W^2$ the vectorial coupling of the SM electron to the Z. One can see that, contrary to the general case, the diagrams with off-diagonal A and Z couplings to the VLFs vanish for our choice of parameters. Unfortunately, due to the smallness of $V_e \simeq 0.02$, our scenario does not produce a sizeable modification to the $A \to Z\gamma$ decay channel with respect to the case of an ordinary 2HDM.

We also briefly comment on the case of the WW and ZZ decay channels. As the $A \to \gamma\gamma/Z\gamma$ processes, both $A \to ZZ$ and $A \to WW$ are loop-suppressed (AWW/AZZ vertices are forbidden at tree level by CP-invariance). Moreover, detection of such decays is challenging due to either (i) suppression by reduced branching ratios ($\mathrm{Br}(Z \to \ell^+\ell^-) \simeq 7\%$, $\ell = e, \mu$) or (ii) final states that are difficult to reconstruct/disentangle from the background (hadronic decays of W, Z and leptonic decays of the W, $W \to \nu\ell$, which involve missing transverse energy). Therefore, we will not consider these channels as they are not as clean and/or competitive as the ones already discussed.

Direct Production of VLLs

We conclude the overview of the collider phenomenology of the scenario under investigation by briefly commenting on possible direct searches of the VLLs. VLLs can be produced at LHC through the Drell-Yann processes [210] $pp \to Z^*/\gamma^* \to EE$, $pp \to Z^* \to NN$, and $pp \to W^* \to NE$ [17]. The results of corresponding LHC searches [182, 265] cannot be, nevertheless applied to our case since they rely on the presence of a mixing with SM leptons. Whereas, in our scenario, in order to guarantee the stability of the DM candidate, we have forbidden such a mixing by imposing a $\mathbb{Z}_2$ symmetry under which the VLL sector is odd and the SM is even (see next section). On the contrary, a possible collider signal would be represented by the production of E_1E_1 or N_2E_1 and their subsequent decay into DM, which can be tested in 2-3 charged leptons plus missing energy final state events. Searches of this kind have been performed in the context of Supersymmetric scenarios [266–268]. In order to take into account possible constraints, we have imposed (exception for the coannihilation regime), in our scans, a lower limit on the mass of the lightest charged VLL of 300 GeV. Direct production of DM, through off-shell Z/h boson or on-shell heavy Higgses, cannot be instead tested, through monojet searches, since constraints from DM Direct Detection imposes, for these states, a negligible branching fraction of decay into DM pairs (see fig. 5.12)

Another potentially interesting channel would be the production of a charged Higgs and its subsequent decay into N_1E_1, followed by $E_1 \to N_1W$. However, for most of the points providing the correct DM relic density and, at the same time, passing the DD constraints, we have that $m_{H^\pm} < m_{N_1} + m_{E_1}$, so that production can occur only through off-shell charged Higgs. Furthermore, the dominant production modes of $H^\pm$ at the LHC, $gg \to tbH^\pm$ and $gb \to tH^\pm$, are phase-space suppressed by the top quark produced in association and typically have a low cross section. The s-channel production of a charged Higgs, $qq' \to H^\pm$ is not a valid option neither: even if the charged Higgs would be on-shell, the low Yukawa couplings of the initial state quarks renders such a process unobservable. For a more detailed discussion, we refer the reader to Ref. [210].

[17] Alternatively, VLLs can be produced from the decay of heavy neutral Higgses [262–264]

We close the section by commenting again on possible production of VLLs from decays of the neutral Higgses. As pointed previously, in the coannihilation scenario sizable branching fractions for the decays $H/A \to E_i E_i$, $i = 1, 2$ are not forbidden by limits from DM phenomenology. However, while E_2, having a sizeable admixture of a $SU(2)_L$ doublet, almost always decays promptly into E_1 plus a $W/Z/h$ boson (on or off-shell), the E_1 can decay only into a N_1 and two fermions through an off-shell W. This decay rate would be doubly suppressed by the very small coupling to the W of the mostly SU(2) singlet DM and by the phase space. Consequently, the E_1 state could be long-lived or even stable on collider scales.

5.3.6 Constraints on the Charged Higgs

Collider limits on the charged Higgs are mostly relevant for very light masses, namely $m_{H^\pm} < m_t$. In this case, light charged Higgses can be searched for in the $t \to H^\pm b$ decays, followed by $H^\pm \to cs$ or $H^\pm \to \tau\nu_\tau$. Searches for this processes have been performed both by ATLAS [269] and CMS [270, 271]. No important variations in the top branching fractions with respect to the SM have been detected, disfavoring masses of the charged Higgs below 160 GeV. The ATLAS collaboration has performed searches for $H^\pm \to \tau\nu_\tau$ [272] also in the high mass regime, i.e. $m_{H^\pm} > m_t$, with the charged Higgs being produced in association with a top quark, i.e. through the process $gb \to tH^\pm$. The limits obtained, however, cannot yet constrain efficiently most of the 2HDM setups considered in this chapter (with the possible exception of the Lepton Specific 2HDM), since the $\tau\nu_\tau$ final state has a low branching fraction at high masses [273].

The mass of the charged Higgs can be also strongly constrained by low energy observables. As these bounds are determined by the value of $\tan\beta$, they are actually dependent on the type of 2HDM realization. For an extensive review we refer, for example, to Ref. [273]. We will instead summarize, in the following, the constraints relevant to our analysis.

We have first of all to consider loop induced contributions to the $B \to X_s\gamma$ process. These depend on the coupling of the charged Higgs to t,b and s quarks. In the type-I and lepton specific models, all the relevant couplings are suppressed by $1/\tan\beta$ and, hence, sizable constraints are obtained only for very low $\tan\beta$ [274]. Much stronger bounds are instead obtained in 2HDM-II, excluding masses of the charged Higgs up to order of 400 GeV [275–278], virtually independently from the value of $\tan\beta$. A second relevant bound comes from the semileptonic decays of the pseudoscalar mesons, in particular $B(B \to \tau\nu)$. By requiring the ratio $r = B(B \to \tau\nu_\tau)/B(B \to \tau\nu_\tau)_{\rm SM}$ to be consistent with the experimental determination $r = 1.56 \pm 0.47$ [107, 279], one obtains, only for the type-II 2HDM, a limit on the bidimensional plane $(m_{H^\pm}, \tan\beta)$ which is relevant for $\tan\beta \gtrsim 20$.

5.3.7 Stability of DM and Flavor Changing Neutral Currents

As previously stated, our analysis has been mostly carried on a purely phenomenological basis. In this subsection we nevertheless take some steps towards a more complete construction, discussing some potential challenges in the model building, the stability of the DM and the suppression of FCNCs.

VLFs with the same quantum numbers of the SM fermions feature allow for a Yukawa coupling of one VLF, one SM fermion and one Higgs boson. Such a coupling would generate a mass mixing between VL and SM fermions, which would force all the VLF to decay into a SM fermion and a gauge or Higgs boson. In order to have the lightest neutral VLF as a viable DM candidate, this kind of mixing should be strongly suppressed or possibly forbidden. The most simple option to achieve this goal would be represented by the introduction of

a $\mathbb{Z}_2$ symmetry, which we label $\mathbb{Z}_2^{\text{VLL}}$, under which the VLLs are odd (with the SM states being instead even), so that the coupling which sources the mixing between the VLLs and the SM fermions would be actually forbidden.

Another potential challenge is represented by the presence of FCNCs. FCNCs induced by the coupling of the SM fermions with the Higgs doublet have been forbidden by assuming four specific configurations for these couplings. These can be realized by assuming suitable discrete symmetries, which were listed in subsection 4.1.3. Possible UV completions for these 2HDM realizations have been studied in e.g. [280–282].

The addition of VLFs, freely coupled to both Higgs doublets, provides a further potential source of FCNCs, induced at one-loop in this case. The determination of possible bounds for generic couplings of the VLF, as considered here, is not in the purpose of this thesis. A possible workaround would be to make also some of the VLFs odd under the $\mathbb{Z}_2^{\text{2HDM}}$ symmetry. Drawing inspiration from the simple flavor conserving 2HDMs, where the the SM quark doublet and the up-type right-handed quarks are, by convention, even under $\mathbb{Z}_2^{\text{2HDM}}$, we choose the VLL doublet and the $N'_{L,R}$ singlet VL neutrino ("up-type" VLL) to be, similarly, even under $\mathbb{Z}_2^{\text{2HDM}}$. This leaves us with two possibilities for $E'_{L,R}$:

1. $E'_{L,R}$ is also even under $\mathbb{Z}_2^{\text{2HDM}}$, meaning that all VLLs couple to H_2;
2. $E'_{L,R}$ is odd under $\mathbb{Z}_2^{\text{2HDM}}$, which implies that VL electrons couple to H_1, while VL neutrinos couple to H_2.

As evident from the discussion above, $\mathbb{Z}_2^{\text{2HDM}}$ and $\mathbb{Z}_2^{\text{VLL}}$ should be distinct symmetry groups since the VLLs have the same charge under $\mathbb{Z}_2^{\text{VLL}}$ but different charges under $\mathbb{Z}_2^{\text{2HDM}}$. Once the two symmetries are imposed, the Higgs+VLL Lagrangian reads as follows (for simplicity, mass terms have been omitted since not relevant for the discussion):

$$-\mathcal{L}_{VLL} = y_{N_R}\overline{L}_L\tilde{H}_2 N'_R + y_{N_L}\overline{N}'_L\tilde{H}_2{}^\dagger L_R + y_{E_R}\overline{L}_L H_i E'_R + y_{E_L}\overline{E}'_L H_i^\dagger L_R + \text{h.c.}, \tag{5.57}$$

where $i = 1, 2$ corresponds to the two cases mentioned above. After EWSB, the interaction Lagrangian of the VL neutrinos with the neutral Higgs scalars is the same in both cases and reads:

$$\begin{aligned} -\sqrt{2}\,\mathcal{L}_{\phi NN} = \begin{pmatrix} N_L^\dagger & N_L'^\dagger \end{pmatrix} \Bigg[h \begin{pmatrix} 0 & y_{N_R} s_\beta \\ y_{N_L} s_\beta & 0 \end{pmatrix} + H \begin{pmatrix} 0 & -y_{N_R} c_\beta \\ -y_{N_L} c_\beta & 0 \end{pmatrix} \\ + A \begin{pmatrix} 0 & -i\, y_{N_R} c_\beta \\ i\, y_{N_L} c_\beta & 0 \end{pmatrix} \Bigg] \begin{pmatrix} N_R \\ N'_R; \end{pmatrix} + \text{h.c.}\,. \end{aligned} \tag{5.58}$$

On the contrary, in the case of the VL electrons we distinguish the following two possibilities:

$$\begin{aligned} -\sqrt{2}\,\mathcal{L}^{(1)}_{\phi EE} = \begin{pmatrix} E_L^\dagger & E_L'^\dagger \end{pmatrix} \Bigg[h \begin{pmatrix} 0 & y_{E_R} c_\beta \\ y_{E_L} c_\beta & 0 \end{pmatrix} + H \begin{pmatrix} 0 & y_{E_R} s_\beta \\ y_{E_L} s_\beta & 0 \end{pmatrix} \\ + A \begin{pmatrix} 0 & -i\, y_{E_R} s_\beta \\ i\, y_{E_L} s_\beta & 0 \end{pmatrix} \Bigg] \begin{pmatrix} E_R \\ E'_R \end{pmatrix} + \text{h.c.}, \end{aligned} \tag{5.59}$$

$$\begin{aligned} -\sqrt{2}\,\mathcal{L}^{(2)}_{\phi EE} = \begin{pmatrix} E_L^\dagger & E_L'^\dagger \end{pmatrix} \Bigg[h \begin{pmatrix} 0 & y_{E_R} s_\beta \\ y_{E_L} s_\beta & 0 \end{pmatrix} + H \begin{pmatrix} 0 & -y_{E_R} c_\beta \\ -y_{E_L} c_\beta & 0 \end{pmatrix} \\ + A \begin{pmatrix} 0 & i\, y_{E_R} c_\beta \\ -i\, y_{E_L} c_\beta & 0 \end{pmatrix} \Bigg] \begin{pmatrix} E_R \\ E'_R \end{pmatrix} + \text{h.c.}. \end{aligned} \tag{5.60}$$

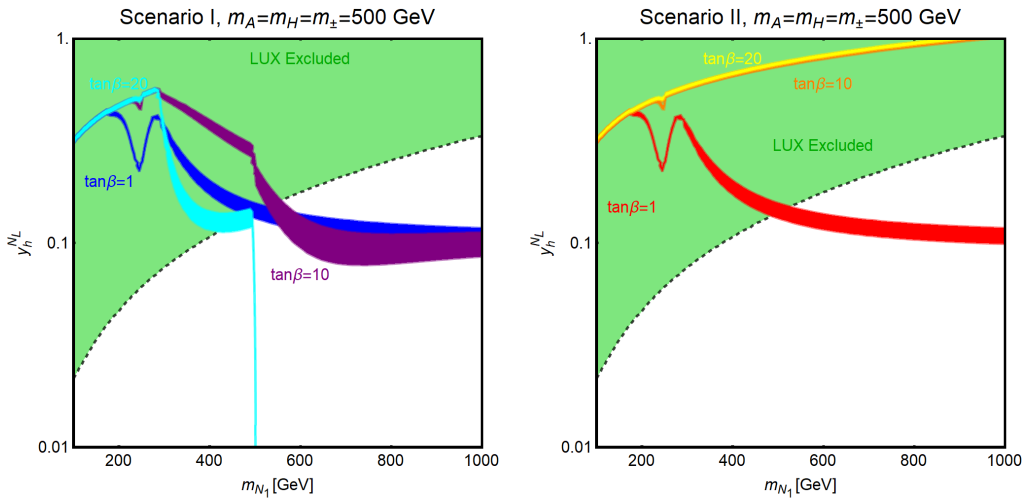

Figure 5.16 – Main constraints from Dark Matter phenomenology, i.e. in the two proposed scenarios for a flavor conserving VLF sector.

For what regards the interactions of the VLLs with the charged Higgs we have:

$$
\begin{aligned}
-\mathcal{L}^{(1)}_{H^\pm NE} &= H^+ \begin{pmatrix} N_L^\dagger & N_L'^\dagger \end{pmatrix} \begin{pmatrix} 0 & y_{E_R} s_\beta \\ y_{N_L} c_\beta & 0 \end{pmatrix} \begin{pmatrix} E_R \\ E_R' \end{pmatrix} \\
&\quad + H^- \begin{pmatrix} E_L^\dagger & E_L'^\dagger \end{pmatrix} \begin{pmatrix} 0 & y_{N_R} c_\beta \\ y_{E_L} s_\beta & 0 \end{pmatrix} \begin{pmatrix} N_R \\ N_R' \end{pmatrix} + \text{h.c.}, \qquad (5.61) \\
-\mathcal{L}^{(2)}_{H^\pm NE} &= H^+ \begin{pmatrix} N_L^\dagger & N_L'^\dagger \end{pmatrix} \begin{pmatrix} 0 & -y_{E_R} c_\beta \\ y_{N_L} c_\beta & 0 \end{pmatrix} \begin{pmatrix} E_R \\ E_R' \end{pmatrix} \\
&\quad + H^- \begin{pmatrix} E_L^\dagger & E_L'^\dagger \end{pmatrix} \begin{pmatrix} 0 & y_{N_R} c_\beta \\ -y_{E_L} c_\beta & 0 \end{pmatrix} \begin{pmatrix} N_R \\ N_R' \end{pmatrix} + \text{h.c.} \qquad (5.62)
\end{aligned}
$$

The couplings introduced in this subsection can be related the ones used in our analysis by reabsorbing a factor s_β (c_β), in the case that $E_{L,R}$ ($E'_{L,R}$) couples to $H_1(H_2)$, into the definitions of the VLL Yukawa couplings to the 125 GeV Higgs boson, h. For the VL neutrinos, the redefined couplings to the scalars would read:

$$
y_h^{N_{L,R}} \equiv y_{N_{L,R}} s_\beta, \quad y_H^{N_{L,R}} \equiv -y_{N_{L,R}} c_\beta = -y_h^{N_{L,R}} t_\beta^{-1}, \qquad (5.63)
$$

whereas for the VL electrons we have:

$$
y_h^{E_{L,R}} \equiv y_{E_{L,R}} c_\beta, \quad y_H^{E_{L,R}} \equiv y_{E_{L,R}} s_\beta = y_h^{E_{L,R}} t_\beta \qquad (5.64)
$$

$$
y_h^{E_{L,R}} \equiv y_{E_{L,R}} s_\beta, \quad y_H^{E_{L,R}} \equiv y_{E_{L,R}} c_\beta = -y_h^{E_{L,R}} t_\beta^{-1}. \qquad (5.65)
$$

in the cases of, respectively, couplings with H_1 and H_2.

We then notice that, as opposed to the case where the VLLs couple to both scalar doublets, t_β now plays a role also in the VLL sector. More specifically, one finds, in the VLL couplings to H, A (relative to their couplings to h), the same type of t_β^{-1} suppression or t_β enhancement as for the SM fermions.

The impact of this feature on DM phenomenology has been sketched in fig. (5.16). Here we have reported in the two panels the isocontours of the correct DM relic density, as well as the excluded region by LUX, in the bidimensional plane $(m_{N_1}, y_h^{N_L})$ (we have used the

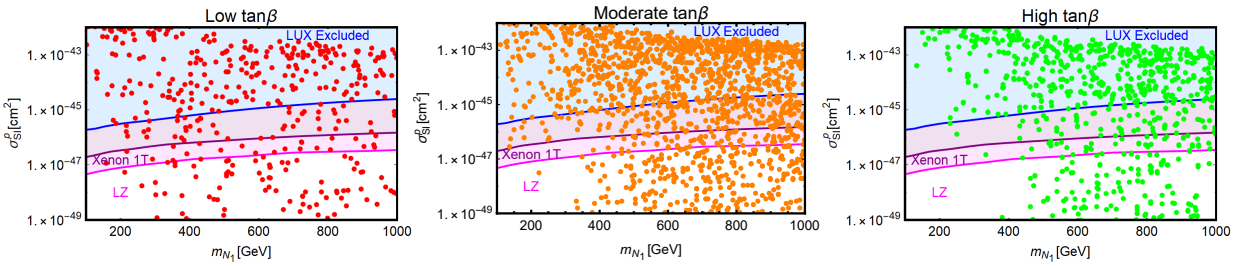

Figure 5.17 – Summary plots including all the constraints discussed throughout this chapter. Each of the three panels of the figure refers to a different regime of values of $\tan\beta$ (see main text for details), indicated on the top of each panel.

relations above to adopt the same variables as the rest of the text; as usual, we have assumed $y_h^{N_R} = 0$), and for three values of $\tan\beta$, namely 1,10 and 20, while keeping fixed $y_h^{E_L} = 0.1$, $y_h^{E_R} = 0$ and $M_L = M_E = 2M_N$.

The more constrained structure of the couplings – with respect to general case discussed in the rest of the text – influences the scenarios for the correct relic density (i.e. s-channel resonances and annihilation into heavy Higgses) in the following way. The relation between the couplings $y_h^{N_L}$, $y_H^{N_L}$ tends to disfavor the case of resonant annihilations since they make the constraints from DD stronger with respect to the case in which this two couplings can be regarded as independent. The effectiveness of these constraints increases with $\tan\beta$ since the couplings of the DM with the H and A bosons are now suppressed as $1/\tan\beta$. The regime of annihilations into heavy Higgses is perfectly viable in the case from eq. (5.64) ("Scenario I") where the coupling $y_H^{E_L}$ can be be even enhanced at high $\tan\beta$. More contrived is instead the case from eq. (5.65) ("Scenario II") where DM annihilation into H^+H^- is suppressed at high $\tan\beta$, thus increasing the tension with DD constraints. The light DM regime is, instead, negligibly affected since the relic density is mostly determined by the couplings of the DM with the W and Z boson which depend only on $y_h^{N_L}$ and $y_h^{E_L}$. For the same reason the constraints from Direct Detection are mostly unchanged (notice that the shape of the LUX excluded region is different with respect to the one shown in fig. 5.7 since in the latter M_L and M_E were fixed to the value of 500 GeV, while here the ratio with M_N is constant, so that the behaviour of the angles $\theta_N^{L,R}$ with $y_h^{N_L}$ is different for the two figures).

5.3.8 Summary of Results

The results of the study carried out in this chapter are summarized in fig. (5.17). Here we put together the results for DM phenomenology with theoretical constraints, i.e. scalar quartic couplings RGEs, EWPT constraints, limits from collider searches, mostly $H/A \to \tau\tau$, and constraints from low energy observables (for the latter we have adopted the limits on $(m_{H^\pm}, \tan\beta)$ as reported in Refs. [274, 283]).

The three panels of fig. (5.17) show, for three regimes of values of $\tan\beta$, i.e low, moderate and high, in the plane $(m_{N_1}, \sigma^{\rm SI}_{N_1 p})$, the model points providing the correct DM relic density and satisfying the constraints listed above.

The results shown in fig. (5.17) can be explained as follows. The distribution of the points in the three panels of the figure appears rather similar. As discussed in the text, under the assumption that the VLL can couple with both Higgs doublets, the dependence on $\tan\beta$ of the couplings of the DM is reabsorbed in the definition of the couplings themselves. We notice nevertheless that low DM masses, i.e. lighter than approximately 400 GeV, become

progressively disfavored as the value of $\tan\beta$ increases. DD limits are mostly evaded if the DM relic density is achieved either through s-channel resonances or via annihilations involving heavy Higgses, in particular the charged ones, as final states. The former possibility becomes increasingly contrived at higher values of $\tan\beta$ because the reduced decay width of the H/A states requires a stronger fine tuning in the $|m_{N_1} - m_{A,H}/2|$ difference (a possible exception would be represented by the flipped 2HDM at very high $\tan\beta$, i.e. $\gtrsim 45$). This problem is partially overcome by considering high enough values of the masses of H and A. The case of the annihilations into heavy Higgses is influenced by several aspects, according the configuration, i.e. type I, type II, lepton specific or flipped, chosen for the couplings with SM fermions. The type-II configuration is excluded for m_A below 400 GeV in the moderate $\tan\beta$ regime, and for considerably higher masses in the high $\tan\beta$ regime, by LHC searches in the $\tau\tau$ channel (cf. fig. 5.13). Values of m_A below 400 GeV are also excluded in the flipped configuration for high $\tan\beta$. These constraints also partially influence the other Higgs masses since for moderate/high $\tan\beta$ the constraints (5.26)-(5.27) and EWPT tend to favor a mass degenerate heavy Higgs spectrum. In the type II model, the mass of the charged Higgs is, nevertheless, individually forced to lie above approximately 400 GeV by constraints from low energy processes.

5.4 Discussion

In this chapter, we have performed an extensive study of the impact of the addition of a family of vector like fermions, with suitable quantum numbers such as to provide a DM candidate, to the SM and to various types of 2HDMs.

The SM+VLLs realization is strongly constrained. The correct relic density implies too strong interactions with the Z-boson, ruled out by DM Direct Detection unless the DM, and hence in turn the whole spectrum of the new fermions, lie above the TeV scale.

Lower DM masses can instead be achieved in 2HDM realizations. Indeed, s-channel enhancement, in correspondence with the H/A poles, can provide the correct relic density even for a small hypercharge/SU(2) component of the Dark Matter. In addition, efficient DM annihilations can also be achieved in the $H^{\pm}H^{\mp}$ and $W^{\pm}H^{\mp}$ final states. The corresponding cross-section is not directly correlated with the DM DD cross-section, such that it would be possible to evade current and even future bounds. On the other hand, the DM relic density depends on the masses of the new Higgs states. Complementary constraints thus come from their experimental searches. Given the variation of SM fermion Yukawas with $\tan\beta$, the allowed parameter space actually depends on the type of couplings of the Higgs doublets with the SM fermions.

Type-II, and, to a lesser extent, flipped 2HDMs, are the most constrained realizations, since low values of $m_{H^{\pm}}$ (and in turn DM masses) are excluded by low energy observables. Moreover, a large part of the type-II parameter space is excluded by limits from searches of $A/H \to \tau\tau$. Combining these constraints, DM masses below 400 GeV are strongly disfavored. For the other two 2HDM realizations, constraints from searches of extra Higgses are not yet competitive with DM constraints and lower DM masses are accessible.

Although the size of the Yukawa couplings of the charged VLLs can account for the correct DM relic density, it cannot account for a significant enhancement of the diphoton production rates observable at colliders. This happens because the limits from EWPT and RGE forbid values greater than ~ 1 for this couplings. Moreover, the possibility of a direct observation of the VLLs appears similarly contrived.

Chapter 6

Diboson Resonances in the Custodial Warped Extra-Dimension Scenario

6.1 The Custodial Randall-Sundrum Model

Briefly introduced in the second chapter of this thesis, the simple RS models based on the SM $SU(3)_c \times SU(2)_L \times U(1)_Y$ gauge group, with bulk matter and gauge fields, have difficulties in coping with the constraints coming from electroweak precision tests (EWPT). More precisely, in such models, the T (or, equivalently, ρ) parameter receives dangerous contributions originating from the mixing between the SM EW gauge bosons and their Kaluza-Klein counterparts. Consequently, agreement with the measured value of T forces the lowest-lying KK resonances to have masses of the order of 10 TeV [284], rendering them unobservable at the LHC. Moreover, 10 TeV KK particles aggravate the little hierarchy problem from which RS models suffer.

However, as was realised during the previous decade, there is an elegant way of keeping under control the KK contributions to the T parameter in warped extra-dimensional models: in Ref. [140], the authors enlarged the gauge group with an extra $SU(2)$, considering the gauge

$$G = SU(3)_c \times SU(2)_R \times SU(2)_L \times U(1)_X. \tag{6.1}$$

The addition of $SU(2)_R$ endows the resulting 4D effective theory with a custodial symmetry, which protects the ρ parameter from dangerous contributions. The 5D action of this model can be written as

$$S^{5\text{D}} = S^{5\text{D}}_{\text{gauge}} + S^{5\text{D}}_{\text{fermion}} + S^{4\text{D}}_{\text{Planck}} + S^{4\text{D}}_{\text{Higgs}}. \tag{6.2}$$

$S^{5\text{D}}_{\text{gauge}}$ contains the kinetic terms for the $SU(3)_c \times SU(2)_R \times SU(2)_L \times U(1)_X$ gauge fields, with $S^{5\text{D}}_{\text{fermion}}$ playing the same role, but for fermions. In both cases, the "$5D$" superscript is used because the gauge and fermion fields propagate in the bulk. On the other hand, the "$4D$" superscript indicates that the fields are confined on either the Planck ($S^{4\text{D}}_{\text{Planck}}$) or the TeV brane ($S^{4\text{D}}_{\text{Higgs}}$). While $S^{4\text{D}}_{\text{Planck}}$ contains the fields responsible for breaking $U(1)_R \times U(1)_X$ down to $U(1)_Y$, $S^{4\text{D}}_{\text{Higgs}}$ contains the kinetic and potential terms for the brane-localized Higgs field.

In the rest of the section, we briefly discuss the features of the so-called Custodial RS model, focusing on its (electroweak) gauge and Higgs sectors and on its the pattern of symmetry breaking. The discussion presented below serves as a starting point for the current chapter and for the next one.

6.1.1 The Gauge Sector

We start by introducing the gauge kinetic terms present in the Custodial RS model. They are given by

$$S^{5\mathrm{D}}_{\mathrm{gauge}} = -\frac{1}{4}\int \mathrm{d}^5x\sqrt{g}\, g^{AM}g^{BN}\left(\mathrm{tr}\, W_{AB}W_{MN} + \mathrm{tr}\, W'_{AB}W'_{MN} + B'_{AB}B'_{MN}\right), \tag{6.3}$$

with W, W', and B' being the non-abelian 5D gauge field strengths associated to $SU(2)_L$, $SU(2)_R$, and $U(1)_X$, respectively:

$$W^a_{MN} = \partial_M W^a_N - \partial_N W^a_M - g^{5\mathrm{D}}_L \epsilon^{abc} W^b_M W^c_N, \tag{6.4}$$

$$W'^a_{MN} = \partial_M W'^a_N - \partial_N W'^a_M - g^{5\mathrm{D}}_R \epsilon^{abc} W'^b_{M,b} W'^c_N, \tag{6.5}$$

$$B'_{MN} = \partial_M B'_N - \partial_N B'_M, \tag{6.6}$$

where a, b, c are $SU(2)$ indices running from 1 to 3. We denote the corresponding 5D gauge couplings as $g^{5\mathrm{D}}_L$, $g^{5\mathrm{D}}_R$, and $g^{5\mathrm{D}}_X$, whose 4D counterparts can be determined by tree-level matching and are given by $g_{L,R,X} \equiv g^{5\mathrm{D}}_{L,R,X}/\sqrt{L}$. We do not include the gluon since it does not play a central role in the remainder of this thesis.

As any model of new physics, the Custodial RS has to incorporate the SM low energy spectrum. Since there are two 5D $SU(2)$ fields, one has to make sure that only one of them possesses 0-modes, corresponding to the measured W and Z bosons. This is easily achievable by considering appropriate boundary conditions (BCs) for the 5D fields. To start with, we impose $(-+)$ BCs to the μ components of the 5D gauge fields $\tilde{W}^{1,2}$, and $(++)$ BC to all the other 5D gauge fields. Such an assignation plays a double role: (i) it assures that the charged W' bosons have no light zero modes and (ii) it breaks $SU(2)_R$ down to $U(1)_R$ on the Planck brane. The surviving group, $U(1)_R \times U(1)_X$, is further broken on the Planck brane to the hypercharge group $U(1)_Y$. This symmetry breaking pattern is realized by a scalar field which develops a VEV on the Planck brane ($S^{4\mathrm{D}}_{\mathrm{Planck}}$). Thus, we end up with SM gauge group on the Planck brane:

$$SU(3)_c \times SU(2)_R \times SU(2)_L \times U(1)_X \overset{\text{Planck-brane}}{\longrightarrow} SU(3)_c \times SU(2)_L \times U(1)_Y. \tag{6.7}$$

Consequently, the W'^3_μ and B'_μ mix with each other to give

$$\begin{pmatrix} Z'_\mu \\ B_\mu \end{pmatrix} = \begin{pmatrix} \tilde{c}_W & -\tilde{s}_W \\ \tilde{s}_W & \tilde{c}_W \end{pmatrix} \begin{pmatrix} W'^3_\mu \\ B'_\mu \end{pmatrix}, \tag{6.8}$$

where

$$\tilde{c}_W \equiv \cos\tilde{\theta}_W = \frac{g_R}{\sqrt{g_R^2 + g_X^2}}, \quad \tilde{s}_W \equiv \sin\tilde{\theta}_W = \frac{g_X}{\sqrt{g_R^2 + g_X^2}}. \tag{6.9}$$

The resulting gauge coupling of the $U(1)_Y$ group is given by

$$g_Y = g_R\tilde{s}_W = g_X\tilde{c}_W = \frac{g_R\, g_X}{\sqrt{g_R^2 + g_X^2}}, \tag{6.10}$$

while the Z'_μ coupling and charge read

$$g_{Z'} = \sqrt{g_R^2 + g_X^2}, \quad Q_{Z'} = I^3_R - Y\tilde{s}^2_W. \tag{6.11}$$

Here, I^3_R is the third component of the $SU(2)_R$ isospin. Denoting by X the $U(1)_X$ charge, the hypercharge quantum number results from the following expression:

$$Y = X + I^3_R, . \tag{6.12}$$

At this point, one should mention a second role of the VEV on the Planck brane. Coupling the Z'_μ field to this VEV, one mimics to a good approximation $(-+)$ boundary conditions for the aforementioned field [140]. One thus removes 0-mode from the Z' field, and consequently the SM spectrum of EW gauge bosons is correctly reproduced: the only gauge light degrees of freedom are the measured Z and $W^\pm$ bosons (plus, of course, the photon and the gluon).

6.1.2 The Higgs Sector and Electroweak Symmetry Breaking

In the context of the extended gauge group mentioned previously in this section, the brane-localised Higgs doublet gets promoted to a bi-doublet of $\mathrm{SU}(2)_\mathrm{R} \times \mathrm{SU}(2)_\mathrm{L}$, uncharged under $\mathrm{U}(1)_X$. When it develops a vacuum expectation value (VEV), the Higgs bi-doublet thus breaks, on the IR brane, the $\mathrm{SU}(2)_R \times \mathrm{SU}(2)_L \times \mathrm{U}(1)_X$ gauge group down to $\mathrm{U}(1)_{e.m.}$ times a global $\mathrm{SU}(2)_V$, the latter endowing the Higgs sector with a custodial symmetry, which keeps under control the contributions to the T parameter.

After the usual redefinition the Higgs bi-doublet, $H \to \mathrm{e}^{kL} H$, the brane-localised action reads

$$S^{4\mathrm{D}}_{\mathrm{Higgs}} = \int \mathrm{d}^4x \left[\frac{1}{2}\eta^{\mu\nu}\, \mathrm{tr}\, D_\mu H^\dagger D_\nu H - \frac{\lambda_0}{4}\left(\mathrm{tr}\, H^\dagger H - v^2\right)^2 \right]_{y=L}, \tag{6.13}$$

where $v \simeq 246$ GeV (this is true, as shown later on, only in the limit where the KK partners decouple) and $\eta_{\mu\nu}$ is the Minkowski metric. Omitting the gluon, the covariant derivative is given, in general, in terms of the 5D gauge fields, by

$$\begin{aligned} D_\mu &= \partial_\mu - i\left(g^{5\mathrm{D}}_R W'^a_\mu I^a_R + g^{5\mathrm{D}}_L W^a_\mu I^a_L + g^{5\mathrm{D}}_X B'_\mu X\right) \\ &= \partial_\mu - i\left(g^{5\mathrm{D}}_R W'^{1,2}_\mu I^{1,2}_R + g^{5\mathrm{D}}_L W^{1,2}_\mu I^{1,2}_L + \right. \\ &\left. + g^{5\mathrm{D}}_{Z'} Z'_\mu Q_{Z'} + g^{5\mathrm{D}}_L W^3_\mu I^3_R + g^{5\mathrm{D}}_Y B_\mu\right) Y, \end{aligned} \tag{6.14}$$

with $I^a_{L,R}$, $a = 1,2,3$ being the $\mathrm{SU}(2)_{L,R}$ generators, proportional to the usual Pauli matrices. In particular, the covariant derivative acting on the Higgs bi-doublet reads:

$$D_\mu H = \partial_\mu H - i\sqrt{L}\left[g_L (W^a_\mu I^a_L) H + g_R H (W'^a_\mu I^a_R)^T\right]. \tag{6.15}$$

The $\sqrt{L}$ factor above originates from using 4D couplings instead of 5D (dimensionful) couplings. Besides, due to the scalar bi-doublet having null charge under $\mathrm{U}(1)_X$, the B' gauge field does not appear in the covariant derivative acting on H. Upon EWSB, the Higgs bi-doublet can be written in the unitary gauge as

$$H = \frac{v + h_0(x)}{\sqrt{2}} \begin{pmatrix} 0 & -1 \\ 1 & 0 \end{pmatrix}, \tag{6.16}$$

with h_0 being the (4D) Higgs field. As previously mentioned, the VEV acquired by the bi-doublet breaks, on the IR brane, $SU(2)_L \times U(1)_Y$ down to $U(1)_{em}$ (times a global $SU(2)_V$). The resulting 5D gauge bosons are

$$W^{(\prime)\pm}_\mu = \frac{W^{(\prime)1}_\mu \mp W^{(\prime)2}_\mu}{\sqrt{2}}, \quad \begin{pmatrix} Z_\mu \\ A_\mu \end{pmatrix} = \begin{pmatrix} c_W & -s_W \\ s_W & c_W \end{pmatrix} \begin{pmatrix} W^3_\mu \\ B_\mu \end{pmatrix}, \tag{6.17}$$

where

$$c_W \equiv \cos\theta_W \equiv \frac{g_L}{\sqrt{g_L^2 + g_Y^2}}, \quad s_W \equiv \sin\theta_W \equiv \frac{g_Y}{\sqrt{g_L^2 + g_Y^2}}, \tag{6.18}$$

are the cosine and sine of the weak mixing angle θ_W. The coupling and charge of the $U(1)_{em}$ gauge group, whose associated 5D gauge boson is A_μ (the photon), are given by

$$e = g_L s_W = g_Y c_W = \frac{g_L\, g_Y}{\sqrt{g_L^2 + g_Y^2}}, \quad Q_{em} = Y + I_L^3 = X + I_R^3 + I_L^3, \tag{6.19}$$

while for the Z_μ boson we have

$$g_Z = \sqrt{g_L^2 + g_Y^2}, \quad Q_Z = I_L^3 - Q_{em}\, s_W^2. \tag{6.20}$$

As expected, A_μ does not feel EWSB, which means its 0-mode, which corresponds to the SM photon, remains massless.

We now have all the prerequisites to study the properties of the gauge bosons and their associated KK excitations.

6.1.3 KK Gauge Boson Mixing: Masses and Couplings

In this subsection, we outline the procedure for obtaining the exact profiles and masses of the EW gauge bosons and their KK partners. Once these ingredients are known, the relevant couplings can be calculated by simply evaluating overlap integrals.

Putting together several results from the previous subsections, the 4D IR brane-localized action has the following expression:

$$\begin{aligned} S_{\text{Higgs}}^{\text{4D}} = &\int \mathrm{d}^4x\, L \left(1 + \frac{h_0}{v}\right)^2 \left[\bar{m}_W^2 \left(W_\mu - \alpha_W W'_\mu\right)^2 + \frac{\bar{m}_Z^2}{2}\left(Z_\mu - \alpha_Z Z'_\mu\right)^2\right]_{y=L} \\ &+ \int \mathrm{d}^4x \left[\frac{1}{2}(\partial_\mu h_0)^2 - \left(\frac{m_{h_0}^2}{2} h_0^2 + \frac{m_{h_0}^2}{2v} h_0^3 + \frac{m_{h_0}^2}{8v^2} h_0^4\right)\right]. \end{aligned} \tag{6.21}$$

Here, $V_\mu^2 \equiv \eta^{\mu\nu} V_\mu V_\nu$, and

$$\alpha_W = g_R/g_L, \;\; \alpha_Z = \sqrt{g_R^2/g_Z^2 - s_W^2}. \tag{6.22}$$

The masses in the first line of eq. (6.21) are given by $\bar{m}_{W,Z} = \frac{g_{L,Z} v}{2}$; as demonstrated later on in the subsection, they are not equal to the measured W and Z boson masses. Moreover, $m_{h_0}^2 = 2\lambda_0 v^2$ is the bare Higgs mass (to anticipate the discussion in Chapter 7, m_h^0 is different from the physical Higgs mass if the SM scalar mixes with the so-called radion). The expression above is our starting point for deriving the (y-dependent) wave functions of the SM-like W and Z bosons and of their KK partners, as well as their couplings to the Higgs scalar field.

We start by describing the procedure employed for obtaining the masses and profiles of the Z boson and its KK partners. A conceptually identical calculation applies also to the case of the W boson, whereas the photon case is much simpler, as A_μ does not couple to the brane-localized Higgs field.

We denote the observed Z boson by Z_0, while its KK excitations (which here are also mass eigenstates) are referred to as Z_n, with $n = 1$ for the first KK level, $n = 2$ for the second one, and so on. Collecting several terms from eqs. (6.3) and (6.21), the relevant part of the action reads, after EW symmetry breaking, as follows:

$$\begin{aligned} S_{ZZ}^{\text{5D}} = &\int \mathrm{d}^5x \sqrt{g} \left(-\frac{1}{4}\, g^{AB} g^{MN} Z_{AM} Z_{BN} - \frac{1}{4}\, g^{AB} g^{MN} Z'_{AM} Z'_{BN}\right) \\ &+ \int \mathrm{d}^5x\, L\, \delta(y - L) \frac{\bar{m}_Z^2}{2} \left[Z_\mu(x,y) - \alpha_Z Z'_\mu(x,y)\right]^2, \end{aligned} \tag{6.23}$$

We choose to work in a gauge where the fifth component of the 5D gauge fields, $Z_5^{(\prime)}$, is null. [1] Similarly to e.g. Ref. [285], we perform a "mixed" KK decomposition, but applied to the gauge bosons:

$$\begin{aligned} Z_\mu(x,y) &= \frac{1}{\sqrt{L}} \sum_{n\geq 0} g_+^n(y) Z_{n,\mu}(x), \\ Z'_\mu(x,y) &= \frac{1}{\sqrt{L}} \sum_{n\geq 0} g_-^n(y) Z_{n,\mu}(x), \end{aligned} \tag{6.24}$$

where the (dimensionless) profiles $g_\pm^n$ obey $(\pm+)$ boundary conditions. Such a mixed decomposition allows us to include the boundary-localised mixing between the Z and Z' 5D fields into the (coupled) equations of motion for g_+ and g_-, which in turn leads us to the exact expressions for the profiles and masses of the KK excitations of the Z boson.

By using the standard technique of varying the action in eq. (6.23) with respect to the Z_μ and Z'_μ fields and then employing the KK decomposition in eqs. (6.24), one gets the following equations of motion (EOMs) for the profiles:

$$\begin{aligned} \partial_5\left(\mathrm{e}^{-2ky}\partial_5 g_+\right) + m^2 g_+ &= \bar{m}_Z^2\, L\, \delta(y-L)\left[g_+(L) - \alpha_Z\, g_-(L)\right], \\ \partial_5\left(\mathrm{e}^{-2ky}\partial_5 g_-\right) + m^2 g_- &= -\alpha_Z\, \bar{m}_Z^2\, L\, \delta(y-L)\left[g_+(L) - \alpha_Z\, g_-(L)\right], \end{aligned} \tag{6.25}$$

with the BCs given by

$$g'_+(0) = g'_\pm(L) = g_-(0) = 0, \tag{6.26}$$

where the prime denotes differentiation with respect to y. For better readability, we have suppressed the n indices, which labeled the KK levels.

The presence of the delta functions in the EOMs induces discontinuities in the first derivatives of the profiles at $y = L$. To find out by how much the derivatives "jump", we integrate the EOMs in eq. (6.25) from $L-\epsilon$ to L, and then take $\epsilon \to 0$, which gives us the following relations:

$$\begin{aligned} \bar{m}_Z^2\, L\, \mathrm{e}^{-2kL}\left[g_+(L) - \alpha_Z g_-(L)\right] + g'_+(L_-) &= 0 \\ \alpha_Z\, \bar{m}_Z^2\, L\, \mathrm{e}^{-2kL}\left[g_+(L) - \alpha_Z g_-(L)\right] - g'_-(L_-) &= 0, \end{aligned} \tag{6.27}$$

where we use the notation $\lim_{\epsilon\searrow 0} f(x-\epsilon) \equiv f(x_-)$. We now have all the prerequisites to calculate the profiles and the masses of the Z boson tower. Combining eqs. (6.25), (6.26), and (6.27), we find the well-known expressions for the profiles [42, 43], which are expressed by the Bessel function of the first (J_α) and second (Y_α) kinds:

$$g_\pm^n = N_\pm^n \mathrm{e}^{ky}\left[J_{\frac{1}{2}\mp\frac{1}{2}}\left(x_n \mathrm{e}^{-kL}\right) Y_1\left(x_n \mathrm{e}^{k(y-L)}\right) - Y_{\frac{1}{2}\mp\frac{1}{2}}\left(x_n \mathrm{e}^{-kL}\right) J_1\left(x_n \mathrm{e}^{k(y-L)}\right)\right], \tag{6.28}$$

where $x_n \simeq \sqrt{6}\, m_{Z_n}/m_{KK}$, with $m_{KK} \simeq \sqrt{6} k\, e^{-kL}$ being the mass of the first KK excitation of the photon (or gluon). The normalisation constants $N_\pm^n$ are obtained by requiring that each Z_n field has a canonically normalised kinetic term, which translates to

$$\int_0^L \frac{\mathrm{d}y}{L}\left(g_+^m g_+^n + g_-^m g_-^n\right) = \delta_{mn}. \tag{6.29}$$

We plot in Fig. 6.1 the $(++)$ and $(-+)$ profiles $g_\pm^n$ corresponding to the observed Z boson $(n=0)$ and to its two lightest KK modes $(n=1,2)$. Notice that g_-^0 is slightly shifted from

[1] While the 0-mode of the 5D scalar field $Z_5^{(\prime)}$ is set to 0 by the boundary conditions (BCs), one can interpret the KK modes of $Z_5^{(\prime)}$ as the longitudinal components of the KK Z bosons, $Z_{i\geq 1}^\mu$.

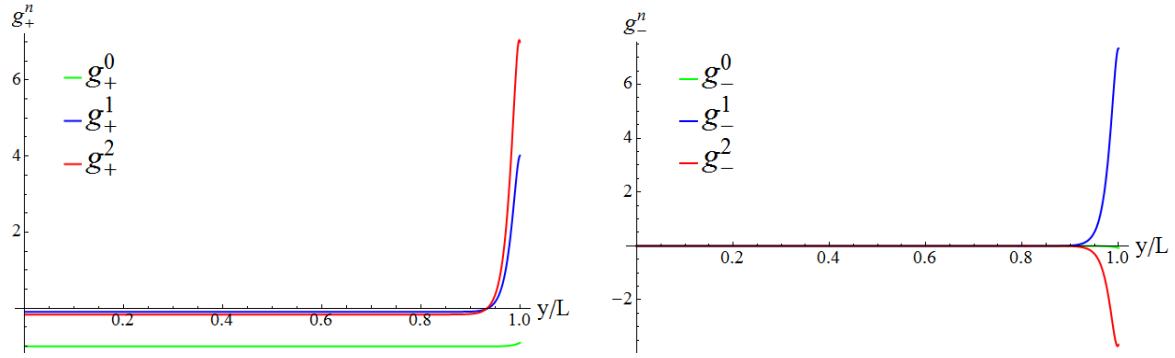

Figure 6.1 – Profiles of the Z_0 (green), Z_1 (blue), and Z_2 (red) fields, corresponding to (left) $(++)$ and (right) $(-+)$ boundary conditions, accordingly to eq. (6.24). We have set $m_{KK} = 3$ TeV.

0 close to $y = L$ due to the $Z - Z'$ mixing. Also, g_+^0 is flat in most of the $[0, L]$ interval, with a small departure close to the IR brane, where the mixing of the SM-like Z boson with the heavier KK partners takes place. As for the lowest KK-Z profiles, i.e. $g_\pm^{1,2}$, they are all of comparable size and peaked towards $y = L$, signaling the usual KK partner localization close to the IR brane.

Meanwhile, the mass spectrum is obtained by solving the system of equations (6.27). One thus obtains

$$\frac{6\bar{m}_Z^2 (kL)^2}{m_{KK}^2} \left[g_+(L) g'_-(L_-) - \alpha_Z^2 \, g'_+(L_-) g_-(L) \right] + g'_+(L_-) g'_-(L_-) = 0. \tag{6.30}$$

Notice that the normalisation constants $N_\pm$ simplify in this equation. Since the lightest mode of the Z KK-tower is identified with the observed Z-boson, its mass should be equal to the measured $m_Z \simeq 91.2$ GeV. Imposing this condition determines the value of $\bar{m}_Z$ (and thus, as discussed later, of v) as a function of the mass of the first KK excitation of the photon/gluon, m_{KK}. In turn, knowing $\bar{m}_Z$, one can compute the masses of the KK mass eigenstates associated to the Z boson.

We display in Fig. 6.2 the first four KK Z mass eigenvalues as a function of the KK photon mass, m_{KK}. As expected, m_{Z_1} and m_{Z_2} are almost degenerate and of the order m_{KK} (the first Z' mode mass is close to m_{KK}), with a mass splitting of the order of the electroweak scale or even smaller (order of the off-diagonal mixing mass term). In the limit of zero mixing, Z_1 (Z_2) would correspond to the first KK mode of the Z' (Z) gauge boson. For similar reasons, m_{Z_3} and m_{Z_4} are nearly degenerate at a scale such that $m_{Z_3} - m_{Z_1}$ is much larger than the electroweak scale.

In fact, $\bar{m}_Z$ quantifies nothing else than the Higgs doublet VEV shift [286]. This phenomenon arises from the fact that the Z boson does not acquire its mass only from the scalar VEV, but also from mixing with the heavier KK partners. Therefore, to reproduce the very precisely measured m_Z, the VEV should be adjusted. To first non-trivial order in m_Z/m_{KK}, the RS VEV v gets shifted from its SM value v_{SM} as

$$\frac{v}{v_{SM}} \equiv \frac{\bar{m}_Z}{m_Z} \simeq 1 + \frac{3m_Z^2}{2m_{KK}^2} \left[\left(1 + \alpha_Z^2 \right) kL - 1 \right]. \tag{6.31}$$

Here, we have dropped all terms suppressed by $\exp(-kL)$ or by $(kL)^{-1}$. In our calculations, we nevertheless use the exact value of the obtained shifted VEV, v, instead of restricting to $\mathcal{O}(m_Z^2/m_{KK}^2)$ corrections. As eq. (6.31) already shows, the shifted VEV is always larger

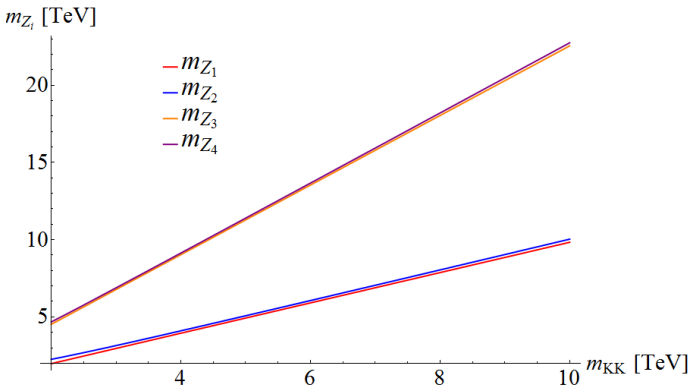

Figure 6.2 – Masses (in TeV) of the first four KK Z boson eigenstates, as a function of the first KK photon mass, m_{KK} (in TeV).

the SM VEV, i.e. $v > v_{SM} = 246$ GeV (in the decoupling limit $m_{KK} \to \infty$, the two VEVs become equal, as expected).

One can easily repeat the same exercise as above for the W boson KK tower, but with certain substitutions, such as $m_Z \to m_W$, $\alpha_Z \to \alpha_W$, and so on. It is nevertheless instructive to look closer at the case of the W boson: as shown below, it allows to see in a transparent way how custodial symmetry is at work in the model we are considering.

An important point is to observe that, as soon as m_Z is fixed to its measured value, the same happens to the VEV: it is fixed as a function of m_{KK} (see eq. (6.31)). Therefore, m_W is not a free parameter to be adjusted to its measured value, but a prediction of the theory, which we shall denote by m_W^{RS}. We write an equation similar to (6.31), but for the W boson:

$$\frac{m_W^{RS}}{\bar{m}_W} \simeq 1 - \frac{3m_W^2}{2m_{KK}^2}\left[\left(1+\alpha_W^2\right)kL - 1\right]. \tag{6.32}$$

Now, using the fact that

$$\bar{m}_W = \frac{g_L v}{2} \equiv m_W \frac{v}{v_{SM}},\ m_W = \frac{g_L v_{SM}}{2}, \tag{6.33}$$

we can calculate the lowest order correction (of $\mathcal{O}(m_Z^2/m_{KK}^2)$) to the predicted W mass. Combining eqs. (6.31),(6.32), and (6.33), we get that

$$\frac{m_W^{RS}}{m_W} \simeq 1 + \frac{3m_Z^2}{2m_{KK}^2}\left\{ kL \underbrace{\left[\left(1+\alpha_Z^2\right) - \frac{m_W^2}{m_Z^2}\left(1+\alpha_W^2\right)\right]}_{=0} - (1 - \frac{m_W^2}{m_Z^2}) \right\}, \tag{6.34}$$

since $m_W/m_Z = c_W$ at tree level in the SM. Thus, we can see that, due to the custodial symmetry coming from the extended gauge sector, the W mass no longer receives kL-enhanced $\mathcal{O}(m_Z^2/m_{KK}^2)$ corrections, which originate from mixing with the heavier KK states. In the non-custodial version RS, the coefficient in front of kL is not vanishing, which leads to the stringent bound that pushes the KK mass scale in the 10 TeV range.

Finally, let us briefly discuss the KK decomposition of the 5D photon field, A_μ, which proceeds in a much simpler way than in the case of the W and Z bosons: as $U(1)_{em}$ remains unbroken, one does not have to impose any jump conditions as the ones in eq. (6.27). As a consequence, the profile of the 0-mode of A_μ, corresponding to the massless photon, remains

flat. The profiles of its Kaluza-Klein excitations are given by $g_+^{n\geq 1}$, which are defined in eq. (6.28), but with $x_n = \sqrt{6} m_{A_n}/m_{KK}$. The boundary conditions for the KK photon profiles are purely (++), i.e. $g'_+(0) = g'_+(L) = 0$; imposing them, one finds that the mass of the first KK partner of the photon is indeed $m_{A_1} = m_{KK}$.

For later use in calculating the WW, WZ, Wh (this chapter) and the radion/Higgs plus Z (next chapter) production cross sections, we give the couplings of the W_i, Z_i, A_i fields to light fermions. Such light fermions constitute the initial states for the processes we shall consider ($e^\pm$ for the a future linear collider and light quark flavours, u, d, s, c, for the LHC). Moreover, we shall only take into account the contribution from the lowest lying KK excitation of the gauge bosons. Namely, in the case of W, Z, we will consider, besides the SM-like 0-modes, only $W_{1,2}$ and $Z_{1,2}$, which are nearly degenerate and have masses close to m_{KK}. Concerning the photon, we will include only its first KK partner.

Again, we use as an illustrative example the couplings of the Z boson KK tower to light fermions. The exact same considerations apply for the W and A KK towers. Such couplings can be inferred from the covariant derivative of the 4D part of the kinetic term of the 5D fermionic field:

$$S_\Psi^{5\mathrm{D}} = \int \mathrm{d}^5x \sqrt{g}\, \bar{\Psi}\, i\Gamma^\mu D_\mu \Psi \to \int \mathrm{d}^5x \sqrt{g}\, \sqrt{L}\, \bar{\Psi}\, \Gamma^\mu (g_Z Q_Z^\Psi Z_\mu + g_{Z'} Q_{Z'}^\Psi Z'_\mu)\Psi, \tag{6.35}$$

where Ψ denotes a generic 5D fermion, whose zero mode is a light SM fermion. The $\sqrt{L}$ factor allows us to use the 4D couplings g_Z and $g_{Z'}$ (defined in the previous subsections) instead of their (dimensionful) 5D equivalents. Meanwhile, $Q_{Z^{(\prime)}}^\Psi$ is the $Z^{(\prime)}$ charge of the fermion Ψ. Denoting by $\exp(3ky/2)\, f(y)$ the profile of the light SM fermion originating from Ψ, one obtains its couplings to the Z_i bosons by plugging the KK decomposition in eq. (6.24) into eq. (6.35), thus obtaining

$$g_Z Q_Z^\Psi \int_0^L \frac{\mathrm{d}y}{L}\, f^2(y)\, g_+^i(y) + g_{Z'} Q_{Z'}^\Psi \int_0^L \frac{\mathrm{d}y}{L}\, f^2(y)\, g_-^i(y) \equiv g_Z Q_Z^\Psi c_i. \tag{6.36}$$

These couplings can easily be deduced from profile overlap considerations. First, note that the light fermion profiles, which are be relevant for the initial state particles, are peaked towards the UV brane, with very small values close to the IR brane. Meanwhile, as shown in Fig. 6.1, the $g_\pm^{i=0,1,2}$ profiles are almost constant along the extra dimension, the sole exception being a small region near the IR brane, where they get peaked. Consequently, the overlap between the $g_\pm$'s and the light fermion profiles will effectively take place only in a region close to the UV brane, where the gauge boson profiles are almost constant. Therefore, bearing in mind that the fermion profiles are orthonormalised, the overlap between the light fermionic profiles and the gauge boson wave function are excellently approximated by the simple expression

$$c_i \simeq g_+^i(0) \int_0^L \frac{\mathrm{d}y}{L}\, f^2(y) = g_+^i(0). \tag{6.37}$$

The g_- profiles do not appear in this expression simply because their boundary conditions imply $g_-^i(0) = 0$. Therefore, in some sense, the light fermions couple only to the $\mathrm{SU(2)_L} \times \mathrm{U(1)_Y}$ "part" of the Z KK tower (same applies to the W KK tower), which means that only their (SM-like) representations under the aforementioned gauge group will be relevant for their coupling to the $Z_{0,1,2}$ states. Similar considerations apply for the A and W KK towers, the difference being that the couplings involved are different, i.e. g_L for W and e for A.

6.2 The 2 TeV Diboson Anomaly

Compared to the expectations in the context of the Standard Model (SM), one of the very few anomalies that were observed at the earlier run of the LHC with an energy up to 8 TeV and a total luminosity of about 25 fb^{-1} are the excesses in the diboson spectra observed by the ATLAS [287] and, to a lesser degree, by the CMS [288, 289] collaborations. In the former case, searches were performed for di–electroweak gauge bosons, $pp \to VV$ with $V = W/Z$, that were hadronically decaying and identified through jet–substructure techniques [290]. At a diboson invariant mass of about 2 TeV, an excess compared to the SM prediction was observed by ATLAS [287] in all the detection modes WW, WZ and ZZ with a statistical significance of ≈ 2.5–3σ in each channel. Excesses in the same channels and at the same invariant mass were also measured by the CMS collaboration [288], but with a smaller significance. In addition, CMS searched for heavy vector resonances decaying into W and Higgs bosons that lead to $\ell\nu b\bar{b}$ final states and observed a 2.5σ excess also at an invariant mass of approximately 2 TeV [289].

Unfortunately, as in the case of the diphoton excess discussed in the fourth chapter, subsequent batches of data discarded the diboson exces as a statistical fluctuation. As these excesses in the structure of the diboson mass spectra can have several interpretations in terms of new physics, a vast literature appeared at that time on the subject [291]. The most advocated and robust scenario was the production of new spin–one resonances that subsequently decayed into two SM bosons.

In the present chapter, based on Ref. [292], we consider an interpretation of this excess in the context of the warped extra–dimensional model proposed by Randall and Sundrum [25] and in which a bulk gauge custodial symmetry is introduced in order to protect the electroweak observables from large corrections [140]. The main features of the gauge sector of these models are summarized in the previous section. Concerning the SM fermionic sector, if the heavy $Q = t, b$ quarks can be localized towards the so-called TeV-brane where the Higgs boson is confined, large wave function overlaps between these fermions and the Kaluza-Klein excitations of gauge bosons can be generated and would lead to significant changes of the $VQ\bar{Q}$ couplings [138]. These non–standard couplings could explain the puzzles in the forward–backward asymmetries for bottom quark production A_{FB}^b as measured at LEP and for top quark pair production A_{FB}^t as more recently observed at the Tevatron [107].

The new gauge bosons can have masses in the few TeV range and can decay not only into $t\bar{t}, b\bar{b}$ and/or bt modes [293], but also into VV and Vh diboson final states [294]. In fact, such a configuration has already been predicted at the LHC in Ref. [295], where the explanation of (i) the A_{FB}^b discrepancy at LEP [106] and (ii) the A_{FB}^t anomaly at the Tevatron [296, 297] entailed a diboson signal of a 1.5 TeV resonance. In the present chapter, we adapt this analysis in order to comply as much as possible with the ATLAS and CMS data collected at the previous run [287–289]. We also discuss the compatibility of such an interpretation with the constraints set by the electroweak precision data [107] and by the LHC Higgs measurements [173].

6.3 Synopsis of the Model

As stated in previous section, we consider the custodially protected RS scenario, with bulk fermions and gauge bosons, in order to interpret the diboson excess. Besides providing a solution to the gauge hierarchy problem, the version of the RS scenario with bulk matter allows for a new interpretation of the fermion mass hierarchies based on specific localizations of the fermion wave functions along the warped extra dimension [42, 43, 58–61]. Indeed, if

the fermions are placed differently along the extra dimension, the observed patterns among the effective four-dimensional Yukawa couplings are generated as a result of their various wave function overlapping with the Higgs field, which remains confined on the so-called TeV brane for its mass to be protected. A parameter denoted $c_f k$ quantifies the five-dimensional mass attributed to each fermion and fixes its localization with respect to the TeV brane. With decreasing c_f, the zero mode fermions become increasingly closer to the TeV–brane and acquire larger masses.

Hence, the third generation fermions interact more strongly with the gauge bosons KK excitations as a result of the large overlap between their wave functions near the TeV brane. The heavy t, b quarks are thus expected to be most sensitive to new physics effects. For instance, the couplings of the b–quarks to the Z boson, which mixes with the neutral KK gauge boson excitations, can be altered as to solve [106] the longstanding anomaly observed at the LEP collider in the $Z \to b\bar{b}$ forward–backward asymmetry, the only high-energy observable that significantly deviates from the SM prediction [107]. The same occurs for the top quark and, for $m_{KK} \approx 2$ TeV, the KK gluons would contribute to top quark pair production at the Tevatron and could explain [296, 297] the anomaly observed in its forward–backward asymmetry at high invariant masses.

In the present chapter, we consider only the lowest-lying KK excitations of the various states and we denote them, as done at the beginning of this chapter, by $A_1, Z_{1,2}, W_{1,2}$ for the photon and the weak gauge bosons. We assume a relatively low KK mass scale which approximately corresponds to the masses of the first KK excitations, $m_{KK} = m_{A_1} = m_{g_1} \approx m_{Z_{1,2}} \approx m_{W_{1,2}}$. More precisely, we assume a KK mass scale $m_{KK} = 1.97$ TeV, which leads to the following masses for the various heavy neutral and charged resonances (in the mass basis)

$$m_{A_1} = 1.97 \text{ TeV}, \; m_{Z_1} \simeq m_{W_1} \simeq 1.95 \text{ TeV}, \; m_{Z_2} \simeq m_{W_2} = 2 \text{ TeV}. \tag{6.38}$$

Assuming the equality of the two SU(2) gauge couplings, $g_L = g_R$, we gauge boson couplings to the SM heavy quarks (t, b) can be obtained quarks by adopting the following c_f parameters:

$$c_{t_L} = c_{b_L} \equiv c_{Q_L} \simeq 0.4, \; c_{t_R} \simeq 0, \tag{6.39}$$

and calculating the relevant overlap integrals, which are similar to the one in eq. (6.36). We quote here the $V_{1,2}qq^{(\prime)}$ couplings, with $V = A, W, Z$, normalized with respect to the corresponding $V_{SM}qq^{(\prime)}$ couplings:

$$\kappa^{A_1}_{t_L t_L} = \kappa^{A_1}_{b_L b_L} \simeq 1, \; \kappa^{A_1}_{t_R t_R} \simeq 4, \tag{6.40}$$

$$\kappa^{Z_1}_{t_L t_L} \simeq -6.3, \; \kappa^{Z_1}_{b_L b_L} \simeq 4.3, \; \kappa^{Z_1}_{t_R t_R} \simeq 6.8, \tag{6.41}$$

$$\kappa^{Z_2}_{t_L t_L} \simeq 5.5, \; \kappa^{Z_2}_{b_L b_L} \simeq 3, \; \kappa^{Z_1}_{t_R t_R} \simeq 0.3, \tag{6.42}$$

$$\kappa^{W_1}_{t_L b_L} \simeq 1, \; \kappa^{W_1}_{t_R b_R} \simeq 0, \tag{6.43}$$

$$\kappa^{W_2}_{t_L b_L} \simeq 1.5, \; \kappa^{W_2}_{t_R b_R} \simeq 0, \tag{6.44}$$

The rest of the fermions are localized close to the UV brane, hence they have suppressed couplings to the KK gauge bosons do not contribute to the widths of the heavy $V_{1,2}$. The couplings of the heavy vector bosons to light gauge (and Higgs) bosons can be obtained from eqs. (6.3) (for VVV couplings) and (6.21) (for VVh couplings) by inserting the gauge boson KK decomposition and calculating the relevant overlap integrals. We quote below these couplings, which again are normalized to the corresponding $V_{SM}WW/WZ/Wh$ couplings:

$$\kappa^{A_1}_{WW} \simeq 0.025, \; \kappa^{Z_0}_{WW} \simeq 1, \; \kappa^{Z_1}_{WW} \simeq 0.015, \; \kappa^{Z_2}_{WW} \simeq 10^{-3}, \tag{6.45}$$

$$\kappa^{W_0}_{WZ} \simeq 1, \; \kappa^{W_1}_{WZ} \simeq 0.022, \; \kappa^{W_2}_{WZ} \simeq 0.018, \tag{6.46}$$

$$\kappa^{W_0}_{Wh} \simeq 0.42, \; \kappa^{W_1}_{Wh} \simeq -0.9, \; \kappa^{W_2}_{Wh} \simeq -1.7. \tag{6.47}$$

Using the numerical values displayed above, one can derive the total decay widths of the 5 resonances:

$$\Gamma_{A_1} = 123 \text{ GeV},\ \Gamma_{Z_1} = 174 \text{ GeV},\ \Gamma_{Z_2} = 126 \text{ GeV},\ \Gamma_{W_1} = 127 \text{ GeV},\ \Gamma_{W_2} = 134 \text{ GeV}. \quad (6.48)$$

6.4 Interpreting the Diboson Excess

We turn now to the discussion of diboson production at the LHC and our tentative interpretation of some of the excesses observed by the ATLAS and CMS collaborations in our custodially protected RS scenario.

We calculate the cross sections for the production processes $q\bar{q} \to W^+W^-$, $q\bar{q}' \to W^\pm Z$ and $q\bar{q}' \to W^\pm h$, including the s–channel vector boson exchanges and the t– or u–channel light quark exchanges for the first two modes (for the third mode, the Higgs couplings to light quarks are negligible). In the WW case, the exchanged gauge bosons V are the photon and Z boson and their first KK excitations: A_1, Z_1 and Z_2; in the WZ and Wh cases, the exchanged states are the W and the heavier $W_{1,2}$ resonances. The rates, where one should take into account the full interference, depend on the V couplings to the initial $q\bar{q}$ pair and to the W/Z or h bosons as well as on the V total widths. All these ingredients have been given in the previous sections. Although the couplings of the heavy resonances to W, Z, h states are induced by mixing and should in principle be small, the cross sections for longitudinal final states grow with powers of $m^2_{KK}/m^2_{W,Z,h}$ and, thus, can compensate for this suppression. In turn, the $q\bar{q} \to ZZ$ process can be mediated only by t and u–channel quark exchange as there is no coupling of the photon or Z boson to ZZ pairs and, according to the Landau–Yang theorem, heavy spin–one neutral vector bosons such as $Z_{1,2}$ and cannot decay into two light ones.

Figure 6.3 displays the differential cross sections at the LHC with $\sqrt{s} = 8$ TeV as a function of the diboson invariant masses in the three processes, using MSTW parton distributions [298]. As can be seen, the small continuum contributions, which include the SM channels but with possibly significant new contributions at high masses[2], fall with the invariant mass of the diboson systems. However, there are significant excesses at a mass around 2 TeV, which corresponds to the KK mass scale.

The previous example shows that excesses in diboson final states due to resonances can be easily generated in the warped extra–dimensional scenario considered here. While the resonance mass needs to be fixed, the correct magnitude of the signal can be adjusted by simply tuning the various couplings of the KK states to SM particles. More specifically and channel by channel, the ATLAS and CMS data [287, 288] can be interpreted as follows.

The WW mode: The signal is obtained by considering the process $q\bar{q} \to V \to W^+W^-$ with $V = A_1, Z_{1,2}$. Using the input KK masses and couplings given previously, the ATLAS data with a 2.6σ excess in the WW final state at an invariant mass of ≈ 2 TeV can be reproduced. It turns out that the first KK excitation of the photon, A_1, is the main contributor to this particular final state. As the three resonances have very close masses, with differences smaller than the total decay widths, they are indistinguishable.

Besides the SM contribution, there is also a pure QCD reducible background to the $pp \to WW \to$ jets topology: di-jet, W/Z+jet production, and so on. ATLAS has provided a formula that approximately describes this background from a parametrical adjustment of the data that have passed all selection and tagging requirements (it was found to be compatible

[2] These additional contributions result from the anomalous couplings among the SM gauge bosons induced by the RS scenario [295].

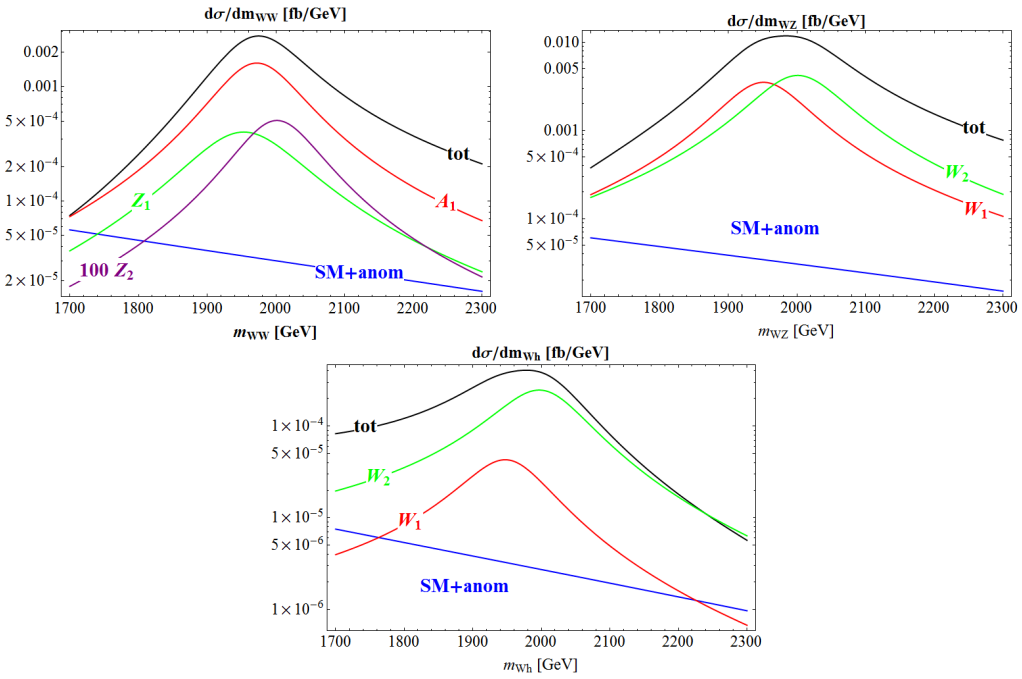

Figure 6.3 – The differential cross sections (in fb/GeV) for the three processes $q\bar{q} \to W^+W^-$ (upper left panel), $q\bar{q}' \to W^\pm Z$ (upper right panel) and $q\bar{q}' \to W^\pm h$ (lower panel) at the LHC with $\sqrt{s} = 8$ TeV as functions of the diboson invariant masses (in GeV). The individual and total contributions of the various heavy resonances with masses close to 2 TeV are shown, together with the SM contributions including the "anomalous" effects in the RS scenario.

both with simulated background events and several sidebands in the data). The function includes all the relatively large uncertainties affecting them[3].

The upper left panel of Fig. 6.4 shows the expected mass distribution of the $pp \to W^+W^-$ process at the LHC at 8 TeV c.m. energy with 20 fb^{-1} data, assuming the efficiency and the purity given by ATLAS. The continuous line corresponds to the predicted background, while the simulated data, with their error bars, are obtained by adding to this background the expected signal in our extra–dimensional scenario, with the numerical values of the parameters given previously. As can be seen, the local $\approx 3\sigma$ excess observed by ATLAS at an invariant mass of ≈ 2 TeV is reproduced within the statistical uncertainties.

The WZ mode: Once the various parameters of our scenario have been adjusted in order to fit the WW data, the WZ data and in particular the $\approx 3.4\sigma$ ATLAS excess in this channel at a 2 TeV invariant mass can be straightforwardly explained in terms of the $W_{1,2}$ contributions to the process $q\bar{q}' \to WZ$, with the parameters given previously. The upper right panel of Fig. 6.4 shows the expected mass distribution of the ZW final state at $\sqrt{s} = 8$ TeV with 20 fb^{-1} data, assuming the efficiency and purity given by the ATLAS collaboration. Again, the continuous line is for the QCD background, while the crosses represent the simulated data corresponding to the expected signal in our scenario added on top of the background..

Compared to other approaches, as, for instance, GUT extensions of the SM, the scenario considered here has two interesting features. First, the $W_{1,2}$ and $Z_{1,2}$ states are predicted to have approximately the same mass, so we indeed have $m_{KK} \approx 2$ TeV for the four resonances.

[3]This means that the QCD background and the genuine WW signal cannot be measured separately. While this has no impact for the observation of a resonance, it forbids measuring possible excesses in the WW component due to possible anomalous couplings as also predicted by our scenario; see e.g. Ref. [295].

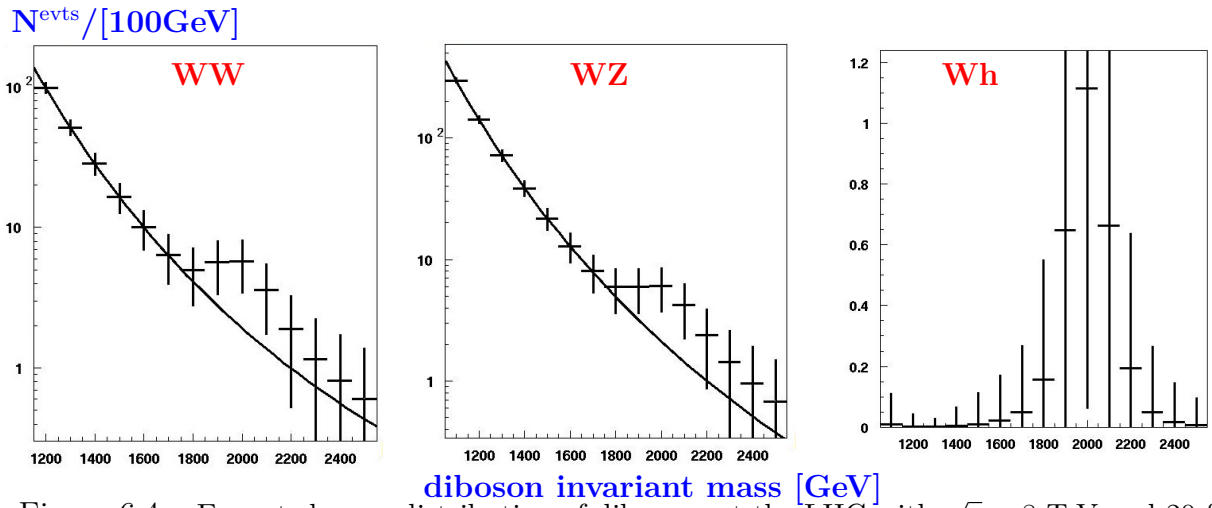

Figure 6.4 – Expected mass distribution of dibosons at the LHC with $\sqrt{s} = 8$ TeV and 20 fb^{-1} data in the WW (left), WZ (center) and Wh (right) channels, assuming the efficiency and purity from the ATLAS (in WW, WZ) or the CMS (in Wh) collaborations. Continuous lines are for the backgrounds and the bars are when adding the expected signals in our scenario.

Second, similar 0-mode–KK-mode mixing for the W and Z KK towers (as enforced by the custodial symmetry) implies that the couplings of the neutral and charged heavy states to W/Z bosons are closely related. Thus, the rates for $q\bar{q}' \to WZ$ are fixed once the parameters entering $q\bar{q} \to WW$ are chosen. Remarkably, they both turn out to be in agreement with the ATLAS data. The only freedom is, as already noticed in Ref. [294], that additional decay modes into heavy quarks, such as $W_{1,2} \to t'b$, with t' a KK top partner, affecting the resonance total widths, are possible. Since these new contributions cannot be predicted accurately, one can leave the total widths free to adjust the data more precisely.

The ZZ mode: In this case, ATLAS observes an excess corresponding to a 2.9σ standard deviation. This excess is difficult to explain in our context since, as mentioned previously, heavy spin–1 neutral gauge bosons such as $Z_{1,2}$, cannot decay into two almost massless neutral ones. One should thus assume that either the heavy resonance is the spin–two KK excitation of the graviton, G_{KK}, with a mass that is close to $m_{KK} \approx 2$ TeV (although in the simplest scenarios the mass of G_{KK} should be higher than this value). Another explanation would be that the uncertainty in the measurement of the dijet mass could make one of the decaying Z bosons resemble a W or a h boson, allowing the possibility to attribute the excess in our RS context to WZ or Wh production.

In fact, while ATLAS provides a good separation between the dibosons and the QCD background, there is a large overlap between W and Z selections and, hence, the existence of the three separate WW, WZ and ZZ channels is not certain, preventing a full comparison with our prediction. The only meaningful attitude would be to sum the excesses in the three different diboson modes. In doing so, our scenario with the parameters chosen above ideally predicts in the three 100 GeV most exciting mass bins around 2 TeV, a total of 9 signal events above the 9 background events which makes a total of 18 events.

The Wh mode: The channel $pp \to Wh$ with the subsequent decays $W \to \ell\nu$ and $h \to b\bar{b}$ has been searched for by CMS [289] and a ≈ 2.5 standard deviation was found at an invariant mass of 2 TeV, at which the SM background is negligible. In our scenario, the excess originates from $pp \to W_{KK} \to Wh$ production. The right–hand side of Fig. 6.4 shows the expected signal in our scenario at $\sqrt{s} = 8$ TeV with 20 fb^{-1} data assuming the

efficiency and the purity given by CMS. Note that the process $pp \to Z_{1,2} \to Zh$ should be also observed at some stage but as the neutral cross section is smaller than that for the charge one and the leptonic $Z \to \ell^+\ell^-$ branching rate is small, this neutral current process cannot be observed with the data collected at the previous LHC run.

We close this section by making two remarks. A first one is that WW, WZ and Wh final states should also have been observed in the semi-leptonic modes with similar sensitivities; nevertheless, ATLAS observes no such signal, while CMS observes a $\approx 2.5\sigma$ effect in Wh. A second remark is that if the ZZ signal is due to a ≈ 2 TeV mass KK graviton, the production would be initiated by gluon–gluon fusion and the significance of the signal could therefore increase when moving from 8 to 13 TeV energy.

6.5 Discussion and future prospects

Let us now discuss the impact of our choice of parameters in the warped extra-dimension scenario that we consider (in particular the $m_{KK} \simeq 2$ TeV choice) on the rates of the 125 GeV Higgs boson as measured at the LHC [173]. The tree–level Higgs couplings to fermions and gauge bosons are first affected by (i) the mixing between the SM fields and their KK excitations and (ii) the modification of the Higgs vacuum expectation value. Second, the loop-induced Higgs vertices receive further contributions from exchanges of the KK towers of bosonic and fermionic modes, as well as from the custodians [108, 285, 286, 299–302].

Within our RS framework, these effects can be parameterized in terms of two parameters besides m_{KK} [303]: the size kL of the extra dimension and the maximum absolute value $y_\star$ of the dimensionless complex Yukawa couplings. For fermion representations promoted to $\mathrm{SU(2)_L \times SU(2)_R \times U(1)_X}$ multiplets, with equal $\mathrm{SU(2)_R}$ and $\mathrm{SU(2)_L}$ gauge coupling constants, the predictions for the Higgs production and decay rates were calculated in Ref. [303]. It was shown that for reasonable kL and $0.5 < y_\star < 3$ values and in two different scenarios, one of a Higgs field localized towards the TeV–brane but with a narrow width profile and another of a purely brane–localized Higgs field, one needs m_{KK} values beyond a few TeV and in any case, $m_{KK} \gtrsim 2.5$ TeV, in order to cope with the Higgs data.

A detailed analysis of the Higgs production and decay rates in the RS scenario considered here is beyond the scope of the analysis carried out in this chapter. Nevertheless, we believe that there is a way to cope with the LHC data on the Higgs signal strengths $\mu_{XX} = \sigma(pp \to h \to XX)/\sigma(pp \to h \to XX)|_{\rm SM}$ for the dominant detection channels, $h \to \gamma\gamma, ZZ^* \to 4\ell, WW^* \to 2\ell 2\nu, b\bar{b}$ and $\tau^+\tau^-$. The reasons behind this optimism are the following.

First, in their combined analyses of the Higgs signals, the ATLAS and CMS collaborations assumed that all uncertainties can be treated as Gaussian, which is not necessarily correct, as the theoretical uncertainties, which are at the level of 10–15% and have been underestimated by the experiments, should be treated as a bias; see Refs. [120, 121, 130] for detailed discussions. The total uncertainties on the signal strengths are thus larger and, at the 2σ level, one could still allow for a deviation of order of 50% that a mass scale of $m_{KK} \simeq 2$ TeV can generate on the most precisely measured μ_{WW}, μ_{ZZ} and $\mu_{\gamma\gamma}$ signal strengths.

Second, one could include the effects of the new quarks t' and b' that we do not completely specify here, as we are mainly focusing on the bosonic sector (the effects of the fermionic KK excitations have been included in the analysis of Ref. [303] in an approximate way but not the ones of the "custodians" [304]. They could generate global modifications to the loop induced processes, such as the dominant $gg \to h$ production mechanism and the precisely measured $h \to \gamma\gamma$ decay mode. These new partners also alter the tree–level $t\bar{t}h$ (and $b\bar{b}h$)

couplings through fermion mixing.

Finally, a third point is that these indirect constraints are also subject to uncertainties from higher dimensional non-renormalisable operators originating from the ultra-violet completion of the model. The latter can potentially lead to large (and hopefully compensating) effects; see for instance the analysis of Ref. [305] in a similar context.

In fact, a similar problem occurs when addressing the indirect constraints from electroweak precision data: there are large contributions in the so–called oblique corrections that affect the W boson mass and the effective mixing angle $\sin^2\theta_W$ at high orders. Indeed, even under the hypothesis of a custodial symmetry $\mathrm{SU(2)_L \times SU(2)_R \times U(1)_X}$ gauged in the bulk that should in principle allow for some protection, analyses of oblique corrections lead to a lower bound of a few TeV on the mass m_{KK} in the simplest realisations [306].

In conclusion, we consider the KK resonance mass scale $m_{KK} \simeq 2$ TeV to be viable despite the potentially problematic corrections to the Higgs signal rates and the electroweak precision data as they can be alleviated by introducing additional degrees of freedom or new contributions. In some sense, we adopt the spirit of a bottom-up approach and consider that the direct signal of new physics, as the production of new gauge bosons should probably be taken more seriously than the indirect constraints from virtual heavy particle exchanges.

6.6 Summary

We have considered the diboson excesses observed by the LHC experiments in both the WW, WZ and Wh production channels and interpreted them in terms of the production of heavy spin–one resonances: the Kaluza–Klein excitations of the electroweak gauge bosons in the context of a custodially protected model of warped extra space–time dimensions. We have focused our attention on scenarios that also address two anomalies in the heavy quark sector of the SM: the bottom and (to a lesser extent) top quark forward–backward asymmetries as measured respectively at LEP and at the Tevatron.

We have indeed found a set of parameters of the model that fits the ATLAS and CMS diboson data, except for the excess in the ZZ channel, which is difficult to explain unless one assumes (i) a comparable mass for KK gravitons and gauge bosons or (ii) a mismeasurement of the dijet invariant mass, which would imply that a W or h boson is misidentified as a Z. The price to pay for this scenario with a resonance mass scale $m_{KK} = 2$ TeV is some tension with the LHC Higgs and electroweak precision data, but which can be alleviated by allowing for additional contributions from other sectors of the model, such as heavy top and bottom quark partners.

Nevertheless, there is no more interest in addressing any possible shortcomings of the model presented in this chapter, as the 2 TeV excess was not reconfirmed by subsequent data [307–310].

Chapter 7

Scalar Production in Association with a Z Boson at the LHC and ILC: the Mixed Higgs-Radion Case of Warped Models

7.1 Context

After the discovery of the Higgs boson and the completion of the Standard Model (SM), the search for new particles at the Large Hadron Collider (LHC) is more and more intense. Precise measurements of Higgs couplings are the natural complement of these direct searches given that Higgs couplings could be influenced by virtual exchanges and/or mixing effects of exotic particles. Interestingly, new scalar fields (S), arising in various SM extensions, could both be directly produced and mix with the Higgs boson. Such scalars can still be as light as a few tens of GeV given that, for example, the sensitivity of the LEP collider searches is drastically reduced when the ZZS coupling reaches $\sim 1/10$ of the ZZh (Higgs) coupling. LHC searches for scalars also suffer from limited sensitivity to light scalars; for instance the powerful investigation performed in the diphoton decay channel becomes inefficient for masses below ~ 60 GeV given the trigger limitations. The future e^+e^- International Linear Collider (ILC) and CLIC, which shall collect more than 100 times the LEP luminosities and reach the TeV scale, are expected to improve the low scalar mass searches.

From the theoretical point of view, the warped extra dimension scenario proposed by L.Randall and R.Sundrum (RS) [25] with a Higgs boson localised at (or close to) the TeV-brane, being dual to composite Higgs models [62–65], remains one of the most attractive extensions of the SM, in particular due to its elegant solution of the the gauge hierarchy problem and its simple geometrical explanations of the fermion mass hierarchies [42,43,59–61] – in case of matter in the bulk. The RS paradigm – including the dual composite Higgs scenarios – constitutes an alternative to the supersymmetric SM extensions of a completely different nature. Nevertheless, both these kinds of SM extensions predict the existence of new scalar particles which could lead to clear experimental signatures at colliders. In the case of warped models, a predicted scalar is the so-called radion, which corresponds to the dilaton field through the AdS/CFT correspondence.

The collider phenomenology of the RS scenario is guided by the indirect constraints on the masses of the various Kaluza-Klein (KK) excitations. Let us thus shortly review the constraints on such a scenario arising from the electroweak precision tests (EWPT). In the RS model with a custodial symmetry gauged in the bulk [140], the bounds from

EWPT can be reduced down to gauge boson masses $m_{KK} \gtrsim 3-5$ TeV [125, 306, 311] for the first KK excitation of, say, the photon, in case of a purely brane-localised Higgs [1]. In RS versions with a bulk Higgs field unprotected by a custodial symmetry, these bounds become $m_{KK} \gtrsim 7.5$ TeV for a Higgs profile still addressing the gauge hierarchy problem ($\beta = 0$) [312, 313] [2], and, $m_{KK} \gtrsim 13.5$ TeV for the brane-Higgs limit ($\beta \to \infty$) [313].

In contrast, within custodially protected warped models, the lightest KK excitations of fermions (custodians) can reach masses as low as the TeV scale while satisfying the EWPT affected by their loop contributions to the oblique parameters S,T [65] or their direct (mixing) corrections to the Zbb vertex [125].

The radion scalar field, corresponding to the fluctuations of the metric along the extra dimension, has a typical mass around the EW energy scale [317], within the standard mechanism of radius stabilisation based on a bulk scalar field [47]. The EWPT (via the S,T,U parameters) and LEP limits allow radion masses between $\sim$ 10 GeV and the TeV scale, depending on the curvature-scalar Higgs mixing (for SM fields on the IR brane) [318].

Given those mass bounds, the radion might be the lightest new particle and thus appear as the first signature of warped models at colliders – before KK fermion [79, 319] or KK gauge boson [293, 320–325] production. The detection of the radion would constitute the discovery of a second scalar field, after the Higgs boson observation. This new boson should then be disentangled from other scalar particles predicted by supersymmetric models or other scenarios with extended Higgs sectors.

The radion is mainly produced at LHC by gluon-gluon fusion (see e.g. Ref. [326] for a recent paper) but some model-dependence might affect this process as we discuss now. The LHC data [327, 328] on the Higgs rates [3] lead to $m_{KK} \gtrsim 11$ TeV for a brane-Higgs [4] within a custodially protected RS model [303]. [5] These constraints arise essentially because of the contributions of KK modes to the Higgs production reaction with the highest cross section: the loop-induced gluon-gluon Fusion (ggF) mechanism (see e.g. Ref. [108]). To reduce this limit on the KK scale m_{KK} down to the TeV scale (comparable with EWPT limits), and in turn reconcile the related gravity scale at the IR brane with the fine-tuning problem, one may expect some new physics effects (brane-localised kinetic terms, different fermion representations under the custodial symmetry, cancellations...) in the triangular loop of the ggF production mechanism, thus suppressing the KK mode contributions. This introduces some unknown model-dependence in the Higgs ggF mechanism which would also affect the similar ggF process for radion production.

In contrast, the Higgs (h) production in association with an EW gauge boson ($V \equiv Z, W$), followed by the Higgs decay into a pair of bottom quarks, induces – due to KK mixing [286] – a limit of $m_{KK} \gtrsim 2.25$ TeV (3.25 TeV) with $y^* = 1.5$ ($y^* = 3$) for a brane-Higgs (and slightly above for a narrow bulk-Higgs) in custodial warped models [303]. Such values are acceptable from the fine-tuning point of view. Hence there is no strong reason to assume that the tree-level hV production is sensitive to unknown effects. A similar conclusion then holds for the radion (ϕ) production in association with a gauge boson V.

The ϕZ production in particular possesses other interests in some regions of the RS parameter space. For example, the radion discovery at LHC through its ggF production is challenging if the radion mass satisfies $m_\phi < 2m_Z$, closing kinematically the golden channel

[1] $\sim$ 3 TeV for a bulk Higgs localised towards the TeV-brane [312].

[2] $\sim$ 2 TeV [312] with a deformed metric, with deviations from AdS geometry near the Infra-Red (IR) brane [314–316].

[3] These data constrain the Higgs-radion mixing to be small enough to recover a SM like Higgs boson.

[4] $\sim$ 7.25 TeV for a narrow bulk-Higgs.

[5] Those limits hold for a maximal absolute value $y^* = 1.5$ of the anarchic dimensionless 5D Yukawa coupling constants, and are even more severe for a larger value $y^* = 3$.

$\phi \to ZZ$ [6], and is too small to allow for the detection of the diphoton decay $\phi \to \gamma\gamma$. The ϕZ production would then offer an additional on-shell Z boson which helps for the tagging of the final state. Another situation motivating the ϕZ production search is a suppression of the ggF rate due to a significant decrease of the radion coupling to gluons as occurs in some parameter regions. [7]

Regarding the future e^+e^- ILC machine, the ϕZ production (alongside with vector boson fusion or VBF) would be the dominant radion production mode [329], similarly to the Higgs boson case. The ϕZ production in a leptonic machine is also an important channel because, as for the hZ channel, it allows for a decay independent search – based on the simple $2 \to 2$ body kinematics – that should permit in particular to cover low radion masses, which challenging for the LHC.

Therefore, in this chapter, based on Ref. [330], we study the ϕZ production in custodially protected warped models with a brane-localised Higgs boson. The analytical calculations of the radion couplings allow us to compute the complete ϕZ production cross section, both at the LHC and ILC colliders. The LHC and ILC turn out to constitute complementary machines in regard to the ϕZ investigation. The ϕZ reaction proceeds through the s-channel exchange of the EW Z boson, its KK excitations as well as the extra Z' gauge boson (issued from the extended bulk custodial symmetry). All these contributions together with their interference are taken into account. The effects of the various KK mixings in the radion couplings and KK exchanges in the s-channel are discussed, as well as the possibility to reconstruct the invariant mass of the first two resonant heavy boson eigenstates (mainly KK modes) almost degenerate in mass. Such a spectacular resonance observation would constitute a double discovery of the radion and first KK gauge bosons. The resonant KK gauge boson detection through its decay to hZ is also quantitatively studied. Indeed, the ϕZ and hZ productions should be consistently analysed together due to the $\phi - h$ mixing. In view of the obtained ϕZ and hZ rates, we discuss the possibilities of experimental observations which rely on favoured radion decays, depending on the parameter space and in particular on m_ϕ values.

Furthermore, we propose in this chapter a more general experimental technique to search for an inclusive final state $Z + X$ (where X represents any SM or new particles), followed by the decay $Z \to 2$ charged leptons, based on a cut on the Z boson transverse momentum. The choice of the decay $Z \to \mu^+\mu^-$ is thus a tagging method to allow trigger and detection. Such a technique could also be applied for $X \equiv \phi$ in RS versions different from the present one, e.g. with lower resonant KK Z masses and/or favoured gluon decays for the radion (so that the associated tagged Z becomes crucial for the detection). See for instance Ref. [331] for a recent warped model of this kind.

At this stage we also mention the related work on the search of the radion at colliders [326] as well as the more general literature on the radion phenomenology in warped scenarios with SM fields at the TeV-brane [318, 332, 333], with only the Higgs boson stuck on the IR brane [334, 335] or the whole SM field content propagating in the bulk [336]. Besides, there exists a connected study on the hZ production through resonant neutral KK gauge bosons [337].

This chapter is organised as follows. In Section 7.2, we present all the radion and Higgs couplings and calculate the KK mixing effects – applying the so-called mixed KK decomposition to the gauge boson sector. Then we provide the analytical and numerical

[6] Below this threshold, the channel $\phi \to ZZ^*$, into a virtual Z boson, may still allow to reconstruct one on-shell Z boson decaying to charged lepton pairs.

[7] $m_\phi \gtrsim 200$ GeV and $\xi = \mathcal{O}(1)$, as shown in Ref. [326] (where the effect of the coloured KK fermions on the ϕgg loop is neglected).

results for the ϕZ and hZ (Section 7.3) production cross sections at the LHC and ILC. The behaviours of these rates along the theoretical parameter space are explained there. In Section 7.4, experimental methods are proposed to detect the radion and/or (extra) KK gauge bosons. Finally, we present a summary in the last section.

7.2 Radion and Higgs Couplings

7.2.1 Model Description

Our model is the RS scenario with the Higgs doublet localised on the IR brane, while the remaining fermionic and gauge fields are propagating in the bulk. The SM fermion mass hierarchy is generated through their wave function overlaps with the Higgs boson, as usually in this framework.

In the $(+----)$ convention that is used throughout this thesis, the well-known RS metric reads

$$\mathrm{d}s^2 = \mathrm{e}^{-2k\,y}\eta_{\mu\nu}\mathrm{d}x^\mu\mathrm{d}x^\nu - \mathrm{d}y^2 \equiv g_{MN}\mathrm{d}x^M\mathrm{d}x^N, \tag{7.1}$$

where upper case roman letters refer to 5D Lorentz indices and greek letters to 4D indices and k being the 5D curvature scale, which is typically of the order of the Planck scale. The y coordinate, which parametrizes the position along the extra-dimension, spans in the interval $[0, L]$. Throughout this work, we will consider that kL, the so-called volume factor, is equal to 35, such that the hierarchy problem is addressed. For the time being, we denote by g_{MN} the unperturbed metric, and postpone the inclusion of the scalar fluctuations for subsection 7.2.2.

We consider the custodial gauge symmetry implementation with a Left-Right Parity [138] as well as a more general implementation allowing potentially to address the A_{FB}^b [106] and A_{FB}^t [296, 297] anomalies. Both implementations predict the same gauge field content. The gauge sector of such models has been presented in detail at the beginning of the previous chapter, so now we move on to the Higgs and radion couplings to the Z boson and its KK partners.

7.2.2 Higgs and Radion Couplings Before Mixing

We now focus on the radion and how it couples to the Z boson KK tower. We start by taking the background RS metric from eq. (7.1) and including the scalar perturbation $F(x, y)$ as in Ref. [334, 335],

$$\mathrm{d}s^2 = \mathrm{e}^{-2(k\,y+F)}\eta_{\mu\nu}\mathrm{d}x^\mu\mathrm{d}x^\nu - (1+2F)^2\mathrm{d}y^2 \equiv \bar{g}_{MN}\mathrm{d}x^M\mathrm{d}x^N, \tag{7.2}$$

where we used $\bar{g}_{MN}$ to denote the 5D metric with scalar perturbations included, in order to differentiate it from its unperturbed counterpart, g_{MN}. The linearized metric perturbations read

$$\bar{g}_{MN} - g_{MN} \equiv \delta g_{MN} \simeq -2F\,\mathrm{diag}\left(\mathrm{e}^{-2k\,y}\eta_{\mu\nu}, 2\right). \tag{7.3}$$

The situation is slightly different for terms localised on the IR brane, i.e. terms that contain the Higgs bi-doublet. On this brane, the line element is written as

$$\mathrm{d}s^2_{\mathrm{IR}} = \mathrm{e}^{-2[kL+F(x,L)]}\eta_{\mu\nu}\mathrm{d}x^\mu\mathrm{d}x^\nu \to \mathrm{e}^{-2F(x,L)}\eta_{\mu\nu}\mathrm{d}x^\mu\mathrm{d}x^\nu \equiv \bar{\eta}_{\mu\nu}\mathrm{d}x^\mu\mathrm{d}x^\nu, \tag{7.4}$$

where the arrow was used to indicate that the redefinition of the Higgs bidoublet H absorbs away the e^{-2kL} factor. Therefore, the linearized metric perturbations on the IR brane are

given by

$$\bar{\eta}_{\mu\nu} - \eta_{\mu\nu} \equiv \delta\eta_{\mu\nu} \simeq -2F(x,L)\eta_{\mu\nu}. \tag{7.5}$$

In the limit of small backreaction (of the field F on the metric curvature), the scalar perturbation $F(x,y)$ can be parametrized as follows [334, 335]:

$$F(x,y) = \frac{\phi_0(x)}{\Lambda} \mathrm{e}^{2k(y-L)}, \tag{7.6}$$

where ϕ_0 is the (unmixed) 4D radion field [8] and Λ is the radion VEV, which is an $\mathcal{O}$ (TeV) energy scale that sets the length of the extra dimension [47]. At linear order, the radion's interaction with the gauge fields and the Higgs can be obtained by making the following replacements:

- $g^{MN} \to \bar{g}^{MN}$ in eq. (6.3) for interactions originating from the bulk terms,
- $\mathrm{d}^4x \to \mathrm{d}^4x\sqrt{\bar{\eta}}$, $\eta^{\mu\nu} \to \bar{\eta}^{\mu\nu}$ in eq. (6.21) for brane-localised interactions,

and then keep only the terms linear in F. [9] Finally, to derive the effective 4D couplings, and take into account the KK Z mixing, one should employ the KK expansion from eq. (6.24) and perform the usual integration over y (or, for the brane-localised terms, just evaluate the profiles at $y = L$). Thus, putting all these elements together, we arrive at the complete 4D Lagrangian describing the h_0ZZ and ϕ_0ZZ interactions:

$$\mathcal{L}^{\mathrm{4D}}_{\varphi Z_i Z_j} = \bar{m}_Z^2 \left(\frac{h_0}{v} - \frac{\phi_0}{\Lambda}\right) C_i^{\mathrm{4D}} C_j^{\mathrm{4D}} Z_{i,\mu} Z_j^\mu - \frac{\phi_0}{\Lambda}\left[\frac{m_{KK}^2}{3(kL)^2} C_{ij}^{5D} Z_{i,\mu} Z_j^\mu + \frac{1}{2}\tilde{C}_{ij}^{\mathrm{5D}} Z_{i,\mu\nu} Z_j^{\mu\nu}\right], \tag{7.7}$$

where we have used the following notations:

$$C_i^{\mathrm{4D}} = g_+^i(L) - \alpha_Z\, g_-^i(L), \tag{7.8}$$

$$C_{ij}^{\mathrm{5D}} = L\int_0^L \mathrm{d}y \left[(g_+^i)'(g_+^j)' + (g_-^i)'(g_-^j)'\right], \tag{7.9}$$

$$\tilde{C}_{ij}^{\mathrm{5D}} = \frac{1}{L}\int_0^L \mathrm{d}y\, \mathrm{e}^{2k(y-L)} \left(g_+^i g_+^j + g_-^i g_-^j\right). \tag{7.10}$$

Let us now trace the origin of each term appearing in eq. (7.7). The first term, proportional to $\bar{m}_Z^2$, originates from the brane-localised mass term in the first line of eq. (6.21), whereas the terms between square brackets come from the 5D gauge kinetic terms in eq. (6.3). More precisely, in terms of 5D fields, the first term between the square brackets originates from the $Z_{5\mu}Z^{5\mu}$ term, while the second one stems from $Z_{\mu\nu}Z^{\mu\nu}$.

We now have all the ingredients to derive the mixed Higgs-radion couplings to the Z_i bosons, which is what we do in the next section.

7.2.3 Higgs-Radion Mixing and Couplings

The Higgs-radion mixing arises at the renormalisable level by coupling the 4D Ricci scalar R_4 to the trace of $H^\dagger H$ via a possible gauge invariant term [318, 332, 333] as follows:

$$S_\xi^{\mathrm{4D}} = \xi \int \mathrm{d}^4x\, \sqrt{\bar{\eta}}\, R_4(\bar{\eta}_{\mu\nu}) \frac{1}{2}\,\mathrm{tr}\left(H^\dagger H\right), \tag{7.11}$$

[8] The KK radion modes are absorbed into the (longitudinal) degrees of freedom of the massive KK gravitons.

[9] Equivalently, one can find the radion couplings by varying the action with respect to the metric and keeping only the linear metric perturbations [334, 335].

with $\bar{\eta}_{\mu\nu}$, the perturbed IR brane metric, defined in eq. (7.4). As it involves the brane-localised Higgs field, the Higgs-radion mixing sources from the IR brane. A non-zero ξ coupling in eq. (7.11) induces a kinetic mixing between the two scalars after EW symmetry breaking, the Higgs-radion Lagrangian being given, at the quadratic level, by [318, 326, 332–335]

$$\mathcal{L}^{\text{4D}}_{\varphi\varphi} = -\frac{1}{2}\begin{pmatrix}\phi_0 & h_0\end{pmatrix}\begin{pmatrix}1+6\xi\ell^2 & -3\xi\ell \\ -3\xi\ell & 1\end{pmatrix}\begin{pmatrix}\Box\phi_0 \\ \Box h_0\end{pmatrix} - \frac{1}{2}m^2_{\phi_0}\phi_0^2 - \frac{1}{2}m^2_{h_0}h_0^2, \tag{7.12}$$

where $\ell \equiv v/\Lambda$ is the ratio between the Higgs and radion VEVs and $\Box$ is the flat-space d'Alembertian. The transition to the mass eigenstates, ϕ and h, is achieved through a non-unitary transformation diagonalising the kinetic terms of eq. (7.12):

$$\begin{pmatrix}\phi_0 \\ h_0\end{pmatrix} = \begin{pmatrix}a & -b \\ c & d\end{pmatrix}\begin{pmatrix}\phi \\ h\end{pmatrix}. \tag{7.13}$$

Using notations similar to the ones in Ref. [334, 335], the elements of this matrix are $a = \cos\theta/Z$, $b = \sin\theta/Z$, $c = \sin\theta + t\cos\theta$, and $d = \cos\theta - t\sin\theta$, with $t = 6\xi\ell/Z$ and $Z^2 = 1 + 6\xi\ell^2(1-6\xi)$ being the determinant of the kinetic mixing matrix from eq. (7.12). The mixing angle is given by

$$\tan\theta = \frac{m^2_{h_0} - m^2_h}{t\, m^2_{h_0}} = -\frac{t\, m^2_{h_0}}{m^2_{h_0} - m^2_\phi}. \tag{7.14}$$

The squared mass $m^2_{h_0}$ can then be expressed in terms of the physical mass eigenvalues $m_{h,\phi}$ as follows [318, 332, 333]:

$$m^2_{h_0} = \frac{Z^2}{2}\left[m^2_h + m^2_\phi + \text{sign}(m^2_h - m^2_\phi)\sqrt{(m^2_h - m^2_\phi)^2 - \frac{144\,\xi^2\ell^2 m^2_h m^2_\phi}{Z^2}}\right], \tag{7.15}$$

while $m^2_{\phi_0}$ can be deduced from $m^2_{h_0}m^2_{\phi_0} = Z^2 m^2_h m^2_\phi$, which results from evaluating the mass matrix determinant in both bases. As it is clear from the expression of $m^2_{h_0}$ above, we use the sign convention in which m_h (m_ϕ) coincides with m_{h_0} (m_{ϕ_0}) when $\xi = 0$.

Summing up, the Higgs-radion system is described by four parameters: the mixing parameter ξ, the radion VEV Λ, the physical radion mass m_ϕ, and the physical Higgs mass m_h, which we fix at 125 GeV. There is also a fifth parameter, the first KK photon mass m_{KK}, which enters indirectly into this interplay by shifting the Higgs VEV. However, one cannot take arbitrary values for these parameters, as there are two theoretical consistency conditions which constrain the parameter space. The first condition is the absence of ghost fields in the theory, which restricts the kinetic mixing matrix determinant to positive values, i.e. $Z^2 > 0$. The second one concerns the square root appearing in eq. (7.15), whose argument should be positive in order to have positive $m^2_{h_0,\phi_0}$ and thus a hermitian Lagrangian. This gives the following mathematical condition:

$$Z^2(m^2_h - m^2_\phi)^2 \geq 144\,\xi^2\ell^2 m^2_h m^2_\phi, \tag{7.16}$$

which actually supersedes the no-ghost condition, $Z^2 > 0$, in the whole parameter space. Note that, in the case of exact degeneracy between the Higgs and the radion, there can be no Higgs-radion mixing, as the condition in eq. (7.16) imposes $\xi = 0$ if $m_h = m_\phi$.

We can now express the couplings of the physical Higgs and radion states to the gauge bosons. To ease the notations, we will use the following definitions, which are similiar to the ones in Ref. [334, 335]:

$$g_\phi = c - \ell a, \quad g_h = d + \ell b, \quad g^r_\phi = -\ell a, \quad g^r_h = \ell b. \tag{7.17}$$

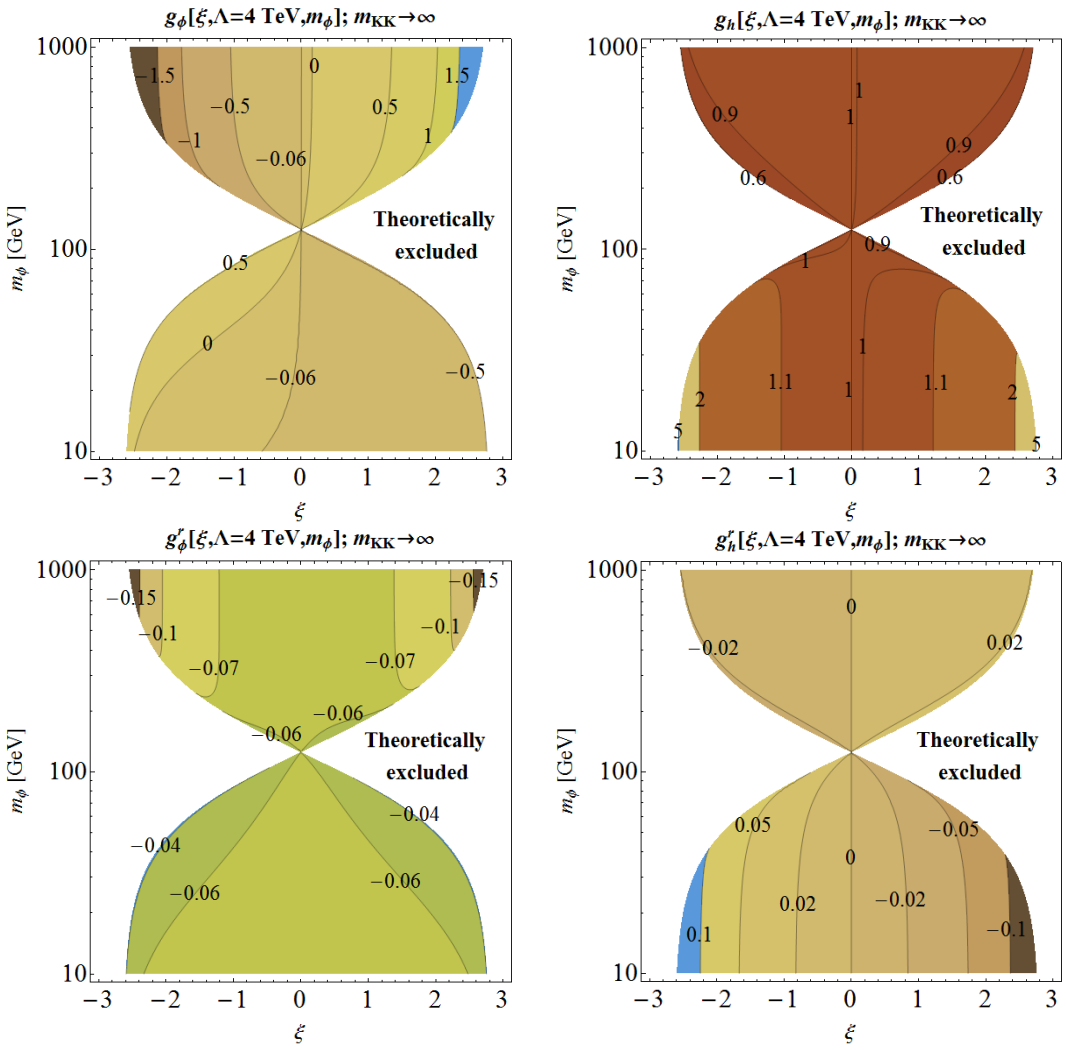

Figure 7.1 – Iso-contours of the couplings (upper left) g_ϕ, (upper right) g_h, (lower left) g^r_ϕ, and (lower right) g^r_h, in the $\{\xi, m_\phi\}$ plane. The four dimensionless couplings plotted above are defined in eq. (7.17). The white region is excluded by the theoretical consistency condition displayed in eq. (7.16). The radion VEV Λ has been fixed at 4 TeV, while we have taken, for simplicity, $m_{KK} \to \infty$.

Using these definitions and the couplings of ϕ_0, h_0, which were derived in the previous section, one can straightforwardly write down the couplings for the scalar mass eigenstates, ϕ and h. As we are focusing on the $Z\phi$ (and Zh) production mechanism, we first list the Lagrangian for $\phi Z_i Z_j$ interactions, which is obtained by inserting the definitions of eq. (7.17) in eq. (7.7):

$$\begin{aligned}\mathcal{L}^{\rm 4D}_{\phi Z_i Z_j} &= \frac{\bar{m}_Z^2}{v}\left(g_\phi\, C_i^{\rm 4D} C_j^{\rm 4D} + \frac{g^r_\phi\, m_{KK}^2}{3\bar{m}_Z^2 (kL)^2} C_{ij}^{5D}\right)\phi Z_{i,\mu} Z_j^\mu + \frac{g^r_\phi}{2v}\tilde{C}^{\rm 5D}_{ij}\phi Z_{i,\mu\nu} Z_j^{\mu\nu} \\ &\equiv \frac{\bar{m}_Z^2}{v}\phi\left[C^\phi_{ij}\, Z_{i,\mu} Z_j^\mu + \frac{\tilde{C}^\phi_{ij}}{2\,\bar{m}_Z^2}\, Z_{i,\mu\nu} Z_j^{\mu\nu}\right]. \end{aligned} \tag{7.18}$$

The hZ_iZ_j interactions are obtained by simply substituting $\phi \to h$ in the above equation.

We plot in Fig. 7.1, as a function of ξ and m_ϕ, the four couplings defined in eq. (7.17), namely $g_{\phi,h}$ and $g^r_{\phi,h}$. We have chosen $\Lambda = 4$ TeV, and, for simplicity, $m_{KK} \to \infty$. In fact, a finite m_{KK} would produce a shift in v and, as the four couplings depend on Λ only through

the combination $\ell = v/\Lambda$, such a VEV shift can be compensated by adjusting Λ to give the same ℓ. Hence, the value of m_{KK} is not crucial in this context, which is why we have set it to infinity. As the four plots indicate, in most of the parameter space $g_{\phi,h}$ dominates over the $g^r_{\phi,h}$ coupling values. In practice, at currently accessible collider energies, one can ignore the $g^r_{\phi,h}$ couplings when calculating the $Z\phi$ or Zh production cross section (even if those coupling contributions are included in our numerical calculations). An exception to this rule applies in the vicinity of the $g_\phi = 0$ contour [10]: in this region, g^r_ϕ becomes dominant, and the radion's coupling to a pair of Z bosons is dramatically reduced, as is the $Z\phi$ production cross section, which tends to render this region blind to current hadronic or even future leptonic colliders. To conclude on this figure, in the limit of KK decoupling (where $C_0^{4\mathrm{D}} \to 1$), the radion coupling to two Z bosons corresponds mainly to g_ϕ [dimensionless with the normalisation of eq. (7.18)] and is thus driven by the Higgs-radion mixing [see eq. (7.17)].

Before closing this section, let us a remark on the correlation between the first KK photon/gluon mass, m_{KK}, and the radion VEV, Λ. The two quantities are related in the following way:

$$\frac{m_{KK}}{\Lambda} \simeq \frac{k}{M_{\mathrm{Pl}}} \,, \tag{7.19}$$

M_{Pl} being the effective 4D Planck mass. In order to avoid significant 5D quantum gravitational corrections, the above ratio should satisfy $k/M_{\mathrm{Pl}} \lesssim 3$ [338]. Throughout this chapter we indeed systematically consider m_{KK} to be smaller than $3\,\Lambda$. Even when the $m_{KK} \to \infty$ limit is considered, it means in fact that the KK partners are sufficiently heavy so as to not influence the numerical results, i.e. $m_{KK} = \mathcal{O}(10)$ TeV. Such values of m_{KK} do not conflict with the considered values of $\Lambda = 4, 5$ TeV.

7.3 The ϕZ and hZ Production

We now turn to the study of the $\phi Z/hZ$ production at the LHC and at the ILC, which proceeds through the s-channel exchange of Z_i bosons, $q\bar{q}/e^+e^- \to Z_i \to Z_0\phi/Z_0 h$. As higher KK levels are to a very good approximation decoupled, we only consider the Z boson plus its first two KK excitations, i.e. $i = 0, 1, 2$, as intermediate s-channel states. Moreover, in the LHC case, we consider only the dominant first and second generation quarks as initial state partons. The Feynman rule for the $Z_i Z_0 \phi$ vertex can be straightforwardly deduced from the Lagrangian piece in eq. (7.18). We display below the squared absolute value of the spin-averaged and polarisation-summed Lorentz invariant amplitude:

$$\overline{|\mathcal{M}_{\phi Z}|^2} = \frac{g_Z^4 (v_f^2 + a_f^2)}{8} \sum_{i,j=0}^{2} \frac{c_i c_j s^2}{(s - m_{Z_i}^2 + \mathrm{i}\, m_{Z_i}\Gamma_{Z_j})(s - m_{Z_j}^2 - \mathrm{i}\, m_{Z_j}\Gamma_{Z_j})} \times$$
$$\times \left[\frac{\bar{m}_Z^2}{m_Z^2} (\lambda \sin^2\theta^* + 4 r_Z)(C_{ij}^\phi)^2 + 8\sqrt{\lambda + 4 r_Z}\, C_{ij}^\phi \tilde{C}_{ij}^\phi + \frac{s}{\bar{m}_Z^2} \left(\lambda(1 + \cos^2\theta^*) + 12 r_Z \right) (\tilde{C}_{ij}^\phi)^2 \right] , \tag{7.20}$$

where the coupling factors c_i are defined in eq. (6.37). The notations we used are as follows: v_f and a_f are, respectively, the vectorial and axial couplings of the initial state fermions to the Z boson (i.e. $v_f = I_{3L}^f/2 - Q_\gamma^f \sin^2\theta_W$ and $a_f = I_{3L}^f/2$, with I_{3L}^f the weak isospin of the fermion f, and Q_γ^f its electric charge), $\sqrt{s}$ the e^+e^-/partonic center-of-mass energy, and θ^* the scattering angle in the center-of-mass frame. Moreover, $\lambda = (1 - r_\phi - r_Z)^2 - 4 r_\phi r_Z$, with $r_A = m_A^2/s$, is the usual 2-body phase space function. The wave function overlap integrals

[10] At high enough m_ϕ, the $g_\phi = 0$ condition becomes equivalent to the so-called conformal limit, $\xi = 1/6$.

c_i were defined previously in eq. (6.37). As before, the amplitude for the Zh production process is obtained trivially from eq. (7.20) by changing $\phi \to h$. The expression of the $\phi Z/hZ$ production cross section (in the case of LHC, at the partonic level) is obtained from the integration over $\cos\theta^*$ of the amplitude displayed in eq. (7.20).

As it is customary, we denote by Γ_{Z_i} the widths of the observed Z boson ($i = 0$) and of its first two KK excitations ($i = 1, 2$). In our calculations, as the (partonic) center-of-mass energy is always above m_{Z_0}, we can safely neglect Γ_{Z_0}. Regarding $Z_{1,2}$, their widths are approximately equal to 10% of their masses. For example, if one takes $m_{KK} = 3$ TeV, we get

$$m_{Z_1} \simeq 2.96 \text{ TeV}, \ \Gamma_{Z_1} \simeq 270 \text{ GeV} \quad \text{and} \quad m_{Z_2} \simeq 3.15 \text{ TeV}, \ \Gamma_{Z_2} \simeq 300 \text{ GeV}, \tag{7.21}$$

where we have chosen the dimensionless bulk mass parameters of the top and bottom quarks to be $c_{Q_L} = 0.4$, $c_{t_R} = 0$, and $c_{b_R} = -0.57$, such that their measured masses are reproduced and the left and right Zbb couplings are close to their SM values. These are values of the c-parameters that we will use in our analysis. On the other hand, in order to explain the anomaly on the bottom quark forward-backward asymmetry $A_{\rm FB}^b$ at LEP (and, to a lesser extent, the anomalous top quark asymmetry $A_{\rm FB}^t$ measured at Tevatron), a more suitable choice would be $c_{Q_L} = 0.51$, $c_{t_R} = -1.3$, and $c_{b_R} = 0.53$ [106, 296, 297]. In this case, the widths of the KK Z partners change, but not dramatically: $\Gamma_{Z_1} \simeq 350$ GeV and $\Gamma_{Z_2} \simeq 275$ GeV. In both cases mentioned above, the Higgs-radion parameters have been fixed as follows: $\xi = 1$, $\Lambda = 4$ TeV, and $m_\phi = 750$ GeV. However, the width dependence on these parameters is weak, as the decay to $Z\phi$ is always subdominant. Throughout most of the parameter space spanned by ξ, Λ, and m_ϕ, with the c-parameters chosen above, the dominant decay channel for Z_1 (Z_2) is to WW (Zh).

7.3.1 At the LHC

Radion Production

The LHC cross-section is obtained by convoluting the cross section for the hard scattering, $\sigma(q\bar{q} \to Z_i \to Z\phi)$, with the parton distribution functions (PDFs). In the following, we use the MSTW set of PDFs at NNLO [298].

We first show in Fig. 7.2 the $Z\phi$ production cross section as a function of m_ϕ and m_{KK}, for a proton-proton center-of-mass energy $\sqrt{s} = 13$ TeV, with $\xi = 1$ and $\Lambda = 4$ TeV. We consider m_{KK} values above ~ 2 TeV as allowed from the direct Zh searches at LHC (potentially affected by KK Z mixing), since there is no specific reason to expect unknown effects in this tree-level production – as discussed in the the first section of this chapter. The radion mass range was discussed as well in Section 7.1.

For $m_{KK} \gtrsim 5$ TeV, we see on Fig. 7.2 that the KK partners of the Z boson no longer play a significant role in the $Z\phi$ production, thus effectively decoupling. This is due to the fact that, at partonic center-of-mass energies $\sqrt{\hat{s}}$ bigger than ~ 5 TeV, or equivalently $\hat{s}/s \equiv \tau \gtrsim (5/13)^2$, the quark-anti-quark luminosity drops down to a negligible level which restricts the on-shell production of $Z_{1,2}$ states. On the contrary, for $m_{KK} \lesssim 5$ TeV, the Z_1 and Z_2 states play an important role, but only for a radion heavier than ~ 500 GeV. This is because, in order to produce a radion plus a Z boson, $\sqrt{\hat{s}}$ should surpass $m_\phi + m_Z$, which means that, for a 500 GeV radion, the virtual Z boson contribution to the $Z\phi$ production is cut off by the $\sqrt{\hat{s}}$ threshold and hence becomes comparable to the contribution of its KK partners, Z_1 and Z_2. However, as one goes to lower radion masses, the cross section dependence on m_{KK} becomes less and less important, as the exchanged virtual Z boson becomes less and less off-shell and starts to dominate over the contributions coming from

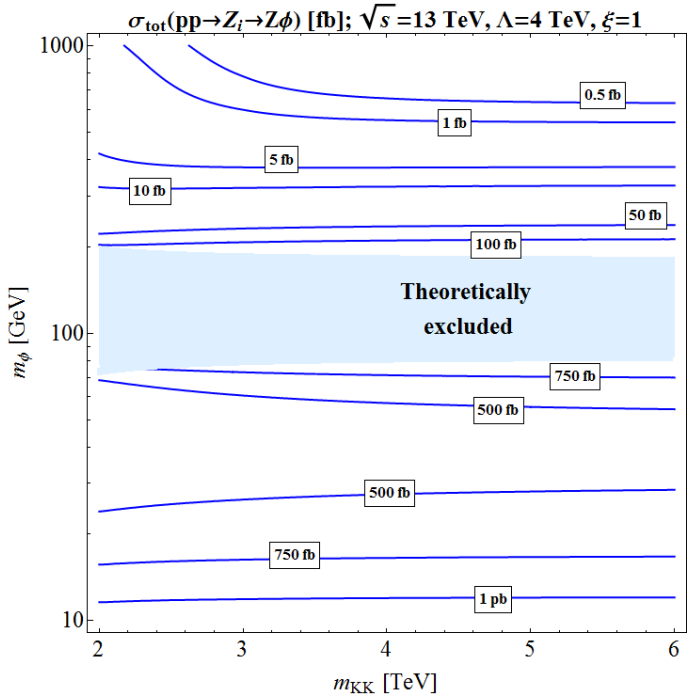

Figure 7.2 – Contour lines of the $Z\phi$ production cross section (in fb and pb) at the LHC in the plane m_ϕ (in GeV) versus m_{KK} (in TeV). The values of the other involved parameters are $\xi = 1$ and $\Lambda = 4$ TeV. The light blue region is excluded by the theoretical constraint from eq. (7.16).

the exchanges of Z_1 and Z_2. Nevertheless, we observe a small dependence on m_{KK} for small radion masses as well: its origin lies in the dependence of the $\phi Z_0 Z_0$ coupling on m_{KK}, which is a result of the mixing of the SM-like Z boson with its KK partners.

To better illustrate our argument from the previous paragraph, we show in Fig. 7.3 the $Z\phi$ invariant mass distribution for $\Lambda = 4$ TeV, $\xi = 1$, $m_{KK} = 3$ TeV, and two radion masses, $m_\phi = 10$ GeV (left panel) and $m_\phi = 750$ GeV (right panel). As the total cross section is obtained from the integration of the invariant mass distribution over values greater than the kinematical threshold, $\sqrt{\hat{s}} = m_{Z\phi} > m_\phi + m_Z$, it is clear why the KK Z partners play a role only for the associated production of a heavy radion: in this case, the integral does not cover the region at low $\hat{s}$, where the invariant mass distribution is enhanced by the reduced "off-shellness" of the Z boson contribution, thus giving more weight to the invariant mass region around the KK peak.

Moreover, one notices on the right panel of Fig. 7.3 that the two nearly-degenerate KK Z bosons produce a single peak in the $Z\phi$ invariant mass distribution. In fact, as shown in this figure, this peak mostly originates from the Z_2 resonance, as it is, in general, more strongly coupled to $Z\phi$ than Z_1. The other reason is that the Z_1 eigenstate is mainly composed of the Z' boson which has vanishing couplings to the light initial quarks localised towards the Planck-brane. The interference term was taken at zero to draw those two resonance distributions separately. The spectacular observation of such a resonant $Z\phi$ production would represent the simultaneous direct manifestation of the radion and the first KK Z boson, the rate of the extra boson Z' (mainly constituting the Z_1 state) resonance being probably too small to expect a detection at LHC.

In addition, we have investigated the impact of varying the value of g_R on the $Z\phi$ production cross section at the LHC. For this, we have chosen a point in the plane displayed in Fig. 7.2 and computed the corresponding cross section for $g_R = g_L$ (Left-Right Parity

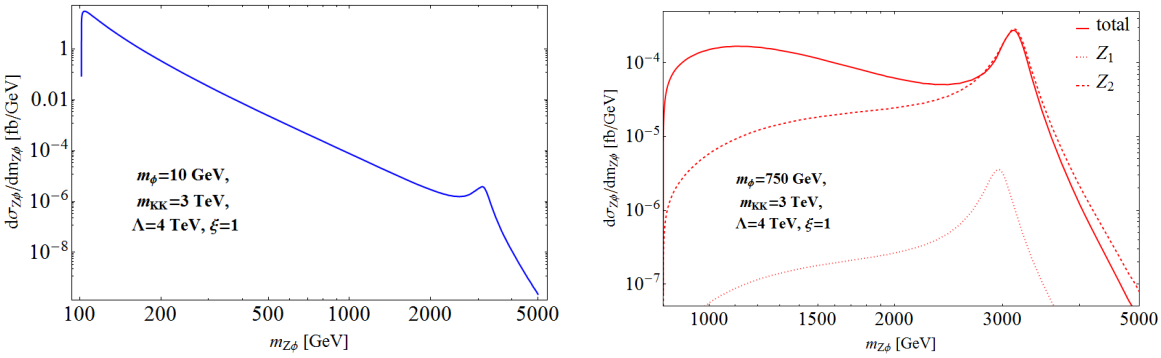

Figure 7.3 – $Z\phi$ invariant mass distribution at LHC (in fb/GeV) for (left) $m_\phi = 10$ GeV and (right) $m_\phi = 750$ GeV. The other parameters are fixed as follows: $m_{KK} = 3$ TeV, $\Lambda = 4$ TeV, and $\xi = 1$. On the right plot, we also display the individual contributions from the two KK boson eigenstates, Z_1 and Z_2.

case [138]) and $g_R = 2g_L$ ($g_R \neq g_L$ is possible in different custodial symmetry implementations). Since one expects that changing g_R would affect mostly the KK Z bosons (not through small mixing effects, as is the case of Z_0), Z_1 and Z_2, we have considered $m_\phi = 800$ GeV, such that the heavy KK resonances have a sizeable contribution to the $Z\phi$ production. Furthermore, we have taken $m_{KK} = 3$ TeV and the other parameters as specified above the plot in Fig. 7.2. The $Z\phi$ production cross sections for the two values of g_R are of the same order of magnitude: while for $g_R = g_L$ we find ~ 0.5 fb, for $g_R = 2g_L$ the cross section value is ~ 0.15 fb. The difference comes mostly from the $Z_i Z_0 \phi$ ($i = 1, 2$) couplings, which are approximately two times stronger in the first case compared to the second case. The impact of the g_R variation on the cross section is independent of the ξ and Λ parameters.

In Fig. 7.4, we present the total $Z\phi$ production cross section at the LHC as a function of ξ and m_ϕ, for two values of the radion VEV, $\Lambda = 3, 4$ TeV, with m_{KK} fixed at 3 TeV in both cases. We observe that for $m_\phi > m_h$ the cross section contours have roughly the same behaviours as the g_ϕ ones (see Fig. 7.1). Indeed, the dimensionless g_ϕ coupling corresponds to a good approximation to the radion coupling to two Z bosons, as described in the comments of Fig. 7.1. This is no longer true for $m_\phi < m_h$: in this region, as explained in the previous paragraphs, the cross section typically increases as m_ϕ decreases, this being a result of the behaviour of PDFs, which increase at lower values of $\tau = \hat{s}/s$. However, even for $m_\phi < m_h$, the lowest $Z\phi$ production cross sections are achieved in the vicinity of the $g_\phi = 0$ contour.

Higgs Production

In Fig. 7.5, we show the Zh invariant mass distribution, focusing on the region close to the resonant peak produced by the almost degenerate Z_1 and Z_2 states (the peak, as in the case of $Z\phi$ production, originates mostly from Z_2). We have chosen the following realistic parameters: $m_\phi = 750$ GeV, $\Lambda = 4$ TeV, $\xi = 0$ and a mass of $m_{KK} = 3$ TeV. The Zh channel is a favoured discovery avenue for Z_2, as the largest branching ratio of Z_2 is into Zh (meanwhile, Z_1 has its highest branching ratio for the WW decay). The observability potential for the KK resonance is discussed in Section 7.4.1.

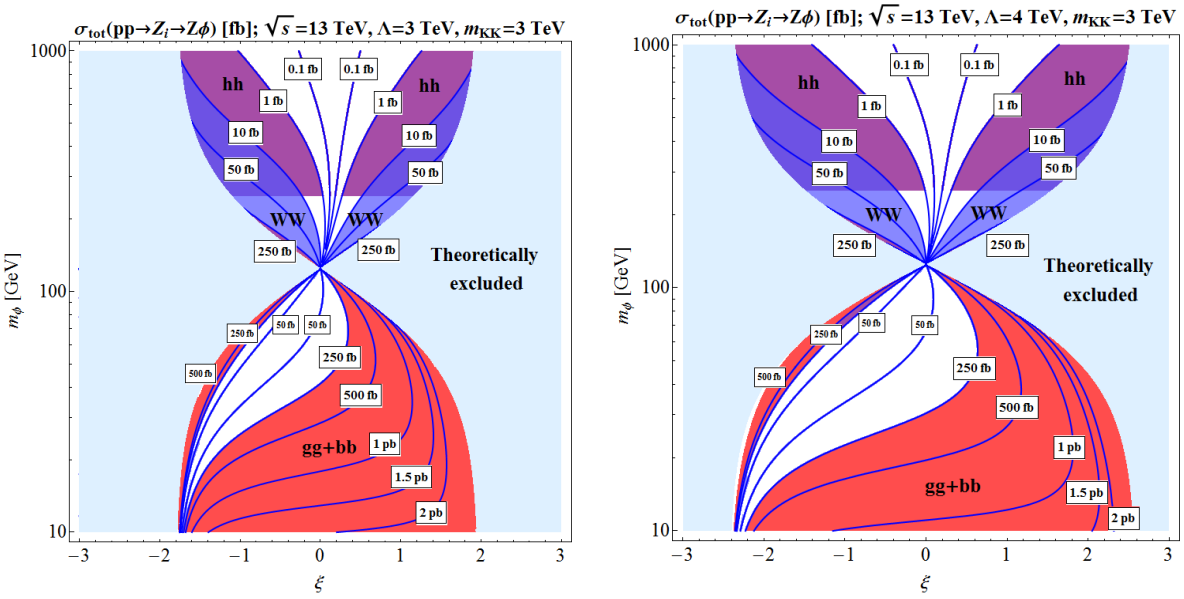

Figure 7.4 – Iso-contours of $Z\phi$ production cross section (in fb and pb) at the LHC with $\sqrt{s} = 13$ TeV, as a function of ξ and m_ϕ (in GeV), for (left) $\Lambda = 3$ TeV and (right) $\Lambda = 4$ TeV with $m_{KK} = 3$ TeV. The light blue regions are excluded by the theoretical constraint from eq. (7.16), while the purple, red, and blue zones approximately indicate parameter space regions that will be probed with 300 fb^{-1} at the LHC via radion decays into hh, dijets ($gg + bb$), and WW final states, respectively.

7.3.2 At the ILC

We now focus our attention on the $Z\phi$ production at a linear electron-positron collider, taking as an example the International Linear Collider (ILC). For an e^+e^- collider, the problem is simpler, as the center-of-mass energy is a known quantity and one does not need to convolute the cross section with PDFs.

Another simplifying aspect is the fact that, for ILC center-of-mass energies, which in principle could go up to 1 TeV, the s-channel exchange of the KK partners of the Z boson is negligible. Indeed as EWPT require that m_{KK} is larger than $\sim 2-3$ TeV, the two heavy resonances, Z_1 and Z_2, are significantly off-shell even at $\sqrt{s} = 1$ TeV, which renders their contribution negligible. Therefore, effectively, only the Z boson exchange in the s-channel has to be considered for the $Z\phi$ production, as we have numerically checked. Concerning the KK Z mixing effect on the ϕZZ coupling, for a given $Z\phi$ production cross section, varying m_{KK} translates to at most a percent-level shifting of ξ for a fixed m_ϕ.

We plot in Fig. 7.6 the $Z\phi$ production cross section in fb at the ILC, for e^+e^- center-of-mass energies of 250 and 500 GeV. We have chosen $\Lambda = 5$ TeV and, to ease the calculations, $m_{KK} \to \infty$ (see previous paragraph). As described in Section 7.3.1, the $e^+e^- \to Z\phi$ production cross section at the ILC has typically the same dependence on the two parameters ξ and m_ϕ as the g_ϕ coupling itself, whose values are illustrated on Fig. 7.1 (as a matter of fact, to a very good approximation, the aforementioned cross section is proportional to g_ϕ^2). This explains the relative similarity of iso-contour behaviours between Fig. 7.6 and Fig. 7.1 (upper left).

Note that, similarly to the SM Zh production, the $Z\phi$ cross section, for a given radion mass, is proportional to $1/s$. [11] Consequently, in order to present the regions with maximal

[11] Deviations from this behaviour are proportional to g_ϕ^r, and in turn subdominant for most of the parameter

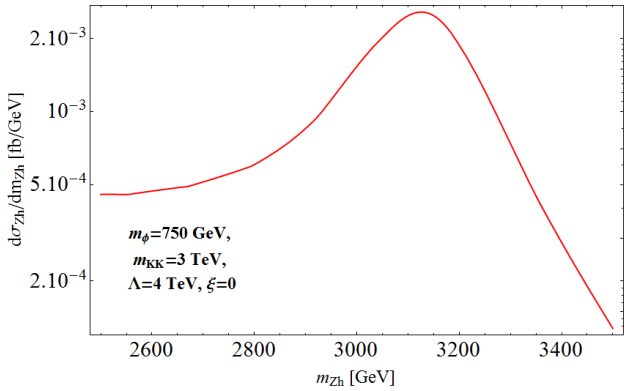

Figure 7.5 – Zh invariant mass distribution (in fb/GeV) in the neighbourhood of the KK Z resonance peak, for $m_\phi = 750$ GeV. The values of the other relevant parameters are: $m_{KK} = 3$ TeV, $\Lambda = 4$ TeV, and $\xi = 0$.

rates, we show in Fig. 7.6 only small radion masses, $m_\phi < m_h$ for $\sqrt{s} = 250$ GeV, while, for $\sqrt{s} = 0.5$ TeV, we show only moderate to high radion masses, $m_\phi > m_h$.

7.4 Radion, Higgs and KK Mode Detection

7.4.1 At the LHC

Radion Decay to $b\bar{b}$

For the full reaction $pp \to Z\phi$ followed by the radion decay into a bottom quark pair, $\phi \to b\bar{b}$ (possibly including the decay channel into two gluons), the SM background comes from double gluon radiation in the process $q\bar{q} \to Z$+2jets which has been well studied at LHC [339]. At a 13 TeV LHC energy, the full rate for the Z boson production followed by a muonic decay is $\sigma(pp \to Z)B(Z \to \mu^+\mu^-) \simeq 1900$ pb.

A drastic reduction of this background is therefore needed: it can come from a cut on the transverse momentum of the reconstructed Z, $p_T(\mu\mu) > 100$ GeV (see the $p_T(\mu\mu)$ distribution in Ref. [339]). Such a cut would also induce a penalty on the $Z\phi$ production rate approximately equivalent to imposing a cut on the $Z\phi$ invariant mass distribution, $m_{Z\phi} > 200$ GeV, which would lead to a drastic reduction factor of 1/40 for example for the distribution of Fig. 7.3 (left plot), obtained for a radion mass $m_\phi = 10$ GeV. For heavier radions, $m_\phi \gtrsim 100$ GeV, the effect of this optimal cut, $p_T(\mu\mu) > 100$ GeV, is not significant since the $Z\phi$ invariant mass distribution is defined on the range, $m_{Z\phi} > m_Z + m_\phi$. A softer cut, $p_T(\mu\mu) > 30$ GeV, would not alter significantly the signal, even for $m_\phi = 10$ GeV, and the background would be affected by a still efficient rejection factor of ~ 20.

Let us now present guidelines on the main techniques to detect the $Z\phi$ production, depending on the radion mass.

- $m_\phi \gtrsim 20$ GeV. When $m_\phi \gtrsim 20$ GeV, it is justified to request two jets which further decreases by an order of magnitude the background (see Ref. [340] for an ATLAS analysis and Ref. [341] for a CMS one). Then a mass selection should gain a similar factor which brings us to a rate of ~ 1000 fb for the background. A bottom quark selection should gain an additional factor of $10 - 100$ [342]. Therefore, assuming a future integrated luminosity of 300 fb^{-1} at the LHC, with a 20% reconstruction efficiency on the signal and background,

space.

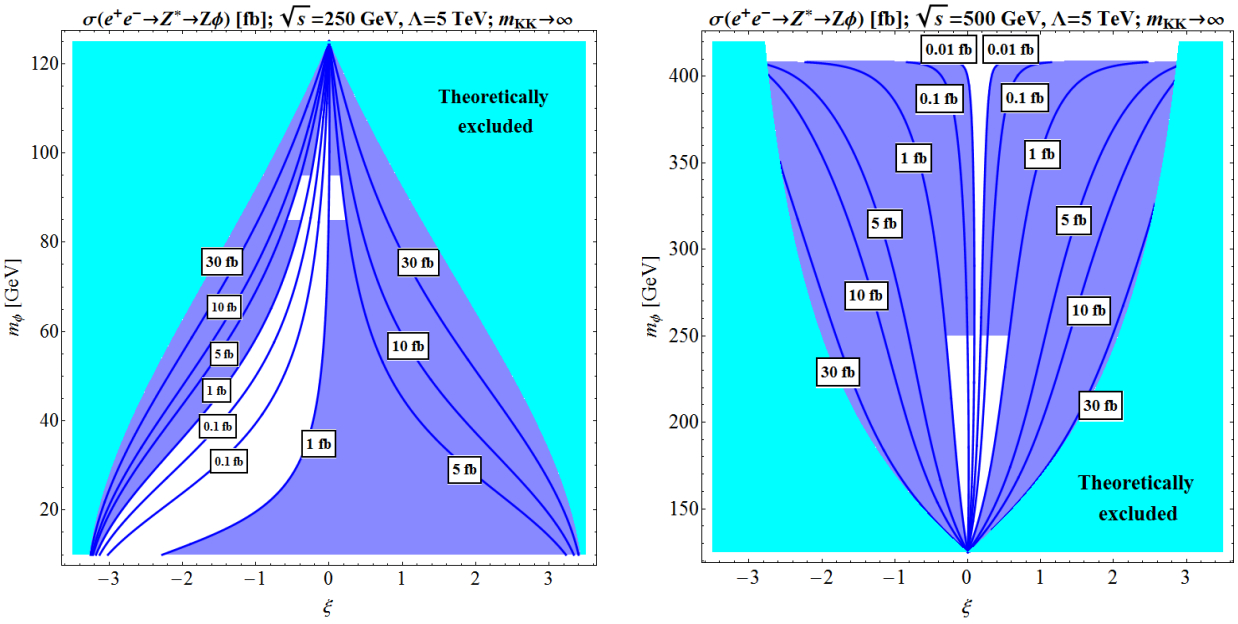

Figure 7.6 – Iso-contours of the $Z\phi$ production cross section (in fb) at the ILC with (left) $\sqrt{s} = 250$ GeV or (right) $\sqrt{s} = 500$ GeV, in terms of ξ and m_ϕ (in GeV), for $\Lambda = 5$ TeV and $m_{KK} \to \infty$. The cyan regions are excluded by the theoretical constraint from eq. (7.16), while the blue zones indicate the parameter space regions estimated to be probed at the ILC through the Z boson recoil mass technique.

gives a 250 fb sensitivity limit at 2σ on the cross section $\sigma_{tot}(Z\phi)$, for a branching fraction $B(\phi \to b\bar{b}) + B(\phi \to gg) \simeq 1$. This corresponds to selecting experimentally two inclusive jets (including two gluons or two b's). This LHC potential reach is illustrated on Fig. 7.4. On the obtained domains of the parameter space to which the LHC is potentially sensitive, one has indeed $B(\phi \to b\bar{b}) + B(\phi \to gg) \simeq 1$, assuming standard radion branching ratios without unknown physics entering the radion-gluon-gluon triangular loop. With b-tagging, the background should improve by about a factor 2 to 10 (corresponding to a factor up to $\sqrt{10}$ in the limit), depending on the tagging purity and efficiency, due to the further background reduction.

- $m_\phi > 100$ GeV. At higher masses, say $m_\phi > 100$ GeV, the $p_T(\mu\mu)$ selection cut can be increased up to 100 GeV without damaging the signal acceptance. Besides, for these masses, the mass resolution increases and therefore the sensitivity limit on $\sigma_{tot}(Z\phi)$ should reach about 100 fb. This LHC potential reach covers higher mass regions in Fig. 7.4.

Radion Decay to W^+W^-

- $m_\phi > 160$ GeV. In the regime $m_\phi > 160$ GeV, one benefits from the kinematical opening of the WW channel: $pp \to Z\phi$, $\phi \to W^+W^-$ [12]. The radion branching ratio into ZZ is smaller. The associated SM background composed of the WWZ production has a cross section of ~ 200 fb at 14 TeV including NLO QCD corrections [343]. Assuming an integrated luminosity of 300 fb^{-1} at the LHC and selecting semi-leptonic decays for the WW system for a reconstruction efficiency of 20% (not including leptonic branching ratios), one expects 170 events for this SM background. The radion mass selection then selects 20 events

[12] One could as well benefit from a cut on the transverse momentum of the reconstructed Z based on such a $p_T(\mu\mu)$ distribution for the associated WWZ background.

corresponding to a ~ 20 fb sensitivity limit on the $\sigma_{tot}(Z\phi)$ cross section, for a relevant branching $B(\phi \to W^+W^-) \simeq 0.5$; the associated sensitive region, for $m_\phi > 160$ GeV. This sensitivity order of magnitude is indicated on Fig. 7.4.

Radion Decay to hh

- $m_\phi > 250$ GeV. Finally, for $m_\phi > 250$ GeV, the LHC can become sensitive to the channel $pp \to Z\phi$, $\phi \to hh$. The Zhh production background opens up with a cross section of 0.25 fb [344]. Assuming a 20% reconstruction efficiency, including b-tagging, would give a 0.5 event background. So 3 events from the $Z\phi$ signal would be sufficient for a 2σ detection. Hence one obtains a ~ 5 fb cross section sensitivity limit for $\sigma_{tot}(Z\phi)$, with a realistic branching $B(\phi \to hh) \simeq 0.3$; the corresponding domain, for $m_\phi > 250$ GeV. The order of magnitude of this sensitivity is indicated on Fig. 7.4 as well.

This domain and the above sensitivity regions are clearly coarse estimates and a full analysis would be needed. Those regions however show that the $Z\phi$ search at LHC could be complementary, in testing some specific regions of the $\{\xi, m_\phi\}$ plane, to the search for the gluon-gluon fusion radion production, in case this loop-induced process is not affected by some unknown physics underlying the SM. We mention that the gluon fusion production of the radion allows to cover large domains of the RS parameter space, as shown in the figures of Ref. [326] (regions below $m_\phi = 80$ GeV were not studied there).

KK Resonances

The $Z\phi$ production can exhibit degenerate KK mode resonances made of Z boson excitations as described in Section 7.3.1. These resonances show up in the bump of Fig. 7.3. In order to discuss the possibility of a KK resonance observation in the radion production, we now consider some optimised but realistic parameter values, $\Lambda = 3$ TeV, $\xi = 1.5$, and $m_\phi = 500$ GeV (see the upper left plot of Fig. 7.1). Then the integrated rate of such a resonant process, obtained by considering an interval $m_{Z_2} \pm 2\,\Gamma_{Z_2}$ on Fig. 7.3, is of ~ 10 fb (~ 1 fb) for $m_{KK} = 2$ TeV (3 TeV). For a (HL-)LHC luminosity of 300(0) fb^{-1}, the induced number of events might lead to a possible but challenging observation. The kinematic selection of the interval around m_{KK} in the $Z\phi$ invariant mass distribution would reduce the associated SM background. The $p_T(\mu\mu)$ selection cut keeps a good efficiency if the production of $Z\phi$ is dominated by the exchange of a KK Z resonance. For $m_{KK} \simeq 2$ TeV and a radion mass below ~ 120 GeV, a simple kinematical study shows that a cut $p_T(\mu\mu) \gtrsim 1$ TeV would select the signal peaked in this area while eliminating significantly the QCD background. A complete Monte Carlo simulation of the signal and background would be needed to conclude on the observability of such a resonance.

This $p_T(\mu\mu)$ selection method is generic and can even be applied for the various processes of the type $q\bar{q} \to Y \to XZ$ where Y is a heavy vector boson which can be produced on-shell and X is a lighter resonance, either SM-like (W, Z, h) or exotic, as is the case for the radion. An additional advantage of this process is that it provides a combination of two resonances allowing a double discrimination. In this respect, the LHC could be competitive with ILC where the production of an on-shell Y resonance is only possible for a mass $m_Y < 1$ TeV.

Similarly, the Zh production can occur through KK Z boson resonances as shown in Fig. 7.5. For the optimised parameter values, $\Lambda = 4$ TeV, $\xi = 1$, $m_\phi = 500$ GeV (see the upper right plot of Fig. 7.1), and an optimistic low mass $m_{KK} \simeq 2$ TeV, the obtained integrated rate is of ~ 11.5 fb. Similar remarks as for the $Z\phi$ production hold regarding the KK resonance observability.

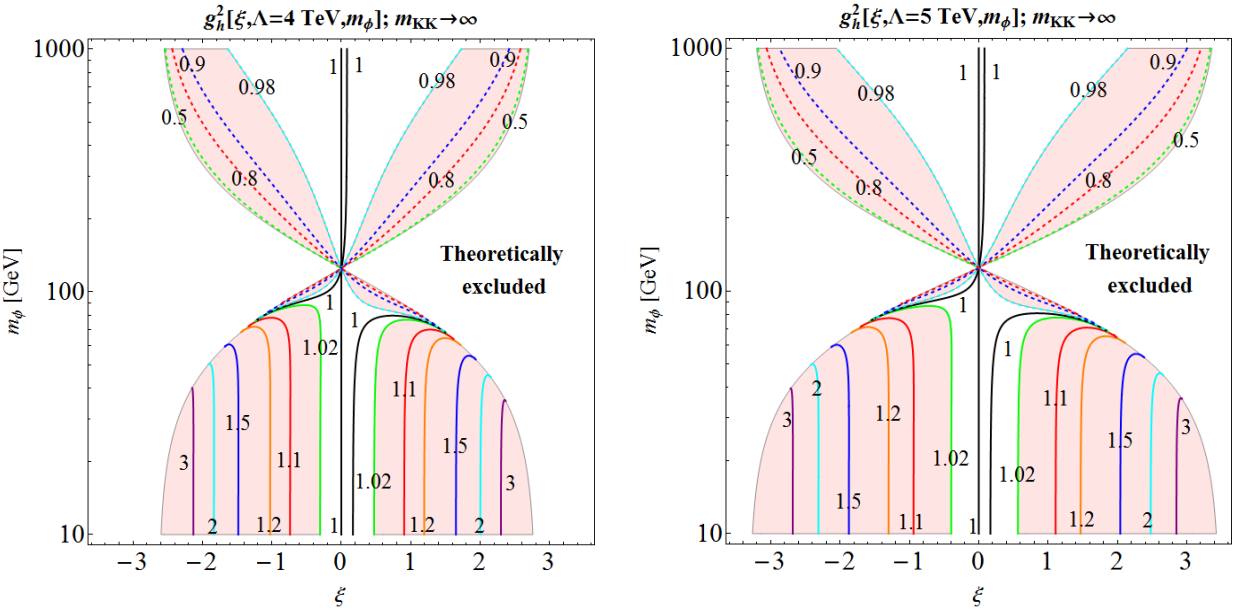

Figure 7.7 – Iso-contours of g_h^2 in the $\{\xi, m_\phi\}$ plane, for (left) $\Lambda = 4$ TeV and (right) $\Lambda = 5$ TeV, with m_{KK} taken to infinity. The coloured region indicates the future indirect sensitivity of the ILC on the Higgs-radion parameter space, corresponding to a $\sim 2\%$ accuracy (at 2σ) on the measurement of the squared hZZ coupling, i.e. $0.98 < g_h^2 < 1.02$.

Higgs Production

The Higgs coupling to two Z bosons has been measured at the LHC, via the Higgs production in association with a Z boson. Assuming decoupling KK modes (which do not affect significantly the $Z\phi$ production), the Higgs couplings are modified only by the Higgs-radion mixing. Taking this into account, the experimental values for the hZZ coupling exclude some domains of the $\{\xi, m_\phi\}$ plane. However, as we shall see later on in Section 7.4.2, these domains are not significant when compared to the ILC sensitivity.

A first LHC analysis combines the run 1 measurements (ATLAS and CMS) [53], with global fits reporting a central value of ~ 1 (i.e. SM value) and a $\sim 10\%$ error at 1σ on g_h (defined in eq. (7.17) [13] and denoted by κ_Z in Ref. [53]), assuming that the Higgs decays only into SM states. Therefore, in our case, this constraint is relevant only for $m_\phi > m_h/2$. Moreover, it allows for $0.6 < g_h^2 < 1.4$ at 2σ, which covers a tiny region in the g_h^2 plot from Fig. 7.7.

Ref. [53] also presents global fits allowing for Higgs boson decays to non-SM states, but with the extra assumption that $g_h < 1$ (or $\kappa_Z < 1$ in their notation), which is not justified in our framework. Their result indicates that, at two sigma, $0.6 < g_h^2 < 1$, which means that, once again, only a tiny region from Fig. 7.7 is covered.

Even though, regarding the hZZ coupling measurement, the LHC is much less competitive than the ILC, these exclusions can still be seen as a new interpretation of the constraints on the RS model from the LHC Higgs data, in the presence of a Higgs-radion mixing (see also Ref. [345]). Higgs physics appears naturally as complementary to the radion sector in testing their common $\{\xi, m_\phi\}$ parameter space.

[13] In the $m_{KK} \to \infty$ limit employed here (where $C_0^{4D} \to 1$), g_h represents indeed the hZZ coupling normalised to its SM value, since the second term in eq. (7.18) is vanishing in this limit and the third one is more than 2 orders of magnitude smaller.

7.4.2 At the ILC

Radion Production

For the associated $Z\phi$ production at ILC, one can use the same missing mass technique as for the Zh production [346] which is independent of the radion branching ratio values. This powerful method is only feasible using the large luminosity provided by this machine which plans to collect 2000 fb^{-1} at 250 GeV (H-20 scenario [347]), 4000 fb^{-1} at 500 GeV and 8000 fb^{-1} at 1 TeV. This is to be compared to the LEP collider which could only collect a few fb^{-1} per experiment so that LEP was not able to significantly exclude the presence of a radion at any mass. This recoil mass technique works best near the $Z\phi$ threshold where the center-of-mass energy is about $m_\phi + m_Z$. One then achieves the most precise recoil mass reconstruction. For this reason the low mass domain, $m_\phi \lesssim 160$ GeV, will be covered by running at a center-of-mass energy of 250 GeV.

- $m_\phi < m_Z$. When $m_\phi < m_Z$, one has an easy situation. The Z background from ZZ^*/γ^* is distributed as a Breit Wigner with a small tail at low masses due to the virtual photon contribution from $Z\gamma^*$. The sensitivity reaches a limit on the $\sigma(Z\phi)$ of ~ 1 fb at the 2σ statistical level. When the $b\bar{b}$ decay mode is considered, this sensitivity limit goes even down to 0.02 fb.
- $m_\phi \sim m_Z$. For $m_\phi \sim m_Z$, the ZZ background is the largest but still giving a sensitivity limit on $\sigma(Z\phi)$ of ~ 3 fb at 2σ.
- $m_\phi > m_Z$. If $m_\phi > m_Z$, one ends up with a similar situation as for Zh: the main background comes from ZZ+ISR, where ISR stands for initial state radiation (i.e. a photon radiated off e^+/e^-) which, in most cases, remains undetected. The missing mass however includes both the Z and this photon, creating what one calls a radiative tail (for $m_\phi \sim m_Z$, the mass reconstruction of the Z into hadrons is too imprecise to allow a separation of m_ϕ from m_Z). From Ref. [346], one can easily evaluate the $\sigma(Z\phi)$ sensitivity in this mass region, which is at the 1 fb level. The Zh channel itself creates a background which generates a small blind zone for $m_\phi \simeq m_h$ but in this case the Higgs properties can also be altered, thus allowing one to feel the presence of the radion.
- $m_\phi > 130$ GeV. At $m_\phi > 130$ GeV, it becomes possible to eliminate the radiative tail effect by reconstructing the radion mass through its decays into two jets. The $\sigma(Z\phi)$ sensitivity improves to 0.5 fb.
- $m_\phi > 150$ GeV. When $m_\phi > 150$ GeV, one starts crossing the kinematical limit for the $Z\phi$ production and it becomes necessary to use data taken at a 500 GeV center-of-mass energy. The recoil mass precision is poor since one operates far above the $Z\phi$ threshold, but the good energy resolution on jets ($\sigma E_j/E_j \sim 3\%$) allows to use direct mass reconstruction with a mass resolution on the radion at the 2% level. One can then include the leptonic and neutrino decay modes from Z, gaining a factor ~ 10 in efficiency. Since one is no more suffering from the ISR effect this method turns out to give a sensitivity for $\sigma(Z\phi)$ at the 0.1 fb level.
- $m_\phi > 160$ GeV. For $m_\phi > 160$ GeV, the situation changes radically since the WW, ZZ channels become accessible for the radion decay, which helps the recoil techniques. For the SM background, the Ref. [348] on WWZ cross sections shows that the WWZ contribution can be reduced down to 10 fb by using right-handed polarization (e_R) for the electron beam. The SM ZZZ background is at the 1 fb level. For ZWW one can simply use the $Z \to \mu\mu$ tagging. The WW component can be identified through semi-leptonic decays where a W decays hadronically and the other leptonically. Taking into account the branching ratios, one expects 350 background events. At the counting level one reaches a 1 fb sensitivity on $\sigma(Z\phi)$. One can then select the ϕ mass allowing an increased sensitivity of about 0.3 fb.

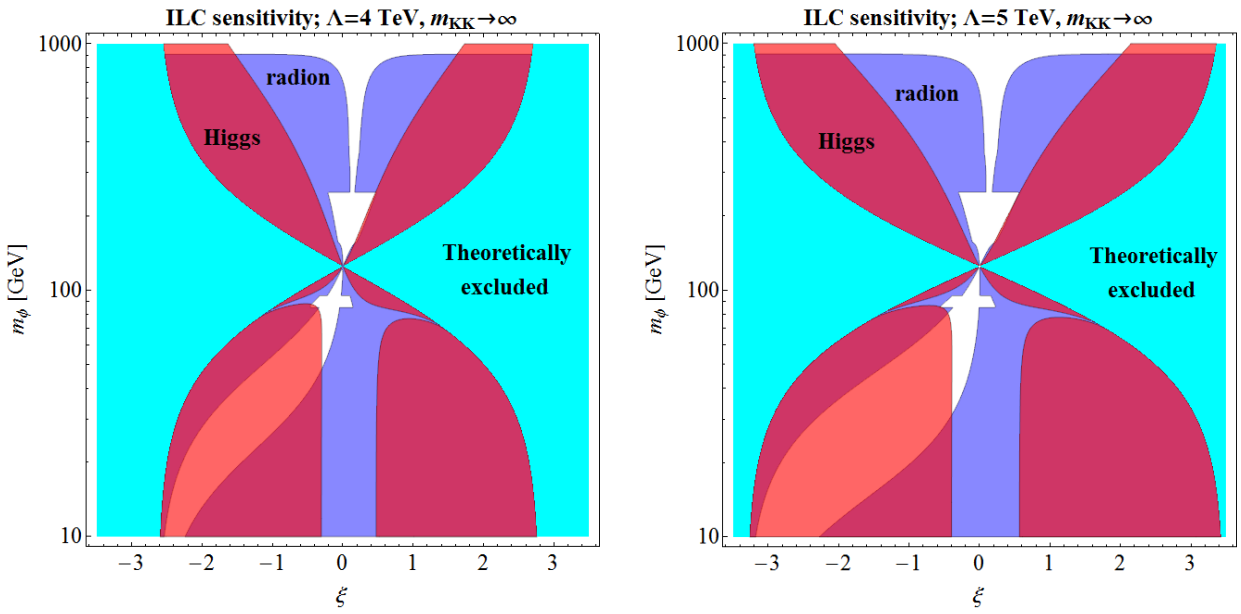

Figure 7.8 – Summary plots for direct and indirect radion searches at the three stages of operation of the ILC ($\sqrt{s}$ = 250 GeV, 500 GeV, and 1 TeV), in the $\{\xi, m_\phi\}$ plane, for (left) $\Lambda = 4$ TeV and (right) $\Lambda = 5$ TeV, with m_{KK} taken to be infinite. The blue region covers the Higgs-radion parameter space estimated to be probed by the ILC through direct radion searches, while the red region represents the domain potentially probed by the precise measurement of the hZZ coupling. The theoretical constraint is superimposed once more, as the cyan domain.

- $m_\phi > 250$ GeV. For $m_\phi > 250$ GeV, the hh channel becomes accessible for the radion decay. The Zhh SM background [349] is even smaller and with strong signatures given by the Higgs decay into $b\bar{b}$. Assuming a 50% efficiency with a relevant $B(\phi \to hh) \sim 0.3$ and low extra backgrounds (from ZZZ essentially), one could reach a sensitivity on $\sigma(Z\phi)$ at the 0.01 fb level. For the ILC option with a 1 TeV center-of-mass energy and an integrated luminosity of 8000 fb^{-1}, the factor 2 increase in luminosity (with respect to the 500 GeV scenario) induces a factor $\sqrt{2}$ of improvement in the cross section sensitivity (the Zhh background is only slightly smaller).

The various estimates given so far constitute a reasonable first guess of the ILC sensitivity for a radion search. All the obtained orders of magnitude for the sensitivities on $\sigma(Z\phi)$ given in the text are drawn as indicative coloured regions in Fig. 7.6. On Fig. 7.8, we summarize on a unique plot the covered regions issued from two possible ILC runs respectively at 250 GeV, 500 GeV and 1 TeV, for infinite m_{KK} (i.e. decoupled KK resonances) and two values of the radion VEV, $\Lambda = 4, 5$ TeV. A dedicated analysis would be needed to fully assess such performances but it is clear that ILC can dig into the radion scenario with excellent sensitivity.

We notice that the region corresponding to $\xi = 0$ and $m_\phi \simeq 60 - 110$ GeV, left uncovered on Fig. 7.8, might be tested via the search for the reaction $gg \to \phi \to \gamma\gamma$ at the HL-LHC extension with an integrated luminosity of 3000 fb^{-1}: this is the conclusion of Ref. [350] in the case of SM fields localised on the TeV-brane.

Besides, as for the SM Higgs case, the vector boson fusion mechanism could provide additional information on the radion, in particular allowing the determination of the total width and in turn of absolute widths [349].

Higgs Production

The Higgs coupling to two Z bosons would possibly be measured at the 0.51% (1.3%) 1σ error level at the ILC with an energy option of 1 TeV (250 GeV), for a luminosity of 2500 fb^{-1} (250 fb^{-1}) [351], via the Higgs production in association with a Z boson. Such measurements would exclude at 2σ the regions of the $\{\xi, m_\phi\}$ plane, as illustrated in Fig. 7.7, assuming a central value equal to the predicted SM hZZ coupling constant. Notice that this measurement is independent of the Higgs branching ratio values due to the recoil technique used to tag the associated Z boson. The future precision Higgs physics at ILC would thus be extremely efficient in testing the $\{\xi, m_\phi\}$ parameter space, as illustrated in Fig. 7.7. The obtained exclusion regions are superimposed as well on the summary plot of Fig. 7.8, showing the whole parameter space than can be covered using both the $Z\phi$ and Zh production at ILC.

7.5 Discussion

Let us finish this chapter on radion production by a short discussion, now that the numerical results have been studied in detail with respect to the possibilities of observation. The investigation of the reaction $q\bar{q} \to Z\phi$ at LHC could allow to cover significant parts of the RS parameter space. This reaction could even benefit from the resonance of degenerate neutral KK vector bosons, which would enhance the reaction rate and allow for tight selections against the QCD background. It will take the ILC program at high luminosity, though, to cover most of the theoretically allowed parameter space, via the $e^+e^- \to Z\phi$ process. The ILC, by investigating this process, is indeed complementary to the LHC for testing the low radion masses (below the Higgs mass), while the reaction $gg \to \phi \to \gamma\gamma$ is quite efficient in principle to probe the high mass regime. The ILC benefits also from the complementarity between the direct radion searches and the high accuracy measurements of the Higgs couplings, in the exploration of the RS parameter space (typically the $\{\xi, m_\phi\}$ plane).

Chapter 8

Summary and Outlook

The idea of extra spatial dimensions, either flat or warped, has proven to be a very fruitful ground for both theoretical and phenomenological studies. While motivated mainly by the gauge hierarchy problem, this paradigm can nonetheless provide solutions to a wide range of problems of the Standard Model. The most prominent examples in this direction are the Dark Matter abundance in the Universe, the flavour hierarchy, neutrino masses, and Grand Unification. Furthermore, such extra-dimensional scenarios have a valid theoretical motivation, since they can be embedded into (Super)String Theory, which is, up to date, one of the few candidates for a fundamental theory of Nature.

In this thesis, we adopted two approaches towards the phenomenological study of these models. In a first part, we focused on effective models inspired from extra-dimensional scenarios, considering minimal and non-minimal scalar sectors extended with Vector-Like Fermions (VLFs), whose existence is predicted in theories with extra dimensions. Firstly, we showed how Vector-Like Quarks (VLQs), through SM quark - VLQ mixing, can simultaneously explain two anomalies related to the third generation of SM quarks: the b-quark forward-backward asymmetry, $A_{\rm FB}^b$, measured at LEP, and the excess in the $t\bar{t}h$ production cross section, observed in the LHC 8 TeV data. Moreover, we estimated the indirect reach of the HL-LHC in probing VLQs. For our estimation, we considered two so-called Higgs decay ratios, $D_{\gamma\gamma}$ and D_{bb}, and reached the conclusion that VLQs in the 5-10 TeV range can be indirectly probed through either their contribution to the $h\gamma\gamma$ loop-induced coupling ($D_{\gamma\gamma}$), or through their mixing with the SM b-quark (D_{bb}). Moreover, a precise measurement of the $D_{\gamma\gamma}$ decay ratio would be essential for the future of particle physics: with a projected 1% accuracy in the measurement of the hZZ coupling at the LHC, one would thus have a precise experimental handle on the loop-induced $h\gamma\gamma$ coupling.

Afterwards, we provided an interpretation for the 750 GeV resonance, which appeared in the first batch of data collected at the 13 TeV LHC, but was discarded as a statistical fluctuation with in the subsequent data. In our model, the bump was due to a superposition of two (almost) mass-degenerate particles, a CP-odd scalar A and a CP-even scalar H. Such new fields arise naturally in the Minimal Supersymmetric Standard Model (MSSM) or in Two Higgs Doublet Models (2HDMs). However, as we showed, the particle content of these two theories was not enough to explain the abnormally high diphoton decay rate of the "resonance". Therefore, we added several families of charged Vector-Like Leptons (VLLs), with the purpose of enhancing the diphoton branching ratios of the two heavy scalars, A and H.

Focusing on a similar 2HDM plus VLL scenario, we then proposed a plausible Dark Matter (DM) candidate in the guise of a mostly SM-singlet vector-like neutrino. While in the case of a minimal Higgs sector as in the SM, the DM particle has to be heavier than ~ 2 TeV,

we showed that extending the SM scalar sector with an extra doublet can lower the DM mass till $m_{DM} \sim 200$ GeV. Such a dramatic lowering of the bound on the DM mass came essentially from two mechanisms which improved the annihilation rate of the DM: resonant annihilation mediated by the heavy neutral scalars from a 2HDM, and annihilation into final states involving at least one non-SM scalar, typically the charged scalar $H^{\pm}$. At the same time, the DM-nucleon scattering cross section was kept under control, allowing our model to pass the stringent constraints coming from DM direct detection from LUX. Moreover, we showed that our model shall be tested at future DM direct detection experiments such as Xenon1T and LZ, the upgraded version of LUX.

In a second part of this thesis, we considered a more concrete extra-dimensional scenario, namely the custodially protected version of the warped ED model of Randall and Sundrum. In the context of this model, we first interpreted the 2 TeV diboson excess(es) in the WW, WZ, and Wh final states, observed in the 8 TeV data at LHC, as a first signal of the KK excitations of the neutral (and charged, depending on the final state) gauge bosons predicted by the enlarged bulk gauge group. Unfortunately, as the diphoton excess, this would-be resonance was not confirmed in subsequent data.

Finally, in the last chapter of this thesis, we studied in detail the scalar sector of the custodial RS model, which is comprised of the SM-like Higgs and a new scalar, dubbed the radion (denoted as ϕ), which arises as a fluctuation of the length of the extra dimension. More precisely, we focused on the process of radion production in association with a Z boson at the LHC and at the ILC, taking into account also the effects of the KK partners of the Z boson. We argued that, even if this production channel can test the mixed Higgs-radion hypothesis quite well at the LHC, it is the ILC (or another future linear collider) who will be able to dig deep into this scenario, especially in the case of a light radion. Moreover, we showed that the precise measurement of the hZZ coupling ($\sim 1\%$) at the ILC would also provide important (indirect) constraints on the mixed Higgs-radion parameter space. We also noticed an interesting complementarity between the direct ($Z\phi$ production) and indirect (hZZ coupling) searches for a radion at the ILC: indeed, at low radion masses, a region of the h–ϕ parameter space to which the $Z\phi$ production is blind can be excellently covered by the precise measurement of the hZZ coupling.

All in all, the past three years, during which the content of this thesis was written, have proved both exciting and agonizing for particle physics. The few anomalies/excesses that showed up in the LHC data at various stages lead us to the study of various interesting and testable scenarios, such as the ones in chapters 3, 4, and 6 of this thesis. Clearly, those were the exciting times. The agonizing times came afterwards, first while waiting for more LHC data, and then, even more, when the new data arrived and the excesses were not confirmed. Thus, it might seem that, at present times, the high-energy community has lost some of its hope of discovering new physics (however, the current Lepton Flavour Universality Violation hints reported in LHCb data have caused a new stir in the community).

In any case, the future has many important new information to bring. To start with, the High-Luminosity LHC will measure the Higgs signal strengths to an impressive accuracy of order 5%, which will bring us closer to knowing if and where the long-sought New Physics lives. Furthermore, various theoretical groups are now working to reduce the theoretical uncertainty on Higgs production and decay rates by trying to reach higher orders in the QCD (and electroweak) perturbative calculations (and trying to go beyong the large quark mass limits in the loop amplitudes). Moreover, the $D_{\gamma\gamma}$ ratio will be one of the most interesting Higgs-related observables, mainly because of the very high accuracy to which it will be measured (order 1%). As shown in chapter 3, $D_{\gamma\gamma}$ would allow the (indirect) probing of new

particles living in the multi-TeV range. Through this ratio, the HL-LHC will stride into the new era of Higgs precision physics.

Moreover, the value of the $D_{\gamma\gamma}$ ratio will become an invaluable piece of information when a lepton collider, such as the ILC, will be built. At a first stage of the ILC, the $\sqrt{s} = 250$ GeV electron-positron collisions will produce around 5×10^5 $h + Z$ pairs (assuming 2000 fb^{-1} of integrated luminosity) which, if analyzed through the so-called missing mass technique, would allow a 1% measurement of the hZZ coupling in a model-independent way. Thus, combining $D_{\gamma\gamma}$ and the precise measurement of the hZZ vertex would allow one to infer the absolute value of the $h\gamma\gamma$ loop-induced coupling independently of other Higgs couplings (to be contrasted with LHC, where only products of Higgs couplings are directly measured). Furthermore, at a later stage, the ILC can be used to perform indirect searches for new physics through precision top physics, by scanning the $t\bar{t}$ production threshold, similarly to how LEP scanned the W^+W^- threshold during its Run 2. For example, it was shown in Ref. [352] that top quark pair production at the ILC can probe new Kaluza-Klein states in the 10-20 TeV range, in the realistic case of matter propagating in the bulk.

Besides Higgs physics, the $\sqrt{s} = 250$ GeV ILC run will have an immense potential of discovering light scalar particles that couple to pairs of Z bosons. As for the case of the Higgs boson, the missing mass (or Z recoil mass) technique will allow the detection of such a scalar (if it exists) without even demanding a certain final state to which the new scalar should decay. In chapter 7, we provided an example of such a scalar, namely the radion, which is predicted in extra-dimensional scenarios. Moreover, a light scalar (e.g. a light radion) that mixes with the Higgs will be tested also indirectly by measuring the hZZ vertex, which is sensitive to scalar mixing effects. Interestingly, a light radion is an example of a new particle that might escape detection at the LHC but be discovered the ILC.

Gazing even further into the future, a 100 TeV machine, such as the FCC-hh hadron collider, would also have a huge potential for discovering or constraining new physics. New particles, with masses in the range of tens of TeVs, such as very heavy superpartners or KK partners, could be studied at such a collider, thus putting the idea of naturalness to a stringent test.

Finally, let us point out that new physics does not hide only in a particle collider tunnel below us: it also hides above us, in the skies, as Dark Matter remains, up to date, as elusive as its name suggests. Current Dark Matter direct detection experiments, such as LUX, can probe WIMP-nucleon scattering cross sections as low as 10^{-45} cm^2. In a particle physicist's language, this number is equal to the remarkably low value of 10^{-6} fb. These measurements tightly constrain WIMP scenarios, as we have seen in chapter 5. There are reasons for excitement, as this cross-section value will be pushed down by two orders of magnitude by next-generation direct-detection experiments, such as XENON1T and LZ. With this in mind, probably the best course of action for a high-energy physicist would be to keep one eye on the collider tunnel and the other one on the skies.

Bibliography

[1] ATLAS, G. Aad *et al.*, "Measurements of the Higgs boson production and decay rates and coupling strengths using pp collision data at $\sqrt{s} = 7$ and 8 TeV in the ATLAS experiment", *Eur. Phys. J.* **C76** (2016) no. 1, 6, arXiv:1507.04548 [hep-ex].

[2] CMS, V. Khachatryan *et al.*, "Precise determination of the mass of the Higgs boson and tests of compatibility of its couplings with the standard model predictions using proton collisions at 7 and 8 TeV", *Eur. Phys. J.* **C75** (2015) no. 5, 212, arXiv:1412.8662 [hep-ex].

[3] M. Baak, M. Goebel, J. Haller, A. Hoecker, D. Ludwig, K. Moenig, M. Schott, and J. Stelzer, "Updated Status of the Global Electroweak Fit and Constraints on New Physics", *Eur. Phys. J.* **C72** (2012) 2003, arXiv:1107.0975 [hep-ph].

[4] Fermi-LAT, MAGIC, M. L. Ahnen *et al.*, "Limits to dark matter annihilation cross-section from a combined analysis of MAGIC and Fermi-LAT observations of dwarf satellite galaxies", *JCAP* **1602** (2016) no. 02, 039, arXiv:1601.06590 [astro-ph.HE].

[5] Fermi-LAT, M. Ackermann *et al.*, "Searching for Dark Matter Annihilation from Milky Way Dwarf Spheroidal Galaxies with Six Years of Fermi Large Area Telescope Data", *Phys. Rev. Lett.* **115** (2015) no. 23, 231301, arXiv:1503.02641 [astro-ph.HE].

[6] ATLAS, G. Aad *et al.*, "Search for neutral Higgs bosons of the minimal supersymmetric standard model in pp collisions at $\sqrt{s} = 8$ TeV with the ATLAS detector", *JHEP* **11** (2014) 056, arXiv:1409.6064 [hep-ex].

[7] CMS, V. Khachatryan *et al.*, "Search for neutral MSSM Higgs bosons decaying to a pair of tau leptons in pp collisions", *JHEP* **10** (2014) 160, arXiv:1408.3316 [hep-ex].

[8] S. L. Glashow, "Partial Symmetries of Weak Interactions", *Nucl. Phys.* **22** (1961) 579–588.

[9] S. Weinberg, "A Model of Leptons", *Phys. Rev. Lett.* **19** (1967) 1264–1266.

[10] A. Salam and J. C. Ward, "Electromagnetic and weak interactions", *Phys. Lett.* **13** (1964) 168–171.

[11] F. Englert and R. Brout, "Broken Symmetry and the Mass of Gauge Vector Mesons", *Phys. Rev. Lett.* **13** (1964) 321–323.

[12] P. W. Higgs, "Broken Symmetries and the Masses of Gauge Bosons", *Phys. Rev. Lett.* **13** (1964) 508–509.

[13] G. S. Guralnik, C. R. Hagen, and T. W. B. Kibble, "Global Conservation Laws and Massless Particles", *Phys. Rev. Lett.* **13** (1964) 585–587.

[14] ATLAS, G. Aad *et al.*, "Observation of a new particle in the search for the Standard Model Higgs boson with the ATLAS detector at the LHC", *Phys. Lett.* **B716** (2012) 1–29, arXiv:1207.7214 [hep-ex].

[15] CMS, S. Chatrchyan *et al.*, "Observation of a new boson at a mass of 125 GeV with the CMS experiment at the LHC", *Phys. Lett.* **B716** (2012) 30–61, arXiv:1207.7235 [hep-ex].

[16] M. C. Gonzalez-Garcia and Y. Nir, "Neutrino masses and mixing: Evidence and implications", *Rev. Mod. Phys.* **75** (2003) 345–402, arXiv:hep-ph/0202058 [hep-ph].

[17] F. Zwicky, "Die Rotverschiebung von extragalaktischen Nebeln", *Helv. Phys. Acta* **6** (1933) 110–127. [Gen. Rel. Grav.41,207(2009)].

[18] F. Zwicky, "On the Masses of Nebulae and of Clusters of Nebulae", *Astrophys. J.* **86** (1937) 217–246.

[19] V. C. Rubin and W. K. Ford, Jr., "Rotation of the Andromeda Nebula from a Spectroscopic Survey of Emission Regions", *Astrophys. J.* **159** (1970) 379–403.

[20] V. C. Rubin, N. Thonnard, and W. K. Ford, Jr., "Rotational properties of 21 SC galaxies with a large range of luminosities and radii, from NGC 4605 /R = 4kpc/ to UGC 2885 /R = 122 kpc/", *Astrophys. J.* **238** (1980) 471.

[21] Planck, P. A. R. Ade *et al.*, "Planck 2015 results. XIII. Cosmological parameters", arXiv:1502.01589 [astro-ph.CO].

[22] P. W. Graham, D. E. Kaplan, and S. Rajendran, "Cosmological Relaxation of the Electroweak Scale", *Phys. Rev. Lett.* **115** (2015) no. 22, 221801, arXiv:1504.07551 [hep-ph].

[23] V. V. Khoze and M. Spannowsky, "Higgsplosion: Solving the Hierarchy Problem via rapid decays of heavy states into multiple Higgs bosons", arXiv:1704.03447 [hep-ph].

[24] P. Fayet and S. Ferrara, "Supersymmetry", *Phys. Rept.* **32** (1977) 249–334.

[25] L. Randall and R. Sundrum, "A Large mass hierarchy from a small extra dimension", *Phys. Rev. Lett.* **83** (1999) 3370–3373, arXiv:hep-ph/9905221 [hep-ph].

[26] T. Kaluza, "On the Problem of Unity in Physics", *Sitzungsber. Preuss. Akad. Wiss. Berlin (Math. Phys.)* **1921** (1921) 966–972.

[27] O. Klein, "Quantum Theory and Five-Dimensional Theory of Relativity. (In German and English)", *Z. Phys.* **37** (1926) 895–906. [Surveys High Energ. Phys.5,241(1986)].

[28] N. Arkani-Hamed, S. Dimopoulos, and G. R. Dvali, "The Hierarchy problem and new dimensions at a millimeter", *Phys. Lett.* **B429** (1998) 263–272, arXiv:hep-ph/9803315 [hep-ph].

[29] I. Antoniadis, N. Arkani-Hamed, S. Dimopoulos, and G. R. Dvali, "New dimensions at a millimeter to a Fermi and superstrings at a TeV", *Phys. Lett.* **B436** (1998) 257–263, arXiv:hep-ph/9804398 [hep-ph].

[30] N. Arkani-Hamed, S. Dimopoulos, and G. R. Dvali, "Phenomenology, astrophysics and cosmology of theories with submillimeter dimensions and TeV scale quantum gravity", *Phys. Rev.* **D59** (1999) 086004, arXiv:hep-ph/9807344 [hep-ph].

[31] N. Arkani-Hamed, S. Dimopoulos, and J. March-Russell, "Stabilization of submillimeter dimensions: The New guise of the hierarchy problem", *Phys. Rev.* **D63** (2001) 064020, arXiv:hep-th/9809124 [hep-th].

[32] T. Appelquist, H.-C. Cheng, and B. A. Dobrescu, "Bounds on universal extra dimensions", *Phys. Rev.* **D64** (2001) 035002, arXiv:hep-ph/0012100 [hep-ph].

[33] G. Servant and T. M. P. Tait, "Is the lightest Kaluza-Klein particle a viable dark matter candidate?", *Nucl. Phys.* **B650** (2003) 391–419, arXiv:hep-ph/0206071 [hep-ph].

[34] K. R. Dienes, E. Dudas, and T. Gherghetta, "Extra space-time dimensions and unification", *Phys. Lett.* **B436** (1998) 55–65, arXiv:hep-ph/9803466 [hep-ph].

[35] K. R. Dienes, E. Dudas, and T. Gherghetta, "Grand unification at intermediate mass scales through extra dimensions", *Nucl. Phys.* **B537** (1999) 47–108, arXiv:hep-ph/9806292 [hep-ph].

[36] E. A. Mirabelli and M. Schmaltz, "Yukawa hierarchies from split fermions in extra dimensions", *Phys. Rev.* **D61** (2000) 113011, arXiv:hep-ph/9912265 [hep-ph].

[37] K. R. Dienes, E. Dudas, and T. Gherghetta, "Neutrino oscillations without neutrino masses or heavy mass scales: A Higher dimensional seesaw mechanism", *Nucl. Phys.* **B557** (1999) 25, arXiv:hep-ph/9811428 [hep-ph].

[38] N. Arkani-Hamed, S. Dimopoulos, G. R. Dvali, and J. March-Russell, "Neutrino masses from large extra dimensions", *Phys. Rev.* **D65** (2001) 024032, arXiv:hep-ph/9811448 [hep-ph].

[39] E. Fermi, "Tentativo di una teoria dell'emissione dei raggi beta", *Ric. Sci.* **4** (1933) 491–495.

[40] L. Randall and R. Sundrum, "An Alternative to compactification", *Phys. Rev. Lett.* **83** (1999) 4690–4693, arXiv:hep-th/9906064 [hep-th].

[41] J. M. Maldacena, "The Large N limit of superconformal field theories and supergravity", *Int. J. Theor. Phys.* **38** (1999) 1113–1133, arXiv:hep-th/9711200 [hep-th]. [Adv. Theor. Math. Phys.2,231(1998)].

[42] T. Gherghetta and A. Pomarol, "Bulk fields and supersymmetry in a slice of AdS", *Nucl. Phys.* **B586** (2000) 141–162, arXiv:hep-ph/0003129 [hep-ph].

[43] Y. Grossman and M. Neubert, "Neutrino masses and mixings in nonfactorizable geometry", *Phys. Lett.* **B474** (2000) 361–371, arXiv:hep-ph/9912408 [hep-ph].

[44] A. Pomarol, "Grand unified theories without the desert", *Phys. Rev. Lett.* **85** (2000) 4004–4007, arXiv:hep-ph/0005293 [hep-ph].

[45] K. Agashe, A. Delgado, and R. Sundrum, "Grand unification in RS1", *Annals Phys.* **304** (2003) 145–164, arXiv:hep-ph/0212028 [hep-ph].

[46] K. Agashe, A. Falkowski, I. Low, and G. Servant, "KK Parity in Warped Extra Dimension", *JHEP* **04** (2008) 027, arXiv:0712.2455 [hep-ph].

[47] W. D. Goldberger and M. B. Wise, "Phenomenology of a stabilized modulus", *Phys. Lett.* **B475** (2000) 275–279, arXiv:hep-ph/9911457 [hep-ph].

[48] A. Djouadi and A. Lenz, "Sealing the fate of a fourth generation of fermions", *Phys. Lett.* **B715** (2012) 310–314, arXiv:1204.1252 [hep-ph].

[49] A. Denner, S. Dittmaier, A. Muck, G. Passarino, M. Spira, C. Sturm, S. Uccirati, and M. M. Weber, "Higgs Production and Decay with a Fourth Standard-Model-Like Fermion Generation", *Eur. Phys. J.* **C72** (2012) 1992, arXiv:1111.6395 [hep-ph].

[50] E. Kuflik, Y. Nir, and T. Volansky, "Implications of Higgs searches on the four generation standard model", *Phys. Rev. Lett.* **110** (2013) no. 9, 091801, arXiv:1204.1975 [hep-ph].

[51] S. L. Adler, "Axial vector vertex in spinor electrodynamics", *Phys. Rev.* **177** (1969) 2426–2438.

[52] J. S. Bell and R. Jackiw, "A PCAC puzzle: pi0 –> gamma gamma in the sigma model", *Nuovo Cim.* **A60** (1969) 47–61.

[53] The ATLAS and CMS Collaborations, "Measurements of the Higgs boson production and decay rates and constraints on its couplings from a combined ATLAS and CMS analysis of the LHC pp collision data at $\sqrt{s} = 7$ and 8 TeV",.

[54] K. Kumar, R. Vega-Morales, and F. Yu, "Effects from New Colored States and the Higgs Portal on Gluon Fusion and Higgs Decays", *Phys. Rev.* **D86** (2012) 113002, arXiv:1205.4244 [hep-ph]. [Erratum: Phys. Rev.D87,no.11,119903(2013)].

[55] D. Das, A. Kundu, and I. Saha, "Higgs data does not rule out a sequential fourth generation", arXiv:1707.03000 [hep-ph].

[56] ATLAS, G. Aad *et al.*, "Search for long-lived stopped R-hadrons decaying out-of-time with pp collisions using the ATLAS detector", *Phys. Rev.* **D88** (2013) no. 11, 112003, arXiv:1310.6584 [hep-ex].

[57] G. Isidori, Y. Nir, and G. Perez, "Flavor Physics Constraints for Physics Beyond the Standard Model", *Ann. Rev. Nucl. Part. Sci.* **60** (2010) 355, arXiv:1002.0900 [hep-ph].

[58] S. J. Huber and Q. Shafi, "Neutrino oscillations and rare processes in models with a small extra dimension", *Phys. Lett.* **B512** (2001) 365–372, arXiv:hep-ph/0104293 [hep-ph].

[59] G. Moreau and J. I. Silva-Marcos, "Neutrinos in warped extra dimensions", *JHEP* **01** (2006) 048, arXiv:hep-ph/0507145 [hep-ph].

[60] G. Moreau and J. I. Silva-Marcos, "Flavor physics of the RS model with KK masses reachable at LHC", *JHEP* **03** (2006) 090, arXiv:hep-ph/0602155 [hep-ph].

[61] G. Moreau, "Realistic neutrino masses from multi-brane extensions of the Randall-Sundrum model?", *Eur. Phys. J.* **C40** (2005) 539–554, arXiv:hep-ph/0407177 [hep-ph].

[62] R. Contino, Y. Nomura, and A. Pomarol, "Higgs as a holographic pseudoGoldstone boson", *Nucl. Phys.* **B671** (2003) 148–174, arXiv:hep-ph/0306259 [hep-ph].

[63] K. Agashe, R. Contino, and A. Pomarol, "The Minimal composite Higgs model", *Nucl. Phys.* **B719** (2005) 165–187, arXiv:hep-ph/0412089 [hep-ph].

[64] K. Agashe and R. Contino, "The Minimal composite Higgs model and electroweak precision tests", *Nucl. Phys.* **B742** (2006) 59–85, arXiv:hep-ph/0510164 [hep-ph].

[65] R. Contino, L. Da Rold, and A. Pomarol, "Light custodians in natural composite Higgs models", *Phys. Rev.* **D75** (2007) 055014, arXiv:hep-ph/0612048 [hep-ph].

[66] N. Arkani-Hamed, A. G. Cohen, and H. Georgi, "Electroweak symmetry breaking from dimensional deconstruction", *Phys. Lett.* **B513** (2001) 232–240, arXiv:hep-ph/0105239 [hep-ph].

[67] N. Arkani-Hamed, A. G. Cohen, E. Katz, and A. E. Nelson, "The Littlest Higgs", *JHEP* **07** (2002) 034, arXiv:hep-ph/0206021 [hep-ph].

[68] J. Kang, P. Langacker, and B. D. Nelson, "Theory and Phenomenology of Exotic Isosinglet Quarks and Squarks", *Phys. Rev.* **D77** (2008) 035003, arXiv:0708.2701 [hep-ph].

[69] C. Kilic, K. Kopp, and T. Okui, "LHC Implications of the WIMP Miracle and Grand Unification", *Phys. Rev.* **D83** (2011) 015006, arXiv:1008.2763 [hep-ph].

[70] F. del Aguila, J. A. Aguilar-Saavedra, and R. Miquel, "Constraints on top couplings in models with exotic quarks", *Phys. Rev. Lett.* **82** (1999) 1628–1631, arXiv:hep-ph/9808400 [hep-ph].

[71] J. A. Aguilar-Saavedra, "Pair production of heavy Q = 2/3 singlets at LHC", *Phys. Lett.* **B625** (2005) 234–244, arXiv:hep-ph/0506187 [hep-ph]. [Erratum: Phys. Lett.B633,792(2006)].

[72] J. A. Aguilar-Saavedra, "Identifying top partners at LHC", *JHEP* **11** (2009) 030, arXiv:0907.3155 [hep-ph].

[73] G. Cacciapaglia, A. Deandrea, L. Panizzi, N. Gaur, D. Harada, and Y. Okada, "Heavy Vector-like Top Partners at the LHC and flavour constraints", *JHEP* **03** (2012) 070, arXiv:1108.6329 [hep-ph].

[74] G. Moreau, "Constraining extra-fermion(s) from the Higgs boson data", *Phys. Rev.* **D87** (2013) no. 1, 015027, arXiv:1210.3977 [hep-ph].

[75] G. Cacciapaglia, A. Deandrea, L. Panizzi, S. Perries, and V. Sordini, "Heavy Vector-like quark with charge 5/3 at the LHC", *JHEP* **03** (2013) 004, arXiv:1211.4034 [hep-ph].

[76] M. Buchkremer, G. Cacciapaglia, A. Deandrea, and L. Panizzi, "Model Independent Framework for Searches of Top Partners", *Nucl. Phys.* **B876** (2013) 376–417, arXiv:1305.4172 [hep-ph].

[77] S. Gopalakrishna, T. Mandal, S. Mitra, and R. Tibrewala, "LHC Signatures of a Vector-like b'", *Phys. Rev.* **D84** (2011) 055001, arXiv:1107.4306 [hep-ph].

[78] J. A. Aguilar-Saavedra, R. Benbrik, S. Heinemeyer, and M. Pérez-Victoria, "Handbook of vectorlike quarks: Mixing and single production", *Phys. Rev.* **D88** (2013) no. 9, 094010, arXiv:1306.0572 [hep-ph].

[79] S. Gopalakrishna, T. Mandal, S. Mitra, and G. Moreau, "LHC Signatures of Warped-space Vectorlike Quarks", *JHEP* **08** (2014) 079, arXiv:1306.2656 [hep-ph].

[80] S. Dawson and E. Furlan, "Yukawa Corrections to Higgs Production in Top Partner Models", *Phys. Rev.* **D89** (2014) no. 1, 015012, arXiv:1310.7593 [hep-ph].

[81] C.-Y. Chen, S. Dawson, and I. M. Lewis, "Top Partners and Higgs Boson Production", *Phys. Rev.* **D90** (2014) no. 3, 035016, arXiv:1406.3349 [hep-ph].

[82] G. Cacciapaglia, A. Deandrea, N. Gaur, D. Harada, Y. Okada, and L. Panizzi, "Interplay of vector-like top partner multiplets in a realistic mixing set-up", *JHEP* **09** (2015) 012, arXiv:1502.00370 [hep-ph].

[83] N. Vignaroli, "Z-peaked excess from heavy gluon decays to vectorlike quarks", *Phys. Rev.* **D91** (2015) no. 11, 115009, arXiv:1504.01768 [hep-ph].

[84] C.-Y. Chen, S. Dawson, and Y. Zhang, "Higgs CP Violation from Vectorlike Quarks", *Phys. Rev.* **D92** (2015) no. 7, 075026, arXiv:1507.07020 [hep-ph].

[85] F. del Aguila, M. Perez-Victoria, and J. Santiago, "Effective description of quark mixing", *Phys. Lett.* **B492** (2000) 98–106, arXiv:hep-ph/0007160 [hep-ph].

[86] F. del Aguila, M. Perez-Victoria, and J. Santiago, "Observable contributions of new exotic quarks to quark mixing", *JHEP* **09** (2000) 011, arXiv:hep-ph/0007316 [hep-ph].

[87] A. Atre, M. Carena, T. Han, and J. Santiago, "Heavy Quarks Above the Top at the Tevatron", *Phys. Rev.* **D79** (2009) 054018, arXiv:0806.3966 [hep-ph].

[88] A. Atre, G. Azuelos, M. Carena, T. Han, E. Ozcan, J. Santiago, and G. Unel, "Model-Independent Searches for New Quarks at the LHC", *JHEP* **08** (2011) 080, arXiv:1102.1987 [hep-ph].

[89] R. Barcelo, A. Carmona, M. Chala, M. Masip, and J. Santiago, "Single Vectorlike Quark Production at the LHC", *Nucl. Phys.* **B857** (2012) 172–184, arXiv:1110.5914 [hep-ph].

[90] A. Atre, M. Chala, and J. Santiago, "Searches for New Vector Like Quarks: Higgs Channels", *JHEP* **05** (2013) 099, arXiv:1302.0270 [hep-ph].

[91] S. Fajfer, A. Greljo, J. F. Kamenik, and I. Mustac, "Light Higgs and Vector-like Quarks without Prejudice", *JHEP* **07** (2013) 155, arXiv:1304.4219 [hep-ph].

[92] A. K. Alok, S. Banerjee, D. Kumar, S. U. Sankar, and D. London, "New-physics signals of a model with a vector-singlet up-type quark", *Phys. Rev.* **D92** (2015) 013002, arXiv:1504.00517 [hep-ph].

[93] A. K. Alok, S. Banerjee, D. Kumar, and S. Uma Sankar, "Flavor signatures of isosinglet vector-like down quark model", *Nucl. Phys.* **B906** (2016) 321–341, arXiv:1402.1023 [hep-ph].

[94] N. Bizot and M. Frigerio, "Fermionic extensions of the Standard Model in light of the Higgs couplings", *JHEP* **01** (2016) 036, arXiv:1508.01645 [hep-ph].

[95] P. Lodone, "Vector-like quarks in a 'composite' Higgs model", *JHEP* **12** (2008) 029, arXiv:0806.1472 [hep-ph].

[96] J. P. Araque, N. F. Castro, and J. Santiago, "Interpretation of Vector-like Quark Searches: Heavy Gluons in Composite Higgs Models", *JHEP* **11** (2015) 120, arXiv:1507.05628 [hep-ph].

[97] M. Gillioz, R. Gröber, A. Kapuvari, and M. Mühlleitner, "Vector-like Bottom Quarks in Composite Higgs Models", *JHEP* **03** (2014) 037, arXiv:1311.4453 [hep-ph].

[98] R. N. Mohapatra and Y. Zhang, "TeV Scale Universal Seesaw, Vacuum Stability and Heavy Higgs", *JHEP* **06** (2014) 072, arXiv:1401.6701 [hep-ph].

[99] ATLAS, G. Aad *et al.*, "Search for vector-like B quarks in events with one isolated lepton, missing transverse momentum and jets at $\sqrt{s} = 8$ TeV with the ATLAS detector", *Phys. Rev.* **D91** (2015) no. 11, 112011, arXiv:1503.05425 [hep-ex].

[100] ATLAS, G. Aad *et al.*, "Search for production of vector-like quark pairs and of four top quarks in the lepton-plus-jets final state in pp collisions at $\sqrt{s} = 8$ TeV with the ATLAS detector", *JHEP* **08** (2015) 105, arXiv:1505.04306 [hep-ex].

[101] ATLAS, G. Aad *et al.*, "Search for pair production of a new heavy quark that decays into a W boson and a light quark in pp collisions at $\sqrt{s} = 8$ TeV with the ATLAS detector", *Phys. Rev.* **D92** (2015) no. 11, 112007, arXiv:1509.04261 [hep-ex].

[102] M. E. Peskin and T. Takeuchi, "Estimation of oblique electroweak corrections", *Phys. Rev.* **D46** (1992) 381–409.

[103] G. Altarelli and R. Barbieri, "Vacuum polarization effects of new physics on electroweak processes", *Phys. Lett.* **B253** (1991) 161–167.

[104] A. Djouadi, J. H. Kuhn, and P. M. Zerwas, "B Jet Asymmetries in Z Decays", *Z. Phys.* **C46** (1990) 411–418.

[105] F. Boudjema, A. Djouadi, and C. Verzegnassi, "A General Sum Rule for the Top Mass From b Physics on Z Resonance", *Phys. Lett.* **B238** (1990) 423–430.

[106] A. Djouadi, G. Moreau, and F. Richard, "Resolving the A(FB)**b puzzle in an extra dimensional model with an extended gauge structure", *Nucl. Phys.* **B773** (2007) 43–64, arXiv:hep-ph/0610173 [hep-ph].

[107] Particle Data Group, K. A. Olive *et al.*, "Review of Particle Physics", *Chin. Phys.* **C38** (2014) 090001.

[108] A. Djouadi and G. Moreau, "Higgs production at the LHC in warped extra-dimensional models", *Phys. Lett.* **B660** (2008) 67–71, arXiv:0707.3800 [hep-ph].

[109] A. Azatov, O. Bondu, A. Falkowski, M. Felcini, S. Gascon-Shotkin, D. K. Ghosh, G. Moreau, and S. Sekmen, "Higgs boson production via vector-like top-partner decays: Diphoton or multilepton plus multijets channels at the LHC", *Phys. Rev.* **D85** (2012) 115022, arXiv:1204.0455 [hep-ph].

[110] N. Bonne and G. Moreau, "Reproducing the Higgs boson data with vector-like quarks", *Phys. Lett.* **B717** (2012) 409–419, arXiv:1206.3360 [hep-ph].

[111] D. Carmi, A. Falkowski, E. Kuflik, and T. Volansky, "Interpreting LHC Higgs Results from Natural New Physics Perspective", *JHEP* **07** (2012) 136, arXiv:1202.3144 [hep-ph].

[112] V. Barger, M. Ishida, and W.-Y. Keung, "Total Width of 125 GeV Higgs Boson", *Phys. Rev. Lett.* **108** (2012) 261801, arXiv:1203.3456 [hep-ph].

[113] P. Huang, A. Ismail, I. Low, and C. E. M. Wagner, "Same-Sign Dilepton Excesses and Light Top Squarks", *Phys. Rev.* **D92** (2015) no. 7, 075035, arXiv:1507.01601 [hep-ph].

[114] G. Couture, M. Frank, C. Hamzaoui, and M. Toharia, "Top and bottom partners, Higgs boson on the brane, and the tth signal", *Phys. Rev.* **D95** (2017) no. 9, 095038, arXiv:1704.02269 [hep-ph].

[115] M. Hashimoto, "Revisiting Vector-like Quark Model with Enhanced Top Yukawa Coupling", arXiv:1704.02615 [hep-ph].

[116] A. Angelescu, A. Djouadi, and G. Moreau, "Vector-like top/bottom quark partners and Higgs physics at the LHC", *Eur. Phys. J.* **C76** (2016) no. 2, 99, arXiv:1510.07527 [hep-ph].

[117] A. Djouadi, "Precision Higgs coupling measurements at the LHC through ratios of production cross sections", *Eur. Phys. J.* **C73** (2013) 2498, arXiv:1208.3436 [hep-ph].

[118] A. Djouadi, J. Quevillon, and R. Vega-Morales, "Into the multi-TeV scale with a Higgs golden ratio", *Phys. Lett.* **B757** (2016) 412–419, arXiv:1509.03913 [hep-ph].

[119] LHC Higgs Cross Section Working Group, S. Dittmaier *et al.*, "Handbook of LHC Higgs Cross Sections: 1. Inclusive Observables", arXiv:1101.0593 [hep-ph].

[120] J. Baglio and A. Djouadi, "Higgs production at the lHC", *JHEP* **03** (2011) 055, arXiv:1012.0530 [hep-ph].

[121] S. Fichet and G. Moreau, "Anatomy of the Higgs fits: a first guide to statistical treatments of the theoretical uncertainties", *Nucl. Phys.* **B905** (2016) 391–446, arXiv:1509.00472 [hep-ph].

[122] "Projections for measurements of Higgs boson signal strengths and coupling parameters with the ATLAS detector at a HL-LHC", ATL-PHYS-PUB-2014-016, CERN, Geneva, Oct, 2014. http://cds.cern.ch/record/1956710.

[123] CMS, "Projected Performance of an Upgraded CMS Detector at the LHC and HL-LHC: Contribution to the Snowmass Process", in *Proceedings, 2013 Community Summer Study on the Future of U.S. Particle Physics: Snowmass on the Mississippi (CSS2013): Minneapolis, MN, USA, July 29-August 6, 2013*. 2013. arXiv:1307.7135 [hep-ex]. http://inspirehep.net/record/1244669/files/arXiv:1307.7135.pdf.

[124] ATLAS, "Physics at a High-Luminosity LHC with ATLAS", in *Proceedings, 2013 Community Summer Study on the Future of U.S. Particle Physics: Snowmass on the Mississippi (CSS2013): Minneapolis, MN, USA, July 29-August 6, 2013*. 2013. arXiv:1307.7292 [hep-ex]. http://inspirehep.net/record/1245017/files/arXiv:1307.7292.pdf.

[125] C. Bouchart and G. Moreau, "The precision electroweak data in warped extra-dimension models", *Nucl. Phys.* **B810** (2009) 66–96, arXiv:0807.4461 [hep-ph].

[126] B. Batell, S. Gori, and L.-T. Wang, "Higgs Couplings and Precision Electroweak Data", *JHEP* **01** (2013) 139, arXiv:1209.6382 [hep-ph].

[127] D. Choudhury, T. M. P. Tait, and C. E. M. Wagner, "Beautiful mirrors and precision electroweak data", *Phys. Rev.* **D65** (2002) 053002, arXiv:hep-ph/0109097 [hep-ph].

[128] A. Djouadi, "The Anatomy of electro-weak symmetry breaking. I: The Higgs boson in the standard model", *Phys. Rept.* **457** (2008) 1–216, arXiv:hep-ph/0503172 [hep-ph].

[129] M. Frank, N. Pourtolami, and M. Toharia, "Higgs Bosons in Warped Space, from the Bulk to the Brane", *Phys. Rev.* **D87** (2013) no. 9, 096003, arXiv:1301.7692 [hep-ph].

[130] A. Djouadi and G. Moreau, "The couplings of the Higgs boson and its CP properties from fits of the signal strengths and their ratios at the 7+8 TeV LHC", *Eur. Phys. J.* **C73** (2013) no. 9, 2512, arXiv:1303.6591 [hep-ph].

[131] M. Spira, A. Djouadi, D. Graudenz, and P. M. Zerwas, "Higgs boson production at the LHC", *Nucl. Phys.* **B453** (1995) 17–82, arXiv:hep-ph/9504378 [hep-ph].

[132] CMS, V. Khachatryan *et al.*, "Search for the standard model Higgs boson produced through vector boson fusion and decaying to $b\bar{b}$", *Phys. Rev.* **D92** (2015) no. 3, 032008, arXiv:1506.01010 [hep-ex].

[133] A. Djouadi, J. Kalinowski, and M. Spira, "HDECAY: A Program for Higgs boson decays in the standard model and its supersymmetric extension", *Comput. Phys. Commun.* **108** (1998) 56–74, arXiv:hep-ph/9704448 [hep-ph].

[134] R. Barbieri, L. J. Hall, Y. Nomura, and V. S. Rychkov, "Supersymmetry without a Light Higgs Boson", *Phys. Rev.* **D75** (2007) 035007, arXiv:hep-ph/0607332 [hep-ph].

[135] L. Lavoura and J. P. Silva, "The Oblique corrections from vector - like singlet and doublet quarks", *Phys. Rev.* **D47** (1993) 2046–2057.

[136] Gfitter Group, M. Baak, J. Cúth, J. Haller, A. Hoecker, R. Kogler, K. Mönig, M. Schott, and J. Stelzer, "The global electroweak fit at NNLO and prospects for the LHC and ILC", *Eur. Phys. J.* **C74** (2014) 3046, arXiv:1407.3792 [hep-ph].

[137] A. Freitas, "Higher-order electroweak corrections to the partial widths and branching ratios of the Z boson", *JHEP* **04** (2014) 070, arXiv:1401.2447 [hep-ph].

[138] K. Agashe, R. Contino, L. Da Rold, and A. Pomarol, "A Custodial symmetry for $Zb\bar{b}$", *Phys. Lett.* **B641** (2006) 62–66, arXiv:hep-ph/0605341 [hep-ph].

[139] L. Da Rold, "Solving the A_{FB}^b anomaly in natural composite models", *JHEP* **02** (2011) 034, arXiv:1009.2392 [hep-ph].

[140] K. Agashe, A. Delgado, M. J. May, and R. Sundrum, "RS1, custodial isospin and precision tests", *JHEP* **08** (2003) 050, arXiv:hep-ph/0308036 [hep-ph].

[141] H. Fusaoka and Y. Koide, "Updated estimate of running quark masses", *Phys. Rev.* **D57** (1998) 3986–4001, arXiv:hep-ph/9712201 [hep-ph].

[142] H. Fritzsch and Z.-z. Xing, "Mass and flavor mixing schemes of quarks and leptons", *Prog. Part. Nucl. Phys.* **45** (2000) 1–81, arXiv:hep-ph/9912358 [hep-ph].

[143] O. Matsedonskyi, F. Riva, and T. Vantalon, "Composite Charge 8/3 Resonances at the LHC", *JHEP* **04** (2014) 059, arXiv:1401.3740 [hep-ph].

[144] W. Beenakker, S. Dittmaier, M. Kramer, B. Plumper, M. Spira, and P. M. Zerwas, "NLO QCD corrections to t anti-t H production in hadron collisions", *Nucl. Phys.* **B653** (2003) 151–203, arXiv:hep-ph/0211352 [hep-ph].

[145] S. Dawson, C. Jackson, L. H. Orr, L. Reina, and D. Wackeroth, "Associated Higgs production with top quarks at the large hadron collider: NLO QCD corrections", *Phys. Rev.* **D68** (2003) 034022, arXiv:hep-ph/0305087 [hep-ph].

[146] S. Frixione, V. Hirschi, D. Pagani, H. S. Shao, and M. Zaro, "Electroweak and QCD corrections to top-pair hadroproduction in association with heavy bosons", *JHEP* **06** (2015) 184, arXiv:1504.03446 [hep-ph].

[147] A. Denner and R. Feger, "NLO QCD corrections to off-shell top-antitop production with leptonic decays in association with a Higgs boson at the LHC", *JHEP* **11** (2015) 209, arXiv:1506.07448 [hep-ph].

[148] M. L. Mangano, T. Plehn, P. Reimitz, T. Schell, and H.-S. Shao, "Measuring the Top Yukawa Coupling at 100 TeV", *J. Phys.* **G43** (2016) no. 3, 035001, arXiv:1507.08169 [hep-ph].

[149] T. D. Lee, "A Theory of Spontaneous T Violation", *Phys. Rev.* **D8** (1973) 1226–1239.

[150] G. C. Branco, P. M. Ferreira, L. Lavoura, M. N. Rebelo, M. Sher, and J. P. Silva, "Theory and phenomenology of two-Higgs-doublet models", *Phys. Rept.* **516** (2012) 1–102, arXiv:1106.0034 [hep-ph].

[151] A. Djouadi, L. Maiani, A. Polosa, J. Quevillon, and V. Riquer, "Fully covering the MSSM Higgs sector at the LHC", *JHEP* **06** (2015) 168, arXiv:1502.05653 [hep-ph].

[152] J. F. Gunion and H. E. Haber, "The CP conserving two Higgs doublet model: The Approach to the decoupling limit", *Phys. Rev.* **D67** (2003) 075019, arXiv:hep-ph/0207010 [hep-ph].

[153] M. Carena, I. Low, N. R. Shah, and C. E. M. Wagner, "Impersonating the Standard Model Higgs Boson: Alignment without Decoupling", *JHEP* **04** (2014) 015, arXiv:1310.2248 [hep-ph].

[154] L. Wang and X.-F. Han, "Status of the aligned two-Higgs-doublet model confronted with the Higgs data", *JHEP* **04** (2014) 128, arXiv:1312.4759 [hep-ph].

[155] P. S. Bhupal Dev and A. Pilaftsis, "Maximally Symmetric Two Higgs Doublet Model with Natural Standard Model Alignment", *JHEP* **12** (2014) 024, arXiv:1408.3405 [hep-ph]. [Erratum: JHEP11,147(2015)].

[156] J. Bernon, J. F. Gunion, H. E. Haber, Y. Jiang, and S. Kraml, " Scrutinizing the alignment limit in two-Higgs-doublet models: m_h=125 GeV ", *Phys. Rev.* **D92** (2015) no. 7, 075004, arXiv:1507.00933 [hep-ph].

[157] The ATLAS collaboration, "Search for resonances decaying to photon pairs in 3.2 fb^{-1} of pp collisions at $\sqrt{s} = 13$ TeV with the ATLAS detector",.

[158] CMS, The CMS Collaboration, "Search for new physics in high mass diphoton events in proton-proton collisions at 13 TeV",.

[159] The ATLAS collaboration, "Search for scalar diphoton resonances with 15.4 fb^{-1} of data collected at $\sqrt{s}$=13 TeV in 2015 and 2016 with the ATLAS detector",.

[160] The CMS Collaboration, "Search for resonant production of high mass photon pairs using 12.9 fb^{-1} of proton-proton collisions at $\sqrt{s} = 13$ TeV and combined interpretation of searches at 8 and 13 TeV",.

[161] A. Angelescu, A. Djouadi, and G. Moreau, "Scenarii for interpretations of the LHC diphoton excess: two Higgs doublets and vector-like quarks and leptons", *Phys. Lett.* **B756** (2016) 126–132, arXiv:1512.04921 [hep-ph].

[162] L. D. Landau, "On the angular momentum of a system of two photons", *Dokl. Akad. Nauk Ser. Fiz.* **60** (1948) no. 2, 207–209.

[163] C.-N. Yang, "Selection Rules for the Dematerialization of a Particle Into Two Photons", *Phys. Rev.* **77** (1950) 242–245.

[164] ATLAS, G. Aad *et al.*, "Search for new phenomena in dijet mass and angular distributions from pp collisions at $\sqrt{s} = 13$ TeV with the ATLAS detector", *Phys. Lett.* **B754** (2016) 302–322, arXiv:1512.01530 [hep-ex].

[165] CMS, V. Khachatryan *et al.*, "Search for narrow resonances decaying to dijets in proton-proton collisions at $\sqrt{s} = 13$ TeV", *Phys. Rev. Lett.* **116** (2016) no. 7, 071801, arXiv:1512.01224 [hep-ex].

[166] The LHC Higgs Cross Section Working Group. https://twiki.cern.ch/twiki/bin/view/LHCPhysics/LHCHXSWG.

[167] ATLAS, G. Aad *et al.*, "Search for Scalar Diphoton Resonances in the Mass Range $65 - 600$ GeV with the ATLAS Detector in pp Collision Data at $\sqrt{s} = 8\ TeV$", *Phys. Rev. Lett.* **113** (2014) no. 17, 171801, arXiv:1407.6583 [hep-ex].

[168] CMS, V. Khachatryan *et al.*, "Search for diphoton resonances in the mass range from 150 to 850 GeV in pp collisions at $\sqrt{s} = 8$ TeV", *Phys. Lett.* **B750** (2015) 494–519, arXiv:1506.02301 [hep-ex].

[169] J. F. Gunion, H. E. Haber, G. L. Kane, and S. Dawson, "The Higgs Hunter's Guide", *Front. Phys.* **80** (2000) 1–404.

[170] A. Djouadi, "The Anatomy of electro-weak symmetry breaking. II. The Higgs bosons in the minimal supersymmetric model", *Phys. Rept.* **459** (2008) 1–241, arXiv:hep-ph/0503173 [hep-ph].

[171] S. A. R. Ellis, R. M. Godbole, S. Gopalakrishna, and J. D. Wells, "Survey of vector-like fermion extensions of the Standard Model and their phenomenological implications", *JHEP* **09** (2014) 130, arXiv:1404.4398 [hep-ph].

[172] A. Djouadi, L. Maiani, G. Moreau, A. Polosa, J. Quevillon, and V. Riquer, "The post-Higgs MSSM scenario: Habemus MSSM?", *Eur. Phys. J.* **C73** (2013) 2650, arXiv:1307.5205 [hep-ph].

[173] ATLAS, CMS, G. Aad *et al.*, "Measurements of the Higgs boson production and decay rates and constraints on its couplings from a combined ATLAS and CMS analysis of the LHC pp collision data at $\sqrt{s} = 7$ and 8 TeV", *JHEP* **08** (2016) 045, arXiv:1606.02266 [hep-ex].

[174] A. Djouadi, M. M. Muhlleitner, and M. Spira, "Decays of supersymmetric particles: The Program SUSY-HIT (SUspect-SdecaY-Hdecay-InTerface)", *Acta Phys. Polon.* **B38** (2007) 635–644, arXiv:hep-ph/0609292 [hep-ph].

[175] ATLAS, G. Aad *et al.*, "A search for $t\bar{t}$ resonances using lepton-plus-jets events in proton-proton collisions at $\sqrt{s} = 8$ TeV with the ATLAS detector", *JHEP* **08** (2015) 148, arXiv:1505.07018 [hep-ex].

[176] CMS, V. Khachatryan *et al.*, "Search for resonant $t\bar{t}$ production in proton-proton collisions at $\sqrt{s} = 8$ TeV", *Phys. Rev.* **D93** (2016) no. 1, 012001, arXiv:1506.03062 [hep-ex].

[177] A. Arhrib, R. Benbrik, M. Chabab, G. Moultaka, and L. Rahili, "Higgs boson decay into 2 photons in the type II Seesaw Model", *JHEP* **04** (2012) 136, arXiv:1112.5453 [hep-ph].

[178] A. G. Akeroyd and S. Moretti, "Enhancement of H to gamma gamma from doubly charged scalars in the Higgs Triplet Model", *Phys. Rev.* **D86** (2012) 035015, arXiv:1206.0535 [hep-ph].

[179] Z. Lalak, M. Lewicki, and J. D. Wells, "Higgs boson mass and high-luminosity LHC probes of supersymmetry with vectorlike top quark", *Phys. Rev.* **D91** (2015) no. 9, 095022, arXiv:1502.05702 [hep-ph].

[180] Particle Data Group, K. Nakamura *et al.*, "Review of particle physics", *J. Phys.* **G37** (2010) 075021.

[181] A. Joglekar, P. Schwaller, and C. E. M. Wagner, "Dark Matter and Enhanced Higgs to Di-photon Rate from Vector-like Leptons", *JHEP* **12** (2012) 064, arXiv:1207.4235 [hep-ph].

[182] ATLAS, G. Aad *et al.*, "Search for heavy lepton resonances decaying to a Z boson and a lepton in pp collisions at $\sqrt{s} = 8$ TeV with the ATLAS detector", *JHEP* **09** (2015) 108, arXiv:1506.01291 [hep-ex].

[183] CMS, S. Chatrchyan *et al.*, "Inclusive search for a vector-like T quark with charge $\frac{2}{3}$ in pp collisions at $\sqrt{s} = 8$ TeV", *Phys. Lett.* **B729** (2014) 149–171, arXiv:1311.7667 [hep-ex].

[184] S. Gopalakrishna, T. S. Mukherjee, and S. Sadhukhan, "Extra neutral scalars with vectorlike fermions at the LHC", *Phys. Rev.* **D93** (2016) no. 5, 055004, arXiv:1504.01074 [hep-ph].

[185] J. Abdallah *et al.*, "Simplified Models for Dark Matter and Missing Energy Searches at the LHC", arXiv:1409.2893 [hep-ph].

[186] F. Kahlhoefer, K. Schmidt-Hoberg, T. Schwetz, and S. Vogl, "Implications of unitarity and gauge invariance for simplified dark matter models", *JHEP* **02** (2016) 016, arXiv:1510.02110 [hep-ph].

[187] C. Arina *et al.*, "A comprehensive approach to dark matter studies: exploration of simplified top-philic models", arXiv:1605.09242 [hep-ph].

[188] X. Chu, T. Hambye, T. Scarna, and M. H. G. Tytgat, "What if Dark Matter Gamma-Ray Lines come with Gluon Lines?", *Phys. Rev.* **D86** (2012) 083521, arXiv:1206.2279 [hep-ph].

[189] Y. Mambrini, G. Arcadi, and A. Djouadi, "The LHC diphoton resonance and dark matter", *Phys. Lett.* **B755** (2016) 426–432, arXiv:1512.04913 [hep-ph].

[190] M. Backovic, A. Mariotti, and D. Redigolo, "Di-photon excess illuminates Dark Matter", *JHEP* **03** (2016) 157, arXiv:1512.04917 [hep-ph].

[191] F. D'Eramo, J. de Vries, and P. Panci, "A 750 GeV Portal: LHC Phenomenology and Dark Matter Candidates", *JHEP* **05** (2016) 089, arXiv:1601.01571 [hep-ph].

[192] J. Goodman, M. Ibe, A. Rajaraman, W. Shepherd, T. M. P. Tait, and H.-B. Yu, "Constraints on Dark Matter from Colliders", *Phys. Rev.* **D82** (2010) 116010, arXiv:1008.1783 [hep-ph].

[193] P. J. Fox, R. Harnik, J. Kopp, and Y. Tsai, "Missing Energy Signatures of Dark Matter at the LHC", *Phys. Rev.* **D85** (2012) 056011, arXiv:1109.4398 [hep-ph].

[194] ATLAS, G. Aad *et al.*, "Search for new phenomena in final states with an energetic jet and large missing transverse momentum in pp collisions at $\sqrt{s}$ =8 TeV with the ATLAS detector", *Eur. Phys. J.* **C75** (2015) no. 7, 299, arXiv:1502.01518 [hep-ex]. [Erratum: Eur. Phys. J.C75,no.9,408(2015)].

[195] CMS, V. Khachatryan *et al.*, "Search for dark matter, extra dimensions, and unparticles in monojet events in proton–proton collisions at $\sqrt{s} = 8$ TeV", *Eur. Phys. J.* **C75** (2015) no. 5, 235, arXiv:1408.3583 [hep-ex].

[196] G. Arcadi, Y. Mambrini, and F. Richard, "Z-portal dark matter", *JCAP* **1503** (2015) 018, arXiv:1411.2985 [hep-ph].

[197] R. C. Cotta, J. L. Hewett, M. P. Le, and T. G. Rizzo, "Bounds on Dark Matter Interactions with Electroweak Gauge Bosons", *Phys. Rev.* **D88** (2013) 116009, arXiv:1210.0525 [hep-ph].

[198] A. De Simone, G. F. Giudice, and A. Strumia, "Benchmarks for Dark Matter Searches at the LHC", *JHEP* **06** (2014) 081, arXiv:1402.6287 [hep-ph].

[199] O. Lebedev, H. M. Lee, and Y. Mambrini, "Vector Higgs-portal dark matter and the invisible Higgs", *Phys. Lett.* **B707** (2012) 570–576, arXiv:1111.4482 [hep-ph].

[200] A. Djouadi, O. Lebedev, Y. Mambrini, and J. Quevillon, "Implications of LHC searches for Higgs–portal dark matter", *Phys. Lett.* **B709** (2012) 65–69, arXiv:1112.3299 [hep-ph].

[201] A. Djouadi, A. Falkowski, Y. Mambrini, and J. Quevillon, "Direct Detection of Higgs-Portal Dark Matter at the LHC", *Eur. Phys. J.* **C73** (2013) no. 6, 2455, arXiv:1205.3169 [hep-ph].

[202] L. Lopez-Honorez, T. Schwetz, and J. Zupan, "Higgs portal, fermionic dark matter, and a Standard Model like Higgs at 125 GeV", *Phys. Lett.* **B716** (2012) 179–185, arXiv:1203.2064 [hep-ph].

[203] A. Beniwal, F. Rajec, C. Savage, P. Scott, C. Weniger, M. White, and A. G. Williams, "Combined analysis of effective Higgs portal dark matter models", *Phys. Rev.* **D93** (2016) no. 11, 115016, arXiv:1512.06458 [hep-ph].

[204] T. Cohen, J. Kearney, A. Pierce, and D. Tucker-Smith, "Singlet-Doublet Dark Matter", *Phys. Rev.* **D85** (2012) 075003, arXiv:1109.2604 [hep-ph].

[205] L. Calibbi, A. Mariotti, and P. Tziveloglou, "Singlet-Doublet Model: Dark matter searches and LHC constraints", *JHEP* **10** (2015) 116, arXiv:1505.03867 [hep-ph].

[206] C. E. Yaguna, "Singlet-Doublet Dirac Dark Matter", *Phys. Rev.* **D92** (2015) no. 11, 115002, arXiv:1510.06151 [hep-ph].

[207] A. Berlin, S. Gori, T. Lin, and L.-T. Wang, "Pseudoscalar Portal Dark Matter", *Phys. Rev.* **D92** (2015) 015005, arXiv:1502.06000 [hep-ph].

[208] SLD Electroweak Group, DELPHI, ALEPH, SLD, SLD Heavy Flavour Group, OPAL, LEP Electroweak Working Group, L3, S. Schael *et al.*, "Precision electroweak measurements on the Z resonance", *Phys. Rept.* **427** (2006) 257–454, arXiv:hep-ex/0509008 [hep-ex].

[209] A. Angelescu and G. Arcadi, "Dark Matter Phenomenology of SM and Enlarged Higgs Sectors Extended with Vector Like Leptons", *Eur. Phys. J.* **C77** (2017) no. 7, 456, arXiv:1611.06186 [hep-ph].

[210] A. Djouadi, J. Ellis, R. Godbole, and J. Quevillon, "Future Collider Signatures of the Possible 750 GeV State", *JHEP* **03** (2016) 205, arXiv:1601.03696 [hep-ph].

[211] R. Benbrik, C.-H. Chen, and T. Nomura, "Higgs singlet boson as a diphoton resonance in a vectorlike quark model", *Phys. Rev.* **D93** (2016) no. 5, 055034, arXiv:1512.06028 [hep-ph].

[212] C. W. Murphy, "Vector Leptoquarks and the 750 GeV Diphoton Resonance at the LHC", *Phys. Lett.* **B757** (2016) 192–198, arXiv:1512.06976 [hep-ph].

[213] F. Wang, W. Wang, L. Wu, J. M. Yang, and M. Zhang, "Interpreting 750 GeV diphoton resonance as degenerate Higgs bosons in NMSSM with vector-like particles", arXiv:1512.08434 [hep-ph].

[214] Y.-L. Tang and S.-h. Zhu, "NMSSM extended with vectorlike particles and the diphoton excess at the LHC", *Phys. Rev.* **D94** (2016) no. 3, 035010, arXiv:1512.08323 [hep-ph].

[215] P. S. B. Dev, R. N. Mohapatra, and Y. Zhang, "Quark Seesaw, Vectorlike Fermions and Diphoton Excess", *JHEP* **02** (2016) 186, arXiv:1512.08507 [hep-ph].

[216] E. Palti, "Vector-Like Exotics in F-Theory and 750 GeV Diphotons", *Nucl. Phys.* **B907** (2016) 597–616, arXiv:1601.00285 [hep-ph].

[217] B. Dutta, Y. Gao, T. Ghosh, I. Gogoladze, T. Li, Q. Shafi, and J. W. Walker, "Diphoton Excess in Consistent Supersymmetric SU(5) Models with Vector-like Particles", arXiv:1601.00866 [hep-ph].

[218] S. Di Chiara, A. Hektor, K. Kannike, L. Marzola, and M. Raidal, "Large loop-coupling enhancement of a 750 GeV pseudoscalar from a light dark sector", arXiv:1603.07263 [hep-ph].

[219] J. Kawamura and Y. Omura, "Diphoton excess at 750 GeV and LHC constraints in models with vectorlike particles", *Phys. Rev.* **D93** (2016) no. 11, 115011, arXiv:1601.07396 [hep-ph].

[220] S. Gopalakrishna and T. S. Mukherjee, "The 750 GeV diphoton excess in a two Higgs doublet model and a singlet scalar model, with vector-like fermions, unitarity constraints, and dark matter implications", arXiv:1604.05774 [hep-ph].

[221] A. Arhrib, R. Benbrik, S. J. D. King, B. Manaut, S. Moretti, and C. S. Un, "Resonances at 750 GeV in a 2HDM with VLQs", arXiv:1607.08517 [hep-ph].

[222] ATLAS, "Search for resonances decaying to photon pairs in 3.2 fb^{-1} of pp collisions at $\sqrt{s} = 13$ TeV with the ATLAS detector", *ATLAS-CONF-2015-081* (2015) .

[223] CMS, "Search for new physics in high mass diphoton events in 3.3 fb^{-1} of proton-proton collisions at $\sqrt{s} = 13$ TeV and combined interpretation of searches at 8 TeV and 13 TeV", *CMS-PAS-EXO-16-018* (2016) .

[224] ATLAS, "Search for resonances in diphoton events with the ATLAS detector at $\sqrt{s} =$ 13 TeV", *ATLAS-CONF-2016-018* (2016) .

[225] ATLAS, "Search for scalar diphoton resonances with 15.4 fb^{-1} of data collected at $\sqrt{s} = 13$ TeV in 2015 and 2016 with the ATLAS detector", *ATLAS-CONF-2016-059* (2016) .

[226] "Search for resonant production of high mass photon pairs using 12.9 fb^{-1} of proton-proton collisions at $\sqrt{s} = 13$ TeV and combined interpretation of searches at 8 and 13 TeV", *CMS PAS EXO-16-027* (2016) .

[227] P. Gondolo and G. Gelmini, "Cosmic abundances of stable particles: Improved analysis", *Nucl. Phys.* **B360** (1991) 145–179.

[228] G. Bélanger, F. Boudjema, A. Pukhov, and A. Semenov, "micrOMEGAs4.1: two dark matter candidates", *Comput. Phys. Commun.* **192** (2015) 322–329, arXiv:1407.6129 [hep-ph].

[229] G. Jungman, M. Kamionkowski, and K. Griest, "Supersymmetric dark matter", *Phys. Rept.* **267** (1996) 195–373, arXiv:hep-ph/9506380 [hep-ph].

[230] K. Griest and D. Seckel, "Three exceptions in the calculation of relic abundances", *Phys. Rev.* **D43** (1991) 3191–3203.

[231] M. Cirelli, E. Del Nobile, and P. Panci, "Tools for model-independent bounds in direct dark matter searches", *JCAP* **1310** (2013) 019, arXiv:1307.5955 [hep-ph].

[232] LUX, D. S. Akerib *et al.*, "Improved Limits on Scattering of Weakly Interacting Massive Particles from Reanalysis of 2013 LUX Data", *Phys. Rev. Lett.* **116** (2016) no. 16, 161301, arXiv:1512.03506 [astro-ph.CO].

[233] XENON, E. Aprile *et al.*, "First Dark Matter Search Results from the XENON1T Experiment", arXiv:1705.06655 [astro-ph.CO].

[234] G. Degrassi, S. Di Vita, J. Elias-Miro, J. R. Espinosa, G. F. Giudice, G. Isidori, and A. Strumia, "Higgs mass and vacuum stability in the Standard Model at NNLO", *JHEP* **08** (2012) 098, arXiv:1205.6497 [hep-ph].

[235] K. Blum, R. T. D'Agnolo, and J. Fan, "Vacuum stability bounds on Higgs coupling deviations in the absence of new bosons", *JHEP* **03** (2015) 166, arXiv:1502.01045 [hep-ph].

[236] D. Bečirević, E. Bertuzzo, O. Sumensari, and R. Zukanovich Funchal, "Can the new resonance at LHC be a CP-Odd Higgs boson?", *Phys. Lett.* **B757** (2016) 261–267, arXiv:1512.05623 [hep-ph].

[237] S. Kanemura, Y. Okada, E. Senaha, and C. P. Yuan, "Higgs coupling constants as a probe of new physics", *Phys. Rev.* **D70** (2004) 115002, arXiv:hep-ph/0408364 [hep-ph].

[238] A. Barroso, P. M. Ferreira, I. P. Ivanov, and R. Santos, "Metastability bounds on the two Higgs doublet model", *JHEP* **06** (2013) 045, arXiv:1303.5098 [hep-ph].

[239] S. Davidson and G. J. Grenier, "Lepton flavour violating Higgs and tau to mu gamma", *Phys. Rev.* **D81** (2010) 095016, arXiv:1001.0434 [hep-ph].

[240] E. Bertuzzo, P. A. N. Machado, and M. Taoso, "Di-Photon excess in the 2HDM: hasting towards the instability and the non-perturbative regime", arXiv:1601.07508 [hep-ph].

[241] R. Franceschini, G. F. Giudice, J. F. Kamenik, M. McCullough, A. Pomarol, R. Rattazzi, M. Redi, F. Riva, A. Strumia, and R. Torre, "What is the $\gamma\gamma$ resonance at 750 GeV?", *JHEP* **03** (2016) 144, arXiv:1512.04933 [hep-ph].

[242] J. Gu and Z. Liu, "Physics implications of the diphoton excess from the perspective of renormalization group flow", *Phys. Rev.* **D93** (2016) 075006, arXiv:1512.07624 [hep-ph].

[243] M. Son and A. Urbano, "A new scalar resonance at 750 GeV: Towards a proof of concept in favor of strongly interacting theories", *JHEP* **05** (2016) 181, arXiv:1512.08307 [hep-ph].

[244] A. Salvio and A. Mazumdar, "Higgs Stability and the 750 GeV Diphoton Excess", *Phys. Lett.* **B755** (2016) 469–474, arXiv:1512.08184 [hep-ph].

[245] A. Salvio, F. Staub, A. Strumia, and A. Urbano, "On the maximal diphoton width", *JHEP* **03** (2016) 214, arXiv:1602.01460 [hep-ph].

[246] K. J. Bae, M. Endo, K. Hamaguchi, and T. Moroi, "Diphoton Excess and Running Couplings", *Phys. Lett.* **B757** (2016) 493–500, arXiv:1602.03653 [hep-ph].

[247] Y. Hamada, H. Kawai, K. Kawana, and K. Tsumura, "Models of the LHC diphoton excesses valid up to the Planck scale", *Phys. Rev.* **D94** (2016) 014007, arXiv:1602.04170 [hep-ph].

[248] G. Arcadi, P. Ghosh, Y. Mambrini, and M. Pierre, "Scrutinizing a di-photon resonance at the LHC through Moscow zero", arXiv:1608.04755 [hep-ph].

[249] F. Goertz, J. F. Kamenik, A. Katz, and M. Nardecchia, "Indirect Constraints on the Scalar Di-Photon Resonance at the LHC", *JHEP* **05** (2016) 187, arXiv:1512.08500 [hep-ph].

[250] A. Bharucha, A. Djouadi, and A. Goudelis, "Threshold enhancement of diphoton resonances", arXiv:1603.04464 [hep-ph].

[251] F. D'Eramo, J. de Vries, and P. Panci, "A 750 GeV Portal: LHC Phenomenology and Dark Matter Candidates", *JHEP* **05** (2016) 089, arXiv:1601.01571 [hep-ph].

[252] A. Hektor, L. Marzola, and T. Tuvi, "Gamma-ray line constraints on Coy Dark Matter", arXiv:1702.02580 [hep-ph].

[253] B. Dutta, Y. Gao, T. Ghosh, and L. E. Strigari, "Confronting Galactic center and dwarf spheroidal gamma-ray observations with cascade annihilation models", *Phys. Rev.* **D92** (2015) no. 7, 075019, arXiv:1508.05989 [hep-ph].

[254] LHC Higgs Cross Section Working Group, D. de Florian *et al.*, "Handbook of LHC Higgs Cross Sections: 4. Deciphering the Nature of the Higgs Sector", arXiv:1610.07922 [hep-ph].

[255] R. V. Harlander, S. Liebler, and H. Mantler, "SusHi: A program for the calculation of Higgs production in gluon fusion and bottom-quark annihilation in the Standard Model and the MSSM", *Comput. Phys. Commun.* **184** (2013) 1605–1617, arXiv:1212.3249 [hep-ph].

[256] J. Hajer, Y.-Y. Li, T. Liu, and J. F. H. Shiu, "Heavy Higgs Bosons at 14 TeV and 100 TeV", *JHEP* **11** (2015) 124, arXiv:1504.07617 [hep-ph].

[257] S. Gori, I.-W. Kim, N. R. Shah, and K. M. Zurek, "Closing the Wedge: Search Strategies for Extended Higgs Sectors with Heavy Flavor Final States", *Phys. Rev.* **D93** (2016) no. 7, 075038, arXiv:1602.02782 [hep-ph].

[258] N. Craig, J. Hajer, Y.-Y. Li, T. Liu, and H. Zhang, "Heavy Higgs Bosons at Low $\tan\beta$: from the LHC to 100 TeV", arXiv:1605.08744 [hep-ph].

[259] M. Carena and Z. Liu, "Challenges and opportunities for heavy scalar searches in the $t\bar{t}$ channel at the LHC", arXiv:1608.07282 [hep-ph].

[260] A. Djouadi, J. Ellis, and J. Quevillon, "Interference effects in the decays of spin-zero resonances into $\gamma\gamma$ and $t\bar{t}$", *JHEP* **07** (2016) 105, arXiv:1605.00542 [hep-ph].

[261] Search for BSM physics in di-photon final states at CMS, 2016.

[262] R. Dermisek, E. Lunghi, and S. Shin, "Two Higgs doublet model with vectorlike leptons and contributions to $pp \to WW$ and $H \to WW$", *JHEP* **02** (2016) 119, arXiv:1509.04292 [hep-ph].

[263] R. Dermisek, E. Lunghi, and S. Shin, "New decay modes of heavy Higgs bosons in a two Higgs doublet model with vectorlike leptons", *JHEP* **05** (2016) 148, arXiv:1512.07837 [hep-ph].

[264] R. Dermisek, E. Lunghi, and S. Shin, "New constraints and discovery potential for Higgs to Higgs cascade decays through vectorlike leptons", *JHEP* **10** (2016) 081, arXiv:1608.00662 [hep-ph].

[265] ATLAS, G. Aad *et al.*, "Search for type-III Seesaw heavy leptons in pp collisions at $\sqrt{s} = 8$ TeV with the ATLAS Detector", *Phys. Rev.* **D92** (2015) no. 3, 032001, arXiv:1506.01839 [hep-ex].

[266] ATLAS, G. Aad *et al.*, "Search for direct production of charginos, neutralinos and sleptons in final states with two leptons and missing transverse momentum in pp collisions at $\sqrt{s} = 8$ TeV with the ATLAS detector", *JHEP* **05** (2014) 071, arXiv:1403.5294 [hep-ex].

[267] ATLAS, G. Aad *et al.*, "Search for the electroweak production of supersymmetric particles in $\sqrt{s}$=8 TeV pp collisions with the ATLAS detector", *Phys. Rev.* **D93** (2016) no. 5, 052002, arXiv:1509.07152 [hep-ex].

[268] CMS, V. Khachatryan *et al.*, "Searches for electroweak neutralino and chargino production in channels with Higgs, Z, and W bosons in pp collisions at 8 TeV", *Phys. Rev.* **D90** (2014) no. 9, 092007, arXiv:1409.3168 [hep-ex].

[269] ATLAS, G. Aad *et al.*, "Search for a light charged Higgs boson in the decay channel $H^+ \to c\bar{s}$ in $t\bar{t}$ events using pp collisions at $\sqrt{s} = 7$ TeV with the ATLAS detector", *Eur. Phys. J.* **C73** (2013) no. 6, 2465, arXiv:1302.3694 [hep-ex].

[270] CMS, S. Chatrchyan *et al.*, "Search for a light charged Higgs boson in top quark decays in pp collisions at $\sqrt{s} = 7$ TeV", *JHEP* **07** (2012) 143, arXiv:1205.5736 [hep-ex].

[271] CMS, V. Khachatryan *et al.*, "Search for a light charged Higgs boson decaying to $c\bar{s}$ in pp collisions at $\sqrt{s} = 8$ TeV", *JHEP* **12** (2015) 178, arXiv:1510.04252 [hep-ex].

[272] ATLAS, G. Aad *et al.*, "Search for charged Higgs bosons decaying via $H^{\pm} \to \tau^{\pm}\nu$ in fully hadronic final states using pp collision data at $\sqrt{s} = 8$ TeV with the ATLAS detector", *JHEP* **03** (2015) 088, arXiv:1412.6663 [hep-ex].

[273] A. G. Akeroyd *et al.*, "Prospects for charged Higgs searches at the LHC", arXiv:1607.01320 [hep-ph].

[274] T. Hermann, M. Misiak, and M. Steinhauser, "$\bar{B} \to X_s\gamma$ in the Two Higgs Doublet Model up to Next-to-Next-to-Leading Order in QCD", *JHEP* **11** (2012) 036, arXiv:1208.2788 [hep-ph].

[275] L. F. Abbott, P. Sikivie, and M. B. Wise, "Constraints on Charged Higgs Couplings", *Phys. Rev.* **D21** (1980) 1393.

[276] M. Ciuchini, G. Degrassi, P. Gambino, and G. F. Giudice, "Next-to-leading QCD corrections to $B \to X_s\gamma$: Standard model and two Higgs doublet model", *Nucl. Phys.* **B527** (1998) 21–43, arXiv:hep-ph/9710335 [hep-ph].

[277] F. Borzumati and C. Greub, "2HDMs predictions for anti-B —> X(s) gamma in NLO QCD", *Phys. Rev.* **D58** (1998) 074004, arXiv:hep-ph/9802391 [hep-ph].

[278] F. Borzumati and C. Greub, "Two Higgs doublet model predictions for anti-B —> X(s) gamma in NLO QCD: Addendum", *Phys. Rev.* **D59** (1999) 057501, arXiv:hep-ph/9809438 [hep-ph].

[279] CKMfitter Group, J. Charles, A. Hocker, H. Lacker, S. Laplace, F. R. Le Diberder, J. Malcles, J. Ocariz, M. Pivk, and L. Roos, "CP violation and the CKM matrix: Assessing the impact of the asymmetric B factories", *Eur. Phys. J.* **C41** (2005) no. 1, 1–131, arXiv:hep-ph/0406184 [hep-ph].

[280] P. M. Ferreira, L. Lavoura, and J. P. Silva, "Renormalization-group constraints on Yukawa alignment in multi-Higgs-doublet models", *Phys. Lett.* **B688** (2010) 341–344, arXiv:1001.2561 [hep-ph].

[281] J. Bijnens, J. Lu, and J. Rathsman, "Constraining General Two Higgs Doublet Models by the Evolution of Yukawa Couplings", *JHEP* **05** (2012) 118, arXiv:1111.5760 [hep-ph].

[282] H. Serodio, "Yukawa Alignment in a Multi Higgs Doublet Model: An effective approach", *Phys. Lett.* **B700** (2011) 133–138, arXiv:1104.2545 [hep-ph].

[283] H. Flacher, M. Goebel, J. Haller, A. Hocker, K. Monig, and J. Stelzer, "Revisiting the Global Electroweak Fit of the Standard Model and Beyond with Gfitter", *Eur. Phys. J.* **C60** (2009) 543–583, arXiv:0811.0009 [hep-ph]. [Erratum: Eur. Phys. J.C71,1718(2011)].

[284] C. Csaki, J. Erlich, and J. Terning, "The Effective Lagrangian in the Randall-Sundrum model and electroweak physics", *Phys. Rev.* **D66** (2002) 064021, arXiv:hep-ph/0203034 [hep-ph].

[285] A. Azatov, M. Toharia, and L. Zhu, "Higgs Production from Gluon Fusion in Warped Extra Dimensions", *Phys. Rev.* **D82** (2010) 056004, arXiv:1006.5939 [hep-ph].

[286] C. Bouchart and G. Moreau, "Higgs boson phenomenology and VEV shift in the RS scenario", *Phys. Rev.* **D80** (2009) 095022, arXiv:0909.4812 [hep-ph].

[287] ATLAS, G. Aad *et al.*, "Search for high-mass diboson resonances with boson-tagged jets in proton-proton collisions at $\sqrt{s} = 8$ TeV with the ATLAS detector", *JHEP* **12** (2015) 055, arXiv:1506.00962 [hep-ex].

[288] CMS, V. Khachatryan *et al.*, "Search for massive resonances in dijet systems containing jets tagged as W or Z boson decays in pp collisions at $\sqrt{s} = 8$ TeV", *JHEP* **08** (2014) 173, arXiv:1405.1994 [hep-ex].

[289] CMS, V. Khachatryan *et al.*, "Search for massive WH resonances decaying to $\ell\nu\mathrm{b\bar{b}}$ final state in the boosted regime at $\sqrt{s} = 8\,\mathrm{TeV}$",.

[290] G. P. Salam, "Towards Jetography", *Eur. Phys. J.* **C67** (2010) 637–686, arXiv:0906.1833 [hep-ph].

[291] See A. Angelescu, A. Djouadi, G. Moreau, and F. Richard, arXiv:1512.03047 [hep-ph] and references therein.

[292] A. Angelescu, A. Djouadi, G. Moreau, and F. Richard, "Diboson resonances within a custodially protected warped extra-dimensional scenario", arXiv:1512.03047 [hep-ph].

[293] A. Djouadi, G. Moreau, and R. K. Singh, "Kaluza-Klein excitations of gauge bosons at the LHC", *Nucl. Phys.* **B797** (2008) 1–26, arXiv:0706.4191 [hep-ph].

[294] K. Agashe, S. Gopalakrishna, T. Han, G.-Y. Huang, and A. Soni, "LHC Signals for Warped Electroweak Charged Gauge Bosons", *Phys. Rev.* **D80** (2009) 075007, arXiv:0810.1497 [hep-ph].

[295] F. Richard, "Diboson production at LHC with warped extra dimensions", arXiv:1203.1762 [hep-ph].

[296] A. Djouadi, G. Moreau, F. Richard, and R. K. Singh, "The Forward-backward asymmetry of top quark production at the Tevatron in warped extra dimensional models", *Phys. Rev.* **D82** (2010) 071702, arXiv:0906.0604 [hep-ph].

[297] A. Djouadi, G. Moreau, and F. Richard, "Forward-backward asymmetries of the bottom and top quarks in warped extra-dimensional models: LHC predictions from the LEP and Tevatron anomalies", *Phys. Lett.* **B701** (2011) 458–464, arXiv:1105.3158 [hep-ph].

[298] A. D. Martin, W. J. Stirling, R. S. Thorne, and G. Watt, "Parton distributions for the LHC", *Eur. Phys. J.* **C63** (2009) 189–285, arXiv:0901.0002 [hep-ph].

[299] M. Carena, S. Casagrande, F. Goertz, U. Haisch, and M. Neubert, "Higgs Production in a Warped Extra Dimension", *JHEP* **08** (2012) 156, arXiv:1204.0008 [hep-ph].

[300] S. Casagrande, F. Goertz, U. Haisch, M. Neubert, and T. Pfoh, "The Custodial Randall-Sundrum Model: From Precision Tests to Higgs Physics", *JHEP* **09** (2010) 014, arXiv:1005.4315 [hep-ph].

[301] F. del Aguila, A. Carmona, and J. Santiago, "Tau Custodian searches at the LHC", *Phys. Lett.* **B695** (2011) 449–453, arXiv:1007.4206 [hep-ph].

[302] M. Carena, E. Ponton, J. Santiago, and C. E. M. Wagner, "Light Kaluza Klein States in Randall-Sundrum Models with Custodial SU(2)", *Nucl. Phys.* **B759** (2006) 202–227, arXiv:hep-ph/0607106 [hep-ph].

[303] R. Malm, M. Neubert, and C. Schmell, "Higgs Couplings and Phenomenology in a Warped Extra Dimension", *JHEP* **02** (2015) 008, arXiv:1408.4456 [hep-ph].

[304] M. Carena, E. Ponton, J. Santiago, and C. E. M. Wagner, "Electroweak constraints on warped models with custodial symmetry", *Phys. Rev.* **D76** (2007) 035006, arXiv:hep-ph/0701055 [hep-ph].

[305] B. M. Dillon and S. J. Huber, "Non-Custodial Warped Extra Dimensions at the LHC?", *JHEP* **06** (2015) 066, arXiv:1410.7345 [hep-ph].

[306] R. Malm, M. Neubert, K. Novotny, and C. Schmell, "5D Perspective on Higgs Production at the Boundary of a Warped Extra Dimension", *JHEP* **01** (2014) 173, arXiv:1303.5702 [hep-ph].

[307] ATLAS, M. Aaboud *et al.*, "Searches for heavy diboson resonances in pp collisions at $\sqrt{s} = 13$ TeV with the ATLAS detector", *JHEP* **09** (2016) 173, arXiv:1606.04833 [hep-ex].

[308] CMS, V. Khachatryan *et al.*, "Combination of diboson resonance searches at 8 and 13 TeV",.

[309] CMS, V. Khachatryan *et al.*, "Search for diboson resonances in the semileptonic $X \to ZV \to \ell^+\ell^-$ $q\bar{q}$ final state at $\sqrt{s} = 13$ TeV with CMS",.

[310] CMS, V. Khachatryan *et al.*, "Search for new resonances decaying to $WW/WZ \to \ell\nu qq$",.

[311] S. Fichet and G. von Gersdorff, "Anomalous gauge couplings from composite Higgs and warped extra dimensions", *JHEP* **03** (2014) 102, arXiv:1311.6815 [hep-ph].

[312] A. M. Iyer, K. Sridhar, and S. K. Vempati, "Bulk Randall-Sundrum models, electroweak precision tests, and the 125 GeV Higgs", *Phys. Rev.* **D93** (2016) no. 7, 075008, arXiv:1502.06206 [hep-ph].

[313] P. R. Archer, M. Carena, A. Carmona, and M. Neubert, "Higgs Production and Decay in Models of a Warped Extra Dimension with a Bulk Higgs", *JHEP* **01** (2015) 060, arXiv:1408.5406 [hep-ph].

[314] A. Falkowski and M. Perez-Victoria, "Electroweak Breaking on a Soft Wall", *JHEP* **12** (2008) 107, arXiv:0806.1737 [hep-ph].

[315] J. A. Cabrer, G. von Gersdorff, and M. Quiros, "Warped Electroweak Breaking Without Custodial Symmetry", *Phys. Lett.* **B697** (2011) 208–214, arXiv:1011.2205 [hep-ph].

[316] J. A. Cabrer, G. von Gersdorff, and M. Quiros, "Suppressing Electroweak Precision Observables in 5D Warped Models", *JHEP* **05** (2011) 083, arXiv:1103.1388 [hep-ph].

[317] C. Csaki, M. Graesser, L. Randall, and J. Terning, "Cosmology of brane models with radion stabilization", *Phys. Rev.* **D62** (2000) 045015, arXiv:hep-ph/9911406 [hep-ph].

[318] C. Csaki, M. L. Graesser, and G. D. Kribs, "Radion dynamics and electroweak physics", *Phys. Rev.* **D63** (2001) 065002, arXiv:hep-th/0008151 [hep-th].

[319] R. Barceló, S. Mitra, and G. Moreau, "On a boundary-localized Higgs boson in 5D theories", *Eur. Phys. J.* **C75** (2015) no. 11, 527, arXiv:1408.1852 [hep-ph].

[320] B. Lillie, L. Randall, and L.-T. Wang, "The Bulk RS KK-gluon at the LHC", *JHEP* **09** (2007) 074, arXiv:hep-ph/0701166 [hep-ph].

[321] B. Lillie, J. Shu, and T. M. P. Tait, "Kaluza-Klein Gluons as a Diagnostic of Warped Models", *Phys. Rev.* **D76** (2007) 115016, arXiv:0706.3960 [hep-ph].

[322] F. Ledroit, G. Moreau, and J. Morel, "Probing RS scenarios of flavour at LHC via leptonic channels", *JHEP* **09** (2007) 071, arXiv:hep-ph/0703262 [HEP-PH].

[323] M. Guchait, F. Mahmoudi, and K. Sridhar, "Associated production of a Kaluza-Klein excitation of a gluon with a t anti-t pair at the LHC", *Phys. Lett.* **B666** (2008) 347–351, arXiv:0710.2234 [hep-ph].

[324] K. Agashe, A. Belyaev, T. Krupovnickas, G. Perez, and J. Virzi, "LHC Signals from Warped Extra Dimensions", *Phys. Rev.* **D77** (2008) 015003, arXiv:hep-ph/0612015 [hep-ph].

[325] B. C. Allanach, F. Mahmoudi, J. P. Skittrall, and K. Sridhar, "Gluon-initiated production of a Kaluza-Klein gluon in a Bulk Randall-Sundrum model", *JHEP* **03** (2010) 014, arXiv:0910.1350 [hep-ph].

[326] M. Frank, K. Huitu, U. Maitra, and M. Patra, "Probing Higgs-radion mixing in warped models through complementary searches at the LHC and the ILC", *Phys. Rev.* **D94** (2016) no. 5, 055016, arXiv:1606.07689 [hep-ph].

[327] The ATLAS Collaboration. https://twiki.cern.ch/twiki/bin/view/AtlasPublic.

[328] The CMS Collaboration. http://cms-results.web.cern.ch/cms-results/public-results/publications/.

[329] F. Richard, "Diphoton resonance at e+e- and photon colliders", arXiv:1604.01640 [hep-ex].

[330] A. Angelescu, G. Moreau, and F. Richard, "Scalar production in association with a Z boson at the LHC and ILC: The mixed Higgs-radion case of warped models", *Phys. Rev.* **D96** (2017) no. 1, 015019, arXiv:1702.03984 [hep-ph].

[331] K. S. Agashe, J. Collins, P. Du, S. Hong, D. Kim, and R. K. Mishra, "LHC Signals from Cascade Decays of Warped Vector Resonances", *JHEP* **05** (2017) 078, arXiv:1612.00047 [hep-ph].

[332] G. F. Giudice, R. Rattazzi, and J. D. Wells, "Graviscalars from higher dimensional metrics and curvature Higgs mixing", *Nucl. Phys.* **B595** (2001) 250–276, arXiv:hep-ph/0002178 [hep-ph].

[333] D. Dominici, B. Grzadkowski, J. F. Gunion, and M. Toharia, "The Scalar sector of the Randall-Sundrum model", *Nucl. Phys.* **B671** (2003) 243–292, arXiv:hep-ph/0206192 [hep-ph].

[334] C. Csaki, J. Hubisz, and S. J. Lee, "Radion phenomenology in realistic warped space models", *Phys. Rev.* **D76** (2007) 125015, arXiv:0705.3844 [hep-ph].

[335] A. Ahmed, B. M. Dillon, B. Grzadkowski, J. F. Gunion, and Y. Jiang, "Implications of the absence of high-mass radion signals", *Phys. Rev.* **D95** (2017) no. 9, 095019, arXiv:1512.05771 [hep-ph].

[336] P. Cox, A. D. Medina, T. S. Ray, and A. Spray, "Radion/Dilaton-Higgs Mixing Phenomenology in Light of the LHC", *JHEP* **02** (2014) 032, arXiv:1311.3663 [hep-ph].

[337] K. Agashe, H. Davoudiasl, S. Gopalakrishna, T. Han, G.-Y. Huang, G. Perez, Z.-G. Si, and A. Soni, "LHC Signals for Warped Electroweak Neutral Gauge Bosons", *Phys. Rev.* **D76** (2007) 115015, arXiv:0709.0007 [hep-ph].

[338] K. Agashe, H. Davoudiasl, G. Perez, and A. Soni, "Warped Gravitons at the LHC and Beyond", *Phys. Rev.* **D76** (2007) 036006, arXiv:hep-ph/0701186 [hep-ph].

[339] CMS, V. Khachatryan *et al.*, "Measurements of inclusive and differential Z boson production cross sections in pp collisions at $\sqrt{s} = 13$ TeV",.

[340] ATLAS, T. A. collaboration, "Measurements of the Production Cross Section of a Z Boson in Association with Jets in pp collisions at $\sqrt{s} = 13$ TeV with the ATLAS Detector",.

[341] CMS, V. Khachatryan *et al.*, "Comparison of the Z/γ^* + jets to γ + jets cross sections in pp collisions at $\sqrt{s} = 8$ TeV", *JHEP* **10** (2015) 128, arXiv:1505.06520 [hep-ex]. [Erratum: JHEP04,010(2016)].

[342] ATLAS, G. Aad *et al.*, "Measurement of differential production cross-sections for a Z boson in association with b-jets in 7 TeV proton-proton collisions with the ATLAS detector", *JHEP* **10** (2014) 141, arXiv:1407.3643 [hep-ex].

[343] D. T. Nhung, L. D. Ninh, and M. M. Weber, "NLO corrections to WWZ production at the LHC", *JHEP* **12** (2013) 096, arXiv:1307.7403 [hep-ph].

[344] Q.-H. Cao, Y. Liu, and B. Yan, "Measuring trilinear Higgs coupling in WHH and ZHH productions at the high-luminosity LHC", *Phys. Rev.* **D95** (2017) no. 7, 073006, arXiv:1511.03311 [hep-ph].

[345] A. Chakraborty, U. Maitra, S. Raychaudhuri, and T. Samui, "Mixed Higgs–radion states at the LHC – a detailed study", *Nucl. Phys.* **B922** (2017) 41–61, arXiv:1701.07471 [hep-ph].

[346] ILD Design Study Group, H. Li, K. Ito, R. Poschl, F. Richard, M. Ruan, Y. Takubo, and H. Yamamoto, "HZ Recoil Mass and Cross Section Analysis in ILD", arXiv:1202.1439 [hep-ex].

[347] T. Barklow, J. Brau, K. Fujii, J. Gao, J. List, N. Walker, and K. Yokoya, "ILC Operating Scenarios", arXiv:1506.07830 [hep-ex].

[348] P. Doublet, *Hadrons dans un calorimètre électromagnétique silicium-tungstène hautement granulaire, Production du quark top à l'International Linear Collider*. PhD thesis, LAL Orsay, http://publication.lal.in2p3.fr/2011/These-PhDoublet.pdf, 2011.

[349] H. Baer, T. Barklow, K. Fujii, Y. Gao, A. Hoang, S. Kanemura, J. List, H. E. Logan, A. Nomerotski, M. Perelstein, *et al.*, "The International Linear Collider Technical Design Report - Volume 2: Physics", arXiv:1306.6352 [hep-ph].

[350] S. Bhattacharya, M. Frank, K. Huitu, U. Maitra, B. Mukhopadhyaya, and S. K. Rai, "Probing the light radion through diphotons at the Large Hadron Collider", *Phys. Rev.* **D91** (2015) 016008, arXiv:1410.0396 [hep-ph].

[351] ILC physics and detector study, J. Tian and K. Fujii, "Measurement of Higgs boson couplings at the International Linear Collider", *Nucl. Part. Phys. Proc.* **273-275** (2016) 826–833.

[352] E. De Pree and M. Sher, "Top pair production in Randall-Sundrum models", *Phys. Rev.* **D73** (2006) 095006, arXiv:hep-ph/0603105 [hep-ph].

Titre: Des scalaires dans les dimensions supplémentaires (courbes): modèles effectifs et réalisations concrètes
Mots clés: *Nouvelle Physique, Dimensions Supplémentaires, Boson de Higgs, LHC, Phenomenologie, Matiére Noire*
Résumé: Il y a près de deux décennies, l'utilisation des modèles à dimensions supplémentaires pour résoudre le problème de hiérarchie des théories de jauge a reçu beaucoup d'attention, grâce à d'élégantes propositions: des dimensions supplémentaires (DS) étendues et plates – le modèle d'Arkani-Hamed-Dimopoulos-Dvali, ou ADD – ainsi que des DS courbées – le modèle de Randall-Sundrum, ou RS. Dans cette thèse, nous discutons plusieurs modèles inspirés de tels scénarios de dimension supèrieure. Pour commencer, nous introduisons des éléments-clés de la théorie des champs en cinq dimensions, et nous montrons comment de tels scénarios apportent une réponse au problème de hiérarchie. Ensuite, dans une première partie, nous adoptons une approche "de bas en haut" et étudions plusieurs modèles contenant des fermions vectoriels (FV), prédits génériquement dans les modèles de DS. Nous montrons qu'en ajoutant des quarks vectoriels (QV) au Modèle Standard (MS), on peut expliquer en même temps les anomalies (i) d'asymétrie avant-arrière des quarks b ($A_{\rm FB}^b$) mesurée au Large Electron-Positron collider (LEP) et (ii) de section efficace de production de $t\bar{t}h$ mesurée au Large Hadron Collider (LHC). En utilisant des rapports de taux de désintégration du Higgs, nous estimons aussi la sensibilité du LHC amélioré, le LHC à haute luminosité, à la présence de QV. Puis nous considérons un modèle à deux doublets de Higgs (2HDM), accompagné de leptons vectoriels (LV) pour expliquer le mystérieux excès à 750 GeV observé au LHC fin 2015. Dans un modèle similaire, nous expliquons également l'abondance de matière noire (MN) dans l'Univers, notre candidat pour la MN étant un LV neutre, stabilisé par une symétrie $\mathbb{Z}_2$ appropriée. Dans une deuxième partie de la thèse, nous nous penchons sur le scénario plus concret des DS courbées dotées d'une symétrie custodiale dans l'espace à cinq dimensions, qui protège le modèle vis-à-vis de larges corrections aux observables de précision électrofaibles. Dans ce cadre, nous interprétons tout d'abord la résonance à deux bosons observée à 2 TeV au LHC comme étant une superposition de bosons de jauge de Kaluza-Klein, produits dans le canal s. Dans un deuxième temps, nous étudions la phénoménologie du secteur scalaire du modèle susdit, qui mélange le boson de Higgs et le radion. En particulier, nous estimons la sensibilité du LHC et d'un futur collisionneur électron-positron (l'International Linear Collider - ILC) à la présence d'un radion, via la production de celui-ci en association avec un boson Z.

Title: Scalars in (Warped) Extra Dimensions: Climbing from the Bottom to the Top
Key words: *New Physics, Extra Dimensions, Higgs Boson, LHC, Phenomenology, Dark Matter*
Abstract: Almost two decades ago, the paradigm of extra-dimensional models addressing the gauge hierarchy problem attracted much attention through the elegant proposals of large, flat extra dimensions (EDs) – the Arkani-Hamed-Dimopoulos-Dvali or ADD model – and warped EDs – the Randall-Sundrum or RS model. In this thesis, we discuss several models inspired from such extra-dimensional scenarios. We start by introducing some key elements of field theory in five space-time dimensions and showing how such scenarios provide a solution to the hierarchy problem. Afterwards, in a first part of this work, we adopt a bottom-up approach and study several models containing Vector-Like Fermions (VLFs), which are typically predicted in ED frameworks. We show how adding Vector-Like Quarks (VLQs) to the Standard Model (SM) allows one to simultaneously explain the anomalies in the (i) b-quark forward-backward asymmetry ($A_{\rm FB}^b$) measured at the Large Electron-Positron collider (LEP) and (ii) the $t\bar{t}h$ production cross section measured at the Large Hadron Collider (LHC). Using the so-called Higgs decay ratios, we also estimate the sensitivity of the upgraded LHC, the High-Luminosity LHC, to the presence of VLQs. Then, we consider a Two-Higgs Doublet Model (2HDM) extended with Vector-Like Leptons (VLLs) in order to fit the mysterious 750 GeV excess observed at LHC in late 2015. Within a similar model, we also explain the Dark Matter (DM) abundance in the Universe, our DM candidate being a neutral VLL, which is rendered stable by a suitable $\mathbb{Z}_2$ symmetry. Later on, in a second part of the thesis, we focus on the more concrete warped ED scenario endowed with a bulk custodial symmetry, which protects the model from large electroweak (EW) corrections. In this framework, we first interpret the 2 TeV diboson bump observed at LHC in 2015 as a superposition of Kaluza-Klein (KK) gauge bosons produced in the s-channel. Afterwards, we study the phenomenology of the mixed Higgs-radion scalar sector of the aforementioned model. In particular, we estimate the sensitivity of the LHC and of a future electron-positron collider (the International Linear Collider - ILC) to the existence of a radion via its production in association with a Z boson.

Université Paris-Saclay
Espace Technologique / Immeuble Discovery
Route de l'Orme aux Merisiers RD 128 / 91190 Saint-Aubin, France